

Old Dominion University

## ODU Digital Commons

---

Chemistry & Biochemistry Theses & Dissertations

Chemistry & Biochemistry


---

Summer 2012

# Spectroscopic Characterization of Dissolved Organic Matter: Insights into Composition, Photochemical Transformation and Carbon Cycling

John Robert Helms  
*Old Dominion University*

Follow this and additional works at: [https://digitalcommons.odu.edu/chemistry\\_etds](https://digitalcommons.odu.edu/chemistry_etds)

 Part of the [Analytical Chemistry Commons](#), [Biogeochemistry Commons](#), and the [Oceanography Commons](#)

---

### Recommended Citation

Helms, John R.. "Spectroscopic Characterization of Dissolved Organic Matter: Insights into Composition, Photochemical Transformation and Carbon Cycling" (2012). Doctor of Philosophy (PhD), Dissertation, Chemistry & Biochemistry, Old Dominion University, DOI: 10.25777/1y3p-e444  
[https://digitalcommons.odu.edu/chemistry\\_etds/32](https://digitalcommons.odu.edu/chemistry_etds/32)

This Dissertation is brought to you for free and open access by the Chemistry & Biochemistry at ODU Digital Commons. It has been accepted for inclusion in Chemistry & Biochemistry Theses & Dissertations by an authorized administrator of ODU Digital Commons. For more information, please contact [digitalcommons@odu.edu](mailto:digitalcommons@odu.edu).

**SPECTROSCOPIC CHARACTERIZATION OF DISSOLVED  
ORGANIC MATTER: INSIGHTS INTO COMPOSITION,  
PHOTOCHEMICAL TRANSFORMATION AND CARBON  
CYCLING**

by

John Robert Helms  
B.A. May 1998, Virginia Wesleyan College  
M.S. December 2006, Old Dominion University

A Dissertation Submitted to the Faculty of  
Old Dominion University in Partial Fulfillment of the  
Requirements for the Degree of

DOCTOR OF PHILOSOPHY

CHEMISTRY

OLD DOMINION UNIVERSITY  
August 2012

Approved By:

\_\_\_\_\_  
Kenneth Mopper (Co-Director)

\_\_\_\_\_  
Jingdong Mao (Co-Director)

\_\_\_\_\_  
Patrick Hatcher (Member)

\_\_\_\_\_  
Aron Stubbins (Member)

\_\_\_\_\_  
Richard Zimmerman (Member)

## **ABSTRACT**

# **SPECTROSCOPIC CHARACTERIZATION OF DISSOLVED ORGANIC MATTER: INSIGHTS INTO COMPOSITION, PHOTOCHEMICAL TRANSFORMATION AND CARBON CYCLING**

John Robert Helms  
Old Dominion University, 2012  
Co-Directors: Dr. Kenneth Mopper  
Dr. Jingdong Mao

This dissertation explores processes affecting the composition of dissolved organic matter (DOM) and how DOM composition changes in sunlit surface waters and in the dark interior ocean. Simulated solar irradiations were used to investigate the impact of photochemistry on terrestrial waters and deep ocean DOM. The photochemically mediated processes observed in Dismal Swamp samples included (i) light induced flocculation of up to 12% of the organic matter and 84% of the dissolved iron originally present; (ii) 74-88% mineralization of dissolved organic carbon (DOC) and 95-99% bleaching of chromophoric DOM (CDOM) during 110 days of irradiation; and (iii) nearly complete loss of the biochemical markers for terrestrial DOM: lignin phenols, CDOM absorption and fluorescence, and aromaticity determined by nuclear magnetic resonance (NMR) spectroscopy. Extensively photo-degraded terrestrial DOM exhibited spectroscopic signatures similar to DOM isolated from ocean water (except that it lacked protein-like fluorescence and appeared to contain excess carboxyl carbon), and photo-degraded deep ocean DOM exhibited optical properties similar to surface ocean DOM.

The heretofore-unexamined DOM removal process of light induced flocculation was further investigated using solid-state  $^{13}\text{C}$  NMR and infrared spectroscopy.

Photochemical decarboxylation and production of alkyl functionality drives the initial phase of photochemical flocculation, while adsorption to iron flocculates is important during later phases of the process. Carboxyl amides appeared to resist mineralization, but were susceptible to photochemical flocculation. A fraction of the photodegraded DOM is more susceptible to mineral adsorption, which may be an important pathway for DOM export from surface waters to the sediments and subsequent preservation.

Advanced solid-state  $^{13}\text{C}$  NMR characterization of DOM isolated by reverse osmosis – electrodialysis (RO/ED) from marine environments with varying biogeochemistries revealed new insights into the biodegradation of carbohydrates as well as preservation of carboxyl groups and condensed aromatic structures in the ocean's interior. Quaternary anomeric carbons were identified as a potentially important structural component of the poorly characterized pool of bio-refractory carbohydrates.

The present biogeochemical paradigm for ocean DOC cycling, the “three-pool” model, is re-examined along with the “three-pool photoreactivity” classification system. A new conceptual model is proposed, which incorporates both biological and photochemical reactivity of dissolved organic matter.



This thesis is dedicated to my wife, Rachel; my children, Annabelle and William; and to my parents, Wayne and Claire; all of whom have inspired me, educated me, and brought so much joy into my life.

## ACKNOWLEDGMENTS

I would first like to thank Dr. Kenneth Mopper and Dr. Jingdong Mao for the research, financial, and educational opportunities, as well as advice, critical comments, friendship, and encouragement that led to this document. It would have been impossible for this document to exist without their many hours of hard work. I must also thank the members of my committee, Dr. Patrick Hatcher, Dr. Aron Stubbins, and Dr. Richard Zimmerman who showed incredible patience, were generous with their time, and enthusiastic with their help. I would like to thank Dr. E. Michael Perdue, Hongmei Chen, Nelson Green, and Dr. Aron Stubbins for providing samples concentrated and desalted by RO-ED and for discussing experimental results described here and elsewhere; Dr. David Burdige for use of the spectrofluorometer; Dr. Mark Chappell and Leslie Miller of U.S. Army Corps of Engineers, Vicksburg, MS and Dr. Klaus Schmidt-Rohr of Iowa State University, Ames, IA for providing NMR analyses; Dr. Hussain Abdulla, Dr. Rachel Sleighter, and Dr. Andrew Wozniak for helpful discussions; Dr. Robert Spencer and Rachel Dyda for lignin analyses. Thanks also to Susan Hatcher and Dr. Junyan Zhong of COSMIC, the staff of VCERC, and the faculty and staff of the ODU Department of Chemistry and Biochemistry and Department of Ocean Earth and Atmospheric Science for providing facilities and resources that made this work possible. Thanks to everyone else who discussed, advised, and encouraged me during the preparation of this dissertation. To list you all by name would make this section too long. Wayne and Claire Helms as well as Joanna and Phillip Cole provided emotional, logistical, and financial support during the writing of this dissertation. This research was supported by the following NSF grants: OCE-0096426, OCE-0241946, OCE-0327423, and OCE-0728634.

## TABLE OF CONTENTS

	Page
LIST OF TABLES .....	ix
LIST OF FIGURES .....	xi
 Chapter	
I. INTRODUCTION .....	1
II. PHOTOCHEMICAL FLOCCULATION OF TERRESTRIAL DISSOLVED ORGANIC MATTER AND IRON .....	11
INTRODUCTION .....	11
MATERIALS AND METHODS .....	15
RESULTS .....	21
DISCUSSION .....	40
III. LOSS OF OPTICAL, MOLECULAR, AND STRUCTURAL INDICATORS OF TERRIGENOUS DISSOLVED ORGANIC MATTER DURING LONG-TERM PHOTBLEACHING .....	52
INTRODUCTION .....	52
MATERIALS AND METHODS .....	55
RESULTS .....	64
DISCUSSION .....	88
IV. PHOTOCHEMICAL BLEACHING OF OPEN OCEAN DISSOLVED ORGANIC MATTER .....	98
INTRODUCTION .....	98
MATERIALS AND METHODS .....	99
RESULTS AND DISCUSSION .....	103
V. CHARACTERIZATION OF OCEANIC DISSOLVED ORGANIC MATTER ISOLATED BY REVERSE OSMOSIS COUPLED WITH ELECTRODIALYSIS .....	120
INTRODUCTION .....	120
MATERIALS AND METHODS .....	123
RESULTS .....	127
DISCUSSION .....	140
VI. SUMMARY AND CONCLUSIONS .....	161
REFERENCES .....	170

	Page
APPENDIX .....	213
VITA .....	219

## LIST OF TABLES

Table	Page
1. Summary of Parameters Measured for Each Sample .....	24
2. Functional Group Assignments and Integrated Area for Each CP-TOSS Spectral Region .....	32
3. CP-TOSS Integration Data from Table 2 Normalized to TOC Concentrations and Reported in Concentration of $\mu\text{mol C L}^{-1}$ for Quantitative Comparison of the Samples .....	33
4. Estimated Concentrations of Different Carboxylic Moieties Reported in Units of $\mu\text{mol C L}^{-1}$ .....	38
5. Summary of the Conditions Measured During the Irradiation Experiment .....	66
6. Spectral Components of Fluorescence Excitation Emission Matrix Spectra .....	74
7. Summary of CuO Oxidation Lignin Phenol Results .....	77
8. Integrated Area from $^{13}\text{C}$ CP/TOSS NMR Spectra for BS and FD Samples Irradiated for up to 32 Days (Total Area = 100%), And the Assigned Structural Moieties Associated With the Spectral Region .....	81
9. $^{13}\text{C}$ CP/TOSS Integration Data Normalized to DOC Concentration in Units of $\mu\text{mol C L}^{-1}$ .....	83
10. Carboxyl Functional Groups Quantified Using the De-convoluted FTIR Peak Areas Normalized to the NMR Peak at 160-187 ppm and DOC Concentration in Units of $\mu\text{mol C L}^{-1}$ .....	86
11. Summary of the Microbial Productivity Assay Used to Monitor Potential Biological Artifacts .....	104
12. DOC and UV-visible Measurements of RO/ED Isolates from NELHA 670m Water Samples .....	105
13. Summary of EEMS Peak Intensities and Locations for Irradiated and Dark Control (0d) RO/ED Isolates from NELHA 670m Water Samples .....	113
14. Fluorescence Indices Calculated Based on EEMS .....	114

Table	Page
15. Recovery of DOC by the RO/ED method. Only the "Initial" (seawater) and "Final" (concentrated and desalted) fractions were analyzed as part of this study, and only the "Final" fraction was amenable to solid-state NMR analysis ...	128
16. Summary of Optical Properties Measured for Initial Seawater Samples and RO/ED Isolates .....	130
17. Integration Ranges and Normalized Areas (total=100%) Determined Based on Solid-state $^{13}\text{C}$ CP/TOSS NMR Spectra .....	133
18. The Relative Abundances (%) of Functional Groups in RO/ED Isolated DOC Estimated Based on NMR Integration Data (Table 17) and NMR Spectral Editing Results (Fig. 36) .....	137
19. Comparison of CP/TOSS Results for RO/ED Isolates with CP/MAS Results from Previous Studies .....	141
20. Semi-labile Carbon Characterization Obtained by Subtracting the Refractory Carbon Signature of the Deep N. Pacific Sample From That of Each Sample (DOC Normalized NMR Integrations) .....	151
21. Semi-labile Carbon Characterization Obtained by Subtracting the Refractory Carbon Signature of the Deep N. Pacific Sample from That of Each Sample (DOC Normalized NMR Integrals With Spectral Editing Data) .....	152
22. Semi-labile Carbon Characterization Obtained by Subtracting the Refractory Carbon Signature of the Deep N. Pacific Sample from That of Each Sample (NMR Integrals With Spectral Editing Data Normalized to Total Area=100%) .....	153

## LIST OF FIGURES

Figure	Page
1. The Vertical Distribution of DOC, at the Bermuda Atlantic Time Series (BATS) Site in the Northwestern Sargasso Sea, Highlights the Applicability of the “Three-pool DOC” Model .....	8
2. pH Values of Water Samples Measured at the End of Each Irradiation Time Point .....	22
3. UV-visible Absorption Spectra (Left), First-derivative Absorption Spectra (Center), and Second-derivative Absorption Spectra Were Obtained (Right) for (A, B, and C) Total, Unfractionated Samples in Which Flocculated POM Was Re-dissolved at High pH, (D, E, and F) Dissolved Samples from Which POM Was Removed, and (G, H, and I) POM Obtained by Difference .....	25
4. Natural Log UV-visible Absorption Spectra (Left), First-derivative Natural Log Absorption Spectra (Center), and Second-derivative Natural Log Absorption Spectra (Right) Were Obtained for (A, B, and C) Total Samples in Which Flocculated POM Was Re-dissolved at High pH, (D, E, and F) Dissolved Samples from Which POM Was Removed, and (G, H, and I) POM Obtained by Difference .....	26
5. Concentrations of Dissolved (Gray), Particulate (Black), and Adsorbed (White) Material Quantified As: (A) Organic Carbon, (B) Absorption at 300 nm, (C) Iron by Atomic Absorption, and (D) Total Nitrogen .....	27
6. Distribution of Dissolved (Gray), Particulate (Black), and Adsorbed (White) Material Quantified As: (A) Organic Carbon, (B) Absorption at 300 nm, (C) Iron by Atomic Absorption, and (D) Total Nitrogen .....	28
7. Solid-state CP/TOSS $^{13}\text{C}$ NMR Spectra (Solid Black Lines) Obtained for (A) the Dark Control Sample, (B) the Un-fractionated 10 d Irradiated Sample, (C) Dissolved Material Isolated from the 10 d Irradiated Sample by Centrifugation, and (D) the Particulate Material Isolated from the 10 d Irradiated Sample by Centrifugation .....	31
8. FTIR Spectra Obtained for (A) Dissolved Organic Matter and (B) Particulate Organic Matter .....	35

Figure	Page
9. Partially De-convoluted FTIR Spectra for (A) Unirradiated, Dark Control, (B) 10 day Irradiated, Unfractionated Sample, (C) 10 Day Irradiated Centrifuged (Supernatant) Sample, and (D) Particles Isolated from 10 Day Irradiated Sample .....	37
10. Distribution of Organic Functional Groups After 10 Days Continuous UVA Exposure .....	39
11. Proposed Components of the Photochemical Flocculation Mechanism for Organic Matter and Iron .....	44
12. Hypothetical Schematic Representation of the Photochemical Flocculation Process .....	45
13. (A) Extrapolated 100% Photobleaching at 300nm for Unfractionated Samples and (B) Centrifuged Samples .....	49
14. Comparison of Solar Irradiance Spectrum and UVA340 Lamp Output .....	57
15. (A) Sample pH, (B) Temperature, and (C) Dissolved Oxygen Saturation Measured for FD Samples During Irradiation .....	67
16. (A) Ultraviolet-visible Spectra of BS and (B) FD Sub-samples Collected Over the Course of the First Irradiation Experiment .....	68
17. (A) Natural Log Linearized Spectra for BS and (B) FD Samples .....	69
18. Absorption Coefficients Measured at (A) 254 nm ( $a_{254}$ ) and (B) 300 nm ( $a_{300}$ ) Decreased During the Course of the Irradiation Experiments .....	70
19. Spectral Slopes Calculated for the Range of (A) 300 – 700 nm Decreased During Irradiation .....	72
20. Fluorescence Excitation Emission Matrices Shown for (A) BS-0d, (B) FD-0d, (C) BS-10d, (D) FD-11d, (E) BS-52d, and (F) FD-56d .....	73
21. (A) EEMS Peak M to Peak C ratio (M:C), (B) McKnight Fluorescence Index (FI), (C) Fluorescence Humification Index (HIX), and (D) Biological Fluorescence Index (BIX) Calculated for Samples from the Irradiation Experiments .....	75
22. CP/TOSS Spectra Obtained from the FD Samples (Black Lines) .....	79



Figure	Page
23. Solid-state $^{13}\text{C}$ NMR Spectra Obtained for (A) BS-0d (B) BS-3d, and (C) BS-10d .....	80
24. Infrared (FTIR) Spectra Obtained for (A) FD-0d, (B) FD-11d, (C) FD-21d, and (D) FD-32d Samples .....	84
25. De-convoluted FTIR Spectra for (A) FD-0d, (B) FD-11d, (C) FD-21d, and (D) FD-32d Samples .....	85
26. Variation of Metal Associated Carboxylate (COO-Me), Carboxylic Acid/Carboxylate, Acetate Groups, Carboxylic Esters (Including Lactones) and Carboxylic Amides in FD Samples Measured During UV Irradiation Reported as (A) Concentration in Solution and (B) Percentage of Carboxyl Groups .....	87
27. (A) UV-visible Absorption Spectra, (B) First-derivative Absorption Spectra, (C) Second-derivative Absorption Spectra, (D) Natural Log Absorption Spectra, (E) First-derivative Natural Log Absorption Spectra, (F) Second-derivative Natural Log Absorption Spectra, (G) Amount of Absorption Removed by Photobleaching, (H) Percentage of Absorption Removed by Photobleaching, and (I) Spectral Slope Spectra, Obtained for NELHA RO/ED Isolates Irradiated for 0 d, 5 d, 26 d, and 68 d .....	106
28. The Trends of Decreasing (A) UV-visible Absorption, (B) DOC, and (C) Specific UV Absorbance (SUVA) With Increasing Irradiation Time .....	107
29. (A) Spectral Slope Coefficients for 300-700 nm, 275-295 nm, and 350-400 nm Show Different Trends With Irradiation .....	110
30. Fluorescence Excitation Emission Matrix Spectra Obtained for RO/ED Isolated DOM Samples from (A) a Surface Sample Collected at Station ALOHA, (B) a Sample Pumped from the 670m Water Supply at NELHA, and (C) a Sample Collected at 3500m Depth at Station ALOHA .....	111
31. Depth Profile of Fluorescence Indices Measured for RO/ED Isolated DOM from the North Pacific at Station ALOHA (5 m and 3500 m) and NELHA (670 m) .....	112
32. Fluorescence Excitation Emission Matrix Spectra Shown for (A) a Non-irradiated 670m NELHA DOM Isolate and (B) 670m NELHA DOM That Was Irradiated for 68 d .....	115

Figure	Page
33. UV-visible Absorption Spectra Collected for (A) Filtered Seawater Samples Using 10 cm cuvette, (B) First-derivative, and (C) Second-derivative .....	129
34. Solid-state $^{13}\text{C}$ NMR Spectra Measured by Cross Polarization with Magic Angle Spinning and Total Suppression of Sidebands (CP-TOSS) .....	132
35. A Representative Sample (5 m North Atlantic) Was Measured Using Both (A) Direct Polarization and (B) Cross Polarization $^{13}\text{C}$ NMR .....	134
36. Solid-state $^{13}\text{C}$ CP/TOSS NMR Spectra and CP/TOSS NMR Spectra with Spectral Editing Were Collected for (A) RO/ED Isolated DOM from the North Atlantic and (B) RO/ED Isolated DOM from the North Pacific .....	135
37. (A) Examples of Quaternary Anomeric Carbons in Furanose (Left) and Pyranose (Right) Sugars .....	139
38. Functional Group Relative Abundances Displayed on a Carbon Percentage Basis .....	144
39. Estimated In Situ Concentrations, Assuming That RO/ED Isolates Are Reflective of Total Organic Carbon Pool Irrespective of the Recovery .....	145
40. Comparison of Sample NMR Signals After Subtraction of the Background Refractory (N. Pacific 3500m) DOM Signal Calculated Using (A) DOC Normalized and (B) Total Area=100% Normalized Data .....	154
41. Modifications Expanding the Applicability of the Three-pool DOC Model, Proposed by Carlson (2002), to Include Photochemical Reactivity of DOM, Which Can Limit the Ability of a Given Compound to Cycle Over Time-scales Longer Than Whole-ocean-overtum .....	157

# CHAPTER I

## INTRODUCTION

Dissolved organic matter (DOM) is a complex mixture of biologically produced material in varied states of decomposition. Aquatic DOM is often classified according to its source environment. Allochthonous DOM is imported from outside the aquatic environment and is of mostly terrestrial (or terrigenous) origin, containing mainly degraded vascular plant material. Autochthonous DOM is produced within the aquatic environment and contains mostly algal produced material, much of which has been altered by heterotrophic and/or photochemical processes (Chester 1990). Aquatic DOM is one of the largest reservoirs of reduced carbon on earth (Mopper and Degens 1979). The dissolved organic carbon (DOC) in the ocean is more than 300 times the annual oceanic uptake of atmospheric carbon, giving small perturbations to aquatic DOM processing the potential for profound changes to the global carbon cycle (Carlson 2002; Sexton et al. 2011). The riverine export of DOM is sufficient to maintain the overturn of DOM in the oceans (Williams 1971; Williams and Druffel 1987; Hedges et al. 1997); however, identifiably terrestrial DOM is vanishingly dilute in the open ocean (Hedges et al. 1997; Hernes and Benner 2002). Our ability to fully understand the role DOM plays in the global carbon cycle hinges on our ability to identify its sources and track its biological, chemical and physical changes within the aquatic environment (Hedges et al. 1997; Hansell and Carlson 2001).

The primary aim of this dissertation is to explore the biogeochemical cycling of DOM in the aquatic environment. Recent advances in nuclear magnetic resonance

spectroscopy (NMR), and DOM isolation techniques as well as new approaches to interpreting ultraviolet-visible and infrared spectra, are applied to the structural and compositional changes to DOM that occur during photochemical degradation in natural waters and aging within the deep ocean.

## BACKGROUND

*Photochemical Alteration of Dissolved Organic Matter* – Complete photo-mineralization of DOM produces carbon dioxide (Miller and Zepp 1995; White et al. 2008) and, to a lesser extent, carbon monoxide (Conrad and Seiler 1980; Zafiriou et al. 1984; Zafiriou et al. 2003). Photo-oxidation also generates low molecular weight products such as carbonyl compounds (Mopper and Stahovec 1986; Kieber et al. 1990) and organic acids (Kieber and Mopper 1987; Wetzel et al. 1995). These low molecular weight photoproducts are considered more biologically available than their parent molecules (Kieber et al. 1989; Wetzel et al. 1995; Miller and Moran 1997; Moran and Zepp 1997; Miller et al. 2002) leading to their rapid and complete removal from the aquatic DOM pool.

Investigations of DOM photochemistry have largely focused on the major (Zafiriou et al. 1984; Miller and Zepp 1995; Zafiriou et al. 2003; Stubbins et al. 2008; White et al. 2008) and minor (Zafiriou et al. 1984; Mopper and Stahovec 1986; Kieber and Mopper 1987; Kieber et al. 1990; Wetzel et al. 1995) photo-products that can be quantified individually (or by class) or on overall changes in optical or bulk properties such as UV absorbance (Chin et al. 1994; Yacobi et al. 2003; Helms et al. 2008) and total organic carbon (TOC) (Moran et al. 2000). More recently, the structural changes that

occur in the bulk DOM have been studied by several mass spectral (MS) techniques (Schmitt-Kopplin et al. 1998; Kujawinski et al. 2004; Minor et al. 2007; Dalzell et al. 2009; Gonsior et al. 2009; Stubbins et al. 2010). These studies have shown that aromatic, conjugated, and low oxygen-containing moieties appear to be efficiently removed during irradiation (Kujawinski et al. 2004; Minor et al. 2007; Gonsior et al. 2009), average molecular weight decreases (Dalzell et al. 2009), and methyl groups appear to be replaced by ketones (Kujawinski et al. 2004). Stubbins et al. (2010) suggested that DOM can be classified into three pools (photo-labile, photo-resistant, and photo-produced) and that simple aromatics, condensed aromatics, and carboxylic rich alicyclic molecules (CRAM) were consumed during photochemical degradation, while aliphatics were produced.

Changes to the optical properties of terrestrial DOM caused by photochemical reactions are well studied. Irradiated filtered water samples show an overall decrease in UV-visible light absorption (Blough and Green 1995; Del Vecchio and Blough 2002) and fluorescence (Del Vecchio and Blough 2002; Del Vecchio and Blough 2004a). Spectral slope ( $S$ ), an index related to the shape of the DOM UV-visible absorption spectrum, typically shows an increase in the short wavelength UV and a decrease in the long wavelength UV (Helms et al. 2008; Spencer et al. 2009). Fluorescence excitation emission matrix spectroscopy (EEMS) facilitates the two-dimensional mapping of fluorescence over a range of excitation and emission wavelengths (Christian et al. 1981). Coble (1996) identified five distinct EEMS peaks, which typify DOM in natural waters. By comparing their relative contributions to the EEMS spectra, additional source and structural information is obtained (McKnight et al. 2001; Cory and McKnight 2005;

Fimmen et al. 2007). Dissolved lignin is widely used as a tracer for terrestrial DOM (Benner and Opsahl 2001). Spencer et al. (2009) have shown that dissolved lignin is efficiently removed along with UV-visible absorption during photochemical degradation of riverine DOM. Broad application of this photochemically labile class of compounds, as molecular tracers for terrestrial DOM, may have resulted in a biased understanding of the sources of DOM in the ocean (Benner and Kaiser 2010). The other structural changes that occur in the DOM and are responsible for these optical changes are not well known.

To date, five studies have used  $^{13}\text{C}$  NMR to investigate the bulk chemical and structural changes that occur during photochemical degradation of DOM (Wetzel et al. 1995; Kulovaara et al. 1996; Schmitt-Kopplin et al. 1998; Osburn et al. 2001; Thorn et al. 2010). However, with the exception of Osburn et al., (2001) these studies have only used DOM fractions isolated by adsorption onto resins. None of the above studies observed removal of more than ~35% of the initial light absorption during photochemical degradation. Chapter II and Chapter III focus on the  $^{13}\text{C}$  NMR characterization of unfractionated DOM samples in which up to 90% of absorption was removed by photobleaching.

*Advanced solid-state NMR* – Cross-polarization magic angle spinning (CP/MAS) solid-state NMR is perhaps the most commonly used NMR technique for characterizing DOM (Mopper et al. 2007). CP/MAS spectra obtained for complex mixtures such as DOM consist of broad and overlapping peaks, thus limiting the information that can be obtained to relatively broad overlapping categories of functional groups (Benner et al. 1992; Hedges et al. 1992). In contrast, advanced NMR techniques (Opella and Frey 1979;

Dixon 1982; Wu and Zilm 1993; Bennet et al. 1995; Mao et al. 2001; Mao and Schmidt-Rohr 2004) have been shown to yield detailed structural and compositional information for a wide variety of natural organic matter (NOM) samples (Keeler and Maciel 2000; Conte et al. 2004; Mao et al. 2007a; Helms et al. 2012). Mao et al. (2011) demonstrated a systematic approach for applying advanced solid-state NMR to the characterization of humic substances. Selected advanced techniques were used here with the aim of gaining new insights regarding which moieties within DOM are degraded, altered or preserved during photochemical degradation (Chapter II and III), as well as new information regarding the structural characteristics of DOM isolated by RO/ED (Chapter V).

*Dissolved organic matter isolation by RO/ED* – The differences in DOM (<0.1  $\mu\text{m}$ ) composition found in different regions of the ocean are widely studied but not well understood. Generally, microbial (i.e. algal and bacterial) DOM is less aromatic and of lower molecular weight than terrigenous DOM, while DOM that has aged in the deep ocean or that has undergone photochemical degradation is, at this time, poorly characterized (Mopper et al. 2007; Sulzberger and Durisch-Kaiser 2009). The lack of chemical characterization is mainly due to the low concentration of oceanic DOM (~1 g of DOC per 900-2000 kg of seawater) and the overwhelmingly high concentrations of inorganic salts (~1 g DOC per 35 kg of salt), the former requiring sensitive detection or pre-concentration, and the latter requiring separation of the DOM from its saline medium in order to provide reliable chemical analyses. Previously used methods of concentrating and desalting DOM selectively recover or systematically fractionate the DOM resulting in incomplete or biased characterization of the DOM pool (Mopper et al. 2007).

A system was recently developed that combines DOM concentration by reverse osmosis and de-salting by electrodialysis (Koprivnjak et al. 2006; Vetter et al. 2007; Gurtler et al. 2008; Koprivnjak et al. 2009). The RO/ED system was previously validated using coastal and Gulf Stream seawater samples (Koprivnjak et al. 2009). This evaluation showed that an average DOC concentration factor of 20x, and >95% salt removal was accomplished with an average isolate DOC recovery of 70% and a maximum DOC recovery of ~94%. One aim of the research described below was to obtain new information on the bulk chemical and molecular level characteristics of the resultant RO/ED isolated from 5 water masses with contrasting biogeochemical histories and, consequently, different chemical compositions.

Photobleaching of open ocean DOM has not been examined in great detail (Opsahl and Benner 1998; Ortega-Retuerta et al. 2010), though much has been inferred by comparison with terrestrial DOM photobleaching and differences in optical properties that have been observed in the ocean (Skoog et al. 1996; Stedmon et al. 2000; Kitidis et al. 2006). The scarcity of direct measurements of open ocean CDOM photobleaching is due to the low concentrations of DOM in the open ocean (and the lack of non-fractionating isolation protocols discussed above), the relatively low absorptivity of marine DOM (Nelson and Siegel 2002), the small magnitude of absorbance and fluorescence changes that occur over short irradiation experiments (Stubbins et al. 2006), and potential organic and trace-metal contamination during sample handling (Fitzwater et al. 1982; Faust and Zepp 1993; Sulzberger and Laubscher 1995). Using RO/ED isolated seawater DOM alleviates difficulties associated with the low in situ concentration of open ocean DOM. As with terrestrial DOM photolysis, using a long-term irradiation time



series provides a more realistic understanding of the chemical and optical property changes to marine DOM caused by photochemical degradation over environmentally relevant time scales (Nelson et al. 2007; Swan et al. 2009). Chapter IV describes the first reported optical measurements during photochemical degradation of RO/ED isolated DOM and relates these results to oceanic C-cycling.

*Dissolved organic matter and the ocean carbon cycle* – Ocean DOM constitutes one of the largest pools of reduced carbon on the planet, yet little is known about its composition or the processes which affect its composition, concentration, and distribution within the ocean. Hansel and Carlson (2001) have proposed a conceptual model to describe the biogeochemistry of DOC based on the time-scale over which different components of the DOC pool are recycled biologically. They assign fresh autochthonous DOC, which is respired within minutes to days of being released by primary producers, to the “labile” pool (Fuhrman and Ferguson 1986; Carlson 2002). DOC that cycles on intermediate time scales of weeks to years is assigned to the “semi-labile” pool (Ogura 1972; Carlson 2002). DOC from the deep North Pacific, which is found at low concentrations and with dissolved organic radiocarbon ages of >6000 y is assigned to the “refractory” pool (Williams and Druffel 1987; Carlson 2002).

The vertical distribution of DOC throughout most of the open ocean suggests that the refractory DOM exists as a ubiquitous, amorphous, and poorly characterized background, while semi-labile and labile carbon are detectable above this background (Fig. 1) and more readily identifiable as biomolecules (Hansell and Carlson 2001; Carlson 2002; Hansell et al. 2009). The three-pool DOC model, based on biological

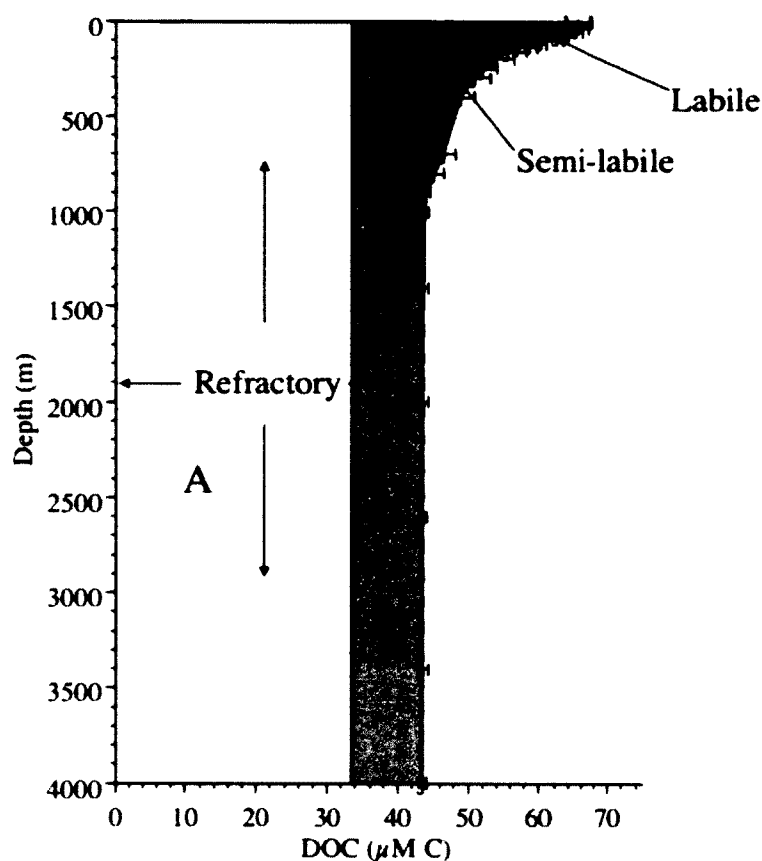


Fig. 1. The vertical distribution of DOC, at the Bermuda Atlantic Time Series (BATS) site in the Northwestern Sargasso Sea, highlights the applicability of the “three-pool DOC” model. Labile DOC does not survive in the ocean long enough to be exported to depth, while semi-labile DOC cycles on timescales of months to years and is mixed to intermediate depths, and refractory components of DOC cycle on (A) millennial and (B) century time scales. Reproduced with permission from Carlson (2002), © Academic Press/Elsevier Publishing, see Appendix.

lability, provides a useful framework upon which to base our understanding of how oceanic DOM cycles and why its composition varies between regions of the ocean (Jiao et al. 2010). This concept, along with the DOM isolation technique of RO/ED and the advanced NMR techniques described above, form the central themes of Chapter V. In contrast to this biologically-based three-pool model, Stubbins et al. (2010) proposed a three-pool photochemically-based DOM model, which is addressed in Chapters III - V.

## THESIS ORGANIZATION AND CHAPTER SYNOPSES

The overarching goal of this research is to improve the understanding of biogeochemical cycling of DOM. This dissertation presents results from four research projects, each of which focuses on a different aspect of DOM characterization or reactivity. Chapter II explores the poorly understood photochemical reactions that lead to flocculation of terrestrial DOM. Chapter III tracks the optical and chemical changes that occur during long-term (up to 110 days) UV-A irradiation of terrestrial DOM (Dismal Swamp, VA, USA) using advanced spectroscopic and standard analytical techniques. Chapter IV combines the use of RO/ED isolated DOM and optical characterization techniques to explore the photochemically-induced changes in DOM that occur when deep ocean water (670m Pacific Ocean collected from the Natural Energy Laboratory of Hawaii) is up-welled or mixed into the euphotic zone. Chapter V demonstrates the use of solid-state  $^{13}\text{C}$  NMR techniques to characterize oceanic DOM isolated using RO/ED.

Several themes are discussed throughout the dissertation. Chapters II, III, and IV are focused on the photochemical reactions that alter the molecular structure and composition of DOM and remove it from surface waters. Chapter II and III investigate

whether the fraction of terrestrial DOM that survives photochemical alteration can be distinguished from open ocean DOM. Chapter IV and V investigate the optical properties and NMR signatures, respectively, of DOM that support the three-pool models of ocean DOM cycling and the build-up of photochemically-refractory material in the subtropical gyres. Both studies reveal new insights into the bulk chemical composition of DOM in the world's oceans and the processes that lead to structural differentiation.

## **CHAPTER II**

### **PHOTOCHEMICAL FLOCCULATION OF TERRESTRIAL DISSOLVED ORGANIC MATTER AND IRON**

#### **INTRODUCTION**

The highly colored waters of the Dismal Swamp contain in excess of 50 mg L<sup>-1</sup> dissolved organic carbon (DOC), which includes significant levels of humic and fulvic acids, polyphenolic material derived from lignin and tannin (Sleighter and Hatcher 2008). The low availability of light for aquatic primary productivity, the low pH of the water, and the dominant contribution of woody tissue and leaf litter in this nearly pristine watershed result in an almost pure terrestrial DOC (Minor et al. 2006; Fimmen et al. 2007; Sleighter and Hatcher 2008). Terrestrial dissolved organic matter (tDOM) appears to be efficiently removed in ocean margin environments including coastal zones, estuaries, and buoyant river plumes; yet the physical, chemical, and biological processes that lead to this removal remain poorly understood (Hedges et al. 1997; Del Vecchio and Blough 2002; Nelson and Siegel 2002; Del Vecchio and Subramaniam 2004; Spencer et al. 2009).

It has been proposed that significant amounts of riverine DOM are delivered to estuarine, continental shelf, and continental slope sediments by various processes: including precipitation, co-precipitation, aggregation, coagulation, micelle formation, hydrophobic interactions, adsorption to or encapsulation of pre-existing particles (Stumm and Morgan 1981; Guo et al. 2007). Here, all physico-chemical processes that convert dissolved material to particulate material are referred to as flocculation. Prior studies investigating the role of abiotic flocculation in estuarine biogeochemistry have focused

on the influences of salt, mixing, particle interactions, and pH on the solubility, stability, or removal of dissolved and colloidal riverine organic matter (Sholkovitz 1976; Turner and Rawling 2001; Turner 2003), humic substances (Eckert and Sholkovitz 1976; Sholkovitz et al. 1978; Fox 1983), carbohydrates (Wang et al. 2010), metals (O'Melia and Stumm 1967; Eckert and Sholkovitz 1976; Boyle et al. 1977; Sholkovitz 1978), phosphorus (Forsgren et al. 1996), clay minerals (Black et al. 1965; O'Melia and Stumm 1967), and algal biomass (Sukenik et al. 1988). In spite of the large number of previous studies, the factors resulting in flocculation remain poorly understood.

Sondergaard et al., (2003) showed that mixing-induced flocculation caused only a 2-5% decrease in DOC along a salinity gradient of 0-25 (Sondergaard et al. 2003). In another study based on end-member mixing experiments and estuarine transects, mixing induced flocculation was insufficient to account for the apparent removal (i.e., non-conservative behavior) of humic acids in the transects (Fox 1983). Guo et al. (2007) showed that salt effects alone were not sufficient to significantly alter the chromophoric DOM (CDOM) composition of a river water sample. Flocculation therefore must be accompanied by additional factors, such as adsorption to mineral surfaces, interactions with pre-existing particles, or other uncharacterized processes.

In addition to salt effects and mixing-induced flocculation, surface-active materials that collect on air bubbles may form particles from DOM upon bubble dissolution (Johnson 1976; Johnson and Cooke 1980) or bursting (Baylor and Sutcliffe 1963; Sutcliffe et al. 1963). Surface-active compounds, including polysaccharides, mucopolysaccharides and glycoproteins, may also play a significant role in the formation of organic-enriched surface micro-layers (Henrichs and Williams 1985; Compiano et al.

1993; Wurl et al. 2009), marine snow (Alldredge and Silver 1988; Mopper et al. 1995; Zhou et al. 1998), or mineral/organic aggregates (Kranck and Milligan 1980).

Photochemical mineralization of DOM (conversion to inorganic forms) and the decrease in ultraviolet and visible absorption, i.e., photobleaching, have been widely studied (Zepp and Schlotzhauer 1981; Zafiriou et al. 1984; Miller 1994; Benner and Biddanda 1998; Del Vecchio and Blough 2002). Photochemical mineralization is a possible removal mechanism for humic acids and colored DOM in estuaries (Del Castillo et al. 1999; Stedmon and Markager 2005; Huguet et al. 2009; White et al. 2010).

However, reports of a link between photochemical alteration of DOM and the flocculation of DOM have received relatively little attention. Thus, little is known about the relationship between these two processes and how photo-induced flocculation may impact processes such as transport and removal of dissolved and particulate materials (Hernes and Benner 2002) and pollutants, biological utilization of organic matter (Miller and Moran 1997) and the organic content of coastal sediments (Cowie and Hedges 1992).

Gao and Zepp (1998) observed that after three days of simulated sunlight exposure, dark-colored particles formed in a 0.22  $\mu\text{m}$ -filtered and oxygen-saturated Satilla River water sample. They reported that particulate matter accounted for 45% of the iron and about 13% of the organic carbon and speculated that the causes of photochemically induced aggregation are changes to double layer repulsion and van der Waals interactions from decarboxylation and to loss of DOM's ability to complex iron leading to formation of polymeric iron oxides. Von Wachenfeldt et al. (2008) found that light exposure correlated with increases in particulate organic carbon (POC) at the expense of DOC for 5 micron filtered humic lake and mire water samples. Thorn et al.

(2010) found that humic and fulvic isolates became decarboxylated, more hydrophobic, much less aromatic, and less soluble after extensive photodegradation. Xie et al. (2004) provided evidence of photochemical decarboxylation of DOM based on changes in carboxylate acidity and production of CO<sub>2</sub>.

Photochemical flocculation of iron and aluminum has also been observed in lakes (Kopáček et al. 2005; Kopáček et al. 2006). The mechanism proposed by Kopáček et al. (2005) proceeds by the iron mediated degradation of organic iron-binding ligands causing release of inorganic iron which is susceptible to oxidation and/or hydrolysis to form insoluble (hydr)oxides. Based on the finding that dissolved iron in terrestrially dominated waters (and in the open ocean) is dominantly organically complexed (Powell and Wilson-Finelli 2003; Laglara and van den Berg 2009) and the fact that the concentration of carboxyl groups affects the solubility of DOM (VanLoon and Duffy 2010) and DOM's ability to form stable complexes with iron (Barbeau 2006), it is anticipated that photochemical decarboxylation of DOM affects solubility of both DOM and iron. Additionally, dissolved O<sub>2</sub> and photochemically produced reactive oxygen species oxidize iron (II) to iron (III), leading to the formation of insoluble iron hydroxides (Faust and Zepp 1993; Kuma et al. 1996).

The residence time of tDOM within the euphotic zone of the oceans is poorly constrained. The fact that most of the world's major rivers form large buoyant plumes often becoming entrained in highly stratified surface waters between 30° S and 30° N latitudes (Moore et al. 1986; Dagg et al. 2004), highlights the importance of photochemical processes as tDOM-containing water masses will receive considerable



light exposure upon export to the ocean margins, thus resulting in its photodegradation and possible photo-flocculation.

The present study examines the photochemical changes to DOM composition that result in abiotic flocculation of organic matter in the absence of salt effects, biological interactions, or interactions with pre-existing particles. Conventional and advanced spectroscopic methods were used to characterize both the POM that forms upon light exposure and the DOM that remains in solution in order to gain insights into the flocculation mechanism(s). This study raises new questions regarding both the mechanisms and magnitude with which photochemistry and flocculation affect the export of terrestrial DOM and POM to the oceans and sediments.

## MATERIALS AND METHODS

Glassware was cleaned with dilute HCl ( $\sim 1 \text{ mol L}^{-1}$ ) and rinsed with MilliQ –UV ultrapure grade water (Millipore), referred to below as MilliQ water. Glassware was combusted at  $450^\circ\text{C}$  overnight ( $>8 \text{ h}$ ). Plasticware was cleaned with  $0.01 \text{ M NaOH}$  followed by MilliQ water and dilute HCl and then rinsed with MilliQ water. All containers were rinsed several times with sample prior to filling. Filter capsules ( $0.1 \mu\text{m}$  pore size, Whatman PolyCap TF) were rinsed with HPLC grade methanol (Alpha Aesar), flushed with  $> 20 \text{ L}$  of MilliQ water, and conditioned with approximately  $1 \text{ L}$  of sample prior to use.

The water sample used for this irradiation experiment was collected at  $76^\circ 22' \text{ W}$ ,  $36^\circ 36' \text{ N}$  from the public boat ramp near the confluence of the Dismal Swamp northwest canal and the Lake Drummond feeder ditch. The water was transported back to the

laboratory in a 20 L Teflon-coated polyethylene jerrycan. The sample was filtered (within 24 hours of collection) through a pre-cleaned 0.1  $\mu\text{m}$  capsule filter into precleaned and combusted 4 L glass Qorpak bottles with acid rinsed Teflon lined caps. Samples were stored (<48 h) at room temperature prior to irradiation. Subsamples were stored at 4-5° C prior to analysis; however, samples were stored at room temperature overnight prior to optical spectroscopic measurements to minimize temperature related artifacts.

Aliquots (450 mL) of the filtered sample were transferred to nine 550 mL quartz round bottom flasks and placed inside a solar simulator containing UVA340 bulbs (Q-panel). These lamps have a spectral output similar to natural sunlight from ~290 to ~365 nm, but under-represent solar irradiance at wavelengths greater than about 365 nm. UVA lamps were chosen because this region of the solar spectrum is quantitatively the most important in the mineralization of dissolved organic carbon (Vähätalo et al. 2000). The light output from the solar simulator was monitored during the course of the irradiation experiment using an IL 1700 radiometer (International Light). The solar simulator is described elsewhere (Minor et al. 2007; Helms et al. 2008; Dalzell et al. 2009). The lamps were kept on constantly during the irradiation. Sub-samples were collected and analyzed at exposure intervals of 0, 10, 20, and 30 days. Dark controls were wrapped in foil and placed inside the solar simulator alongside the irradiated samples. All samples were irradiated at their natural concentration and pH (i.e., not diluted to optically thin conditions or buffered prior to irradiation) in order to collect sufficient organic material for solid-state NMR and FT-IR and to approximately simulate surface conditions in humic lakes during seasonal stratification. The use of added buffers was avoided to minimize potential contamination and artifactual photochemical and dark reactions (e.g.,

iron-phosphate complexation/precipitation) while maximizing the carbon percentage of freeze-dried samples.

At the end of each irradiation time point, a 30 mL aliquot was set aside for measuring pH. pH was measured at room temperature ( $22^{\circ}\text{C} \pm 2^{\circ}$ ) using a calibrated Orion ROSS gel filled pH electrode connected to a Fisher Scientific Accumet pH meter 25.

During the course of the irradiation, particles formed in all samples except for the dark controls. The particles were separated from the remaining supernatant by centrifugation at 6000 rpm ( $\sim 9000\text{ g}$ ) for 15 minutes. For comparison, 15  $\mu\text{L}$  of 50% w/w NaOH (VWR Scientific) was added to 450 mL of un-centrifuged samples in order to re-dissolve the flocculated and adsorbed DOM. In addition, a sub-sample with particles re-suspended was collected. After emptying the irradiation and control flasks, they were rinsed with MilliQ water to remove remaining solution. One flask was then rinsed with 10 mL of 0.5 mM NaOH solution to dissolve adsorbed organic material, while a second flask was rinsed with 0.1 M HCl solution to leach adsorbed iron. A second 10-day irradiation was performed in order to collect sufficient particulate and dissolved material to perform solid-state NMR and FTIR measurements. The samples from that second 10-day irradiation were centrifuged, as above. The particles were rinsed once with cold ( $\sim 4^{\circ}\text{C}$ ) MilliQ water to remove loosely bound DOM. Both dissolved and particulate phases were then freeze-dried.

UV-visible absorption spectra (190-900 nm) were measured for all samples and rinsate solutions using an Agilent 8453 diode array spectrophotometer with a 1 cm quartz cuvette. MilliQ water was used as the blank. Strongly absorbing samples were diluted

with MilliQ water prior to measurement to ensure linear response. Absorbance values were corrected to account for instrument baseline drift, refractive index, and temperature variations according to Green and Blough (1994) and converted to Napierian absorbance coefficients using:

$$(1) \quad a = 2.303A/l$$

where  $a$  = absorbance coefficient ( $\text{m}^{-1}$ ),  $A$  = absorbance, and  $l$  = path length (m). All CDOM UV-visible spectra were assumed to follow an exponential decay approximated by the expression:

$$(2) \quad a_{\lambda} = a_{\lambda_{ref}} e^{-S(\lambda - \lambda_{ref})}$$

where  $\lambda$  = wavelength (nm),  $\lambda_{ref}$  = reference wavelength, and  $S$  = spectral slope. Spectral slopes were calculated by linear regression of the natural log transformed absorption spectra, and spectral slope ratio ( $S_R$ ) was calculated as the ratio of  $S_{275-295}$  to  $S_{350-400}$  (Helms et al. 2008). All samples (dissolved, i.e., supernatant centrifuged, samples; re-dissolved samples; blanks; and dark controls) were analyzed at similar NaOH concentrations (0.5-0.6 mM; pH=10.7  $\pm$  0.2) to avoid pH and refractive index differences between samples and allow direct comparison.

First-derivative UV-visible absorption spectra were obtained by fitting absorption data to linear segments over 11 nm intervals and plotting slope vs. wavelength. The process was repeated using first-derivative data points in order to produce second-derivative spectra.

Non-purgeable organic carbon (NPOC) was measured using high temperature (720°C) catalytic combustion on a Shimadzu TOC-V-CPH carbon analyzer. Samples were acidified with  $\text{H}_3\text{PO}_4$  and sparged with carbon-free air prior to injection. The

instrument was calibrated using dried primary standard grade potassium hydrogen phthalate (Alpha Aesar) dissolved in MilliQ water. Measurements of NPOC for dissolved samples (i.e., centrifuged supernatant) will be referred to as DOC, while NPOC measurements of non-fractionated samples will be referred to as total organic carbon (TOC). POC was determined as the difference between TOC and DOC. Total Nitrogen (TN) was also measured using the Shimadzu TOC-V-CPH. Calibration standards were prepared from  $\text{KNO}_3$  in MilliQ water.

Total iron concentration was measured using a Hitachi Z8100 polarized Zeeman flame atomic absorption spectrophotometer equipped with an iron hollow cathode lamp (VWR Scientific). Iron standards were prepared from puris p.a., ACS grade, iron (II) sulfate heptahydrate (Fluka) in 0.01M HCl and ranged in concentration from 0 to 100  $\mu\text{M}$ . Standards were measured in duplicate and samples were measured in triplicate. Samples were adjusted to pH 1 using ACS grade concentrated hydrochloric acid (Fisher Scientific). Particulate iron concentrations were determined by comparing the iron concentrations of non-fractionated and dissolved samples.

DOM and POM samples from the 10-day irradiation were analyzed by solid-state  $^{13}\text{C}$  cross polarization/total sideband suppression (CP-TOSS) NMR at 100 MHz with a Bruker Biospin DSX-400 spectrometer. Experiments were performed using 4-mm rotors at a spinning speed of 6.5 kHz and a cross polarization (CP) time of 1 ms, with a  $^1\text{H}$   $90^\circ$  pulse-length of 4.1  $\mu\text{s}$  and a recycle delay of 0.4 s. Four-pulse TOSS (Dixon 1982) was applied prior to detection, and two-pulse phase-modulated (TPPM) decoupling was used for optimum resolution (DeAzevedo et al. 2000). Between 16k and 64k scans were accumulated for each spectrum.

In addition to CP-TOSS experiments, spectra showing signals from nonprotonated carbons and mobile groups, like rotating CH<sub>3</sub>, were generated using <sup>13</sup>C CP-TOSS with 40 μs dipolar dephasing (Opella and Frey 1979; Hatcher 1987; Mao et al. 2007b). Between 32k and 64k scans were averaged for each spectrum with dipolar dephasing. To differentiate the signals of anomeric carbons (O-C-O) from those of aromatic carbons that resonate between 90 and 120 ppm, the aromatic carbon signals were selectively suppressed with a five-pulse <sup>13</sup>C chemical-shift anisotropy (CSA) filter (Mao 2004). Between 32k and 64k scans were performed for each CSA-filtered spectrum.

The analytical uncertainty of the NMR spectra due to instrumental and environmental noise was estimated by using the signal to noise ratio of each integration region to calculate relative standard deviation. Additional uncertainty arose from the assignment of chemical shift ranges used for integration. This was partly alleviated through the consistent application of integration ranges to maintain comparability of the samples and by the use of dipolar dephased or CSA-filtered spectra to differentiate overlapping signals.

FTIR spectra were obtained by collecting 200 scans using a Nicolet 370 FTIR spectrometer (DTGS detector) equipped with purge gas generator (Thermo Scientific). Samples were freeze-dried and introduced as KBr disks. The KBr was combusted (24 h, 450 °C) prior to use. The sample and KBr mixtures (1:100 ratio) were homogenized in a glass vial on a grinding mill (Wig-L-Bug) and compressed between two clean, polished iron anvils in a hydraulic press at 20,000 psi to form KBr windows. To minimize wedging effects (Hirschfeld 1979), the disks were pressed for a second time after 90° rotation of the anvils within the press. To avoid CO<sub>2</sub> contamination from lab air, the

sample chamber was purged with dry nitrogen for 4 minutes before beginning the analysis (Abdulla et al. 2010). Spectra were collected with a resolution of  $4\text{ cm}^{-1} \pm 1$  and Happ-Genzel apodization. Background scans consisted of a KBr disk prepared as above, except that no sample was added. Second-derivative spectra were obtained using the second order Savitzky-Golay method as described in Abdulla et al. (2010). The 1900-1500  $\text{cm}^{-1}$  (carboxyl) region of the spectrum was deconvoluted using Voigt line-shape fitting (Griffiths and De Haseth 2007; Abdulla et al. 2010) to facilitate the quantification of different carboxylic functional groups: carboxylic esters, carboxylic amides, carboxylic acids, acetate, and metal associated carboxylate groups. Details of the identification and calibration of the deconvoluted peaks are given in Abdulla et al. (2010).

## RESULTS

*pH shift during irradiation* – As no buffers were added to the water samples prior to or during the irradiation, the pH shifted over the course of the 30 day experiment from ~3.7 to ~5.7 (Fig. 2). While the exclusion of added buffers was necessary to obtain sufficient carbon for solid-state NMR and to avoid artifactual reactions, the gradual increase in pH complicates the interpretation of the iron flocculation mechanism (see Discussion).

*Changes to organic matter during irradiation* – A summary of the parameters measured for each of the samples is given in Table 1. Comparison of these parameters shows that, throughout the course of the irradiation, photo-mineralization and photobleaching caused reductions in both organic matter concentration and absorption at

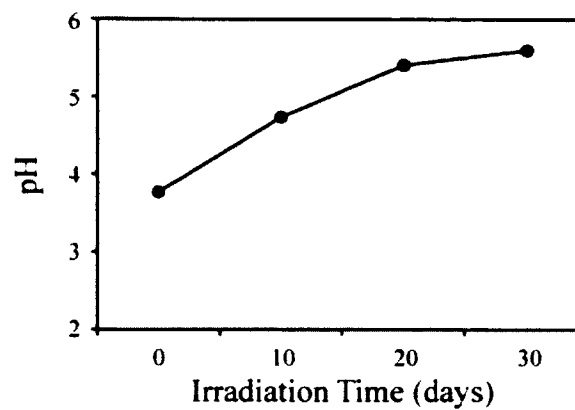


Fig. 2. pH values of water samples measured at the end of each irradiation time point.



300 nm ( $a_{300}$ ). Approximately 22 mg L<sup>-1</sup> or 41% of the original 52.7 mg L<sup>-1</sup> DOC was mineralized during the first 10 days of the irradiation experiment and an additional 4.7 mg L<sup>-1</sup> or 9% of initial DOC was converted to POC. The organic carbon remaining after 10 days was ~15% particulate (Table 1). After 30 days, 95% of the original  $a_{300}$  and 88% of the original DOC were removed (Table 1). Adsorption to the walls of the quartz flasks was responsible for 2.1% of  $a_{300}$  removal and about 6.5% of DOC removal. Flocculation was responsible for 8.3% of  $a_{300}$  removal and 8.0% of DOC removal. After 30 days irradiation, 38% of the remaining TOC was in the particulate phase, and the particulate phase accounted for ~60% of the remaining absorption at 300 nm (Figs. 3 and 4). POC was lower in the 30 day irradiated sample than in the 20-day irradiated sample suggesting that the flocculated particles are susceptible to photobleaching, photomineralization, or photo-dissolution.

While up to 15% of the total remaining  $a_{300}$  adsorbed to the walls of the irradiated quartz flasks (Table 1; Fig. 5B), very little wall adsorption (~0.10% of  $a_{300}$ ) occurred in the dark control. Wall-adsorbed material also exhibited relatively low spectral slope ratios ( $S_R$ ) (Table 1). The spectral slope ratio for the isolated and re-dissolved particles was 0.72 (Table 1) compared to  $S_R$  values of 0.91 ( $\pm 0.01$ ) for the dark control samples, and 1.14 for the dissolved material from the 10 day irradiated sample. In fact, all samples containing re-dissolved POM exhibited lower  $S_R$  values than their particle free counterparts.

UV-visible spectra for unfractionated samples are shown in Fig. 3A along with first and second-derivative absorption spectra (Figs. 3B and 3C). While the absorption spectra all appear relatively featureless, the derivative spectra show that changes in

Table 1. Summary of parameters measured for each sample. Total=whole, unfractionated samples; Diss=dissolved, particle free samples; Ads=adsorbed material; PM=particulate values determined by difference except where denoted with \*. N/D=not determined.

Sample	Irr. Time (days)	TOC (mg L <sup>-1</sup> )	TN (mg L <sup>-1</sup> )	Iron (μmol L <sup>-1</sup> )	$a_{300}$ (m <sup>-1</sup> )	$S_{275:295}$ (nm <sup>-1</sup> )	$S_R$	SUVA <sub>254</sub> (L m <sup>-1</sup> mg <sup>-1</sup> )
0d-Total	0	52.7	1.890	34.8	369.4	0.0151	0.907	11.8
10d-Total	10	31.0	1.692	34.2	211.5	0.0108	1.116	10.8
20d-Total	20	22.0	1.658	34.6	118.9	0.0097	1.133	8.3
30d-Total	30	10.5	1.370	34.2	48.7	0.0094	0.995	6.7
10d-Diss	10	26.3	1.406	34.1	189.1	0.0114	1.149	11.7
20d-Diss	20	15.6	1.309	26.8	102.9	0.0103	1.167	10.5
30d-Diss	30	6.5	1.018	4.5	19.4	0.0182	1.721	5.9
0d-Ads	0	0.3	N/D	0.02	0.4	0.0135	1.145	2.4
10d-Ads	10	2.3	N/D	0.07	5.4	0.0092	0.737	2.8
20d-Ads	20	1.7	N/D	0.36	1.3	0.0115	0.929	1.0
30d-Ads	30	2.5	N/D	0.29	7.4	0.0136	0.772	4.3
10d-PM	10	4.7	0.286	~0	22.4	0.0086*	0.723*	4.8
20d-PM	10	6.4	0.349	7.8	16.0	N/D	N/D	N/D
30d-PM	10	4.0	0.352	29.7	29.3	N/D	N/D	N/D

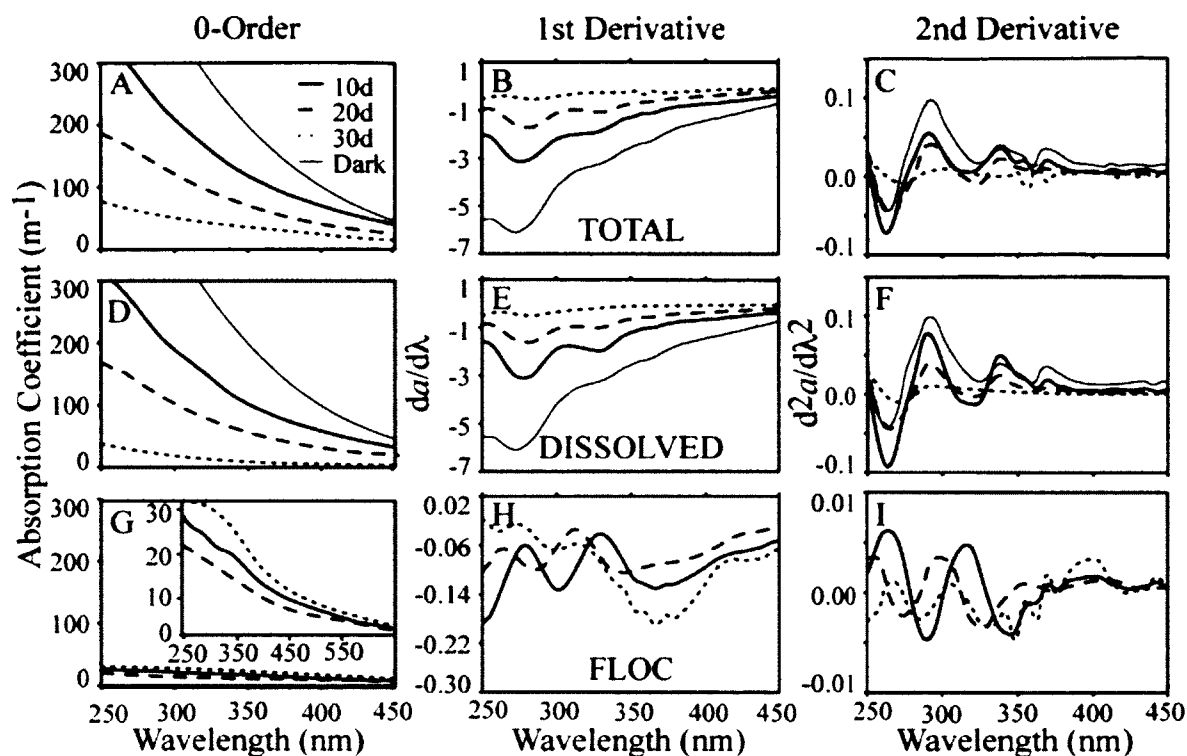


Fig. 3. UV-visible absorption spectra (left), first-derivative absorption spectra (center), and second-derivative absorption spectra (right), were obtained for (A, B, and C) total, unfractionated, samples in which flocculated POM was re-dissolved at high pH, (D, E, and F) dissolved samples from which POM was removed, and (G, H, and I) POM obtained by difference.

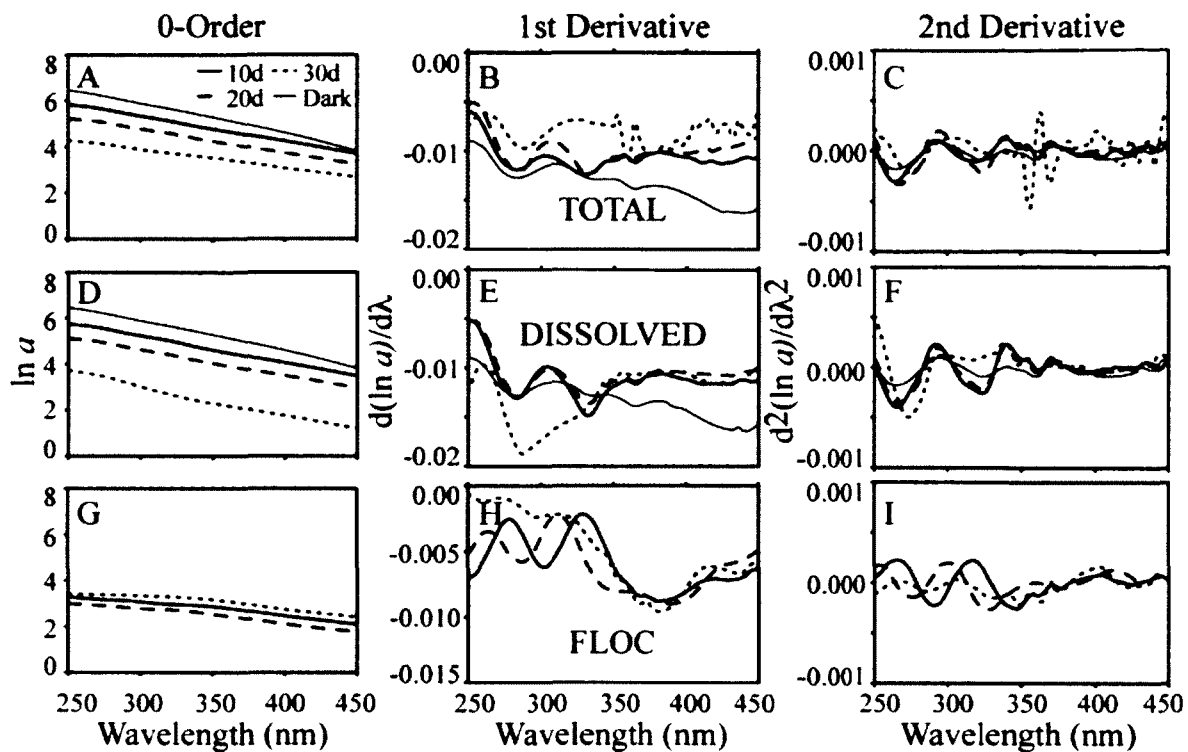


Fig. 4. Natural log UV-visible absorption spectra (left), first-derivative natural log absorption spectra (center), and second-derivative natural log absorption spectra (right), were obtained for (A, B, and C) total samples in which flocculated POM was re-dissolved at high pH, (D, E, and F) dissolved samples from which POM was removed, and (G, H, and I) POM obtained by difference.

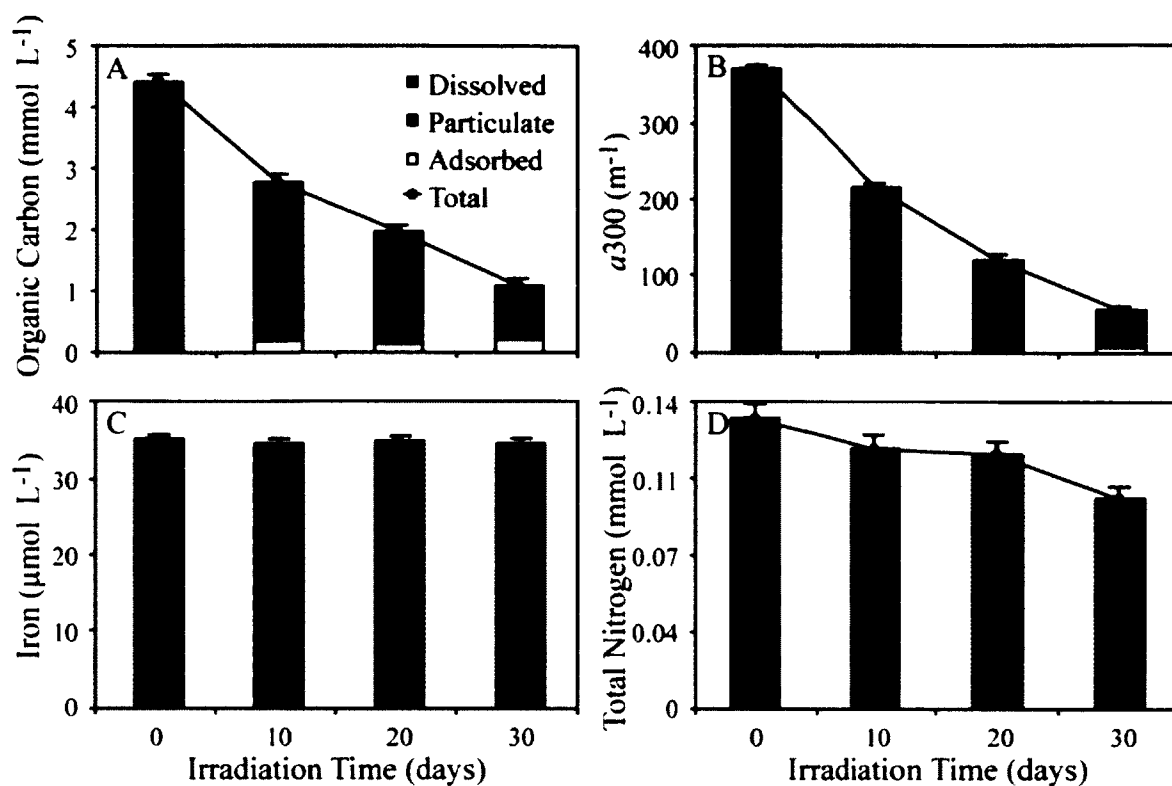


Fig. 5. Concentrations of dissolved (gray), particulate (black), and adsorbed (white) material quantified as: (A) organic carbon, (B) absorption at 300 nm, (C) iron by atomic absorption, and (D) total nitrogen. Error bars represent the combined standard deviations of the “total,” “dissolved,” and “adsorbed” terms from which the “particulate” term was calculated. Total nitrogen was not determined for the “adsorbed” material.

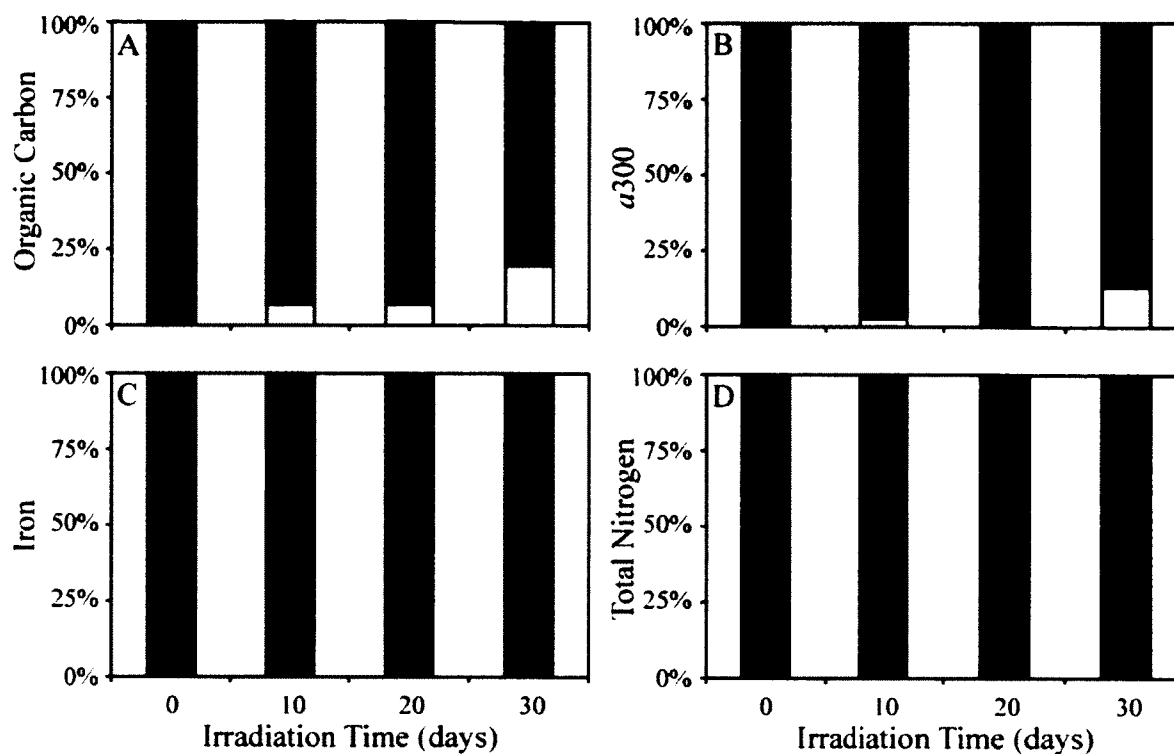


Fig. 6. Percentage distribution of dissolved (gray), particulate (black), and adsorbed (white) material quantified as: (A) organic carbon, (B) absorption at 300 nm, (C) iron by atomic absorption, and (D) total nitrogen.

spectral shape occurred over the course of photobleaching. Absorption and derivative spectra for the dissolved samples are shown in Figs. 3D, 3E, and 3F, and the difference spectra representing the particulate material are shown in Figs. 3G, 3H, and 3I. Natural log spectra (Figs. 4A, 4D, and 4G), first-derivative natural log spectra (Figs. 4B, 4E, and 4H) and second-derivative natural log spectra (Figs. 4C, 4F, and 4I) are also shown. Dissolved and particulate materials exhibit significantly different derivative spectra. Second-derivative spectra of dissolved material show minima between 262 and 271 nm and maxima around 290 nm, while particulate spectra show minima between 273 and 290 nm and maxima between 296 and 315 nm, which shifted during the irradiation. Redissolution of isolated particles from the 10 d sample and dilution with MilliQ water (data not shown) confirm the low spectral slopes exhibited in the difference spectra (Figs. 3 and 4), however, the features observed at ~280 nm and ~340 nm in the difference spectrum were less pronounced (Figs. 3G and 4G).

DOC normalized absorption or “specific UV absorbance” at 254 nm (SUVA<sub>254</sub>), which has been shown to correlate well with aromatic content (Weishaar et al. 2003) and carbon normalized lignin yield (Stubbins et al. 2012), is shown in Table 1. SUVA<sub>254</sub> values decreased throughout the irradiation indicating photochemical degradation of aromatic material, in agreement with the NMR results (discussed below). The SUVA<sub>254</sub> values were generally higher in supernatants than in the unfractionated samples.

Total nitrogen in both the dissolved and unfractionated samples decreased during irradiation (Table 1), while particulate nitrogen increased (Table 1; Fig. 5D). The distribution of dissolved and particulate nitrogen is shown in Figs. 5D and 6D. Total nitrogen includes both organic and inorganic forms of nitrogen. Because inorganic forms

(e.g.,  $\text{NH}_4^+$ ,  $\text{NO}_3^-$ ,  $\text{NO}_2^-$ ) are highly soluble, particulate nitrogen, determined by subtracting TN values of dissolved samples from TN values of unfractionated samples, must dominantly exist as organic nitrogen. The carbon to nitrogen ratio (C:N) of the DOM decreased linearly from 28 to 6.3 during the irradiation. Particulate C:N was 17 after 10 d, 18 after 20 d and 11 after 30 d. The decrease in particulate C:N ratio after 30 days reflects photobleaching of the flocculated material (i.e., preferential loss of carbon; Figs. 5 and 6).

*Flocculation of iron during irradiation* – No detectable flocculation of iron occurred during the first 10 days of irradiation. However, between 10 and 20 days, iron began to flocculate (Figs. 5C and 6C, Table 1) and after 30 days, 87% of the iron originally present was converted to particulate iron. No measurable particle formation occurred in the dark control, and adsorption of iron to the flask wall was negligible (<0.1%).

*Spectroscopic characterization of photodegraded DOM and photochemically flocculated POM* – Solid-state CP-TOSS NMR spectra for the dark control, 10 day irradiated whole sample, supernatant, and particles are shown in Fig. 7. Photodegradation led to a preferential decrease in the aromatic signal (90-160 ppm), in agreement with the SUVA data (Table 1), a broadening of the carboxyl peak (160-190 ppm) and selective preservation of both O-alkyl (carbohydrate-like) material (60-90 ppm) and aliphatic carbon (0-50 ppm). It is noteworthy that the spectrum of the irradiated organic matter remaining in the dissolved phase upon 10 days of irradiation (Fig. 7C) exhibits



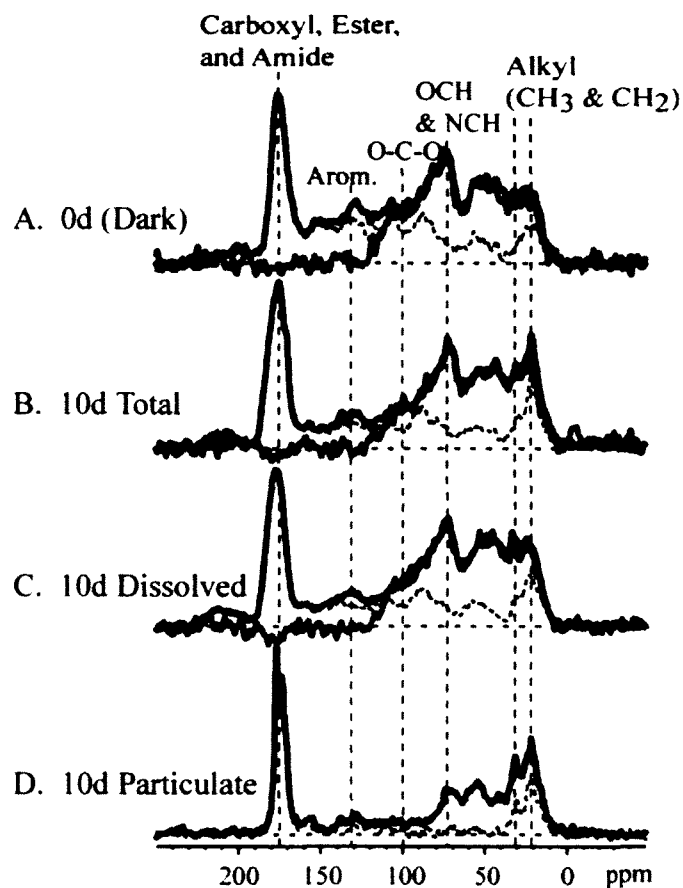


Fig. 7. Solid-state  $^{13}\text{C}$  CP-TOSS NMR spectra (solid black line) obtained for (A) the dark control sample, (B) the un-fractionated 10 d irradiated sample, (C) dissolved material isolated from the 10 d irradiated sample by centrifugation, and (D) the particulate material isolated from the 10 d irradiated sample by centrifugation. Solid-state  $^{13}\text{C}$  CP-TOSS NMR spectra with CSA-filter (gray line) and dipolar dephasing (dashed line) are shown for comparison. CSA-filtered spectra show aliphatic material, while dipolar dephasing shows primarily non-protonated and highly mobile carbons.

Table 2. Functional group assignments and integrated area for each CP-TOSS spectral region. Integrals are given as percentage of total area (i.e. percentage of carbons in powder sample) for qualitative comparison of each sample. Uncertainty was determined using the signal to noise ratio of each integration region and is given as one standard deviation.

	Integration range (ppm)	Dark Control	10d Total	10d Particles	10d Dissolved
Mainly CH <sub>3</sub> (also CH <sub>2</sub> and CH)	0-28	8.4 ±0.2	12.7 ±0.3	19 ±0.4	10.5 ±0.2
Mainly CH <sub>2</sub> (also CH <sub>3</sub> and CH)	28-35	3.8 ±0.1	5.1 ±0.2	7.6 ±0.3	5.4 ±0.1
Mainly CH (also CH <sub>2</sub> )	35-50	9.3 ±0.2	10.6 ±0.3	9.0 ±0.3	11.3 ±0.2
NCH + OCH <sub>3</sub> + OCH <sub>2</sub>	50-65	9.0 ±0.2	9.5 ±0.2	11.3 ±0.5	9.9 ±0.1
Carbohydrate-like C	65-100	21.0 ±0.4	22.0 ±0.4	13.6 ±0.5	23.0 ±0.3
OCHO + arom. C-C-O	100-115	6.3 ±0.2	5.0 ±0.2	3.0 ±0.3	4.8 ±0.1
Aromatic C	115-145	12.1 ±0.3	7.8 ±0.2	6.2 ±0.3	7.9 ±0.1
Aromatic C-O	145-160	4.7 ±0.2	2.8 ±0.2	2.3 ±0.3	2.8 ±0.1
COO +NC=O	160-187	20.5 ±0.4	22 ±0.4	26 ±0.6	20 ±0.3
Aldehyde, ketone, and quinone	187-220	4.6 ±0.2	2.7 ±0.2	1.0 ±0.3	4.1 ±0.1

Table 3. CP-TOSS integration data from Table 2 normalized to TOC concentrations and reported in concentration of  $\mu\text{mol C L}^{-1}$  for quantitative comparison of the samples.

	Integration range (ppm)	Dark Control	10d Total	10d Particles	10d Dissolved
Mainly $\text{CH}_3$ (also $\text{CH}_2$ and $\text{CH}$ )	0-28	370	330	74	240
Mainly $\text{CH}_2$ (also $\text{CH}_3$ and $\text{CH}$ )	28-35	170	130	30	120
Mainly $\text{CH}$ (also $\text{CH}_2$ )	35-50	410	270	35	240
$\text{NCH} + \text{OCH}_3 + \text{OCH}_2$	50-65	400	250	43	220
Carbohydrate-like C	65-100	920	570	55	500
$\text{OCHO} + \text{arom. C-C-O}$	100-115	280	130	12	110
Aromatic C	115-145	530	200	24	170
Aromatic C-O	145-160	210	72	9	61
$\text{COO} + \text{NC=O}$	160-187	920	570	100	440
Aldehyde, ketone, and quinone	187-220	200	70	4	90

pronounced peaks at 35 ppm, 75 ppm, and 175 ppm that are also characteristic of DOM isolated from marine waters (Esteves et al. 2009; Koprivnjak et al. 2009). In comparison with the dissolved material, the flocculated POM from the 10-day irradiated sample (Fig. 2D) contained relatively little aromatic material (90-165 ppm; consistent with SUVA<sub>254</sub> results above). It should be noted that this spectrum exhibits two carboxyl peaks, one at ~178 ppm and the other at ~173 ppm. The CP-TOSS spectra were integrated to provide quantitative information, which is given in Table 2. By normalizing the integration data (Table 2) to the TOC concentrations (Table 1), the concentrations of the various carbon classes were estimated in terms of  $\mu\text{mol L}^{-1} \text{C}$ , and are given in Table 3.

The  $^{13}\text{C}$  NMR spectra with CSA-filter (Fig. 7 grey lines) show that ~85-88% of carbons detected in the 90-115 ppm region were anomeric, i.e., carbohydrate-like, carbons with 12-15% aromatic carbons. No CSA-filtered spectrum was collected for the particulate matter sample as the CP-TOSS spectrum contained very little signal in the region where anomeric and aromatic carbon signals overlap. CP-TOSS spectra with dipolar dephasing (Fig. 7 dashed lines) show that  $80\% \pm 4\%$  of aromatic carbons in the dark control,  $\sim 86\% \pm 3\%$  of aromatic carbons in the unfractionated 10 d irradiated sample,  $\sim 84\% \pm 3\%$  of the aromatic carbons in the 10 d irradiated DOM (supernatant), and  $\sim 78\% \pm 5\%$  of the aromatic carbons in the 10 d irradiated POM (flocculated particles) were non-protonated, i.e. substituted ring carbons or carbons in the interior of condensed polyaromatic structures.

Insufficient particulate material was available from the 20 and 30 d irradiation time points to carry out NMR analyses. However, FTIR spectra were collected for particulate material from all three irradiation time points and for the dissolved material

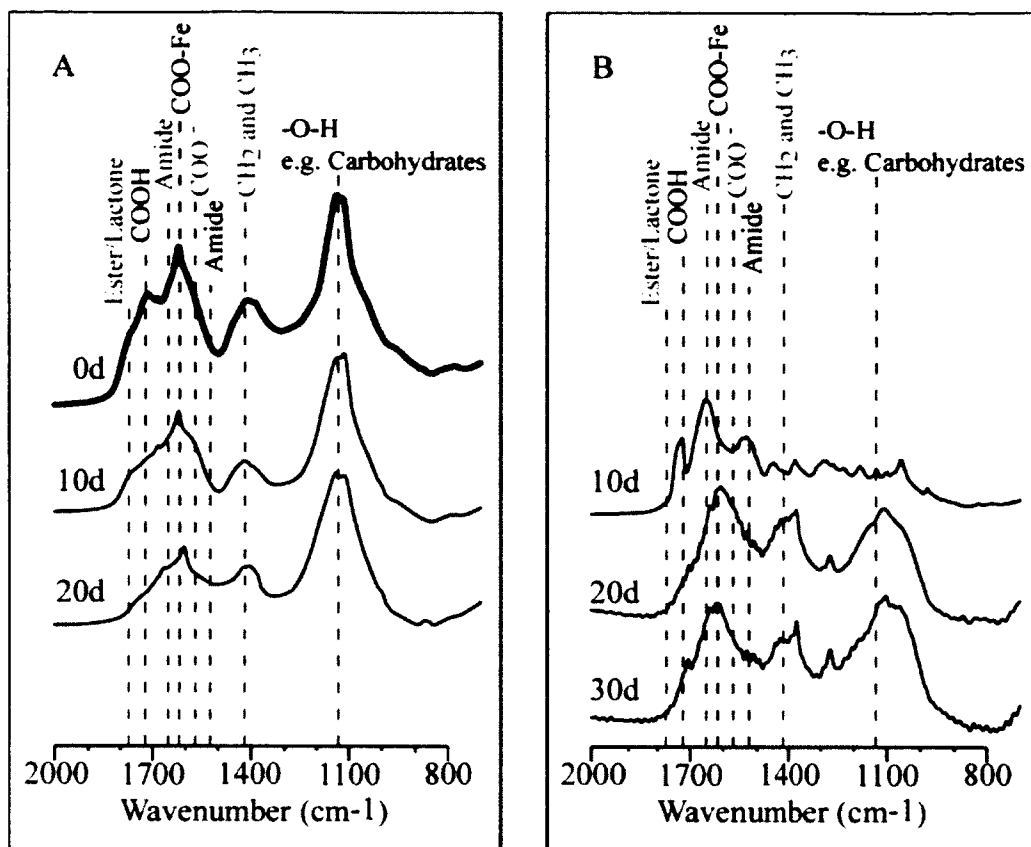


Fig. 8. FTIR spectra obtained for (A) dissolved organic matter and (B) particulate organic matter. Labels to the left of each spectrum refer to the duration of the irradiation.

(supernatant) from the 10 and 20 d time points (Fig. 8). All DOM FTIR spectra exhibit a prominent peak at 1020-1160  $\text{cm}^{-1}$  (carbohydrate region); however, this peak is not observed in the 10 d POM spectrum and is less prominent in the 20 and 30 d POM spectra compared to DOM. The carboxyl region (1500-1800  $\text{cm}^{-1}$ ) of the IR spectrum for the particles that formed during the first ten days (Fig. 8B) is significantly different from the corresponding DOM spectra (Fig. 8A). FTIR spectra for particles from the 20 and 30 d irradiations contain major peaks associated with COOH (1720  $\text{cm}^{-1}$ ), amide (1650 and 1540  $\text{cm}^{-1}$ ), COO-Fe (1620  $\text{cm}^{-1}$ ), and COO<sup>-</sup> (1580  $\text{cm}^{-1}$ ). Peaks were identified by taking the second-derivative of the deconvoluted spectra (Fig. 9) as described in Abdulla et al (2010).

Five main types of carboxyl groups were identified from the deconvoluted second-derivative FTIR spectra and their concentrations for the dark control and 10 d irradiated samples were estimated by combining the TOC normalized carboxyl concentration (Table 3) and the areas obtained by deconvolution and integration of the FTIR spectra (Fig. 9) according to Abdulla et al. (2010). Most notably, the deconvoluted spectrum (Fig. 9D) reveals primarily acetate groups (1745  $\text{cm}^{-1}$ ) and amide groups (1650  $\text{cm}^{-1}$ , 1540  $\text{cm}^{-1}$ , and 1261  $\text{cm}^{-1}$ ) in the particulate spectrum, but no readily observable carboxylate-iron complexes (1620  $\text{cm}^{-1}$ ). This result is consistent with the atomic absorption measurements as no iron flocculation was observed until after the 10 d time point (Figs. 5C and 6C; Table 1). Acetate and amide increased, while the other carboxylate moieties decreased during the irradiation. Nearly all of the amide functionality was present in the particulate phase along with nearly half of the carboxylic acid and carboxylate functionality (Table 4). The partitioning of amide functional groups

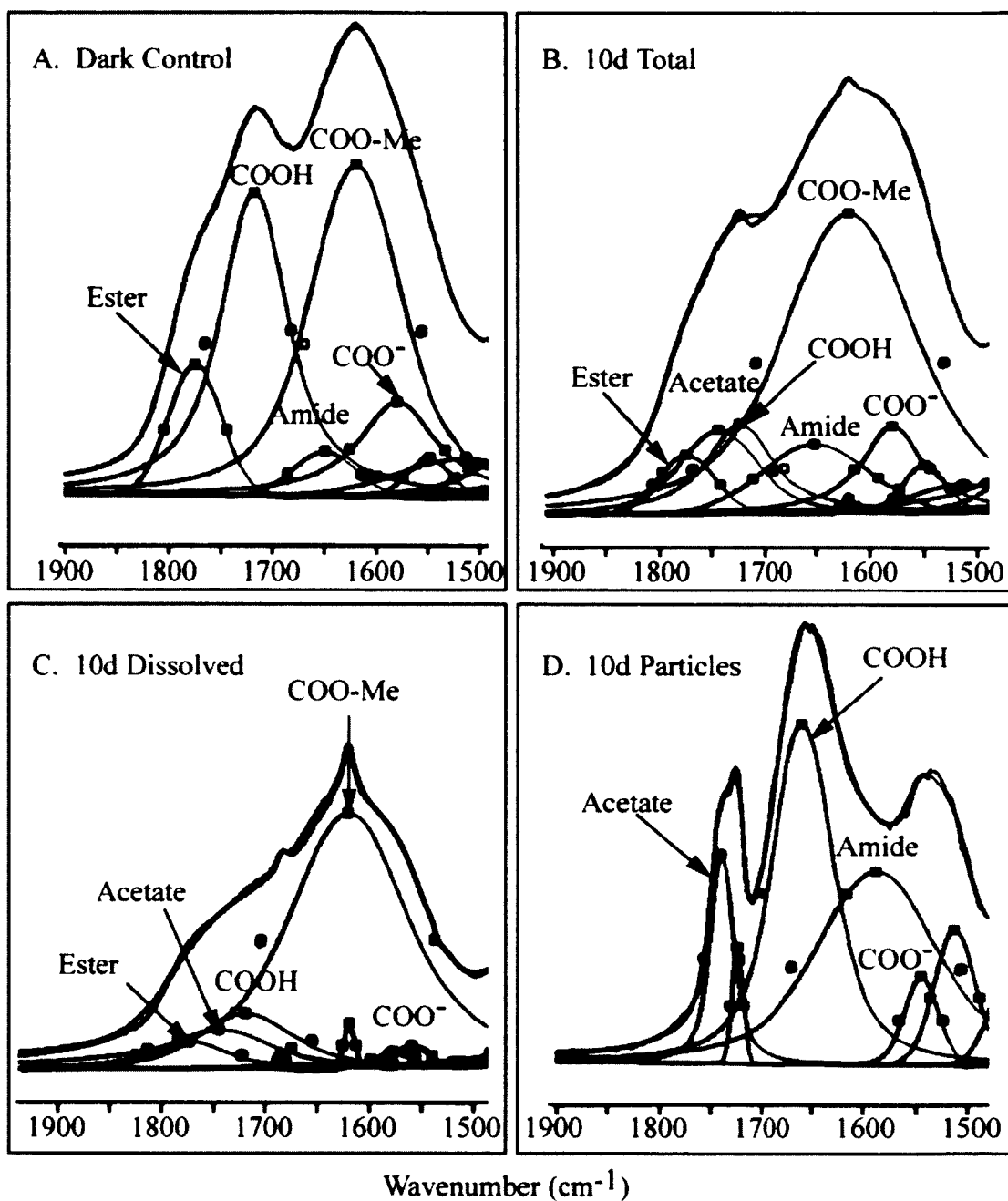


Fig. 9. Partially de-convoluted FTIR spectra for (A) unirradiated, dark control, (B) 10 day irradiated, unfractionated sample, (C) 10 day irradiated dissolved (supernatant) sample, and (D) particles isolated from 10 day irradiated sample.

Table 4. Estimated concentrations of different carboxylic moieties ( $\mu\text{mol C L}^{-1}$ ).

Quantifications are based on deconvoluted FTIR spectra, NMR integration of the 165-190 ppm region, and TOC measurements.

	Peak Center(s) ( $\text{cm}^{-1}$ )	Dark Control	10d Total	10d Particles	10d Dissolved
Ester/Lactone	1775	72	20	0	16
Acetate	1745	0	46	9	32
COOH & COO <sup>-</sup>	1580, 1720	390	94	43	48
COO-Fe	1620	380	280	0	270
Amide	1650	28	44	40	1



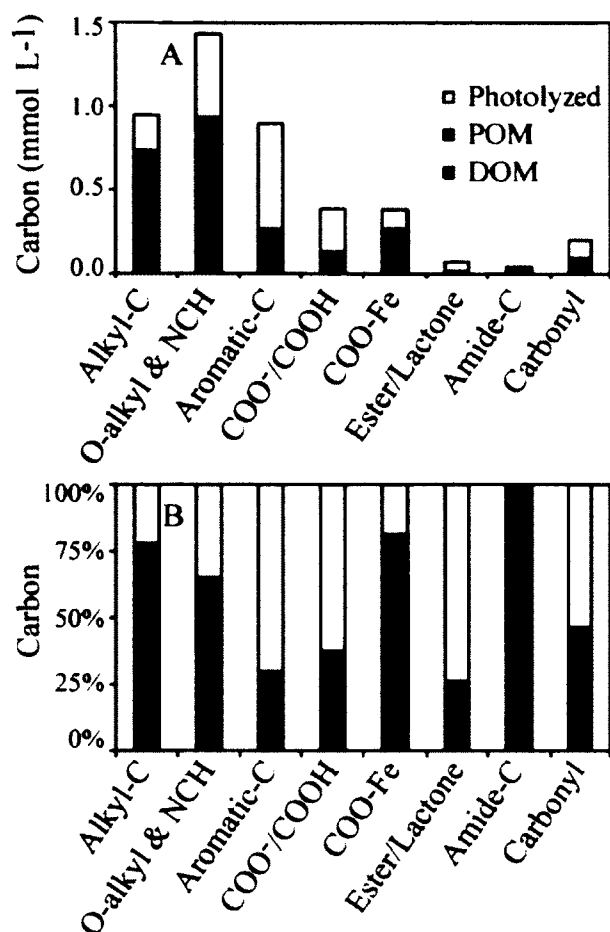


Fig. 10. Distribution of organic functional groups after 10 days continuous irradiation. Photolyzed columns (white) represent organic matter that was completely mineralized or volatilized during irradiation. POM columns (black) represent flocculated organic matter. DOM columns (gray) represent organic matter that remained in dissolved phase after irradiation. Functional group assignments are based on <sup>13</sup>C NMR and FTIR spectra. (A) Quantifications are based on TOC measurements normalized to NMR and/or FTIR spectral integrations. Acetate is included in the “COOH/COO<sup>-</sup>” category. Carbonyl refers to aldehyde, ketone, and quinone moieties.

into the solid phase is consistent with the TN results (Table 1; Fig. 4D). Neither esters nor iron associated carboxylate were apparent in the particle phase after 10 days of irradiation. The FTIR spectra for the 20 d and 30 d samples were not deconvoluted due to their low signal to noise ratios and lack of corresponding NMR data.

The distribution of the major types of DOM structural moieties after 10 days of irradiation (Fig. 10) shows that the most rapidly removed carbons were aromatic. Esters, carboxylic acid/carboxylate groups, and carbonyls were also extensively mineralized. Nearly all of the amide functionality was present in the particulate phase along with a significant fraction of the aliphatic and O-alkyl or amine carbons. The residual (unaltered, photodegraded, and photoproducts) DOM compounds after 10 days irradiation were significantly more aliphatic and less aromatic than the dark control. While carboxyl carbons remained relatively constant as a fraction of total DOC (approximately 20%; Table 2), the distribution of carboxylic groups shifted towards primarily metal associated carboxylate, which was present only in the dissolved phase (Table 4; Fig. 10).

## DISCUSSION

The compositional differences between the photo-flocculated POM and the dissolved phase can be summarized as follows: POM formed after 10 days of irradiation is less aromatic, less carbohydrate-like, contains more amide and aliphatic functionality than the corresponding DOM and contains no metal-associated carboxylate. UV-visible absorption results (Table 1) suggest that photo-flocculated POM (10 day sample) has a higher average molecular weight (lower spectral slope and slope ratio) and less aromatic

functionality (lower SUVA<sub>254</sub>). First- and second-derivative UV-visible spectra (Figs. 3 and 4) suggest that different chromophores are present in the particulate and dissolved phases. These results are supported by the considerable differences between the NMR and FTIR spectra observed for DOM and POM. The C/N ratio of particulate matter decreased during the 10 to 30 d portion of the irradiation because of the preferential mineralization of carbon. The low C:N ratio of the POM that remained after 30 days of irradiation (11) compared to the high DOM C:N ratio of the starting material (28) indicates that photo-flocculation may play an important role in the transport of organic nitrogen from the water column to the sediments.

The combined use of TOC, NMR, and FTIR to quantify carboxyl functionalities reveals a net increase in amide functionality during the early stages of photolysis (Table 4; Fig. 10), nearly all of which appears in the flocculate (Figs. 6D and 10). Amides may have formed via the following mechanism: Ammonia that is produced during photolysis of dissolved organic nitrogen (DON) (Bushaw et al. 1996; Tarr et al. 2001; Stedmon et al. 2007) reacts with esters within DOM to generate alkyl amides (McKee and Hatcher 2010). Since the results show that amides preferentially accumulate in the POM (Table 4; Fig. 10), this process may provide a pathway by which nitrogen is exported from surface waters to sediments. The observed decrease in ester concentration (Table 4) supports this mechanism for amide production. Interestingly, deep ocean DON is largely (up to 76%) in the form of chemically uncharacterized amides that apparently resist both chemical and biological degradation (McCarthy et al. 1997; Aluwihare et al. 2005). An abiotic source of amide functionality within DOM would help explain its refractory nature (McKee and

Hatcher 2010). Further work is needed to determine whether this abiotic mechanism also applies to waters with lower DOM concentrations.

The results of this study suggest that changes in the concentrations and types of carboxyl groups within DOM play critical roles in photo-flocculation. The signal in the carboxyl region of the NMR spectrum for POM for the 10-day sample is partially split into two peaks that are narrower than the single peak observed for DOM (Fig. 7) suggesting that the carboxyl groups in the flocculate phase represent a less diverse mixture than the bulk dissolved material. The narrower, more resolved bands in the carboxyl region for the particulate phase (Fig. 5, day 10) may also be due to the lack or low content of paramagnetic iron in this sample (Pfeffer et al. 1984). Alternatively, similar peaks observed for riverine DOM samples have been attributed to carbonate (Bianchi et al. 2004).

The combined FTIR and NMR results indicate that carboxylic acids, carboxylate groups and metal associated carboxylate groups are removed during the first ten days irradiation (Fig. 10A). In addition, decarboxylation appears to have occurred as indicated by the increase in pH (Fig. 2) in the irradiated samples and the production of dissolved inorganic carbon during UV exposure of Dismal Swamp water (Minor et al. 2006). NMR evidence presented here, and by Thorn et al. (2010) suggests that photochemical decarboxylation leads to decreased DOM aqueous solubility, which is supported by the higher aliphatic content of the POM relative to the DOM (Table 2), thus facilitating flocculation. Abdulla et al. (2010) showed that carboxylic groups in the >1 kDa fraction of DOM decreased downstream along an estuarine transect. They suggested that this decrease was due to flocculation/adsorption, and/or photodegradation/photo-

decarboxylation. In light of the results of the current study, it is reasonable to speculate that a coupled photochemical-flocculation mechanism contributed to this observed estuarine trend.

The mechanism of photochemical flocculation has not previously been directly investigated. Based on the spectroscopic characterization of the DOM and POM remaining after irradiation, it appears that photo-flocculation occurs by two or more pathways (Fig. 11), and that initial flocculation of organic and inorganic material may not occur simultaneously. The processes in Fig. 11 have been subdivided according to whether they occur prior to the flocculation of iron (Phase I) or after iron begins to flocculate (Phase II). The Continuous category includes reactions that likely impact the process of photo-flocculation throughout this experiment, while the Competitive category includes reactions and processes that compete with or counteract the process of photochemical flocculation. During Phase I, loss of DOM solubility may have occurred as a result of selective photodegradation as a portion of the aromatic, polyhydroxyl and polycarboxyl humic material within the DOM matrix becomes more aliphatic and less acidic rendering it more hydrophobic (Gao and Zepp 1998; Thorn et al. 2010). An additional possibility involves the degradation of an amphiphilic fraction of the DOM, which leads to the flocculation of pre-existing hydrophobic “core” material and/or sparingly soluble amphiphiles such as peptides. Similar amphiphilic-hydrophobic interactions have been proposed to explain the enhanced solubility of model pollutants by natural organic matter (Chiou et al. 1986; Abdulla et al. 2009), which suggests that the change in bulk DOM polarity may impact the partitioning of aromatic pollutants. In either case, a photochemically inert fraction of DOM carbohydrate-like material (NMR

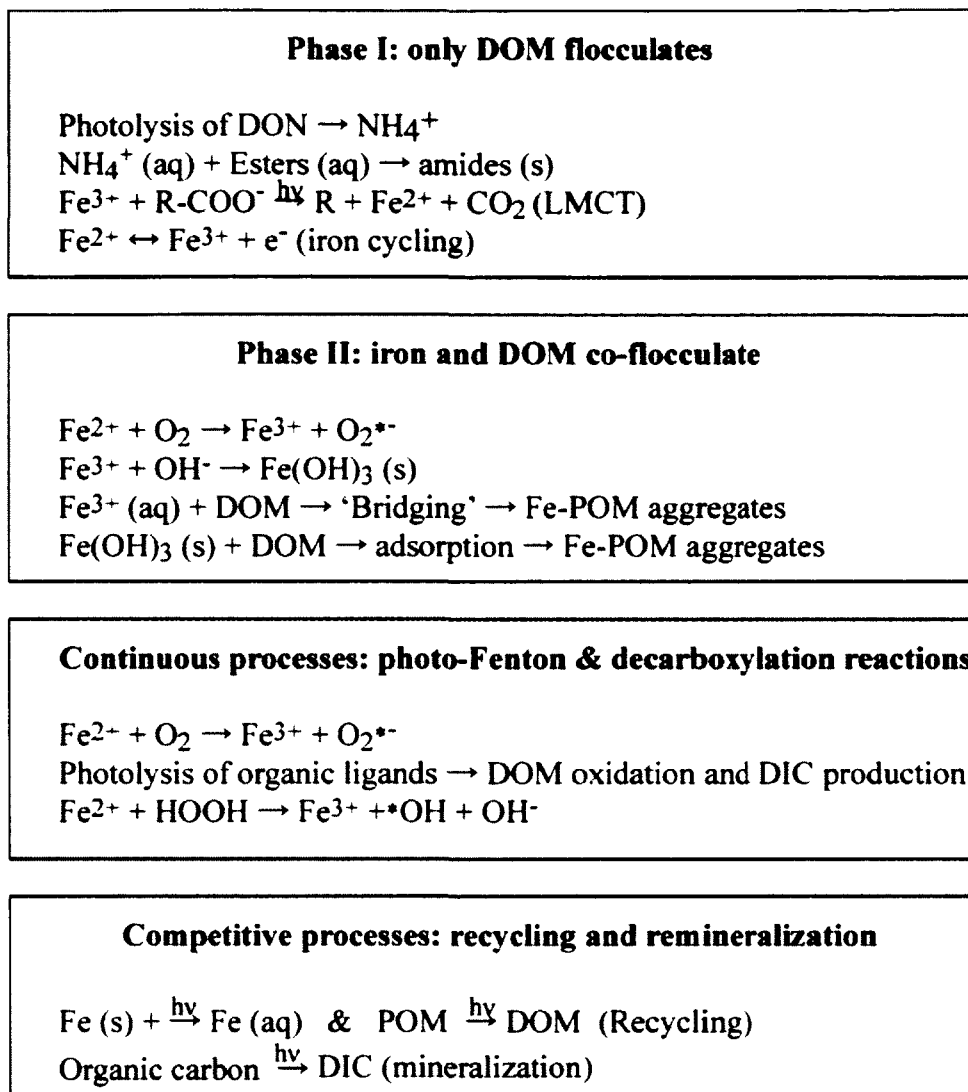


Fig. 11. Proposed components of the photochemical flocculation mechanism for organic matter and iron. During “Phase I” organic matter flocculates, but iron does not. During “Phase II” both organic matter and iron flocculate. The transition from Phase I to Phase II during these experiments may have been caused by loss of soluble iron binding ligands, the increase in pH, and/or the build up of iron (III) as the iron photo-reduction rate decreased relative to Fenton’s reaction. Fe(s) represents solid iron oxyhydroxides.

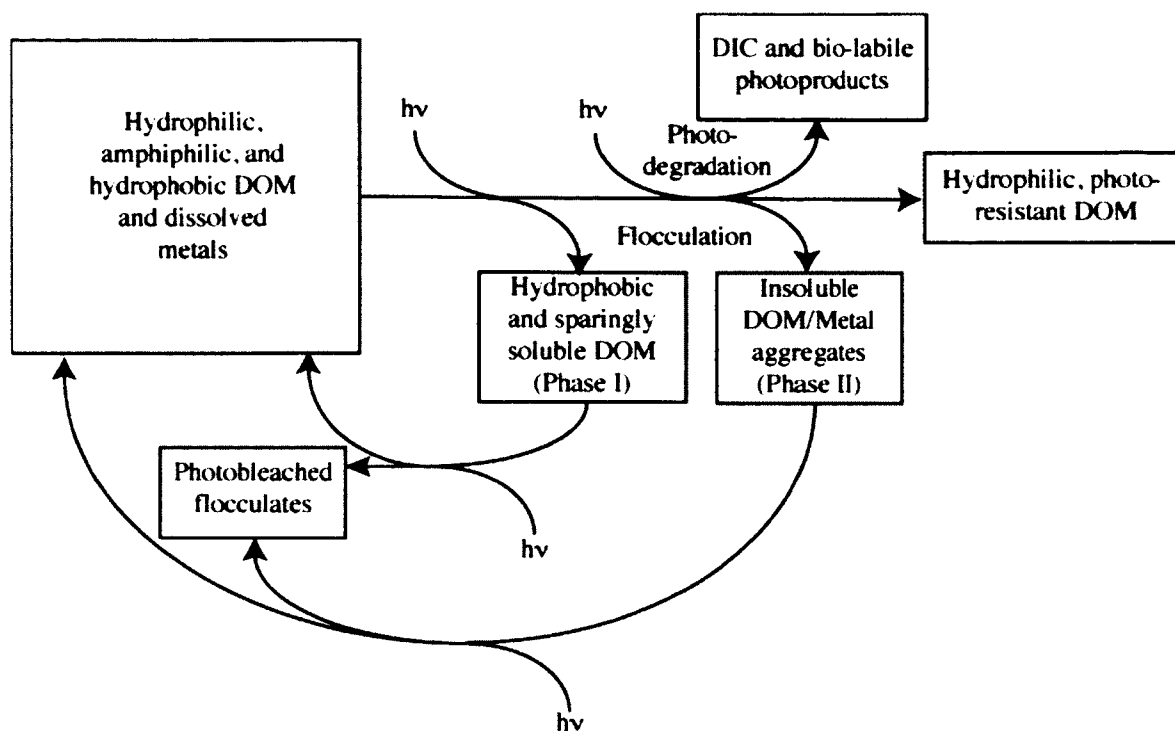


Fig. 12. Hypothetical schematic representation of the photochemical flocculation process.

signal at ~75ppm and ~100ppm, IR peaks from 997 to 1152  $\text{cm}^{-1}$ , and little or no UV-visible absorption) survives long-term UV exposure and remains primarily in the dissolved phase. Fig. 12 shows a simple conceptualization of these processes, wherein a mixture of hydrophilic, amphiphilic, and hydrophobic DOM is photolyzed removing amphiphilic DOM or producing hydrophobic DOM leading to flocculation of the least soluble fractions. Iron and possibly other dissolved metals are also removed from solution by flocculation. A major fraction of DOM is removed from surface waters by formation of inorganic, volatile, or biologically labile photoproducts (Miller and Moran 1994).

Many of the flocculation processes in estuaries are dependent on the presence of suspended particles (Guo et al. 2007; Verney et al. 2009). This dependence was also noted for bubble-induced aggregation in seawater (Batoosingh et al. 1969). Silica particles have been shown to readily adsorb humic substances (Liang et al. 2011), and the adsorption of surface active DOM to minerals and detrital POM has been cited as a possible route for the preservation of organic matter in the sediments (Hedges and Keil 1995; Henrichs 1995; Mead and Goni 2008). Although the experimental protocol used in the current study excluded pre-existing particulate matter greater than 0.1  $\mu\text{m}$ , the extent to which DOM adsorbed to the walls of the quartz flasks was quantified. Negligible adsorption occurred in the dark control (~0.10% of total  $a_{300}$ ), while after 20 days of irradiation, 15% of the residual  $a_{300}$  adsorbed to the walls of the irradiated quartz flasks. TN was not measured for the adsorbed material; however, wall adsorption of DON (along with the formation of volatile nitrogen compounds such as ammonia and amines, which would have been lost during freeze-drying) may help to explain the observed ~20%



decrease in TN during the irradiation experiment (Fig. 5D). As these experiments have shown that a fraction of DOM is susceptible to mineral adsorption, or more strongly adsorbed after photodegradation, this mechanism may be a pathway by which a significant fraction of the tDOM pool is both exported from surface waters to the sediments and subsequently preserved during early diagenesis (Hedges and Keil 1995; Henrichs 1995; Mead and Goni 2008).

The role of iron and other metals in the photochemical flocculation of DOM appears to be complex. Both dissolved and particulate forms of iron likely play roles in the photo-flocculation of DOM. Dissolved iron may form metal ion “bridges” between DOM molecules or colloids resulting in aggregation (Verdugo et al. 2004; Orsetti et al. 2010). Polymeric iron (hydr)oxides as well as soluble forms of iron III, have been found to coagulate DOM (Nierop et al. 2002; Pullin et al. 2004; Honghai et al. 2008). Organic metal-binding ligands have been shown to degrade in sunlit surface seawater transforming organically complexed metals to inorganically complexed or colloidal metals on diel time-scales (Powell and Wilson-Finelli 2003; Shank et al. 2006). Thus, photochemically induced flocculation of dissolved and colloidal iron may be driven by photochemical degradation of metal-complexing ligands within DOM. Even though photo-flocculation of DOM occurred during the first 10 days of the experiment, all the iron essentially remained in solution (Fig. 4), which suggests that, during this period, it either quickly re-cycled back into the dissolved phase by complexation with soluble organic ligands, or it was photo-reduced to iron (II), which is soluble at the initial experimental pH (Fig. 12). Reduction to iron (II) may have occurred via ligand to metal charge transfer reactions (Faust and Zepp, 1993) resulting in oxidative decarboxylation

(Bockman et al. 1996; Thorn et al. 2010), which in turn enhanced the hydrophobicity of the residual DOM molecule (Gao and Zepp 1998; Thorn et al. 2010). It is likely that, as the DOM became increasingly mineralized and/or structurally altered, the abundance of ligands and/or electron donors diminished, causing a shift in the speciation of the iron present and allowing less-soluble iron (III) oxyhydroxides to form (Deng and Stumm 1994). Alternatively or concurrently, iron-binding sites became more abundant in the POM than in the DOM, leading to a transfer of organically complexed iron from the dissolved phase to the particulate phase. Another possibility is that, as the pH increased during the irradiation (Fig. 2), DOM carboxyl groups became progressively deprotonated and thus more readily complexed with metals to form insoluble metal DOM complexes via cation bridged aggregates (Nierop et al. 2002) and/or the solubility of iron III may simply have decreased as a result of the rising pH. It is unclear which of the above was the more important mechanism for iron flocculation or whether the mechanisms shifted during the course of the irradiation. Iron associated carboxylate is clearly present in the 20 and 30 d irradiated particles (Fig. 8B), though it is not known whether these bonds formed in the solution phase or through adsorption of DOM to iron (III) oxyhydroxide particles.

In order to estimate the potential impact of photochemical flocculation on the oceanic carbon cycle, the simple calculations outlined in Fig. 13 are proposed. By plotting TOC removal and DOC removal versus  $a_{300}$  removal and extrapolating to complete photobleaching of the terrestrial organic matter (defined here as  $a_{300}$  removal =100%), and applying these removal terms (Fig. 13) to the total riverine input of DOC to the ocean (Meybeck 1982), it is estimated that  $1.1 \times 10^{13}$  g C  $y^{-1}$  would be removed from

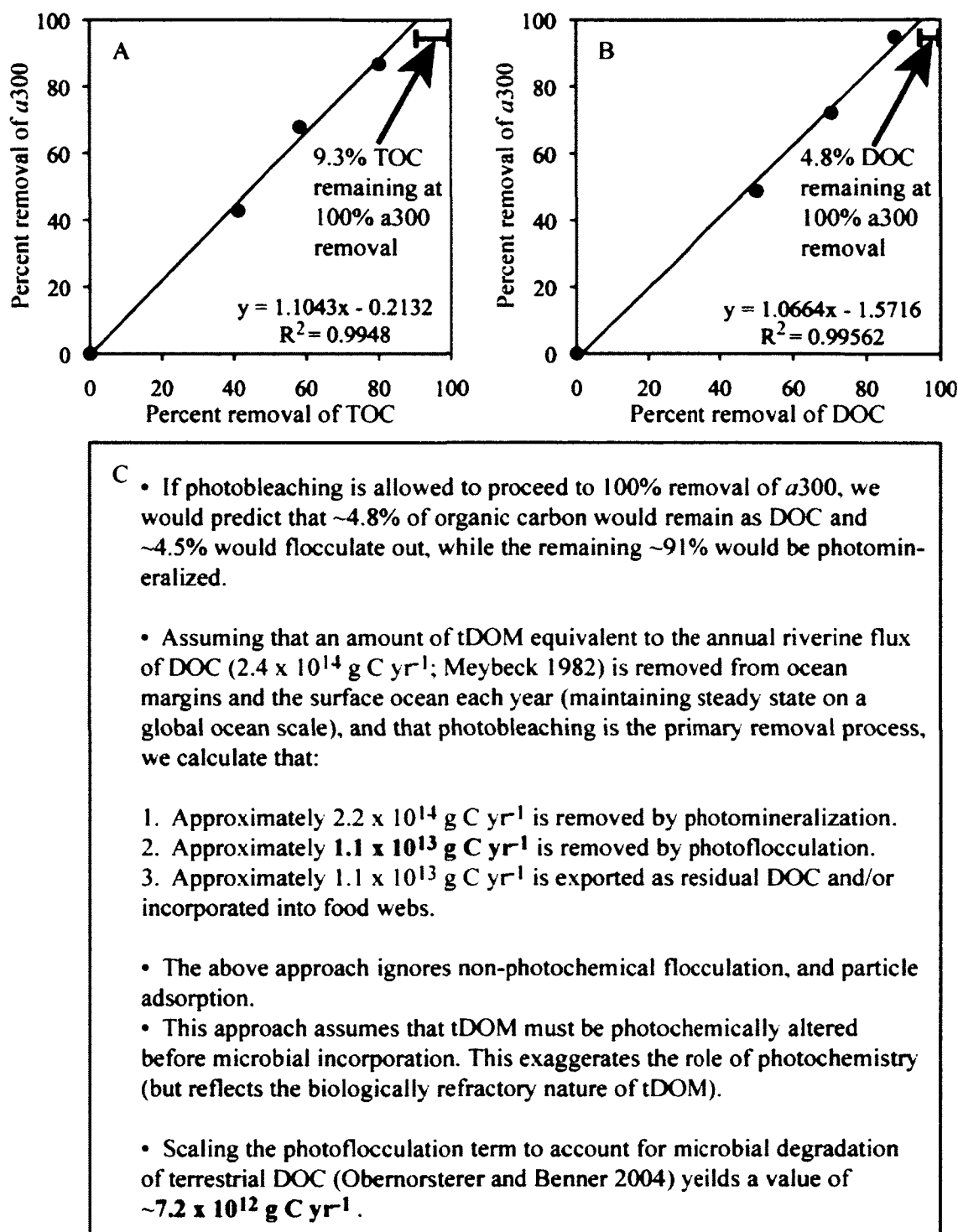


Fig. 13. (A) Extrapolated 100% photobleaching at 300nm for unfractionated samples and (B) dissolved samples. (C) Estimated global impact of photochemical flocculation on the ocean carbon cycle.

surface waters by photochemical flocculation. If our highest POC measurement (from the 20 day time point;  $6.7 \text{ mg C L}^{-1}$  or 12% of initial DOC) and the larger riverine carbon flux estimated by Aitkenhead and McDowell (2000) are considered, then as much as  $4.3 \times 10^{13} \text{ g C y}^{-1}$  could be transported from surface waters to the sediments due to photochemical flocculation. This term may still underestimate the role of photo-flocculation on a global scale as we have neither considered non-riverine sources of tDOM (ground water, tidal wetlands, etc.) nor explored the potential impact of marine DOM photo-flocculation. However, the calculation outlined in Fig. 13 overestimates the role of photochemistry as it assumes that biological degradation of tDOM is limited only to removal of photoproducts, whereas Amon and Benner (1996) reported that (integrated over the water column) biological degradation of non-photo-degraded tDOM is also quantitatively important. Scaling the process of photo-flocculation to account for the estimated biological mineralization of ~27%-34% of terrigenous DOC in the coastal environment (Obernorsterer and Benner 2004) yields an estimated  $\sim 7.5 \times 10^{12} \text{ g C y}^{-1}$  global photochemical flocculation term (using the more conservative term from Fig. 13). Further research is needed to assess the accuracy of these estimates, including investigations of more geographically diverse terrestrial end members, the potential for marine sourced DOM to photo-flocculate, and interactions between photo-degradation/flocculation and biological processing of organic matter.

It should be noted that the POC formation rates of  $0.13\text{-}0.47 \text{ mg C L}^{-1} \text{ d}^{-1}$ , reported here, are lower than the rate of  $0.50 \text{ mg C L}^{-1} \text{ d}^{-1}$  reported by Gao and Zepp (1998) and that all published instances of photochemically mediated DOM flocculation have been reported for high DOC, terrestrial environments with high DOC/TOC ratios.

Furthermore, these estimates do not take into account photo-dissolution of the flocculates in the flasks (Pisani et al. 2011) nor possible dilution effects in the environment. It is not yet known if photo-flocculation affects algal/marine DOM. The need for further investigation in this area of organic matter reactivity is clearly indicated.

Photochemically induced flocculation represents a potentially significant source of organic carbon, organic nitrogen, and iron to the sediments. The abiotic production of amides, which preferentially partition into the particulate phase, may help to explain the presence of biologically refractory carbon and nitrogen in the sediments and deep ocean. This, along with the observed photochemical production of surface-active DOM may significantly contribute to the high rates of organic matter preservation observed in coastal sediments underlying tDOM rich surface waters (Dagg et al. 2004). Furthermore, photochemical flocculation represents a removal mechanism of tDOM from the water column and may partially explain the apparent disconnect between the large riverine source of tDOM and the low abundance of identifiable terrestrial DOM in the oceans.

# CHAPTER III

## LOSS OF OPTICAL, MOLECULAR, AND STRUCTURAL INDICATORS OF TERRIGENOUS DISSOLVED ORGANIC MATTER DURING LONG-TERM PHOTBLEACHING

### INTRODUCTION

Terrestrial dissolved organic matter (tDOM) consists mainly of the biologically refractory components of land plants in varied states of degradation (Hedges and Ertel 1982; Hernes and Hedges 1999; Mannino and Harvey 2000). In comparison with marine derived DOM, tDOM is usually rich in colored or chromophoric DOM (CDOM; Senesi et al. 1989). Past studies have indicated that the oceanic carbon budget is not in balance with respect to riverine carbon inputs (Mantoura and Woodward 1983; Williams and Druffel 1987; Deuser 1988; Hedges et al. 1992; Blough et al. 1993; Opsahl and Benner 1997; Vodacek et al. 1997). Based on riverine inputs alone, the entire dissolved organic carbon (DOC) content of the oceans ( $\sim 10^{17} - 10^{18}$  g-C) can be accounted for in about 600-2000 years (Deuser 1988; Hedges et al. 1992). But, the bulk of the oceanic DOC is in the deep sea, which has an average  $^{14}\text{C}$  age of  $\sim 6000$  years (Williams and Druffel 1987; Druffel et al. 1989) and appears to show little terrestrial character. For example, using bulk properties (such as the C/N ratio, single or dual  $\delta^{13}\text{C}$  and  $\Delta^{14}\text{C}$  isotope signatures of bulk DOM or UV-visible absorption) suggests that only a small portion of terrestrial dissolved organic matter (tDOM) reaches open ocean (Eglinton and Hamilton 1963; Meyers-Schulte and Hedges 1986; Opsahl and Benner 1997; Opsahl et al. 1999; Mitra et al. 2000; Raymond and Bauer 2001; Rochelle-Newall and Fisher 2002b; Hopmans et al. 2004; McCallister et al. 2006). These findings are puzzling since riverine DOC shows a

more or less conservative behavior during estuarine mixing, with coagulation, adsorption and precipitation accounting for only a small fraction of its removal (Sholkovitz 1976; Mantoura and Woodward 1983; Dister and Zafiriou 1993; Guo et al. 1995; Amon and Benner 1996; Opsahl and Benner 1997; Del Castillo et al. 2000; Raymond and Bauer 2001). Therefore, these results suggest either that there exist major unknown sinks for the rapid removal of riverine DOM from the oceans (Kieber et al. 1990; Hedges et al. 1997), and/or that the terrestrial input is diagenetically altered in estuaries and oceanic surface waters to the point that its terrestrial character is substantially lost (Minor et al. 2007; Dalzell et al. 2009; Spencer et al. 2009; Stubbins et al. 2010), and thus the contribution of tDOM to the oceanic DOM pool is largely in an unknown and source unrecognizable form (Dittmar et al. 2007).

Lignin derived phenols have often been used as molecular tracers for tDOM (Hedges and Ertel 1982; Opsahl and Benner 1998; Louchouart et al. 2000). Similarly, the characteristic optical properties of terrigenous chromophoric and fluorescent DOM (CDOM and FDOM respectively) have been used to track the mobility and fate of tDOM in the open ocean (Nelson et al. 2007), coastal zone (Del Vecchio and Blough 2004b; Stedmon et al. 2010), estuaries (Helms et al. 2008), watersheds (Wong 2009), streams, and groundwater (Fasching 2009). As tDOM markers, both lignin and terrestrial CDOM share the advantage that they are relatively slow to biodegrade (Opsahl and Benner 1998; Kowalczyk et al. 2003), however they both degrade photochemically (Opsahl and Benner 1998; Spencer et al. 2009). Therefore, their concentrations appear low in terrestrially influenced water masses that have had a history of high light exposure.

While photochemical reactions are limited to surface waters, the amount of time that tDOM spends in the upper water column can be quite long, e.g., weeks to months during estuarine transit and longer where buoyant plumes are entrained in stratified oceanic surface waters (Moore et al. 1986; Dagg et al. 2004). Few studies of photochemical processes have involved irradiations lasting more than 7 days. However, long-term irradiations can provide relevant information about photochemical alteration of DOM that is anticipated for buoyant river plumes, highly stratified estuaries, shallow environments, and surface ocean waters (Moran et al. 2000; Vähätalo and Wetzel 2004; Stubbins et al. 2010).

$^{13}\text{C}$  NMR has been used previously for the characterization of DOM and its photochemical degradation. Irradiation of decayed plant leachate for up to 4.5 hours with UV-B resulted in only subtle changes to the NMR spectra, probably due to the low signal to noise ratios encountered and the relatively short duration of the irradiation experiment (Wetzel et al. 1995). Irradiation of humic and fulvic acids isolated from Nordic fjords for up to 80 hours using monochromatic 254 nm irradiation (Kulovaara et al. 1996) and the irradiation of sphagnum bog water using natural sunlight for seven days (Osburn et al. 2001) resulted in considerable loss of solid-state cross-polarization magic angle spinning (CP/MAS)  $^{13}\text{C}$  NMR signal in the aromatic region with relatively little change in the aliphatic region and a relative increase in carboxyl signal. Neither study removed more than about 35% of the UV absorption during irradiation. Quantitative solution  $^{13}\text{C}$  NMR was recently used to characterize humic substances irradiated using an unfiltered medium pressure, mercury lamp. The NMR spectra showed that photochemical decarboxylation proceeded rapidly, that initial carbonyl, aromatic, and O-alkyl content were effective



predictors of photo-lability, and that C-alkyl moieties were the most resistant to photochemical degradation followed by O-alkyl moieties (Thorn et al. 2010). Advanced solid-state NMR pulse programs (Mao et al. 2011) provide information beyond that which can be obtained by simply integrating spectra; however, these powerful advanced techniques have not been applied to study the photodegradation of DOM. Fourier transform infrared spectroscopy (FTIR) has also been used extensively to characterize unaltered and photochemically altered DOM (Stevenson 1994; Kalbitz et al. 2003; Abdulla et al. 2010).

In the study described here, photobleaching was monitored throughout long-term solar-simulated UV irradiation of Dismal Swamp water samples (filtered, but otherwise unfractionated) using optical spectroscopy and lignin phenol measurements. In addition, advanced solid-state  $^{13}\text{C}$  NMR and FTIR, as well as a coupled NMR-FTIR data treatment, were applied to investigate the compositional/functionality changes that occurred. This multi-method approach provided new insights into the photo-transformation of tDOM and its fate in the oceans, while the use of un-fractionated DOM at natural concentrations facilitated extrapolation to photochemical transformations in surface waters.

## MATERIALS AND METHODS

*Cleaning procedures* – Glass and quartz-ware were cleaned with dilute ( $\sim 1 \text{ mol L}^{-1}$ ) HCl and rinsed with MilliQ UV-treated ultrapure grade water (Millipore), herein termed MilliQ water, and combusted  $> 4 \text{ h}$  at  $450^\circ\text{C}$ . Plasticware was cleaned with dilute HCl and rinsed with MilliQ water. Stainless steel equipment was cleaned with

mild detergent and copiously rinsed with MilliQ water. All containers were rinsed three times with sample prior to filling. Filter capsules (0.1  $\mu\text{m}$  pore size, Whatman PolyCap) were rinsed briefly with reagent grade acetonitrile, flushed with > 20 L of MilliQ water, and conditioned with approximately 1 L of sample.

*Sample collection, handling, and irradiation* – Two water samples, Burn Site and Feeder Ditch, were collected from the Dismal Swamp National Wildlife Refuge. The Burn Site sample (BS) was collected at 76°31' W, 36°35' N from a ditch adjacent to a fire impacted area. The Feeder Ditch sample (FD) was collected at 76°22' W, 36°36' N from the public boat ramp near the outflow of the Lake Drummond feeder ditch to the Dismal Swamp canal. Samples were transported back to the laboratory in glass 4 L Qorpak bottles with Teflon lined caps and filtered through a pre-cleaned 0.1  $\mu\text{m}$  Whatman PolyCap filter prior to irradiation.

Aliquots (450 mL) of the samples were transferred to ~550 mL quartz round bottom flasks and placed inside a solar simulator containing 12 Q-Panel UVA340 bulbs, which provided a spectral output similar to that of natural sunlight from ~300 to ~365 nm (Q-Panel), but under-represented solar irradiance at wavelengths greater than about 365 nm (Helms et al. 2008; Fig. 14). The light output from the solar simulator was monitored during the course of the irradiation experiment using a Biospherical PUV 2510 radiometer, and absorbed light dose, as applied to spherical flasks (wherein refractive effects were assumed to cancel and thus ignored), was calculated using the absorption spectrum of the sample (see below) and the measured output spectrum of the solar simulator (Leifer 1988). The lamps were kept on constantly during the irradiations.

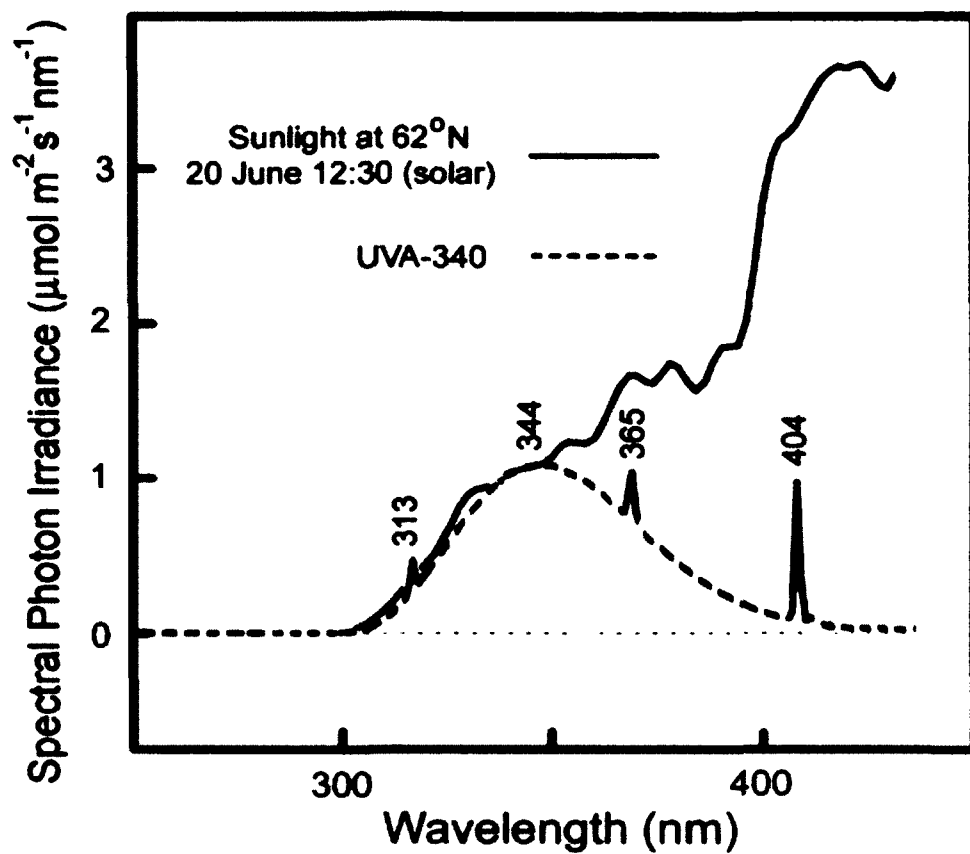


Fig. 14. Comparison of solar irradiance spectrum and UVA340 lamp output.

Reproduced with permission from Tripp et al. (2003) © Nature Publishing, see Appendix.

The radiometer sensor was positioned on a level with the bottom of the sample flasks and approximately 18 inches off center of the 48-inch lamps (samples occupied the center of the solar simulator). Measured irradiance therefore underestimates the light exposure at the top of the samples slightly. Flasks were opened several times each week and stirred to prevent the development of low oxygen conditions. Sub-samples were collected and analyzed at exposure intervals ranging from 1 day to 110 days.

Dissolved oxygen (DO) and temperature were monitored in one of the FD sample flasks using a Thermo-Orion 810A+ meter with DO Probe 081010F. The DO probe was calibrated at room temperature and readings were corrected by applying a multiplication factor derived by dividing the saturated DO concentration at the calibration temperature by the saturated DO concentration at the sample temperature. pH was measured using a Fisher Scientific Accumet pH meter 25 with an Orion ROSS gel filled pH electrode.

The samples were irradiated without dilution in order to collect sufficient organic material for the solid-state NMR analyses. Irradiation of the samples at natural concentrations also provided light conditions similar to those at the surface of humic lakes during summer stratification.

During the course of the irradiation experiment, a small fraction of the DOM precipitated in several flasks by processes investigated and described elsewhere (Chapter II). For the purposes of this study, the particles in the BS samples with irradiation times longer than 15 days were dissolved by adding 15  $\mu$ l of 50% w/w sodium hydroxide (VWR Scientific) to each flask, while the particles that formed in the FD samples were allowed to flocculate. The addition of sodium hydroxide to several of the BS samples prevented the tracking of photochemically induced changes in pH for those samples.

Further, it resulted in bicarbonate and low molecular weight organic acids being retained as sodium salts during freeze-drying prior to solid-state NMR analyses. However, FD samples, which did not receive additions of NaOH, facilitated monitoring of photochemically induced pH changes and provided freeze-dried isolates free of inorganic carbon and volatile organic acids. During the irradiation of FD samples, in situ temperature, and dissolved oxygen were also measured.

Both the dissolved oxygen probe and radiometer were equipped with thermocouple temperature sensors and these agreed to within 1.0 °C. The dark controls were stored in foil-wrapped glass bottles near the irradiated samples. The air temperature in the solar simulator was  $\sim 30\text{ }^{\circ}\text{C} \pm 4\text{ }^{\circ}\text{C}$ .

*Lignin CuO oxidation products* – Lignin analysis is described in detail elsewhere (Hedges and Ertel 1982; Spencer et al. 2010). Briefly, samples were concentrated by freeze-drying, and were reconstituted in 8% NaOH with an excess of CuO and glucose. Eight lignin phenols were quantified using gas chromatography. Acid to aldehyde ratios were calculated for syringyl (Ad/Al)<sub>s</sub> and vanillyl (Ad/Al)<sub>v</sub> phenols, as well as, syringyl to vanillyl (S/V) and cinnamyl to vanillyl (C/V) ratios. The total concentration of the eight index phenols is reported as  $\Sigma_8$  ( $\mu\text{g L}^{-1}$ ), and carbon normalized lignin phenol yields are reported as  $\Lambda_8$  ( $\text{mg mg C}^{-1}$ ).

*UV-visible absorption and fluorescence spectroscopy* – The most commonly measured optical parameter for DOM in natural waters is UV-visible absorbance. CDOM absorption spectra are usually described by an approximate exponential function of

decreasing absorption coefficient with increasing wavelength:

$$(3) \quad a_{\lambda} = a_{\lambda_{ref}} e^{-S(\lambda - \lambda_{ref})}$$

where  $a$  = absorption coefficient ( $\text{m}^{-1}$ ),  $\lambda$  = wavelength (nm),  $\lambda_{ref}$  = reference wavelength (nm), and  $S$  = spectral slope ( $\text{nm}^{-1}$ ) (Helms et al. 2008).

UV-visible absorption spectra (190-900 nm) were measured using an Agilent 8453 diode array spectrophotometer with a 1 cm quartz cuvette. MilliQ water, adjusted to pH = 8.5 with 0.1 M NaOH, was used as the blank. FD samples that contained flocculated particles were adjusted to pH = 11  $\pm$  0.5 with 50% w/w NaOH to dissolve the particles. Highly absorbing samples were diluted with MilliQ water prior to measurement to ensure linear response. All samples were adjusted to pH = 8.5  $\pm$  0.5 with 0.1 M HCl or 0.1 M NaOH, prior to measurement. Absorbance values were corrected to account for instrument baseline drift, refractive index, and temperature variations according to Green and Blough (1994) and converted to Napierian absorbance coefficients using the formula:

$$(4) \quad a = 2.303A/l$$

where  $a$  = absorption coefficient ( $\text{m}^{-1}$ ),  $A$  = absorbance, and  $l$  = path length (m).

Carbon normalized UV absorption, also referred to as specific UV absorption (SUVA), was calculated by dividing the absorption coefficient by the DOC concentration in units of  $\text{mg C L}^{-1}$ . First-derivative UV-visible absorption spectra were obtained by fitting absorption data to linear segments over 11-nm intervals and plotting slope vs. wavelength. The process was repeated using first-derivative data points to produce second-derivative spectra.

Based on  $a_{\lambda}$  measurements, spectral slope ( $S$ ) and slope ratio ( $S_R$ ) may be derived using equation 3, where  $S_R$  is the ratio of  $S_{275-295}$  to  $S_{350-400}$ . The spectral slope across the

wavelength range of 300-700 nm was calculated using non-linear regression of the absorption spectra. Spectral slopes over shorter wavelength ranges were calculated by linear regression of the natural-log transformed absorption spectra (Helms et al. 2008). Spectral slope spectra were generated in a manner similar to Loiselle et al. (2009), except that linear regression of the natural log spectrum was used to determine the slope over a sliding 21-nm interval (10 nm above and below the wavelength for which  $S$  was calculated). Second-derivative natural log absorption spectra were generated as above using the natural log spectra and linear regression slopes calculated over 11-nm intervals.

Fluorescence EEMS were measured using a FluoroMax-2 spectrofluorometer (Spex Industries). Emission spectra (300–550 nm; 2 nm intervals) were measured over a range of excitation wavelengths (240–440 nm for BS and 250–450 for FD; 5-nm intervals). The data integration time was 0.1 - 0.25 s. FD samples that contained particles were adjusted to  $\text{pH} = 11 \pm 0.5$  with 50% w/w NaOH to dissolve particulate organic matter. Strongly absorbing samples were diluted with MilliQ water prior to measurement to reduce inner-filter and other quenching effects (Lakowicz 1999; Cory and McKnight 2005). All samples were adjusted to  $\text{pH} = 7.2 \pm 0.2$  using 0.1 M HCl prior to measurement. EEMS were corrected for inner-filter effects, scattering, and instrument configuration according to Cory and McKnight (2005), normalized to the water Raman peak and then multiplied by the dilution factor. The major DOM component peaks in the EEMS were identified using the wavelength ranges identified by Coble (1996 and 2007): Peak A ( $\lambda_{\text{ex}} \sim 260$  nm;  $\lambda_{\text{em}} = 380\text{--}460$  nm), Peak C ( $\lambda_{\text{ex}} \sim 350$  nm;  $\lambda_{\text{em}} = 420\text{--}480$  nm), Peak M ( $\lambda_{\text{ex}} \sim 312$  nm;  $\lambda_{\text{em}} = 380\text{--}420$  nm), Peak B ( $\lambda_{\text{ex}} \sim 275$  nm;  $\lambda_{\text{em}} \sim 310$  nm), and Peak T ( $\lambda_{\text{ex}} \sim 275$  nm;  $\lambda_{\text{em}} \sim 340$  nm). The fluorescence index (FI), which indicates the relative

influences of terrigenous and autochthonous (i.e., in situ microbial) humic substances, was calculated by dividing the fluorescence at 370ex/470em by that at 370ex/520em (McKnight et al. 2001). The fluorescence humification index (HIX), which compares two broad aromatic dominated fluorescence maxima, was determined at 255 nm excitation by dividing the sum of the emission from 435-480 nm by the sum of the emission from 300-346 nm (Kalbitz et al. 1999). The biological fluorescence index (BIX), which indicates the presence of autochthonous or microbially derived DOM, was determined by dividing the fluorescence at 310ex/380em by that at 310ex/430em (Huguet et al. 2009).

*Dissolved organic carbon* – Non-purgeable total organic carbon (NPOC) was measured using high temperature (720°C) catalytic combustion on a Shimadzu TOC-V-CPH carbon analyzer. The instrument was calibrated using dried primary standard grade potassium hydrogen phthalate (Alpha Aesar) dissolved in MilliQ water. As all samples were 0.1  $\mu\text{m}$ -filtered prior to irradiation, all NPOC measurements are referred to as DOC.

*Solid state  $^{13}\text{C}$  nuclear magnetic resonance spectroscopy* – The semi-quantitative composition of the DOM samples was determined by  $^{13}\text{C}$  cross polarization/total sideband suppression (CP/TOSS) NMR experiments at a spinning speed of 6.5 kHz and a cross polarization (CP) time of 1.0 ms, with a  $^1\text{H}$  90° pulse-length of 4.0 – 4.1  $\mu\text{s}$  and a recycle delay of 0.4 – 1.0 s. Four-pulse TOSS (Dixon 1982) was applied prior to detection, and two-pulse phase-modulated (TPPM) decoupling was used for optimum resolution (Bennet et al. 1995). Between 10,240 and 16,384 scans were accumulated per spectrum.



In addition to CP/TOSS experiments, spectra showing signals from non-protonated carbons and mobile groups, like rotating  $\text{CH}_3$ , were generated using  $^{13}\text{C}$  CP/TOSS with 40  $\mu\text{s}$  dipolar dephasing (Opella and Frey 1979; Hatcher 1987). Between 10,240 and 32,768 scans were collected per spectrum.

In order to separate the signals of anomeric carbons (O-C-O) from those of aromatic carbons, both of which resonate between 90 and 120 ppm, the aromatic carbon signals were selectively suppressed with a five-pulse  $^{13}\text{C}$  chemical-shift anisotropy (CSA) filter with a CSA-filter time of 40 – 47  $\mu\text{s}$  (Mao and Schmidt-Rohr 2004). For BS samples, the CSA-filter technique was combined with dipolar dephasing to isolate signals from deprotonated and highly mobile aliphatics. The CSA-filter was also combined with a short CP (50  $\mu\text{s}$ ) to isolate protonated aliphatics; 12,288 scans were collected per spectrum.

For BS samples, the combined spectrum of  $\text{CH}_2$ , CH, and residual  $\text{CH}_3$  were obtained with good sensitivity in a simple spectral editing experiment. First, a CP/TOSS spectrum was recorded using a short CP of 50  $\mu\text{s}$  (10,240 scans), which shows predominantly protonated carbons in immobile segments; however, residual peaks of quaternary carbons also result from two-bond magnetization transfer. Therefore, a second CP/TOSS spectrum is recorded using a short CP of 50  $\mu\text{s}$  and 40  $\mu\text{s}$  dipolar dephasing (10,240 scans), which contains only the residual signal from quaternary carbons and mobile segments (including  $\text{CH}_3$  groups with > 50% efficiency). The difference of the two spectra provided the spectrum of immobile  $\text{CH}_2$  and CH carbons, with a minor  $\text{CH}_3$  contribution (Mao et al. 2007a).

Analytical uncertainty was estimated for each of the NMR integrals based on the signal to noise ratio. The maximum calculated standard deviation, based on the inverse relationship between signal to noise ratio and relative standard deviation, is reported for each of the spectra.

*Fourier transform infrared spectroscopy* – Samples were freeze-dried and introduced as KBr disks. The KBr was combusted (24 h, 450 °C) prior to use. KBr windows were prepared and spectra were obtained following the procedures in Abdulla et al. (2010) using a Nicolet 370 FTIR spectrometer with a DTGS detector and a purge gas generator (resolution =  $4 \pm 1 \text{ cm}^{-1}$ ; Happ-Genzel apodization). Second-derivative spectra were obtained using the second-order Savitzky-Golay method as described in Abdulla et al. (2010) and the  $1900\text{-}900 \text{ cm}^{-1}$  (carboxyl) region of the spectrum was de-convoluted using Voigt line-shape fitting (Griffiths and De Haseth 2007; Abdulla et al. 2010).

## RESULTS

*Radiometry, temperature, pH, and dissolved oxygen* – The light output of the solar simulator was stable over the course of the experiment (BS irradiation: mean =  $48.3 \text{ (n = 42)}$ , max =  $49.1$ , min =  $46.7 \text{ } \mu\text{W cm}^{-2} \text{ nm}^{-1}$ ; FD irradiation: mean =  $46.3 \text{ (n = 23)}$ , max =  $48.1$ , min =  $44.8 \text{ } \mu\text{W cm}^{-2} \text{ nm}^{-1}$ ; Table 5). The temperature of the irradiated samples was  $33 \pm 2^\circ\text{C}$  during both experiments. The air temperature adjacent to the dark controls was slightly cooler ( $28 \pm 1^\circ\text{C}$ ). The initial FD sample pH was  $\sim 3.8$ , and after increasing to  $\sim 5.4$  during the first 14 days, the pH increased gradually to  $5.6$  by the end of the 89 day

irradiation (Fig. 15A). Dissolved oxygen decreased rapidly at the onset of the light exposure. At no time did the samples drop below 45% oxygen saturation (Fig. 15B).

*UV-vis spectroscopy and DOC* – During the experiment, the UV-visible absorption decreased across all wavelengths (Figs. 16A and 16B). All spectra were approximated by exponential curves (equation 3) and  $\ln(a.)$  exhibited an approximately-linear trend with respect to wavelength (Figs. 17A and 17B). The first-derivative absorption spectra (Figs. 16C and 16D) exhibited pronounced minima at ~274 nm and increased (becoming less negative) with increasing wavelength. The second-derivative absorption spectra and second-derivative natural log absorption spectra (Figs. 16E, 16F, 17E, and 17F) have pronounced minima at  $265 \text{ nm} \pm 2 \text{ nm}$ ,  $300 \text{ nm} \pm 4 \text{ nm}$ ,  $345 \text{ nm} \pm 1 \text{ nm}$ , and  $360 \text{ nm} \pm 2 \text{ nm}$ . The percentage of absorption coefficient lost (% photobleached) is plotted as a function of wavelength in Figs. 16G and 16H. During the first ten days, CDOM absorption was preferentially bleached at ~340 nm (the highest output from the UV solar simulator), although the loss of color became more general by the end of the irradiation (Figs. 16G and 16H). Non-irradiated samples exhibit a broad maximum in spectral slope at 360-390 nm (Figs. 17C and 17D). During the course of the irradiation, the spectral slope increased at wavelengths shorter than 310 nm and decreased at wavelengths longer than 320 nm (Fig. 17C and 17D). After more than 32 days of irradiation, a distinct  $S_x$  maximum developed at ~279-285 nm and a distinct minimum developed near 340 nm (Figs. 17C and 17D).

The BS sample contained considerably more DOC and CDOM than the FD sample (Figs. 16 and 18; Table 5). Approximately 25% of the DOC in the BS sample

Table 5. Summary of the conditions measured during the irradiation experiment.

ND=not determined.

Sample	Irr. Time (days)	Average Irradiance at 340 nm ( $\mu\text{W cm}^{-2} \text{ nm}^{-1}$ )	Sample pH	Average Sample Temp. ( $^{\circ}\text{C}$ )	$a_{300}$ ( $\text{m}^{-1}$ )	DOC ( $\text{mg C L}^{-1}$ )	$S_{275-295}$ ( $\text{nm}^{-1}$ )
BS-0d	0	0	3.21	28.1	692.2	120.7	0.0133
BS-3d	3	47.0	3.28	33.7	572.0	110.2	0.0148
BS-10d	10	47.3	3.34	33.8	446.6	94.9	0.0156
BS-29d	29	48.1	ND	34.3	117.1	49.7	0.0148
BS-52d	52	48.0	ND	33.4	16.8	37.2	0.0253
BS-110d	110	48.3	ND	33.7	8.4	30.4	0.0293
FD-0d	0	0	3.77	28.4	279.2	51.1	0.0134
FD-11d	11	45.2	4.74	33.1	108.2	16.3	0.0156
FD-21d	21	45.8	5.41	33.0	44.7	9.6	0.0166
FD-32d	32	46.1	5.49	32.9	27.3	8.2	0.0125
FD-56d	56	46.1	5.57	33.1	15.9	5.4	0.0260
FD-89d	89	46.3	5.59	32.8	11.9	4.6	0.0255

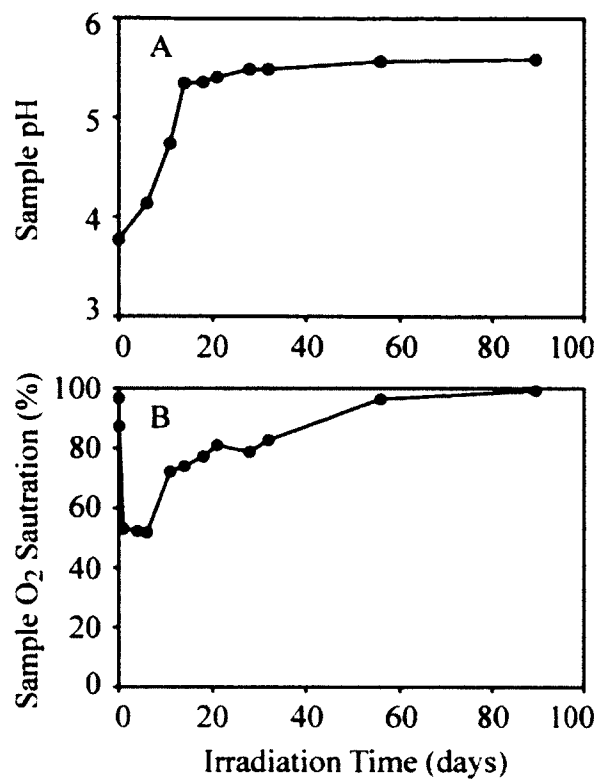


Fig. 15. (A) Sample pH, and (B) dissolved oxygen saturation measured for FD samples during irradiation.

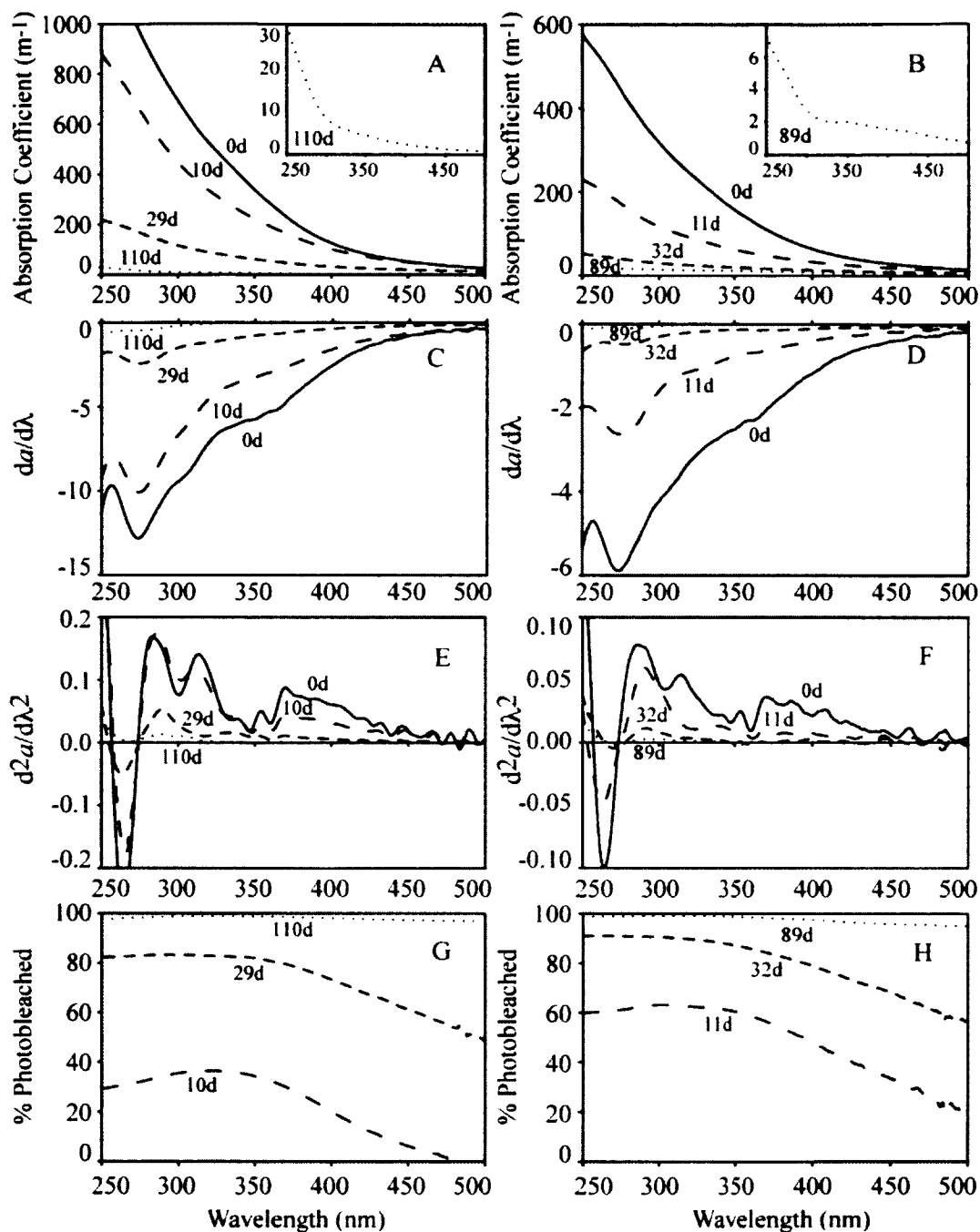


Fig. 16. (A) Ultraviolet – visible spectra of BS and (B) FD sub-samples collected over the course of the irradiation experiments. (C) First-derivative spectra for BS and (D) FD samples. (E) Second-derivative spectra for BS and (F) FD samples. (G) Photobleaching represented as a percentage of initial absorption for BS and (H) FD samples.

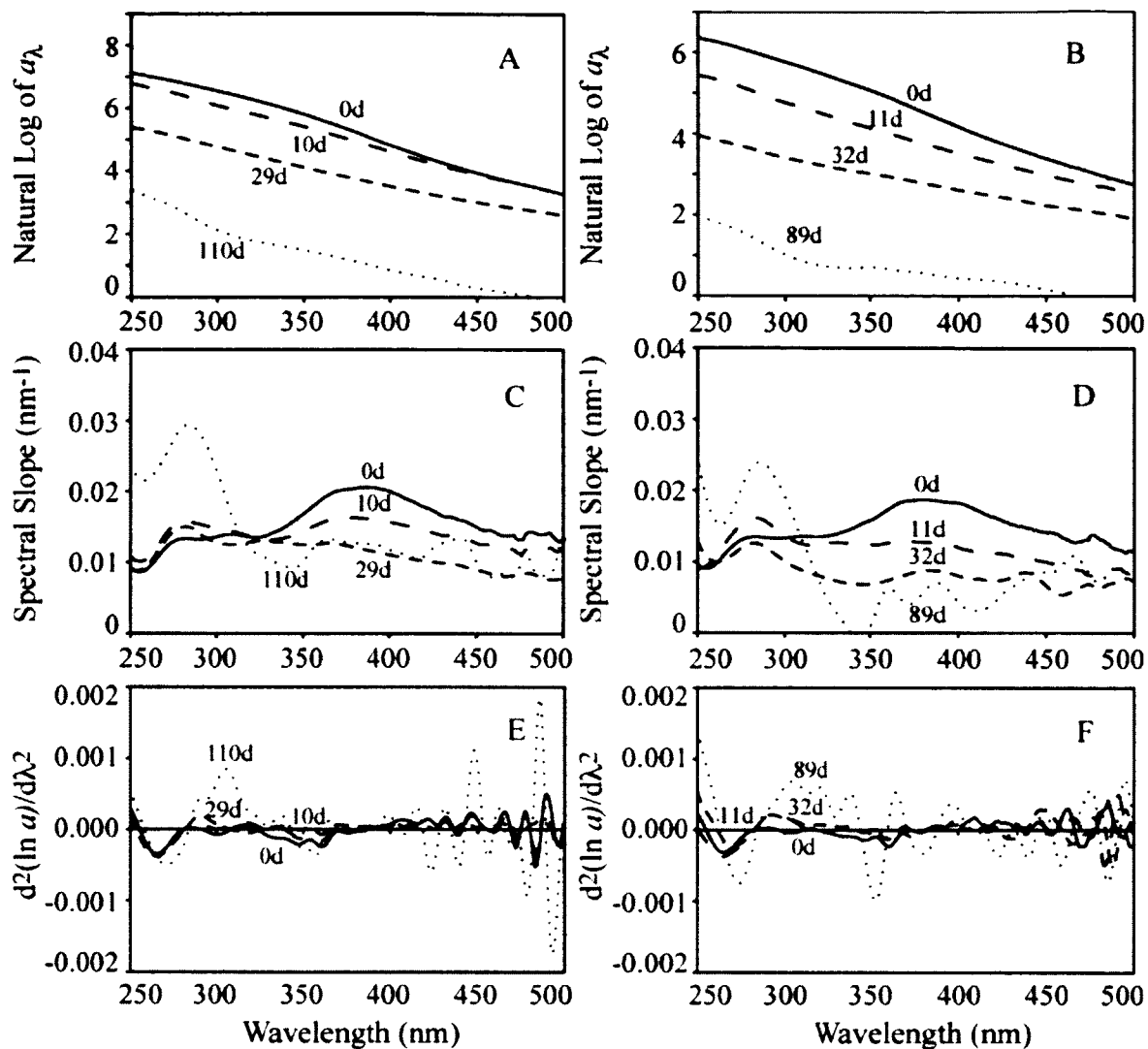


Fig. 17. (A) Natural log linearized spectra for BS and (B) FD samples. (C) Spectral slope was calculated over 21nm intervals for BS and (D) FD samples. (E) Second-derivative natural log spectra for BS and (F) FD samples.

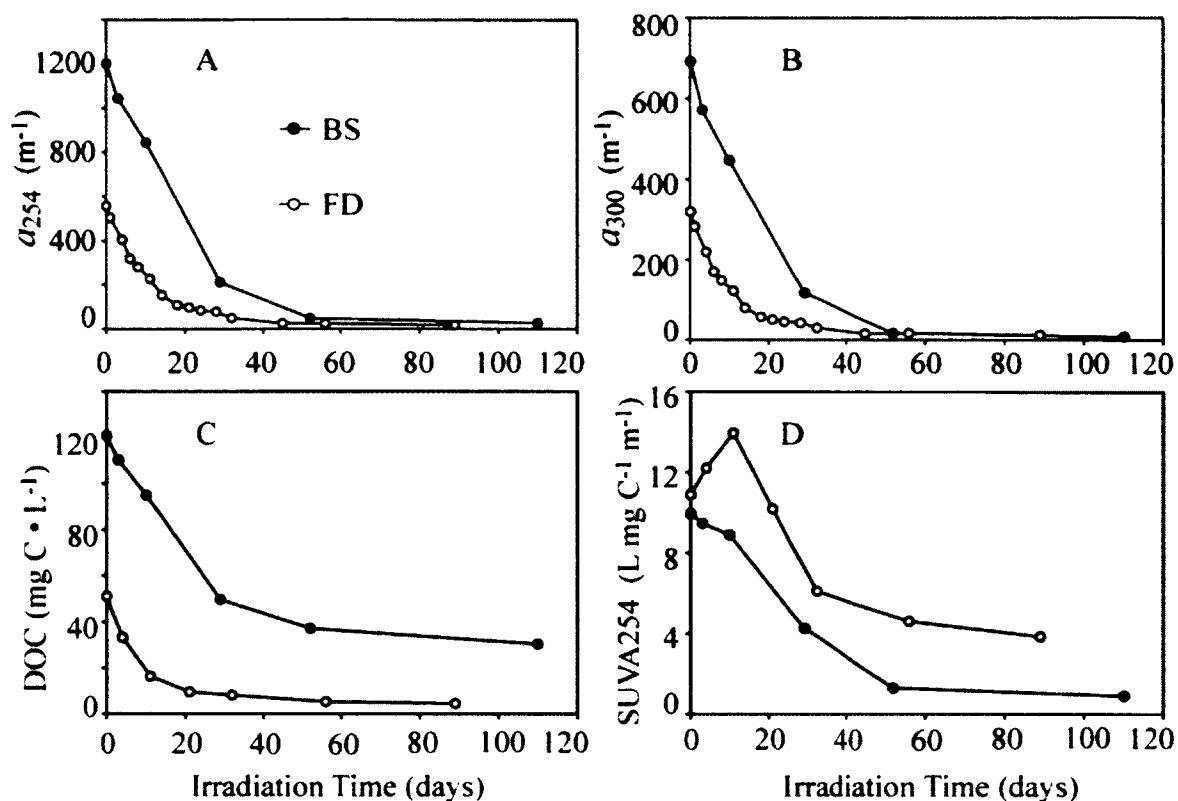


Fig. 18. Absorption coefficients measured at (A) 254 nm ( $a_{254}$ ) and (B) 300 nm ( $a_{300}$ ) decreased during the course of the irradiation experiments. (C) Dissolved organic carbon also decreased. (D) Specific UV absorbance (SUVA) suggested that aromaticity of the remaining DOM decreased over the course of the irradiation. Closed circles represent data from BS sample. Open circles represent data from FD sample. Inset boxes show the same data as above, but the x-axis is in terms of absorbed photons.



did not photochemically degrade, whereas 99% of the absorption at 300 nm was removed after 110 days. In the FD sample, 91% of its initial DOC was lost after 89 days of irradiation, while about 96% of its initial  $a_{300}$  was removed after 89 days. SUVA<sub>254</sub> showed similar long-term trends for the two irradiated samples, though the SUVA<sub>254</sub> values for the FD samples were consistently higher than the BS samples (Fig. 18D).  $S_{300-700}$  (Fig. 19A) and  $S_{350-400}$  (Fig. 19C) decreased during the course of the irradiation, while  $S_{275-295}$  (Fig. 19B) and  $S_R$  (Fig. 19D) increased. Fig. 18 insets depict the same trends plotted using absorbed light dose as the x-axis.

*Fluorescence* – Peak A ( $\lambda_{ex}$ =~260nm;  $\lambda_{em}$ = 380-460 nm) was the most intense peak in all fluorescence EEMS. The wavelength of the emission maximum of this peak shifted during the course of the irradiation from ~450 nm to ~415 nm (Fig. 20; Table 6). The intensity of Peak A also decreased during the course of the irradiation (Table 6). Peak C ( $\lambda_{ex}$ =~350 nm;  $\lambda_{em}$ = 420-480 nm) also underwent a significant decrease in intensity throughout the irradiation. Both  $\lambda_{ex}$  and  $\lambda_{em}$  maxima of peak C shifted during irradiation to a position that is usually referred to as Peak M ( $\lambda_{ex}$ =~312nm;  $\lambda_{em}$ = 380-420 nm; Fig. 20; Table 6). Fluorescence intensity in the Peak B ( $\lambda_{ex}$ =~275 nm;  $\lambda_{em}$ = ~310 nm) and Peak T ( $\lambda_{ex}$ =~275 nm;  $\lambda_{em}$ = ~340 nm) regions were low intensity and/or not well resolved from the larger peaks (Table 6). Only a small fraction of the original fluorescent signal remained in the samples at the end of the irradiation. Peak C of the BS-110 sample contained 0.8% of the signal measured for BS-0 while Peak C of the FD-89 sample was about 2.5% of FD-0 (Table 6).

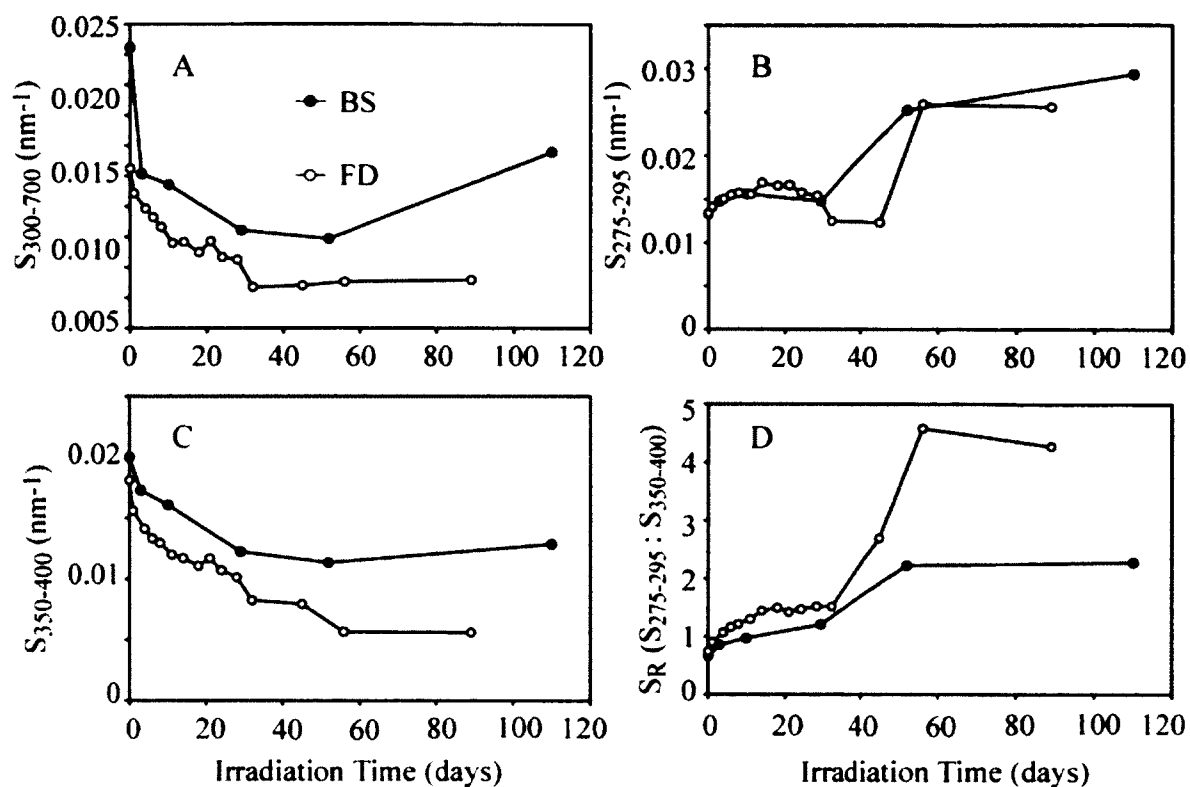


Fig. 19. Spectral slopes calculated for the range of (A) 300 – 700 nm decreased during irradiation. Spectral slopes calculated for (B) 275 – 295 nm increased and, spectral slope in the range of (C) 350-400 nm decreased during irradiation. As a result, (D) slope ratio ( $S_R$ ) increased.

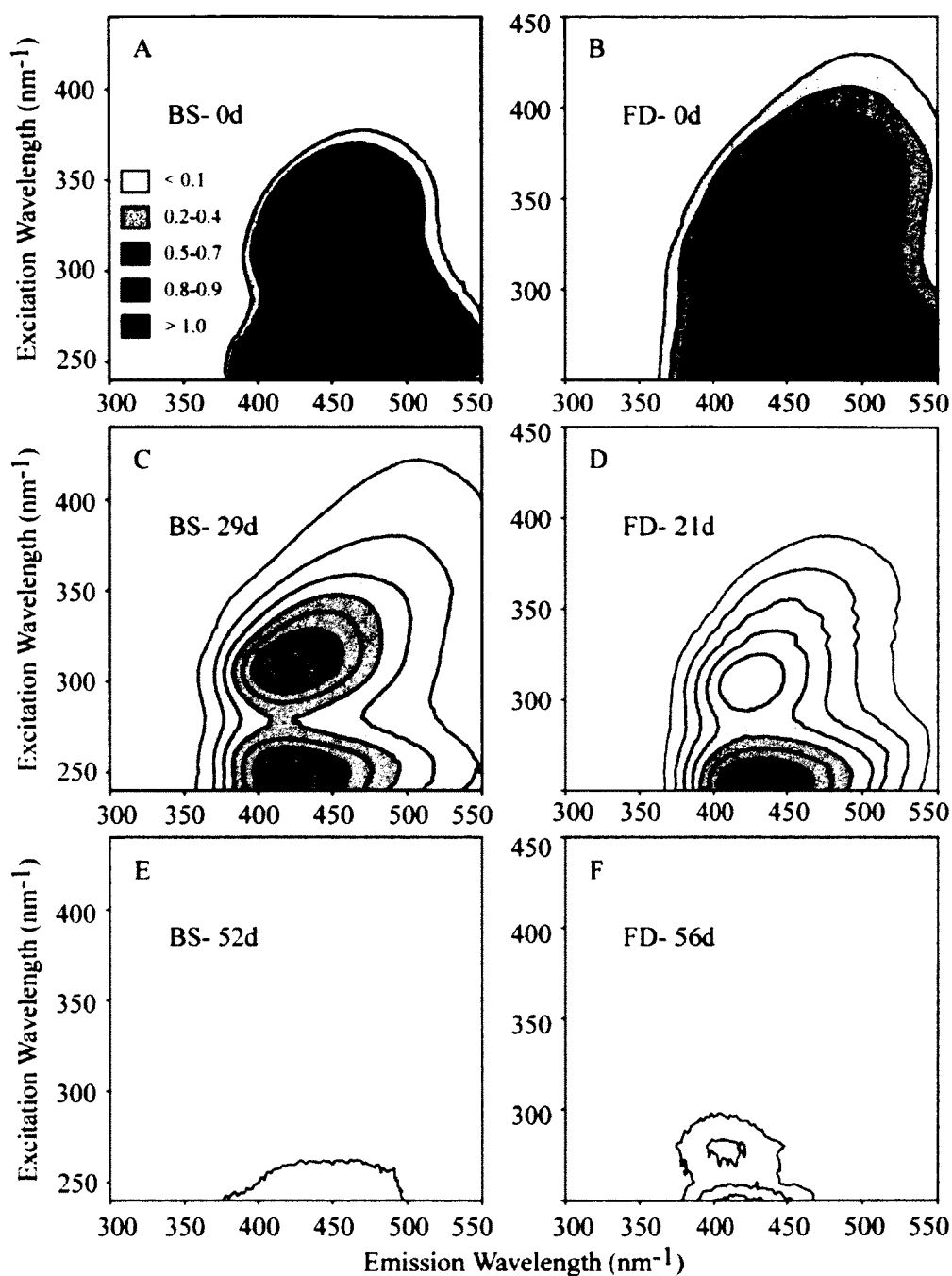


Fig. 20. Fluorescence excitation emission matrices shown for (A) BS-0d, (B) FD-0d, (C) BS-10d, (D) FD-11d, (E) BS-52d, and (F) FD-56d. All samples were diluted to  $a_{450} = 5 \text{ m}^{-1}$ . Peak locations: A $\approx$ 250ex/450em, C $\approx$ 345ex/445em, M $\approx$ 310ex/410em, B $\approx$ 275ex/310em, T $\approx$ 275ex/340em.

Table 6. Spectral components of fluorescence excitation emission matrix spectra.

Intensities have been normalized to the area under the water Raman peak and corrected for dilution.

	BS 0d	BS 3d	BS 29d	BS 110d	FD 0d	FD 11d	FD 21d	FD 56d	FD 89d
<b>Peak A</b>									
(WRU)	1.14	0.478	0.418	0.018	0.982	0.476	0.224	0.041	0.038
$\lambda_{\text{ex}}$ max (nm)	255	254	240	240	250	250	250	250	250
$\lambda_{\text{em}}$ max (nm)	456	458	424	412	450	430	428	414	412
<b>Peak C</b>									
(WRU)	0.727	0.321	0.245*	0.006*	0.668	0.305	0.144*	0.020*	0.017*
$\lambda_{\text{ex}}$ max (nm)	325	320	320	320	330	320	320	320	325
$\lambda_{\text{em}}$ max (nm)	442	446	430	430	444	432	430	420	420
<b>Peak M</b>									
(WRU)	0.572*	0.258*	0.273	0.006*	0.508*	0.304*	0.145	0.027	0.023
$\lambda_{\text{ex}}$ max (nm)	310	310	305	310	310	305	305	290	290
$\lambda_{\text{em}}$ max (nm)	410	410	410	410	410	410	410	396	398
<b>Peak B</b>									
(WRU)	0.021*	0.020*	0.017	0.018	0.018*	0.018*	0.018	0.017	0.017
$\lambda_{\text{ex}}$ max (nm)	275	275	270	275	270	275	275	275	275
$\lambda_{\text{em}}$ max (nm)	316	316	314	312	316	316	316	316	314
<b>Peak T</b>									
(WRU)	0.148*	0.067*	0.040*	0.007*	0.103*	0.049*	0.033*	0.019*	0.017
$\lambda_{\text{ex}}$ max (nm)	270	270	270	270	270	270	275	280	280
$\lambda_{\text{em}}$ max (nm)	360	360	360	348	360	360	360	360	346

\* Not clearly resolved from adjacent peaks or background.

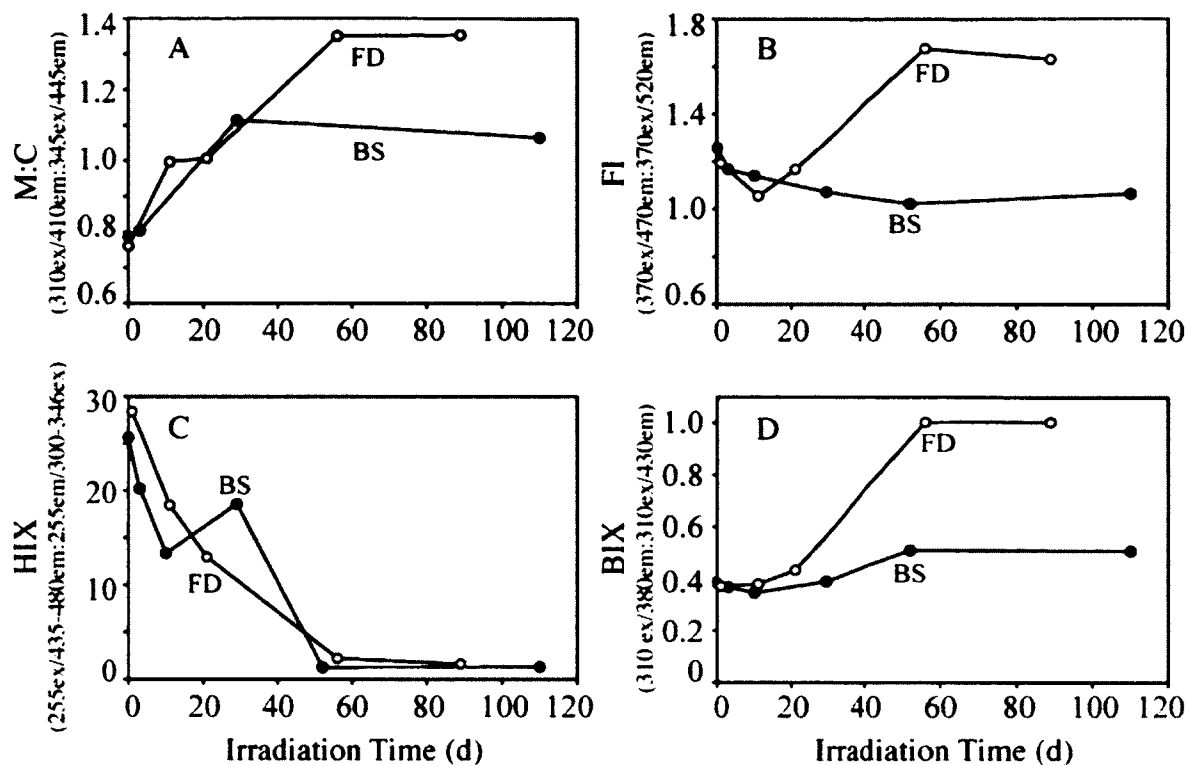


Fig. 21. (A) EEMS Peak M to Peak C ratio (M:C), (B) McKnight fluorescence index (FI), (C) fluorescence humification index (HIX), and (D) biological fluorescence index (BIX) calculated for samples from the irradiation experiments.

Taking the ratio of Peak M intensity to Peak C intensity (M:C) provides a way of comparing spectra from different environments and different photochemical histories (Burdige et al. 2004; Para et al. 2010; Romera-Castillo et al. 2011). FD and BS samples started out with very similar M:C ratios of 0.76 and 0.78 respectively, and increased during the irradiation (Fig. 21A). FD-89d had the highest M:C value at 1.35. For comparison, Pacific Ocean DOM samples (see Chapter IV) yielded M:C values ranging from 1.13 to 1.21.

The FI (McKnight fluorescence index) of the BS samples decreased with increasing irradiation time from 1.09 to 0.88, whereas FI for FD samples increased from 1.19 to 1.63 (Fig. 21B). HIX (humification index) decreased during irradiation for both samples (Fig. 21C) from 25 (BS) and 28 (FD) to 1.3 and 1.6 respectively. Values of BIX (biological fluorescence index) for the BS sample increased from 0.38 to 0.58, while BIX for the FD increased from 0.37 to 1.0 during the irradiation (Fig. 21D).

*Lignin phenols* – The concentration of dissolved lignin decreased rapidly upon irradiation (Table 7). During the 110-day irradiation,  $\Sigma_8$  decreased from an initial concentration of 508 to  $1.35 \mu\text{g L}^{-1}$ , a 99.7% decrease, while  $\Lambda_8$  decreased by ~99% from 0.42 to 0.004 mg lignin mg C<sup>-1</sup>. After the first 10 days of irradiation, the concentrations of index phenols were at or near their limits of detection resulting in larger uncertainties for (Ad/Al)<sub>s</sub>, (Ad/Al)<sub>v</sub> and S/V and C/V ratios for the longer irradiation times. During the initial 10 days of the irradiation, Ad/Al increased for both syringyl and vanillyl phenols, while S:V and C:V ratios decreased.

Table 7. Summary of CuO oxidation lignin phenol results.

Sample	Irr. Time (days)	$\Sigma_8$ ( $\mu\text{g L}^{-1}$ )	$\Lambda_8$ (mg mgOC <sup>-1</sup> )	(Ad/Al) <sub>s</sub>	(Ad/Al) <sub>v</sub>	S:V	C:V
BS-0d	0	507.50	0.420	1.17	1.37	0.27	0.09
BS-3d	3	256.82	0.233	1.56	1.63	0.21	0.08
BS-10d	10	168.10	0.177	1.97	1.94	0.19	0.06
BS-29d	29	4.76*	0.010*	0.42*	11.36*	0.11*	0.17*
BS-52d	52	1.74*	0.005*	0.50*	14.06*	0.15*	0.19*
BS-110d	110	1.35*	0.004*	0.69*	2.18*	0.15*	0.36*

\*these values may be inaccurate, as the index phenols were measured near their detection limits in these three samples.

*Solid-state  $^{13}\text{C}$  NMR and FTIR spectroscopy* – Prior to irradiation, solid-state CP/TOSS  $^{13}\text{C}$  NMR spectra indicate that Dismal Swamp DOM (Figs. 22A and 23A) included significant amounts of aromatic carbon (100 – 160 ppm). After exposure to UV radiation, signals from 100 – 160 ppm (aromatic carbons) and 187 – 220 ppm (carbonyl carbons) decreased (Table 8), while signals from 0 – 100 ppm (alkyl and O-alkyl carbons) increased.

Data for BS-29d, BS-52d and BS-110d are shown in Table 8. Addition of sodium hydroxide to these samples led to the trapping of significant amounts of low molecular weight organic acids and bicarbonate. This can be seen in the spectrum for BS-52 in Fig. 23D by the sharp peaks at 27 ppm (mobile  $\text{CH}_3$ ), 166 ppm (bicarbonate carbons), and 183 ppm (carboxyl carbons). Methyl carbons ( $\sim 27$  ppm  $^{13}\text{C}$ ,  $\sim 2.5$  ppm  $^1\text{H}$ ) show significant correlation with carboxyl carbons ( $\sim 183$  ppm  $^{13}\text{C}$ ,  $\sim 2.5$  ppm  $^1\text{H}$ ; Fig. 23D). FD samples irradiated longer than 32 days were not analyzed using NMR, because at 32 days 84% of the DOC was lost. Based on prior studies (Spencer et al. 2009; Stubbins et al. 2010) further irradiation was considered unlikely to degrade sufficient additional DOC to observe significant structural differences and leave sufficient material to analyze by NMR.

$^{13}\text{C}$  NMR spectra obtained using signal editing pulse sequences elucidated additional aspects of DOM composition. Comparing the CSA-filtered spectrum (Fig. 22 dashed lines) and the CP/TOSS spectrum (Fig. 22 solid black line) provided the percentage of signal from anomeric carbons (O-C-O) in the 100-115 ppm region, where it overlaps with the signal from aromatic carbons. Anomeric carbons represented  $\sim 78\% \pm 2\%$  of the signal in the 100-115 ppm region of the FD-0d spectrum,  $\sim 86\% \pm 2\%$  in the



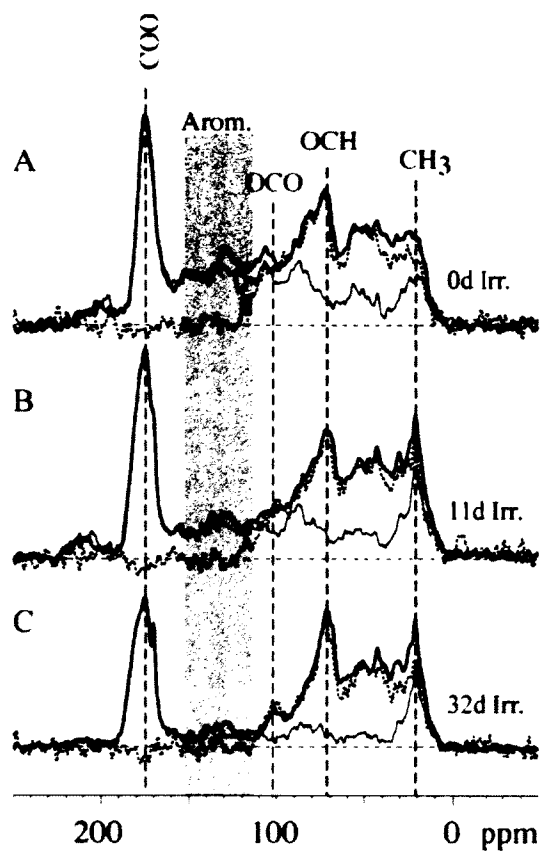


Fig. 22. CP/TOSS spectra obtained from the FD samples (black lines). CP/TOSS spectra with 40  $\mu$ s dipolar dephasing (gray lines), and CP/TOSS spectra with CSA-filter (dashed lines).

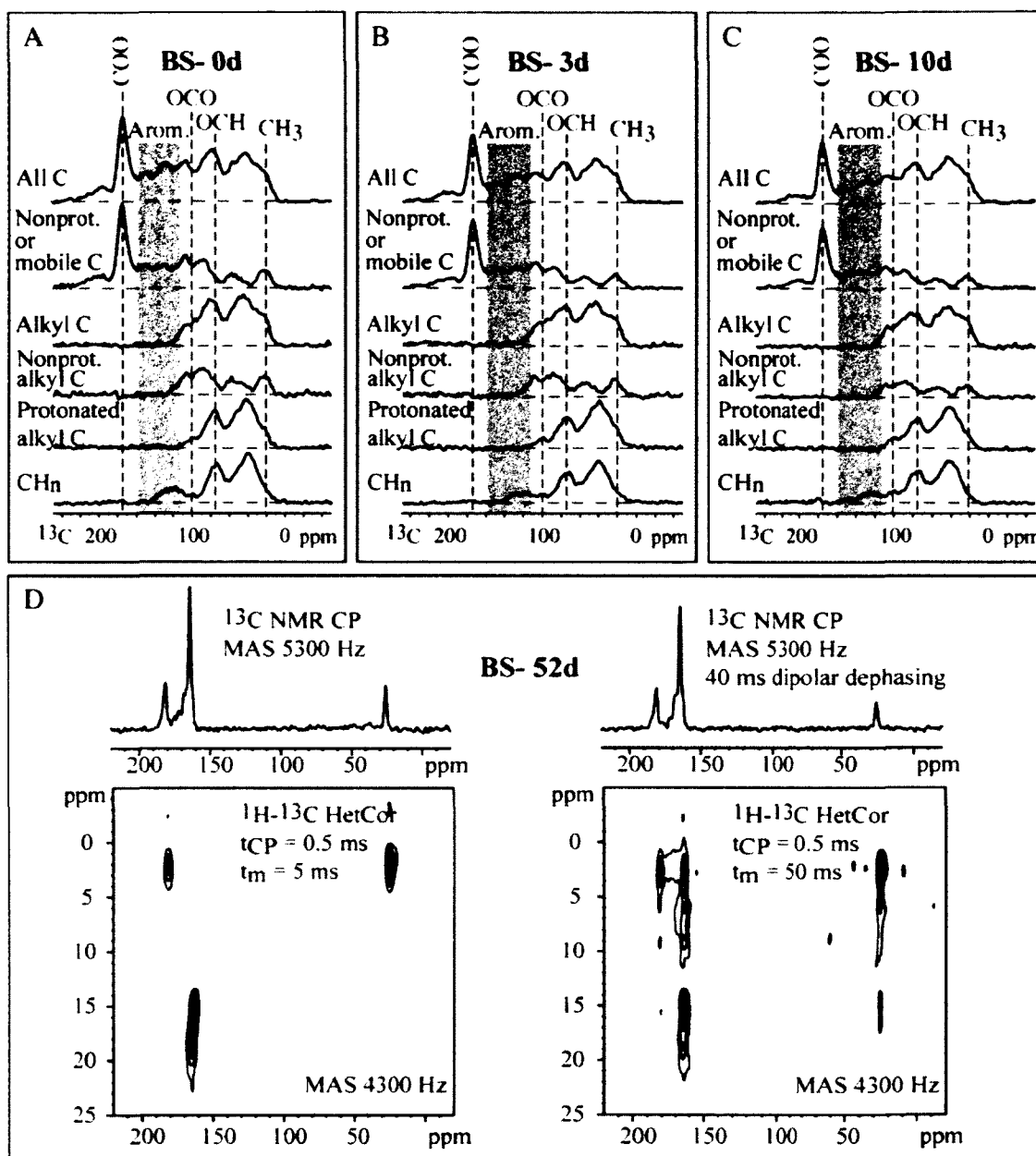


Fig. 23. Solid-state  $^{13}\text{C}$  NMR spectra obtained for (A) BS-0d, (B) BS-3d, and (C) BS-10d. All C: CP/TOSS reference spectrum. Nonprot. & mobile C: CP/TOSS with dipolar dephasing. Alkyl C: CP/TOSS with CSA-filter. Nonprot. alkyl C: CP/TOSS with CSA-filter and dipolar dephasing. Protonated alkyl C: CP/TOSS with short CP (0.05 ms) and CSA-filter.  $\text{CH}_n$ : CP/TOSS with  $\text{CH}_n$  selection. (D) CP/TOSS and  $^1\text{H}$ - $^{13}\text{C}$  2D-HETCOR spectra for BS-52d sample that was amended with NaOH.

Table 8. Integrated area from  $^{13}\text{C}$  CP/TOSS NMR spectra for BS and FD samples (total area = 100%), and the assigned structural moieties associated with the spectral region. BS-29d, BS-52d, and BS-110d are also shown with acetate and bicarbonate peaks excluded (labeled no  $\text{HCO}_3$ ). Maximum uncertainty is based on signal to noise ratio and reported as one standard deviation.

Functional Groups	Integration range (ppm)	BS-0d	BS-3d	BS-10d	FD-0d	FD-11d	FD-32d
$\text{CH}_3$	0-28	5.9	6.9	7.8	9.0	12.7	13.5
$\text{CH}_2$	28-35	4.1	4.7	5.3	3.9	5.1	5.4
$\sim\text{CH}$	35-50	10.2	11.7	13.1	9.4	10.6	12.1
$\text{NCH}+\text{OCH}_3+\text{OCH}_2$	50-65	7.5	8	8.5	8.4	9.5	10.8
Carbohydrate-like C	65-100	20.8	20.6	22.2	23.1	22.0	24.0
O-C-O*	100-115	4.4	5.6	4.9	5.4	4.3	3.2
Arom. C-C-O*	100-115	3.5	1.9	2.6	1.5	0.7	0.4
Arom.**	115-145	4.1	2.2	2.2	2.1	1.3	1.1
Arom. C-O**	145-160	1.7	0.9	0.8	0.8	0.5	0.4
Deprot. Arom.**	115-160	14.4	15.1	12.4	14.5	8.7	5.4
$\text{COO} + \text{NC}=\text{O}$	160-187	18.2	17.8	16.3	19.0	22.0	22.0
Carbonyl C	187-220	5.1	4.6	3.9	2.9	2.6	1.7
Max. Uncertainty (s.d.)		0.5	0.4	0.4	0.8	0.5	0.7
<u>NaOH Added During Irradiation</u>							
Functional Groups	Integration range (ppm)	BS-29d	BS-52d	BS-110d	BS-29d no $\text{HCO}_3$	BS-52d no $\text{HCO}_3$	BS-110d no $\text{HCO}_3$
$\text{CH}_3$	0-28	8.7	9.3	18.6	9.7	12.8	12.7
$\text{CH}_2$	28-35	5.0	2.3	6.2	3.5	4.5	4
$\sim\text{CH}$	35-50	4.5	4.0	5.8	14.9	17.5	20.6
$\text{NCH} + \text{OCH}_3 + \text{OCH}_2$	50-65	3.0	2.4	2.9	11.2	10.5	9.7
Carbohydrate-like C	65-100	6.3	3.7	4.7	21.5	16.4	17.5
O-C-O + Arom. C-C-O	100-115	0.8	0.9	0.9	3	4.4	3.1
Aromatic C	115-145	2.6	2.8	2	9.3	11.5	7.3
Aromatic C-O	145-160	0.7	2.1	0.4	2.4	9.3	1.3
$\text{COO} + \text{NC}=\text{O}$	160-187	66.5	72.4	58.2	21.1	13	23.1
Carbonyl C	187-220	1.8	0	0.3	3.6	0	0.7
Max. Uncertainty (s.d.)		0.8	0.8	1.0	N/D	N/D	N/D

\*Adjusted based on CSA-filtered CP/TOSS spectrum.

\*\*Adjusted based on CP/TOSS spectrum with 40 $\mu\text{s}$  dipolar dephasing.

FD-11d spectrum, and  $\sim 89\% \pm 3\%$  in the FD-32d spectrum. Spectra collected using dipolar dephasing (Fig. 22 gray lines), showed that aromatic carbons (115-165 ppm) in the FD-0d and FD-11d samples were  $\sim 83\% \pm 4\%$  protonated, while aromatic carbons in the FD-32d sample were  $\sim 78\% \pm 3\%$  protonated.

Normalizing NMR integration data (Table 8) to DOC concentrations (Table 5), provides an estimate of the concentration of major functional groups in units of  $\mu\text{mol C L}^{-1}$  (Table 9). Anomeric carbons appear to have increased during the first 3 days of the irradiation of the BS sample, and aliphatic carbons appeared to increase during the first 10 days of the irradiation (Table 9). Phenolic carbons (145-160) were the most photochemically labile structural moieties, while aliphatic carbons (0-35ppm) were the least photochemically reactive organic species (Tables 8 and 9).

FTIR spectra for the irradiated FD samples (Fig. 24) show that a fraction of carbohydrate-like DOM ( $\sim 1100\text{ cm}^{-1}$ ) is preferentially preserved along with aliphatic DOM ( $\sim 1450\text{ cm}^{-1}$ ). The IR signals from carboxyl carbons ( $\sim 1900\text{-}1500\text{ cm}^{-1}$ ) decreased with irradiation. Fig. 25 shows the partially de-convoluted carboxylic region of the FTIR spectra. By combining information from the de-convoluted FTIR spectra, solid-state  $^{13}\text{C}$  CP/TOSS NMR spectra, and DOC measurements for each of the FD samples (after Abdulla et al. 2010), semi-quantitative estimates of carboxylic acid, carboxylate, metal associated carboxylate, amide, and carboxylic ester functional groups were calculated (Table 10). Carboxylic acids, carboxylate ions, and metal associated carboxyl groups decreased in concentration during irradiation (Fig. 26A), as did esters, while the concentration of amide groups remained constant throughout the experiment (Fig. 26B).

Table 9.  $^{13}\text{C}$  CP/TOSS integration data normalized to DOC concentration in units of  $\mu\text{mol C L}^{-1}$ .

Functional Groups	Integration range (ppm)	BS-0d	BS-3d	BS-10d	FD-0d	FD-11d	FD-32d
$\text{CH}_3$	0-28	593	634	617	383	173	92.2
$\text{CH}_2$	28-35	412	432	419	166	69.4	36.9
$\sim\text{CH}$	35-50	1030	1070	1040	400	144	82.6
$\text{NCH} + \text{OCH}_3 + \text{OCH}_2$	50-65	754	735	672	358	129	73.7
Carbohydrate-like C	65-100	2090	1890	1750	984	300	164
O-C-O*	100-115	444	519	391	229	58.8	21.9
Arom. C-C-O*	100-115	350	170	202	65.2	9.3	2.7
Arom.**	115-145	415	205	176	89.4	17.9	7.7
Arom. C-O**	145-160	174	79.6	59.8	35.1	6.5	2.7
Deprot. Arom.**	115-160	1450	1390	981	617	119	36.7
$\text{COO} + \text{NC=O}$	160-187	1830	1640	1290	809	300	150
Carbonyl	187-220	513	422	308	123	35.4	11.6

\*Adjusted based on CSA-filtered CP/TOSS spectrum.

\*\*Adjusted based on CP/TOSS spectrum with  $40\mu\text{s}$  dipolar dephasing.

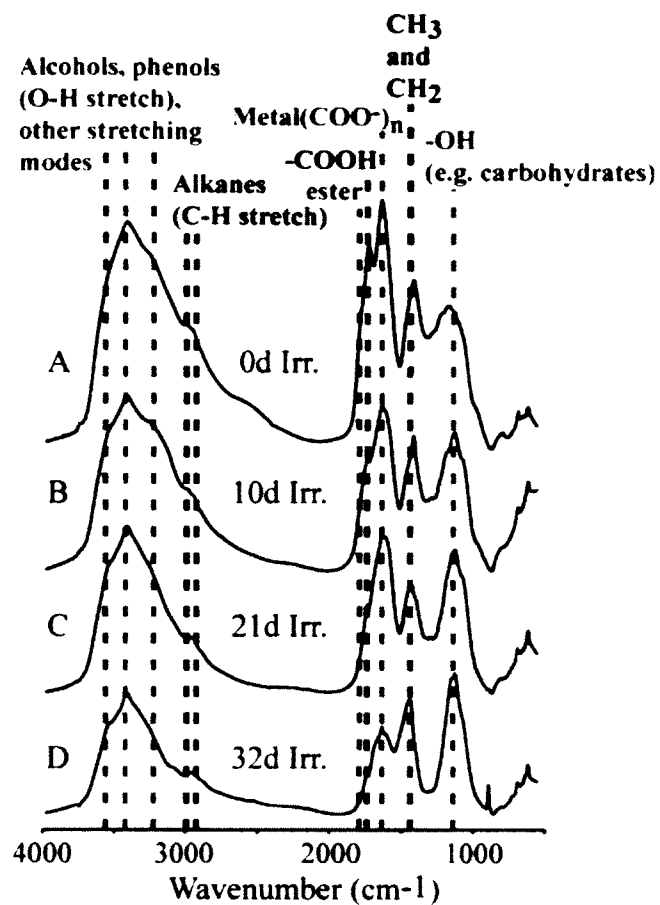


Fig. 24. Infrared (FTIR) spectra obtained for (A) FD-0d, (B) FD-11d, (C) FD-21d, and (D) FD-32d samples.

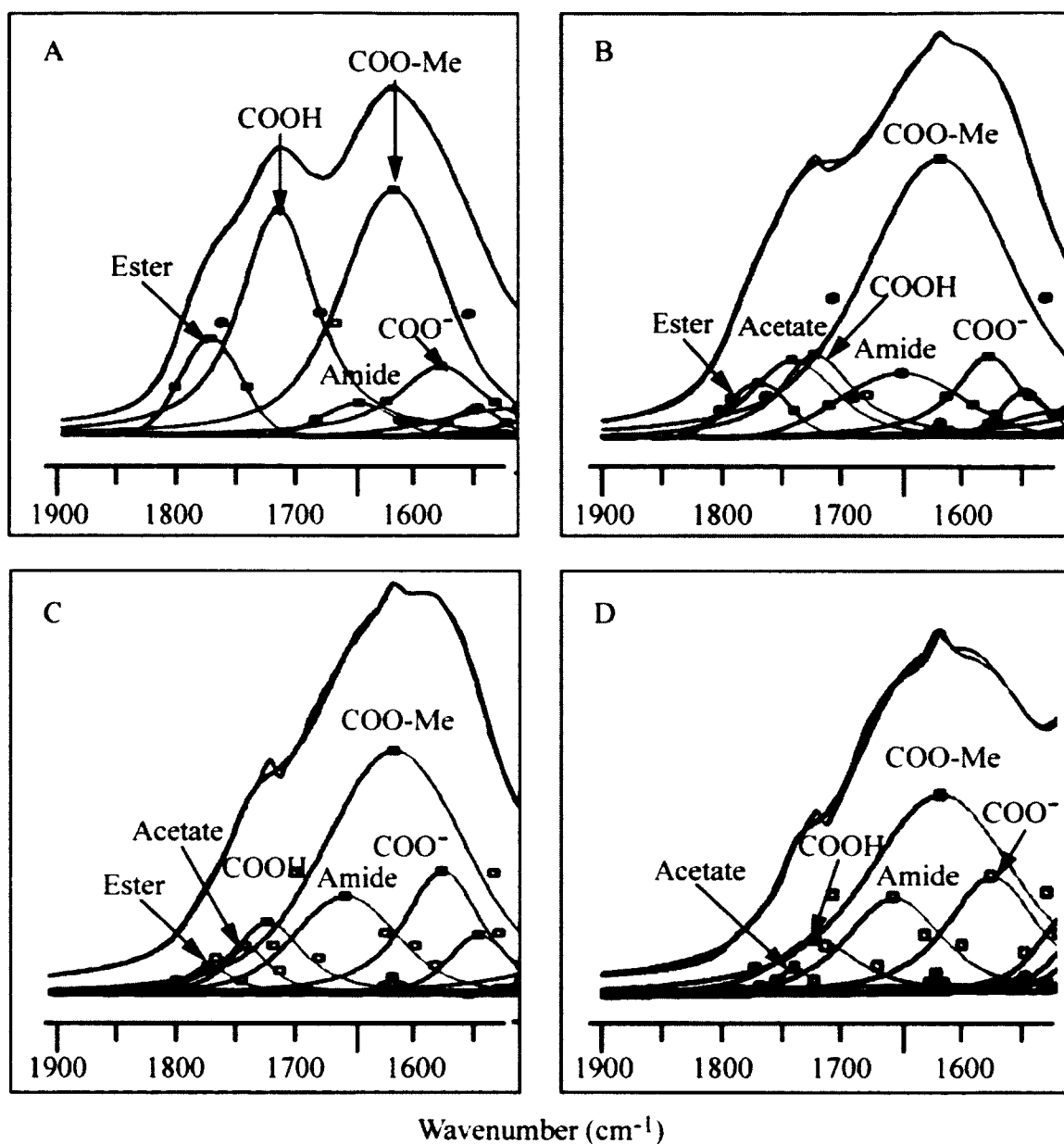


Fig. 25. De-convoluted FTIR spectra for (A) FD-0d, (B) FD-11d, (C) FD-21d, and (D) FD-32d samples. The location of the peak center for each component was identified using second-derivative spectra (not shown) as described by Abdulla et al (2010).

Table 10. Carboxyl functional groups quantified using the de-convoluted FTIR peak areas normalized to the NMR peak at 160-187 ppm and DOC concentration in units of  $\mu\text{mol C L}^{-1}$ .

	Irr. Time (days)	Ester (Lactone)	Acetate	COOH	Amide	COO- Me	COO <sup>-</sup>
	Wavenumber (cm <sup>-1</sup> )	1775	1745	1720	1650	1620	1580
FD-0d	0	72	0	279	28	284	109
FD-11d	11	12	28	30	28	172	28
FD-21d	21	5	7	16	27	91	30
FD-32	32	0.6	2	15	28	88	34



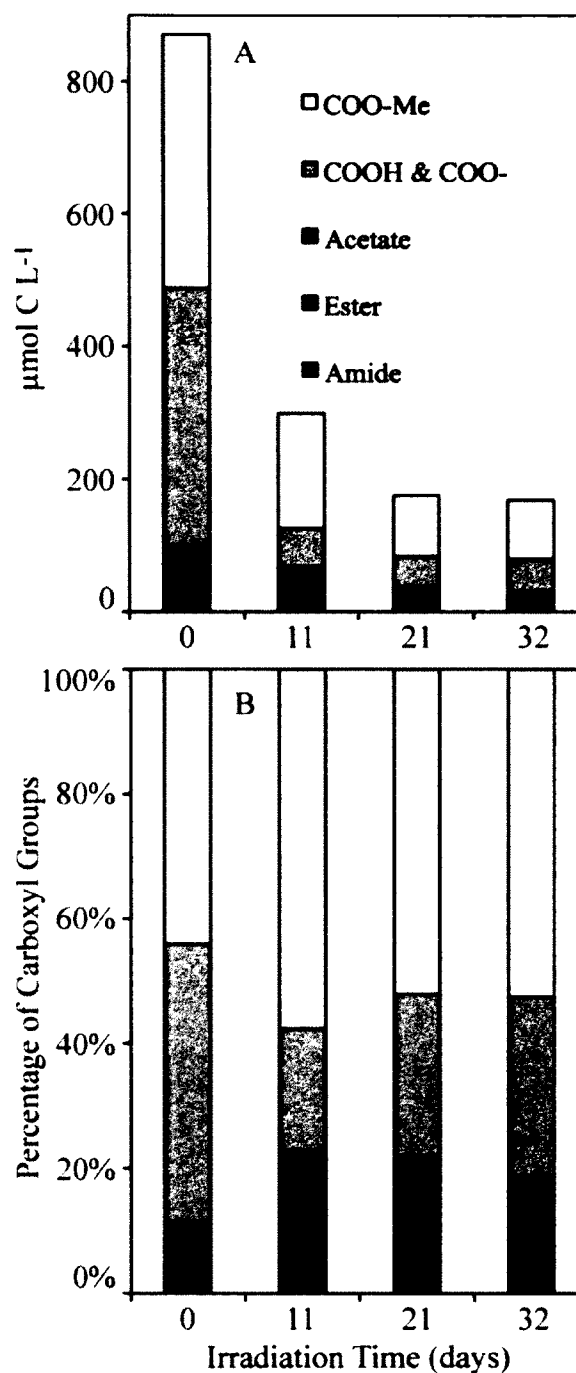


Fig. 26. Variation of metal associated carboxylate (COO-Me), carboxylic acid/carboxylate, acetate groups, carboxylic esters (including lactones) and carboxylic amides in FD samples measured during UV irradiation reported as (A) concentration in solution and (B) percentage of carboxyl groups.

*Summary of results for non-irradiated Dismal Swamp DOM* – The optical spectra recorded for the non-irradiated Dismal Swamp samples are typical of wetland-dominated high-CDOM waters, with high  $a_{300}$ , low  $S_{275-295}$ , low  $S_R$ , high SUVA<sub>254</sub>, high fluorescence at Peaks A and C, FI below 1.5, high HIX, and low BIX (Coble 1996; Kalbitz et al. 1999; McKnight et al. 2001; Weishaar et al. 2003; Helms et al. 2008; Huguet et al. 2009). Prior to irradiation, the BS sample contained high concentrations of lignin phenols (Table 7; Spencer et al. 2009). The NMR (Figs. 22A and 23A) and FTIR (Fig. 25A) spectra presented for the Non-irradiated Dismal Swamp DOM are similar to those recently published (Abdulla et al. 2010).

## DISCUSSION

*Characterization of non-irradiated Dismal Swamp DOM* – Non-irradiated Dismal Swamp DOM displays broad overlapping NMR signals from ~5 ppm to ~165 ppm with a distinct peak in the carboxyl region at ~175 ppm. The relatively large signal observed in the aromatic region (100-165 ppm; Figs. 22A and 23A; Table 9) is consistent with the high lignin phenol concentration (Table 7), with the high absorbance in the 250-300 region, high SUVA<sub>254</sub> values, and low spectral slope observed in the UV-visible spectra (Figs. 16 and 17), with the high fluorescence observed at Peak A and Peak C (Figs. 20A and 20B; Table 6), and with the predominance of lignin- and tannin-like DOM observed by ultrahigh resolution mass spectrometry for Dismal Swamp water samples (Sleighter and Hatcher 2008).

The signal from nonprotonated aromatics in the dipolar dephased CP/TOSS NMR spectra (Figs. 22A and 23A) is likely due to substituted aromatic ring carbons in

polyphenolic structures (such as lignin and tannins) as well as condensed aromatic structures which arise from biomass burning such as forest fires (Mao and Schmidt-Rohr 2003; Hockaday et al. 2006). The peak at ~75 ppm in the CP/TOSS spectrum (Figs. 22A and 23A) and anomeric signal at ~100 ppm (dashed line in Fig. 22A) are likely due to high molecular weight polysaccharides that are solubilized by microbial depolymerization (Green and Highley 1997). The FTIR spectra (Figs. 25 and 26; Table 10) revealed that carboxylic acids and carboxylate ions combined accounted for ~50% of the carboxylic groups. Metal associated carboxylic acids accounted for ~37% of all carboxylic groups. Esters (~9%; e.g. cyclic lactones) and amides (~4%) accounted for the remainder of carboxylic groups.

*Photochemical degradation of Dismal Swamp DOM* – The entire CDOM pool appears to be susceptible to long-term photochemical degradation/bleaching (Figs. 16G and 16H). Long-term photobleaching resulted in a discontinuity in spectral slope in the 290-340 nm region and an increase in slope ratio ( $S_R$ ; Fig. 19D) suggesting a decrease in average CDOM molecular weight in agreement with past studies (Sarpal et al. 1995; Helms et al. 2008; Osburn et al. 2011). Similar results have been reported for irradiations carried out under natural sunlight (Sarpal et al. 1995; Helms et al. 2008). In addition to an apparent decrease in CDOM molecular weight, the observed changes in spectral shape may be attributed to selective bleaching in the 300-350 nm region where both absorbance and irradiance are abundant (Reche et al. 2000; Kieber 2007) and/or to disruption of coupled states such as charge transfer donor-acceptor pairs (Del Vecchio and Blough 2004a).

Photobleaching also caused a shift in EEMS Peak C, which is associated with terrestrial humic materials, to a position that is usually referred to as Peak M (Fig. 20; Table 6), which is associated with marine or microbially produced humic materials (Coble 1996; Coble et al. 1998; Del Castillo et al. 1999). This shift suggests that Peak M fluorescence commonly observed in marine waters may be partly due to photobleached (Boehme et al. 2004; Birdwell and Valsaraj 2010) or photochemically resistant terrestrial FDOM in addition to humic material produced in situ by microbial processes (Coble 1996; Birdwell and Engel 2010). No increase in fluorescent signal associated with microbial activity (e.g. BIX and EEMS Peak T and Peak B) was observed (Coble 2007; Huguet et al. 2009). The intensity of the Peak T region decreased during light exposure, which suggests that indirect photodegradation or limited hydrolysis of tryptophan containing peptides may have resulted during prolonged UV exposure. However, Peak T was not well resolved from the adjacent Peak C/M in these spectra, so this apparent decrease may have been influenced by the behavior of the broader and more intense Peak C/M. The Peak B region did not appear to undergo extensive photodegradation (Fig. 20; Table 6) though, as its fluorescent signal was low at the beginning of the irradiation (intensity of peak B ~ 2% of Peak A), it is difficult to draw conclusions from this result.

The fluorescence index (FI) of the BS sample decreased from 1.09 to 0.88 during irradiation, whereas the FI for FD increased from 1.19 to 1.63 (Fig. 21A), indicating differences exist between the FDOM pools of the two samples. The FI has been shown to negatively correlate with aromaticity, ranging from around 2.0 for predominantly algal derived DOM to 1.5 or less for predominantly terrestrial humic-rich DOM (McKnight et al. 2001). Thus, the increase observed for the FD samples may reflect the presence of

non-humic (i.e. microbial) FDOM. The humification index (HIX) decreased dramatically during irradiation for both samples (Fig. 21B), indicating that aromatic moieties were preferentially removed during light exposure, which is consistent with NMR, SUVA<sub>254</sub>, and lignin phenol results. All values of biological index (BIX) for the BS sample were less than 0.6 indicating that very little autochthonous DOM was present. The BIX for the FD sample reached values of approximately one, which suggests a larger relative contribution from autochthonous microbial derived DOM at longer irradiation times, and may (along with the FI result above) reflect a larger DOM contribution from algae and bacteria at the FD site (downstream from Lake Drummond) than the BS site (stagnant ditch).

The rapid increase in pH, observed upon irradiation, may be explained by two simultaneous processes: the loss/photodegradation of carboxylic acids (typical  $pK_a$  range of 3-5) and photochemical production of inorganic carbon species, i.e, bicarbonate ( $pK_a = 6.35$ ). NMR spectra of samples amended with strong base confirmed substantial photochemical production of DIC (Miller and Zepp 1995; Bianchi et al. 2004; White et al. 2008) and acetate (Wetzel et al. 1995; Bertilsson and Tranvik 1998; Bertilsson et al. 1999) (Fig. 23D). The distribution of  $COO^-$  and  $COOH$  functionalities determined by FTIR (Fig. 25) was likely influenced by the shift in pH during the irradiation (Fig. 15). Thus, changes in protonation of carboxylic acids are not directly attributed to photochemistry. Therefore,  $COO^-$  and  $COOH$  are combined and treated as a single category in Fig. 26, but are listed as separate categories in Table 10 because they were detected as different peaks (Figs. 24 and 25).

The extensive loss of lignin phenols during the irradiation (Table 7) is consistent with the decrease in NMR signal between 100 – 165 ppm as well as the observed decreases in various optical indicators of aromaticity used to trace tDOM, e.g.  $a_{300}$ , SUVA<sub>254</sub>, peak A and C fluorescence, and HIX. The emergence of a more defined peak at 100 ppm in both the CP/TOSS spectrum and the CSA-filtered spectrum (Fig. 22) demonstrated that the anomeric carbons of carbohydrates were much less photochemically reactive than the aromatic carbons adjacent to phenolic carbons (aromatic C-C-O), which also resonate at ~100 ppm. The splitting of the carboxyl peak in the CP/TOSS spectrum of the 32 day-irradiated sample, which contained both DOM and flocculated particles (Fig. 22C), reflects a significant change in the composition of the carboxylic DOM pool. The results presented in Chapter II indicate that the solid phase that flocculates during irradiation is largely responsible for the peak splitting. The second carboxyl peak has not been identified; however, it is speculated to be due to either (i) insoluble carbonate salts (Bianchi et al. 2004), (ii) amides (see Chapter II), (iii) or metal associated carboxylate (based on FTIR results). If the peak splitting is due to carbonate, the total carboxyl C is significantly overestimated in terms of both carbon percentage and concentration. NMR and FTIR results (Fig. 26; Table 10) showed that by the end of the irradiation most of the carboxylic acids, carboxylate ions, and metal associated carboxyl groups were degraded along with nearly all the carboxylic esters, while carboxylic amides were preserved, thus leaving behind mostly metal associated carboxyl groups (53%), carboxylic acid/carboxylate groups (29%), and carboxylic amides (17%). Thus the observed splitting may be related to the preferential preservation of those photo-resistant carboxyl species.

Nearly every structural component of DOM, including those with no absorbance at the irradiated wavelengths, was lost during the irradiation. The latter loss is attributed to indirect or secondary photochemical reactions, such as those induced by the photo-produced radicals and reactive oxygen species, particularly hydroxyl radical and superoxide (Faust and Zepp 1993; Goldstone and Voelker 2000; Goldstone et al. 2002). Based upon their photochemical reactivity, Stubbins et al (2010) recently classified the components of riverine DOM into three pools: (1) “photo-labile DOM,” which is removed during irradiation, (2) “photo-resistant DOM,” which remains unaltered throughout irradiation, and (3) “photo-produced DOM,” which represents DOM that increases in concentration during irradiation or is chemically distinct from the starting material.

*Photo-labile DOM* – Based on the above results, photochemically labile DOM is characterized by absorbance in the UV-visible region, and fluorescence in the EEMS regions of Peaks A and C. Photochemically-induced changes in UV spectral slopes and slope ratios indicated that high molecular weight CDOM is apparently photo-degraded (Fig. 19; Table 5; Helms et al. 2008). Decreases in both SUVA<sub>245</sub> (Fig. 18D; Table 5; Weishaar et al. 2003) and NMR signal in the 100-160 ppm region (Figs. 22 and 23; Tables 8 and 9) suggest that aromatic rings, including condensed aromatic ring systems (deprotonated aromatics in Tables 8 and 9) and lignin phenols (Table 7) are particularly photo-labile. Carboxylic acids, carboxylate ions, metal associated carboxyl groups, and carboxylic esters (Fig. 26; Table 10) were all degraded during the irradiation experiment, though carboxylic acids and carboxylate appear to have mostly photo-degraded during

the first ten days and the metal associated carboxylate changed very little during the final 11 days (21 d – 32 d).

The marked photo-lability of aromatic ring systems reported here is consistent with the ultra-high resolution mass spectral results reported for irradiated Congo River samples in Stubbins et al. (2010). This photo-lability combined with the observed photobleaching is consistent with aromatic moieties being the dominant chromophores in tDOM (Chin et al. 1994; Del Vecchio and Blough 2004a). The extensive photochemical removal of carboxylic functional groups is in agreement with the results reported by Thorn et al. (2010) for UV-irradiated humic substances.

*Photo-resistant DOM* –Terrestrial DOM that underwent long-term photobleaching, in addition to losing most of its UV absorbance and fluorescence, became less aromatic and increasingly dominated by aliphatic material including alkyl carbons, carbohydrate-like compounds (i.e., O-alkyl carbon), amides, and free and metal-complexed carboxyl compounds (Figs. 22, and 23; Tables 8 and 9). Comparing the fluorescence results with the combined NMR/FTIR quantification of amide groups suggests that the loss of protein-like fluorescence (Peak T) may be due to the loss or alteration of the amino acids tryptophan, tyrosine, and phenylalanine, which are mainly responsible for protein fluorescence.

DOM molecules that resisted both direct and indirect photochemical degradation appeared to be mainly amides (e.g., peptides). However, the detection of low concentrations of photo-resistant compounds against the large background of readily photodegraded tDOM, and the differentiation of photo-resistant DOM from photo-



produced DOM were hampered by the use of methods that provided primarily bulk and functional group characterization. This limitation highlights the need for combining this approach with additional molecular-level analytical approaches, e.g., ultra-high resolution mass spectrometry (Kujawinski et al. 2004; Stubbins et al. 2010).

*Photo-produced DOM* – The only readily identified photoproducts, alkyl compounds (Table 9) and acetate (Figs. 23D and 26; Table 10), were produced during the first 10 days of irradiation. The production of alkyl species is consistent with Stubbins et al. (2010), who found that aliphatic molecules accounted for the majority (~76%) of ESI-FTICR-MS detected photoproducts. Previous studies have shown that photochemical alteration of DOM results in the formation of low molecular weight products (Chin et al. 1994; Helms et al. 2008). Some of these photoproducts are volatile and would have been lost during freeze-drying. Thus, in addition to acetate, other low molecular weight acids, carbonyl compounds, and volatile hydrocarbons were likely generated during photolysis (Kieber et al. 1990; Wetzel et al. 1995; Riemer et al. 2000).

*Fate of terrestrial DOM in the ocean* – Kieber et al. (1990) estimated that approximately 10% of the oceans mixed layer undergoes photochemical DOC removal. Further, it has been inferred from ocean circulation, DOC distribution and CDOM distribution that nearly all riverine DOM is likely removed during transport to “blue” ocean waters within tens to hundreds of years (Kieber et al. 1990; Blough and Del Vecchio 2002; Nelson and Siegel 2002). The mechanisms of terrestrial DOM removal are not yet fully understood, but based on the results presented here, it appears that some

fraction of what is considered marine DOC may be photobleached (and bio-refractory) DOM that originated from the terrestrial environment. In addition, the residual DOM (~9-24% of initial DOC) had optical and bulk chemical signatures that were more typical of DOM found in the marine environment, as observed in previous studies (Minor et al. 2006; Minor et al. 2007; Dalzell et al. 2009). The observed increases in  $S$  and  $S_R$  during UV exposure were also consistent with previous studies (Helms et al. 2008; Spencer et al. 2009; Ortega-Retuerta et al. 2010). The observed shifting of the fluorescence intensity maximum from EEMS Peak C to Peak M may be explained by preferential bleaching of the fluorophores responsible for Peak C leaving behind residual Peak M fluorophores, but may also be explained by a decrease in molecular weight and/or decreased conjugation causing a hypsochromic shift in the fluorescence maxima of photochemically altered FDOM. In either case, these results show that the dominant Peak M in marine DOM may be partially attributable to photobleached tDOM in addition to autochthonous “humic” FDOM.

The composition of extensively irradiated DOM, as revealed by  $^{13}\text{C}$  NMR, also more closely resembled marine DOM than the starting material. The dominant emergent peaks at ~25, ~75, ~100, and ~175 ppm in the  $^{13}\text{C}$  NMR spectra for irradiated tDOM (Fig. 22C; See also Chapter II) also dominate marine and estuarine DOM  $^{13}\text{C}$  NMR spectra reported in a number of studies (Benner et al. 1992; Hedges et al. 1992; Abdulla et al. 2010; see also Chapter V); in particular, the loss of signal from the aromatic region of the spectrum and the sharper and more intense peaks in the methyl (0-28 ppm), and O-alkyl/N-alkyl (50-115 ppm) regions of the NMR spectra.

It is important to point out that, despite the similarities, it is unlikely that marine DOM consists primarily of photobleached terrestrial DOM. The similarity between the optical properties and bulk chemical compositions of marine and photobleached tDOM highlights the difficulty that is faced when attempting to quantify the biogeochemical influence of terrestrial DOM on estuarine and ultimately oceanic environments that lie downstream.

Despite these results, lignin and optical properties remain the most unambiguous evidence of terrestrial influence. However, due to the demonstrated photolability of dissolved lignin, CDOM and FDOM, the maxim: “absence of proof is not proof of absence” must be applied. Consequently, the results of this study support Spencer et al. (2009) and Stubbins et al. (2010) in calling for the identification of terrestrially sourced bio-marker molecules that are resistant to both photochemical and microbial degradation, as these would greatly improve our ability to understand and quantify the oceanic carbon cycle. Unfortunately, the present difficulties in optically, chemically and isotopically differentiating the photo-resistant and photo-produced portions of terrigenous DOC (~5-25% of Dismal Swamp DOC in this study) from in situ produced marine DOC (e.g., Spencer et al. 2009) continues to impede efforts to understand and model carbon cycling in aquatic environments.

## **CHAPTER IV**

# **PHOTOCHEMICAL BLEACHING OF OPEN OCEAN DISSOLVED ORGANIC MATTER**

### **INTRODUCTION**

Chromophoric dissolved organic matter (CDOM) is the dominant (non-water) UV light absorbing substance in the open ocean (Zepp 2002; Kitidis et al. 2006). In spite of the large source of allochthonous CDOM from rivers and coastal wetlands (Blough and Del Vecchio 2002; Del Vecchio and Blough 2004b; Spencer et al. 2009), the dominant source of CDOM in the open ocean is thought to be the heterotrophically altered autochthonous material that is produced in and immediately beneath the euphotic zone and also released at depth from sinking particles (Rochelle-Newall and Fisher 2002a; Nelson et al. 2004; Yamashita and Tanoue 2004; Nelson et al. 2007; Swan et al. 2009). CDOM plays an important role in protecting life forms in the upper water column from harmful UV radiation (Williamson et al. 2001; Zepp 2002) and represents a significant interference for the remote sensing of ocean chlorophyll (Carder et al. 1989). Further, the products of CDOM photochemical degradation represent a source of nutrients for phytoplankton (Tarr et al. 2001; Stedmon et al. 2007), metabolic substrates for heterotrophs (Kieber et al. 1989), and climatologically relevant gasses (Johannessen and Miller 2001; Cutter et al. 2004; Stubbins et al. 2006; Toole et al. 2006). The loss of UV and visible light absorbance and fluorescence that occurs during CDOM photochemical degradation is referred to as photobleaching (Zika 1980; Kieber et al. 1990; Skoog et al. 1996). The basin scale impact of CDOM photobleaching in surface waters of the remote Pacific Ocean has recently been highlighted by large scale surveys (Swan et al. 2009;

Yamashita and Tanoue 2009), which show that CDOM absorbance and fluorescence are strongly depleted in the surfaced mixed layer.

While there is substantial evidence for widespread CDOM photobleaching from its distribution in the ocean (Nelson et al. 2007; Swan et al. 2009) and direct observations of photobleaching of CDOM in terrestrially-impacted waters (Skoog et al. 1996; Del Vecchio and Blough 2002; Twardowski and Donaghay 2002; Del Vecchio and Blough 2004a; Helms et al. 2008), open ocean CDOM photobleaching has not been widely examined (Opsahl and Benner 1998; Ortega-Retuerta et al. 2010), and little has been reported with respect to the changes in the spectral distribution of absorption and fluorescence during photodegradation of open ocean CDOM. In the present study, both CDOM absorption and fluorescence were used to investigate the process of photobleaching in open ocean DOM that was concentrated and desalted using reverse osmosis coupled with electrodialysis (RO/ED). The use of open ocean DOM provides starting material with minimal direct contribution from terrestrial environments, while the use of a pre-concentrated sample facilitates the measurement of optical property changes over a much longer irradiation time frame than unconcentrated samples. Isolation of DOM by RO/ED avoids most of the fractionation problems associated with solid phase extraction and ultrafiltration (Koprivnjak et al. 2006; Koprivnjak et al. 2009).

## MATERIALS AND METHODS

*Cleaning procedures* – All glassware was cleaned with dilute ( $\sim 1 \text{ mol L}^{-1}$ ) HCl and rinsed with MilliQ UV ultrapure grade water (Millipore), designated below as “MilliQ water”. Glassware was combusted at  $450^\circ\text{C}$  for  $\geq 4$  hours. Plasticware was cleaned with dilute HCl and rinsed with MilliQ water. Stainless steel equipment was

cleaned with mild detergent and copiously rinsed with MilliQ water. All containers were rinsed several times with sample prior to filling. Filter capsules (0.1  $\mu\text{m}$  pore size, Whatman PolyCap) were rinsed with acetonitrile, flushed with > 20 L of MilliQ water, and conditioned with approximately 1 L of sample prior to use.

*Sample collection, handling, and irradiation* – Water samples were collected from the 670 m depth pumping system at the Natural Energy Lab of Hawaii, Kona, Hawaii (NELHA). The water was pumped through 0.1  $\mu\text{m}$  capsule filters into the polypropylene tank of the RO/ED system. The samples were desalted to a conductivity of  $\sim 10 \text{ mS cm}^{-1}$  by electrodialysis and concentrated by a factor of 11.5 with 76% recovery to a DOC concentration of  $\sim 9.8 \text{ mg C mL}^{-1}$  by reverse osmosis. The isolated sample was frozen and shipped back to the laboratory in Norfolk, VA where it was immediately re-frozen until used in the experiments described below.

Aliquots of the RO/ED concentrate were transferred to  $\sim 550 \text{ mL}$  quartz flasks and placed inside a solar UV simulator containing 12 Q-Panel UVA340 bulbs, which provided a spectral shape similar to that of natural sunlight from approximately 300-365 nm (Q-Panel), but under-represent solar irradiance at wavelengths greater than about 365 nm. The light output from the solar simulator was monitored during the course of the irradiation experiment using a Biospherical PUV 2510 radiometer. The solar simulator is described elsewhere (Minor et al. 2007; Helms et al. 2008; Dalzell et al. 2009). The samples were irradiated constantly during the experiment. Sub-samples were collected and analyzed at exposure intervals ranging from 5 days to 68 days.

At the end of each irradiation period, an aliquot of sample was tested for microbial activity using  $^3\text{H}$  labeled thymidine (TrD) incorporation (Fuhrman and Azam 1982; Smith and Azam 1992). All samples yielded radioactivity measurements less than 1% higher than killed controls; thus, all measured changes to DOM optical properties were principally due to photochemical reactions as microbial growth was negligible.

*UV-visible absorption and fluorescence spectroscopy*– UV-visible absorption spectra (190-900 nm) were measured for irradiated samples and dark controls using an Agilent 8453 diode array spectrophotometer with a 5 cm quartz cuvette. MilliQ water was used as the blank. Absorbance values were corrected for instrument baseline drift, refractive index, and temperature variations according to Green and Blough (1994) and converted to Napierian absorbance coefficients using the formula:

$$(5) \quad a = 2.303A/l$$

where  $a$  = absorbance coefficient ( $\text{m}^{-1}$ ),  $A$  = absorbance, and  $l$  = path length (m). CDOM absorption spectra are usually described by an exponential function of decreasing absorption with increasing wavelength:

$$(6) \quad a_{\lambda} = a_{\lambda_{ref}} e^{-S(\lambda - \lambda_{ref})}$$

where  $a$  = absorption coefficient ( $\text{m}^{-1}$ ),  $\lambda$  = wavelength (nm),  $\lambda_{ref}$  = reference wavelength (nm), and  $S$  = spectral slope ( $\text{nm}^{-1}$ ) (Helms et al. 2008). Specific UV absorbance (SUVA) was determined by dividing the absorption coefficient (at 254 nm and 300 nm) by the DOC concentration.

The spectral slope over the wavelength range of 300-700 nm was calculated using non-linear regression of the absorption spectra (Twardowski et al. 2004). All other

spectral slopes were calculated by linear regression of the natural log transformed absorption spectra (Helms et al. 2008). Spectral slope ratio ( $S_R$ ) was calculated by dividing  $S_{275-295}$  by  $S_{350-400}$  (Helms et al. 2008). First- and second-derivative spectra were obtained for absorption and natural log absorption using linear regression over 21 nm intervals (i.e., central value  $\pm 10$  nm). Slope spectra were generated in a manner similar to Loiselle et al. (2009), except that linear regression of the natural log spectrum was used to determine the slope over a sliding 21 nm interval.

Fluorescence excitation emission matrix spectra were measured using a FluoroMax-2 spectrofluorometer (Spex Industries) and a 1 cm x 1 cm quartz fluorescence cuvette. Emission spectra (300-550 nm; 2 nm intervals) were measured over a range of excitation wavelengths (200-455 nm; 6.375 nm intervals). The data integration time was 1.0 s. EEMS were corrected for inner-filter effects, and scattering peaks were removed (Lakowicz 1999; Zepp et al. 2004; Cory and McKnight 2005). Fluorescence intensities were normalized to the integrated water Raman peak and corrected for the RO/ED volumetric concentration factor.

The major peaks in the EEMS were identified using the wavelength ranges identified by Coble (1996 and 2007): Peak A ( $\lambda_{ex} \sim 260$  nm;  $\lambda_{em} = 380-460$  nm), Peak C ( $\lambda_{ex} \sim 350$  nm;  $\lambda_{em} = 420-480$  nm), Peak M ( $\lambda_{ex} \sim 312$  nm;  $\lambda_{em} = 380-420$  nm), Peak B ( $\lambda_{ex} \sim 275$  nm;  $\lambda_{em} \sim 310$  nm), and Peak T ( $\lambda_{ex} \sim 275$  nm;  $\lambda_{em} \sim 340$  nm). The ratio of Peak M to Peak C fluorescence (M:C) was calculated by dividing the intensity at 310ex/410em by the intensity at 345ex/445em (Burdige et al. 2004; Para et al. 2010; Romera-Castillo et al. 2011). Fluorescence index (FI), which indicates the relative influences of terrigenous and marine (microbial) DOM by comparing the intensity of two



commonly observed humic related fluorescence maxima, was calculated by dividing the intensity at 372ex/470em by the intensity at 372ex/520em (McKnight et al. 2001).

Fluorescence humification index (HIX), which compares two broad aromatically dominated fluorescence maxima, was determined at 253 nm excitation by dividing the integrated emission from 434-480 nm by the integrated emission from 300-346 nm (Kalbitz et al. 1999). The biological fluorescence index (BIX), which indicates the presence of autochthonous or microbially derived DOM, was determined by dividing intensity at 308ex/380em by intensity at 308ex/430em (Huguet et al. 2009).

*Dissolved organic carbon* – Non-purgeable total organic carbon (NPOC) was measured using high temperature (720°C) catalytic combustion on a Shimadzu TOC-V<sub>CPH</sub> carbon analyzer. The instrument was calibrated using dried primary standard grade potassium hydrogen phthalate (Alpha Aesar) dissolved in MilliQ water. As all samples were filtered to less than 0.1  $\mu\text{m}$  prior to RO/ED isolation and irradiation, all NPOC measurements are referred to as DOC.

## RESULTS AND DISCUSSION

*Photobleaching of RO/ED isolated DOM from the open ocean* – Prior to irradiation, the RO/ED isolate yielded an  $a_{254}$  value of 17.9  $\text{m}^{-1}$ , an  $a_{300}$  value of 8.0  $\text{m}^{-1}$ , and a DOC value of 9.47  $\text{mg C L}^{-1}$ . During the irradiation, absorption, DOC and SUVA<sub>254</sub> decreased (Table 12; Figs. 27 and 28). First-derivative absorption spectra (Fig. 27B) show that the steepness of the spectrum generally decreases (becomes less negative) with increasing wavelength and increasing irradiation time. Second-derivative absorption

Table 11. Summary of the microbial productivity assay used to monitor potential biological artifacts. A fresh 5 $\mu$ m filtered pond-water sample was used as a “live-control” to test the effectiveness of the assay. As all irradiated samples showed negligible microbial activity, no calibration was applied and results are reported in raw counts per minute (CPM).

Sample	Irr. Time (days)	Killed Control (CPM)	Non- Poisoned Sample (CPM)	Non- Poisoned Dark Control sample (CPM)	Reference sample “live control” (CPM)	Average Temperature (°C)
NELHA-0d	0	7.4	6.7	6.7	627	22
NELHA-5d	5	7.3	6.1	5.4	627	23
NELHA-26d	26	13.6	6.6	27.8	514	23
NELHA-68d	68	6.0	4.8	8.7	514	23

Table 12. DOC and UV-visible measurements of RO/ED isolates from NELHA 670m water samples.

Sample	DOC (mg C l <sup>-1</sup> )	$a_{254}$ (m <sup>-1</sup> )	$a_{300}$ (m <sup>-1</sup> )	SUVA <sub>254</sub>	$S_{300-700}$ (nm <sup>-1</sup> )	$S_{275-295}$ (nm <sup>-1</sup> )	$S_R$
NELHA-0d	9.47	17.9	8.00	1.89	0.0095	0.0191	2.14
NELHA-5d	7.39	15.6	5.30	2.11	0.0088	0.0273	3.56
NELHA-26d	6.93	9.56	2.37	1.37	0.0112	0.0372	6.30
NELHA-68d	5.85	5.56	1.29	0.95	0.0092	0.0388	8.92

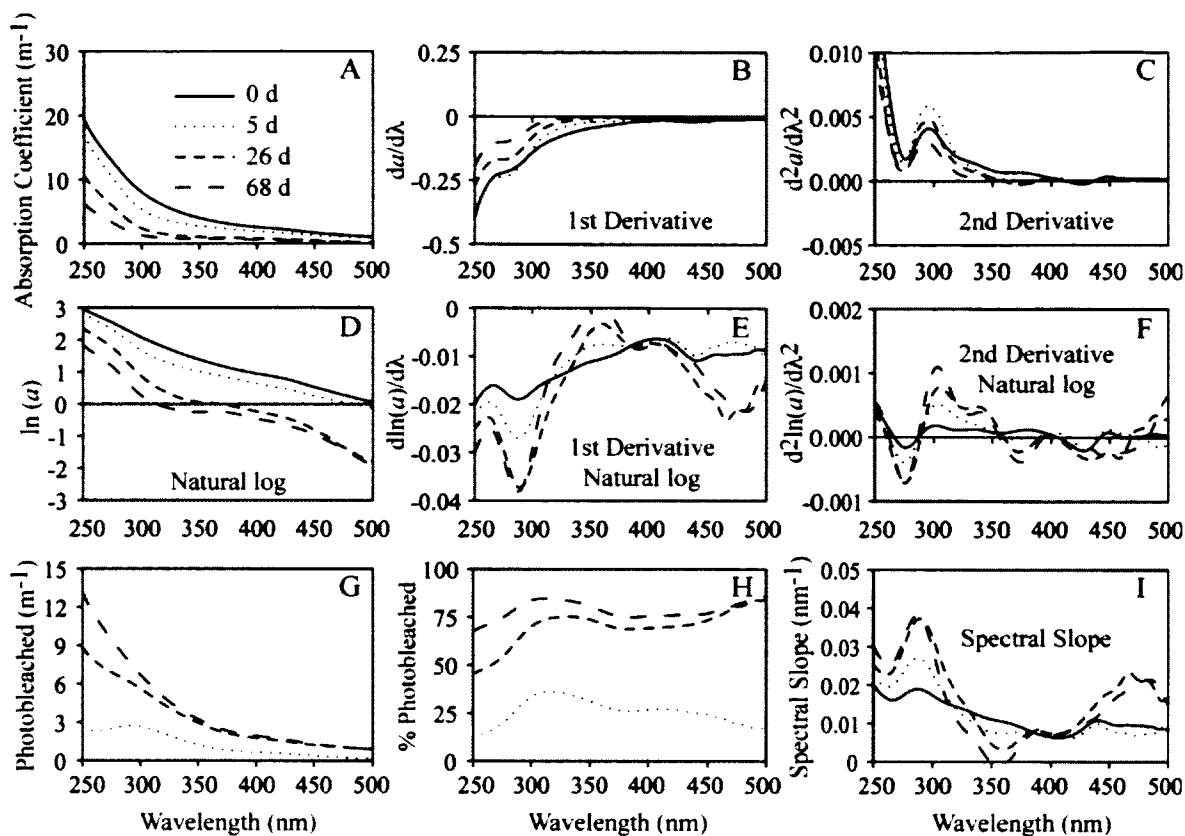


Fig. 27. (A) UV-visible absorption spectra, (B) first-derivative absorption spectra, (C) second-derivative absorption spectra, (D) natural log absorption spectra, (E) first-derivative natural log absorption spectra, (F) second-derivative natural log absorption spectra, (G) amount of absorption removed by photobleaching, (H) percentage of absorption removed by photobleaching, and (I) spectral slope spectra, obtained for NELHA RO/ED isolates irradiated for 0 d, 5 d, 26 d, and 68 d.

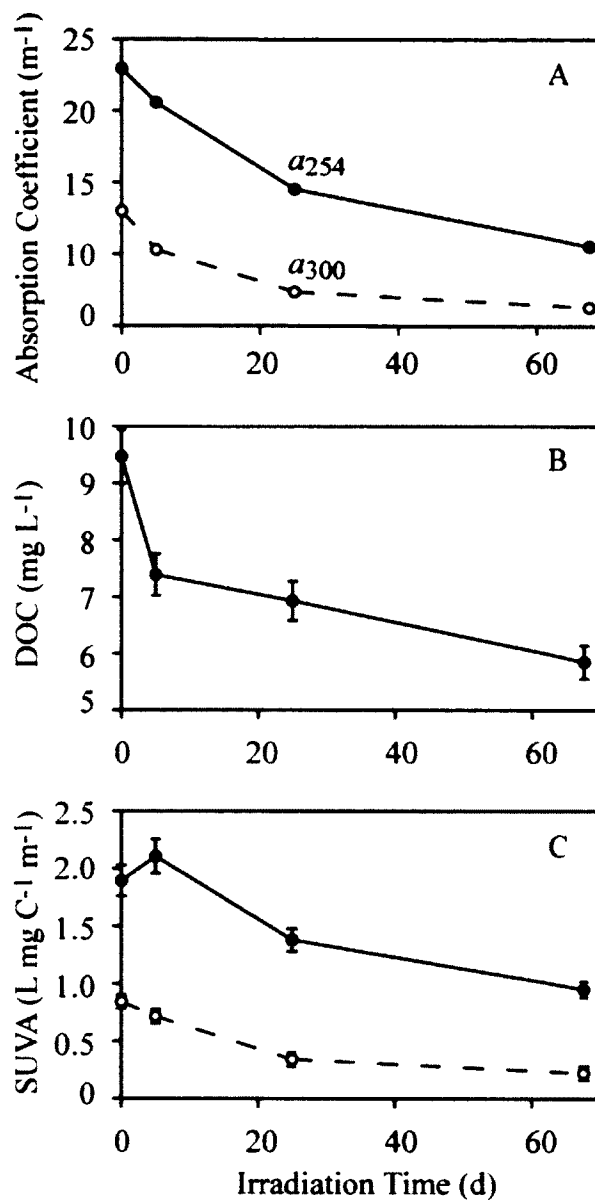


Fig. 28. The trends of decreasing (A) UV-visible absorption, (B) DOC, and (C) specific UV absorbance (SUVA) with increasing irradiation time. Error bars were calculated as two times the standard deviation ( $n \geq 3$ ) plus the blank (absorption coefficient error bars were smaller than the circles).

spectra (Fig. 27C) indicate that the primary UV chromophores may be related to an aromatic (e.g.,  $\pi \rightarrow \pi^*$ ) transition at  $\sim 280$  nm (Summers et al. 1987) with two unidentified absorption bands centered at  $\sim 375$  nm and  $\sim 425$  nm. The minimum in the second-derivative spectrum at  $\sim 280$  nm shifted to somewhat shorter wavelengths during the course of the irradiation, suggesting that the degree of conjugation or molecular size decreased (Pavia et al. 1979; Helms et al. 2008).

The initial natural log absorption spectrum was approximately linear; however, after extensive photobleaching, several new features developed (Fig. 27D). In particular, the spectra become markedly steeper at  $\sim 260$ - $310$  nm, less steep at  $\sim 315$ - $375$  nm, and again steeper at  $\sim 425$ - $575$  nm (Fig. 27D). These changes in the spectral shape are reflected in the first-derivative natural log absorption spectra and in the spectral slope spectra (Figs. 27E and 27I). The second-derivative natural log spectra (Fig. 27F) show that photobleaching led to the emergence of an additional unknown minimum peak at  $\sim 330$  nm. The  $375$  nm minimum peak also intensified during photobleaching. The apparent emergence and/or intensification of negative peaks in the second-derivative natural log spectra could be due to the formation of absorbing photoproducts and/or the preferential degradation of material with absorbance maxima adjacent to those of photo-refractory chromophores. It is clear that photobleaching caused  $a_{\text{CDOM}}$  to decrease over a broad range of wavelengths, but particularly at  $\sim 325$  nm and  $\sim 500$  nm (Figs. 27G and 27H). During the irradiation, decreases were observed for  $a_{254}$  and  $a_{300}$  as well as for DOC and SUVA (Fig. 28).  $a_{300}$  is reported here, because it is frequently used to quantify CDOM, and because  $300$  nm is a region where the solar irradiance spectrum overlaps the CDOM absorption spectrum (Green and Blough 1994; Gao and Zepp 1998; Stedmon et

al. 2000). Decreasing  $a_{254}$  and SUVA<sub>254</sub> indicate degradation of aromatic and/or highly conjugated DOM moieties (Brown 1977; Weishaar et al. 2003).

Prior to irradiation, the RO/ED isolate UV spectrum yielded an  $S_{275-295}$  value of  $0.019 \text{ nm}^{-1}$  and an  $S_R$  value of 2.14. These values are typical for open ocean DOM deeper than ~400m (Table 12; Helms 2006; Helms et al. 2008). Upon irradiation,  $S_{275-295}$  increased to  $0.0388 \text{ nm}^{-1}$ ,  $S_{350-400}$  decreased, while  $S_{300-700}$  remained relatively unchanged (Table 12; Fig. 29).  $S_R$  increased to 8.92, which is typical of stratified surface ocean waters (Helms 2006; Helms et al. 2008). Increases in  $S$  and  $S_R$  have been shown to correlate with (or to be due to) decreases in average CDOM molecular weight (Helms et al. 2008), decreases in CDOM aromaticity (Chapter III), photobleaching of dissolved lignin (Fichot and Benner 2012), selective bleaching in the wavelength region where both absorbance and irradiance are abundant (Reche et al. 2000; Kieber et al. 2007), and to disruption of coupled states such as charge transfer donor-acceptor pairs (Del Vecchio and Blough 2004a).

Prior to irradiation, FDOM in the 670m Pacific Ocean RO/ED isolate exhibited a dominant peak at 253ex/426em (Peak A) (Fig. 30) and had a FI (McKnight Fluorescence index) value of 1.53, a HIX (humification index) value of 3.9, and a BIX (biological fluorescence index) value of 0.74 (Tables 13 and 14). M:C, FI, and BIX differed slightly from those found in surface water RO/ED isolates from the same region (Station ALOHA; Figs. 30 and 31), while HIX was higher than surface waters, but similar to values measured for DOM isolated from 3500 m (Fig. 31). Peak M was slightly more intense than Peak C (Table 13; Fig. 32) with a M:C value of 1.17 (Table 14; Fig. 31). In comparison, M:C values were 1.21 at 5 m and 1.13 at 3500 m.

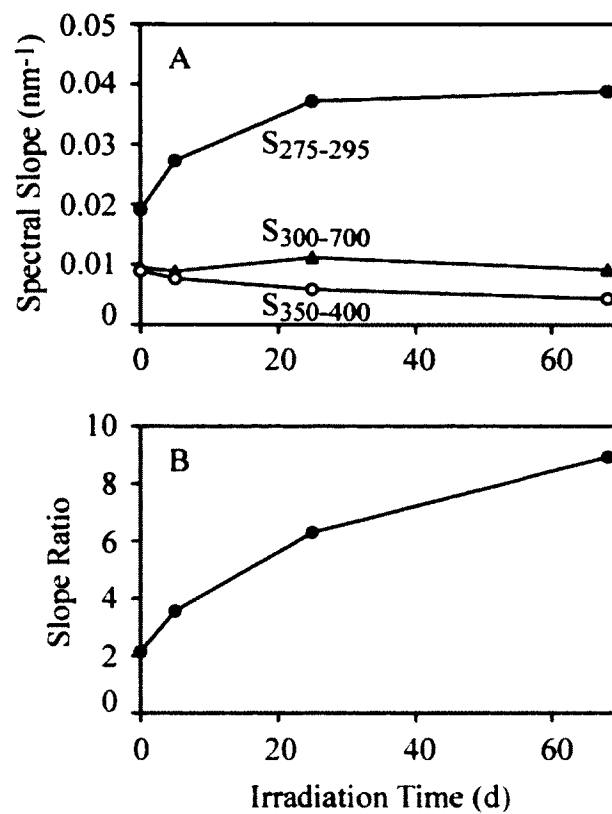


Fig. 29. (A) Spectral slope coefficients for 300-700 nm, 275-295 nm, and 350-400 nm show different trends with irradiation. (B) Slope ratio ( $S_R$ ) increased during irradiation.



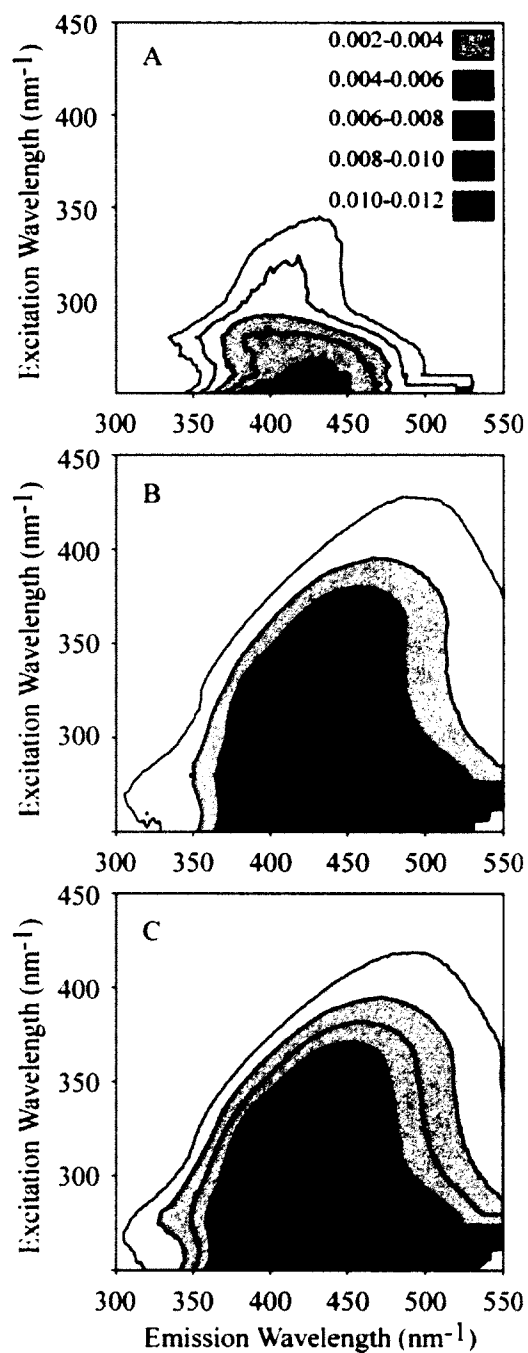


Fig. 30. Fluorescence excitation emission matrix spectra obtained for RO/ED isolated DOM samples from (A) a surface sample collected at station ALOHA, (B) a sample pumped from the 670m water supply at NELHA, and (C) a sample collected at 3500m depth at station ALOHA. Intensity is reported in water Raman units corrected for RO/ED concentration factor.

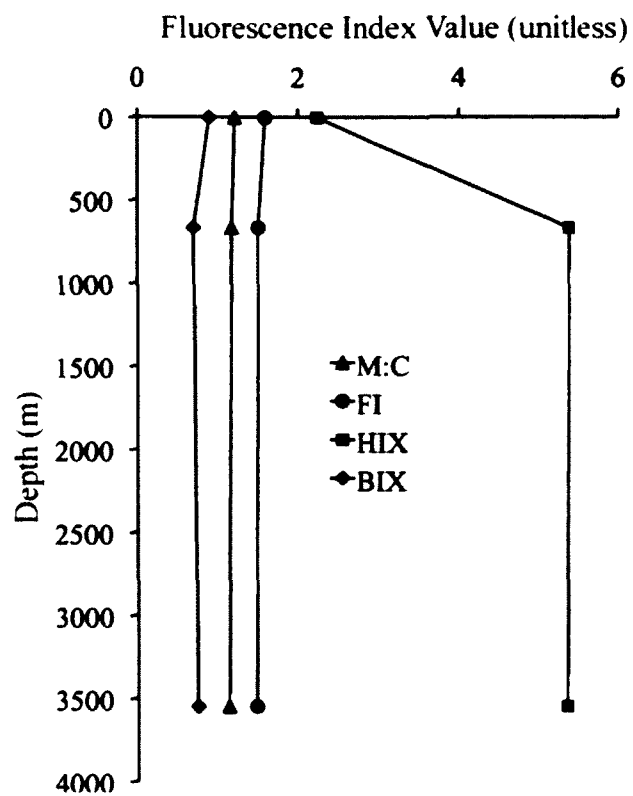


Fig. 31. Depth profile of fluorescence indices measured for non-irradiated RO/ED isolated DOM from the North Pacific at station ALOHA (5 m and 3500 m) and NELHA (670 m).

Table 13. Summary of EEMS peak intensities and locations for irradiated and dark control (0d) RO/ED isolates from NELHA 670m water samples. Maximum peak intensity values are reported as water Raman units (WRU) corrected for RO/ED concentration factor.

	NELHA 0d	NELHA 68d
Peak A (WRU)	0.015	0.0039
$\lambda_{ex}$ max (nm)	253	246
$\lambda_{em}$ max (nm)	426	420
Peak C (WRU)	0.011	0.0017
$\lambda_{ex}$ max (nm)	313	326
$\lambda_{em}$ max (nm)	420	404
Peak M (WRU)	0.012	0.0026
$\lambda_{ex}$ max (nm)	286	286
$\lambda_{em}$ max (nm)	410	410
Peak B (WRU)	0.0065	0.0035
$\lambda_{ex}$ max (nm)	280	280
$\lambda_{em}$ max (nm)	326	318
Peak T (WRU)	0.0094	0.0021
$\lambda_{ex}$ max (nm)	280	275
$\lambda_{em}$ max (nm)	376	378

Table 14. Fluorescence indices calculated based on EEMS.

Sample	M:C	FI	HIX	BIX
NELHA-0d	1.17	1.53	3.90	0.74
NELHA-68d	1.43	1.61	1.40	0.97

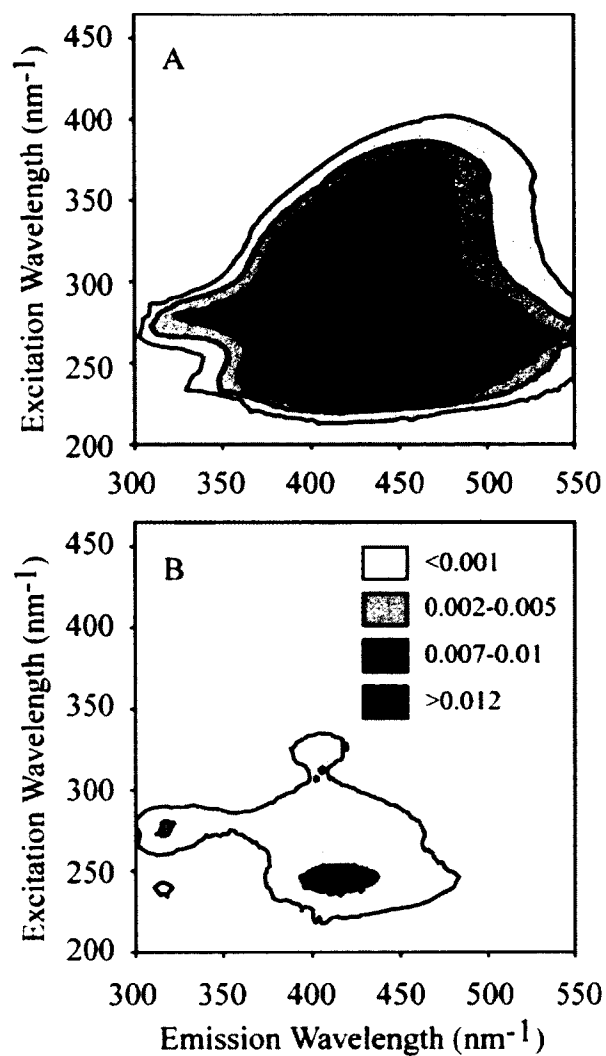


Fig. 32. Fluorescence excitation emission matrix spectra shown for (A) non-irradiated 670 m NELHA DOM isolate and (B) 670 m NELHA DOM that was irradiated for 68 d. Intensity scale is reported as water Raman units corrected for RO/ED concentration factor.

Upon irradiation, fluorescence decreased, similar to  $a_{\text{CDOM}}$ . The largest decrease occurred at Peak C (~84%; Table 13), while the smallest decrease occurred at Peak B (~47%; Table 13). Peaks A, M and T each decreased by  $76\% \pm 2\%$  (Table 13) and the M:C ratio increased to from 1.17 to 1.43. After the 68 d irradiation, Peak A remained the dominant peak (Fig. 32); however, the location of its maximum shifted from 253ex/426em to 246ex/420em. Peak C showed the most significant shift from 313ex/420em to 326ex/404em, while the remaining peaks exhibited relatively minor shifts. The shift in  $\lambda_{\text{ex}}$  observed for Peak B may be partly due to the photobleaching of the broader and more intense fluorescence in the vicinity of Peaks T and M. The comparative photo-stability of the Peak B region fluorophores (tyrosine-like FDOM) is consistent with the results from the irradiation of terrestrial DOM presented in Chapter III.

*Implications for the cycling of CDOM and semi-labile DOM* – Swan et al. (2009) found that CDOM and DOC do not significantly correlate in the Pacific Ocean, and that processes governing CDOM and DOC distributions may be largely decoupled. The shifts in optical properties observed here support the conclusion that the depletion of CDOM in the subtropical gyres is largely due to photochemical degradation (Swan et al. 2009). The residual photo-refractory and photo-produced DOM in the irradiated 670 m sample (~62% of initial DOC; Table 12) suggests that the build-up of DOC in surface waters (Hansell et al. 2009) must involve production of fresh algal DOC, which may, in part, be supported by photochemical release of nutrients (Tarr et al. 2001; Stedmon et al. 2007). In other words, near surface production must overcome a photochemically driven deficit of nearly 40% of the background refractory DOC before any excess could be measured.

CDOM with optical properties similar to subsurface ocean DOM has been shown to accumulate in cultures of aquatic microbial assemblages (Tanoue et al. 1995; Rochelle-Newall and Fisher 2002a; Nelson et al. 2004). It appears that a significant fraction of this “new” CDOM material is biologically semi-labile (Nelson et al. 2004; Yamashita and Tanoue 2004; Yamashita et al. 2007; Yamashita and Tanoue 2008; Yamashita and Tanoue 2009), and based on the findings presented here (and assuming microbial processing is the major source of CDOM in the deep Pacific Ocean), it is largely photo-labile as well. Photo-refractory DOM appears to consist largely of carbohydrates and carboxylated aliphatic material (Chapter III, Stubbins et al. 2010). Further, based on the relatively slow degradation of EEMS Peak B observed here, and the photo-stability of amides observed in Chapter III and based on the observed distribution of amide-nitrogen in the major ocean basins (McCarthy et al. 1997; Aluwihare et al. 2005), there is likely a significant peptide or protein component within the photo-refractory pool as well (McCarthy et al. 1998; Mopper and Kieber 2002; Yamashita and Tanoue 2003a; Yamashita and Tanoue 2003b). Based on the vertical distributions of CDOM presented in Nelson et al. (2008) and Swan et al. (2009) and FDOM described in Yamashita and Tanoue (2008 and 2009) and Yamashita et al. (2007), it appears that an important sink for microbially produced CDOM in surface waters is a coupled photochemical-biological process (Kieber et al. 1989; Miller and Moran 1997; Moran et al. 2000), though the results presented here show that photobleaching alone can remove most of the CDOM and FDOM in the surface mixed layer.

The photo-lability of CDOM depends on its composition. Terrestrially produced CDOM typically contains significantly more aromatic carbon than algal produced CDOM

(Sulzberger and Durisch-Kaiser 2009). As shown in Chapter III, extensively photobleached terrestrial DOM resembles ocean DOM in both bulk composition (see also Chapter II) and in its optical properties (e.g., lower absorptivity and fluorescence, higher spectral slope, and EEMS Peak M becoming larger than Peak C). The sample used in this study was chosen to avoid influences from terrestrial DOM. However, based on the photochemical removal of the optical, molecular, and bulk compositional signature of terrestrial DOM described in Chapter III, it is likely that some terrestrially derived CDOM was present in the sample. EEMS Peak C, while smaller than Peak M, was the most photo-labile fluorophore (Table 13). In fact, the dominance of Peak M relative to Peak C is seen in extensively bleached terrestrial CDOM (Chapter III) and the results of the present study indicate that a more intense Peak M relative to Peak C (e.g., higher M:C ratio) may be an indicator of ongoing or past surface photobleaching as well as an indicator of algal or microbial source (Coble 1996; Yamashita and Tanoue 2003b).

*Conclusions and future directions* – The distributions of DOC and CDOM in the oceans have been extensively investigated, though the processes of production and removal of both CDOM and DOC remain poorly understood. The results presented here help explain the role of photobleaching in the buildup of low absorbance, high spectral slope DOM in the surface waters of the subtropical gyres (Nelson et al. 2007; Swan et al. 2009). This study has also shown (along with Chapter III) that, while EEMS Peak M is associated with surface and sub-surface marine microbial production of FDOM (Rochelle-Newall and Fisher 2002a), the photochemically induced shift of Peak C fluorescence (e.g., from deeper or nearer-shore waters) to shorter wavelengths may result



in a significant source of Peak M fluorescence in surface ocean waters. A greater awareness and further investigation of these photochromic shifts in EEMS spectra are needed to ensure the proper interpretation of FDOM distributions in the upper ~400m of the ocean.

Continued improvement in the molecular level and compositional characterization of ocean DOM with accompanying optical spectroscopic characterization will provide greater understanding of how changes in DOM composition impact the optical properties of CDOM and FDOM. A better understanding of these relationships has implications for the use of in situ optical measurements (Spencer et al. 2007; Menon et al. 2011) and remote sensing technology (Carder et al. 1989; Kutser et al. 2005; Griffin et al. 2011) to track biogeochemically and ecologically important processes over more comprehensive temporal and spatial scales.

# **CHAPTER V**

## **CHARACTERIZATION OF OCEANIC DISSOLVED ORGANIC MATTER ISOLATED BY REVERSE OSMOSIS COUPLED WITH ELECTRODIALYSIS**

### **INTRODUCTION**

The oceans contain approximately  $685 \times 10^{15}$  g of dissolved organic carbon (DOC) (Hansell and Carlson 2001), a pool equivalent to current atmospheric  $\text{CO}_2$  of  $\sim 861 \times 10^{15}$  g C (Forster et al. 2007). Oxidation of 1% of the oceanic DOC pool would exceed the annual (ca. 2000) anthropogenic derived  $\text{CO}_2$  (Hedges 2002). Despite its importance, only a small fraction of the total dissolved organic matter (DOM) in the ocean has been identified (Benner 2002), which has hindered our understanding of sources and cycling of DOM (Hedges, 2002). Determining a comprehensive overview of ocean DOM composition has been impeded by the lack of efficient and non-fractionating methods of isolation and salt removal that can be readily coupled to advanced analytical techniques (Mopper et al. 2007).

Previously used methods of concentrating and desalting DOM have been shown to significantly fractionate the DOM resulting in incomplete and biased characterization (Mopper et al. 2007). The two most widely used isolation techniques are solid phase extraction (SPE) (Leenheer 1981; Leenheer 2009) and ultrafiltration (UF) (Swift 1985; Benner et al. 1992), while ion exchange chromatography, selective precipitation, co-precipitation, azeotropic distillation (Aiken and Leenheer 1993) and other methods have been occasionally used to de-salt samples. These methods have failed to produce a representative and unaltered DOM concentrate with a high recovery (Mopper et al. 2007).

Solid phase extraction as it is typically applied using C-18 silica, XAD resin, or PPL resin, is selective for hydrophobic DOM molecules (and DOM that is rendered hydrophobic upon acidification). Ultrafiltration collects only the higher molecular weight fraction of DOM, typically >1000 Da. In both of these methods, the majority of the ocean DOM is frequently lost during processing resulting in DOC recoveries that range from 17-40% for SPE and 13-35% for UF (Mopper et al. 2007).

A system was recently developed that combines DOM concentration by reverse osmosis and de-salting by electrodialysis (RO/ED) (Koprivnjak et al. 2006; Vetter et al. 2007; Gurtler et al. 2008; Koprivnjak et al. 2009). Koprivnjak et al. (2009) showed that an average DOC concentration factor of 20, and >95% salt removal (estimated from volume and conductivity respectively) was accomplished with an average isolate DOC recovery of 70% and a maximum isolate DOC recovery of 94%. Mass balance recoveries, which also include material recovered from the system by rinsing with 0.01 M sodium hydroxide solution, ranged from 61 - 95% (Koprivnjak et al. 2009).

Despite the recovery and fractionation limitations associated with SPE and UF to isolate DOM from ocean waters, several studies have undertaken the molecular and spectroscopic characterization of these isolates. Hedges et al. (1992) used solid-state cross polarization/magic angle spinning (CP/MAS)  $^{13}\text{C}$  nuclear magnetic resonance (NMR) spectroscopy to investigate the bulk structural characteristics of XAD isolated DOM, often referred to as humic substances (HS), from two sites in the Pacific Ocean (DOC recovery ~10%) and compared them with freshwaters from the Amazon River system (DOC recovery ~30%). Benner et al. (1992) used CP/MAS NMR to characterize UF isolated high-molecular-weight DOM (UDOM) from three depths in the North

Pacific Ocean (DOC recoveries: 22-33%). These studies suggested that DOM isolated from the deep ocean contains more aromatic and/or olefinic carbon than surface ocean DOM, and marine DOM contains much less aromatic material than freshwater DOM. Deep ocean UDOM was shown to be enriched in carbohydrate-like carbons and depleted in unsubstituted alkyl carbons relative to XAD resin extracted deep ocean HS (Benner et al. 1992; Hedges et al. 1992).

Koprivnjak et al. (2009) also applied solid-state CP/MAS  $^{13}\text{C}$  NMR, solution  $^1\text{H}$  NMR, and Fourier transform ion cyclotron mass spectrometry to RO/ED isolates collected in the North Atlantic and observed differences between DOM isolated from coastal and offshore waters. One of the most interesting findings of the study was that the NMR spectra of RO/ED isolates appear to represent an intermediate of DOM isolated by UF and DOM isolated by solid phase extraction, suggesting that RO/ED isolates a more representative and complete fraction of the DOM than either of the previously employed techniques.

In addition to CP/MAS, several complementary and improved solid-state  $^{13}\text{C}$  NMR methods have been developed and applied to many types of natural organic matter (NOM). Mao et al. (2011) demonstrated a systematic approach for characterizing humic substances by advanced solid-state NMR techniques. These techniques were used here to characterize the bulk chemical composition of five RO/ED isolated DOM samples, collected from the Atlantic and Pacific Oceans that were chosen for their marked differences in biogeochemical origins.

## MATERIALS AND METHODS

*Sample collection and DOM isolation by RO/ED* – Three Atlantic Ocean water samples were collected aboard R/V Oceanus, and two Pacific Ocean water samples aboard R/V Kilo Moana. The samples include (i) surface water from the Mauritanian Upwelling Zone (5 m; 20.1° N., 17.5° W.), (ii) North Atlantic Oxygen Minimum Zone (415 m; 19° N., 21.5° W.), (iii) North Atlantic Deep Water (3000 m; 18.5° N., 23.2° W.), (iv) a surface sample from station ALOHA in the North Pacific (5 m; 23° N., 158° W.), and (v) a deep sample from station ALOHA (3500 m; 23° N., 158° W.).

The Mauritanian upwelling zone is an area that experiences high rates of primary production and the RO/ED isolated DOM from this site was intended to represent fresh, primarily algal DOM (Carlson 2002). The 415 m North Atlantic RO/ED isolate was intended to represent DOM from the oxygen minimum layer and was expected to contain DOM that is degraded during and after export to the ocean interior from surface waters or released during the degradation of POM in the nearby shelf sediments (Hansell and Carlson 2001; Carlson 2002; Hansell 2002). The 3000 m North Atlantic sample was collected to represent the Iceland-Scotland overflow water mass (ISOW), which is a component of North Atlantic deep water (NADW) (Hernes and Benner 2006; LeBel et al. 2008). ISOW forms in the sub-polar North Atlantic and is advected to the south and subducted to depths of ~2500-3500 m. The North Atlantic receives considerable input of terrestrial DOM from Arctic rivers, and Hernes and Benner (2006) have suggested that a considerable amount of terrestrial DOM is entrained during deep-water formation. The surface water sample collected at Station ALOHA (5 m North Pacific sample) represents DOM from the oligotrophic surface waters that cover the majority of Earth's surface and

is largely dominated by semi-labile (Carlson 2002) and extensively photobleached DOM (Kitidis et al. 2006). The 3500 m North Pacific sample collected at Station ALOHA represents the Lower Circumpolar Water (LCPW) (Johnson and Toole 1993), which exhibits old apparent  $^{14}\text{C}$  DOC ages ( $\sim 6000$  y) (Williams and Druffel 1987), suggesting that DOM from this water mass consists largely of highly degraded DOM and refractory DOM that resists degradation over multiple ocean overturn cycles (Hedges et al. 1997).

Sample volumes ranging from 133 L to 473 L and averaging  $312 \pm 131$  L were collected using Niskin bottles (General Oceanics) and filtered through pre-cleaned  $0.1 \mu\text{m}$  pore size capsule filters (Whatman, Polycap) prior to processing by RO/ED. The RO/ED isolation method is described in detail elsewhere (Vetter et al. 2007). Briefly, strong electrolytes are removed by ED using a stack of alternating polarity, ion-exchange membranes (Selemon AMV and CMV membranes, Asahi Glass Co., Japan) flanked by electrodes and a counter flow of low-conductivity water. Water is removed by RO at a pressure exceeding two times the osmotic pressure of the sample using an RO membrane (FilmTec TW30-4021, Dow Chemical Co.). The sample passes through both stages of the RO/ED process multiple times until sufficient concentration and de-salting is achieved. RO/ED-isolated samples were freeze-dried (without further treatment) for analysis by solid-state NMR and did not include material recovered during rinsing of the membranes with 0.01 M NaOH because the rinse fractions were not desalted.

*UV-visible spectroscopy and dissolved organic carbon* – Chromophoric dissolved organic matter (CDOM) absorption spectra were collected for seawater and isolate samples using an Agilent 8453 diode array spectrophotometer with either a 1 cm, 5 cm or

10 cm pathlength quartz cuvette according to Helms et al. (2008). Spectral slope ( $S$ ), slope ratio ( $S_R$ ), first- and second-derivative spectra, and DOC-normalized absorbance coefficients, i.e., specific UV absorbance (SUVA) were calculated from the spectra according to Helms et al. (2008).

Dissolved organic carbon (DOC) was measured as non-purgable organic carbon for 0.2  $\mu\text{m}$  filtered seawater samples and RO/ED isolated DOM using high temperature catalytic combustion (Sharp 2002) on a Shimadzu TOC-5000 (N. Atlantic samples) or a Shimadzu TOC-V-CPH (N. Pacific samples). Potassium hydrogen phthalate was used as the calibration standard.

*Solid-state  $^{13}\text{C}$  NMR* –NMR experiments were performed using a 400 MHz ( $^1\text{H}$ ) Bruker Avance II with a dual resonance probe. Samples were packed in 4 mm diameter zircon NMR tubes with Kel-F rotor caps (Bruker-Biospin). Semi-quantitative compositions of the RO/ED isolated samples were investigated using  $^{13}\text{C}$  cross polarization/total sideband suppression (CP/TOSS) NMR experiments at a spinning speed of 6.5 kHz and a cross polarization (CP) time of 0.5 ms with a  $^1\text{H}$   $90^\circ$  pulse-length of 4.0  $\mu\text{s}$  and a recycle delay of 1.0 s. Four-pulse total suppression of sidebands (TOSS) (Dixon 1982) was applied prior to detection, and two-pulse phase-modulated (TPPM) decoupling was used for optimum resolution (Bennet et al. 1995). Signals from nonprotonated carbons or mobile carbons like rotating  $\text{CH}_3$  groups were isolated using  $^{13}\text{C}$  CP/TOSS with 40  $\mu\text{s}$  dipolar dephasing (Opella and Frey 1979). 13312 scans were accumulated for each of these experiments.

The signals of anomeric carbons (e.g., stereoisomeric carbons from cyclic sugars; O-C-O), which resonate between 90 and 120 ppm, were differentiated from those of aromatic and olefinic carbons, which resonate between 100 and 165 ppm, by using a five-pulse  $^{13}\text{C}$  chemical-shift anisotropy (CSA) filter with a CSA-filter time of 40  $\mu\text{s}$  (Mao and Schmidt-Rohr 2004) to selectively suppress the signals of  $\text{sp}^2$  hybridized carbons. The CSA-filter technique was also combined with dipolar dephasing to isolate signals from deprotonated and highly mobile aliphatics and with a short CP time (50  $\mu\text{s}$ ) to isolate protonated aliphatics; 6,144 scans were accumulated for each of these experiments.

Spectra representing only protonated carbons were obtained using a simple spectral editing experiment. First, a CP/TOSS spectrum was recorded using a short CP of 50  $\mu\text{s}$  (6,144 scans). It revealed predominantly protonated carbons in immobile segments, but also residual peaks of quaternary carbons result from two-bond magnetization transfer. Second, a CP/TOSS spectrum was recorded using a short CP of 50  $\mu\text{s}$  and 40  $\mu\text{s}$  dipolar dephasing (6,144 scans), which contains only residual signal from quaternary carbons or mobile segments (including  $\text{CH}_3$  groups with > 50% efficiency). The difference of the two spectra provided the spectrum of immobile  $\text{CH}_2$  and CH carbons, with a small  $\text{CH}_3$  contribution (Mao et al. 2007a).

High-speed  $^{13}\text{C}$  direct polarization/magic angle spinning (DP/MAS) NMR and high-speed quantitative  $^{13}\text{C}$  DP/MAS NMR with recoupled dipolar dephasing provide quantitative structural information. These spectra were run at a spinning speed of 13 kHz. The  $90^\circ$   $^{13}\text{C}$  pulse length was 4  $\mu\text{s}$ . Recycle delays were tested by the cross polarization/spin lattice relaxation time–total suppression of sidebands (CP/ $T_1$ -TOSS) technique to ensure that all carbon sites were fully relaxed (Mao et al. 2000). The recycle



delay was 170 s and 1,536 scans were collected. This technique was fully described elsewhere (Mao and Schmidt-Rohr 2003).

To determine the analytical uncertainty, the signal to noise ratio (S/N) was determined for each integration region. Based on the inverse relationship between S/N and relative standard deviation (RSD), the standard deviation of the integral was calculated. Additional uncertainty arises from the assignment of chemical shift ranges used for integration and from the unrecovered fraction of DOM. The former was partly alleviated by the use of spectral editing to differentiate overlapping signals and by the consistent application of integration ranges to maintain comparability of the samples. The uncertainty resulting from incomplete DOM recovery was not considered in our interpretations based on the assumption that RO/ED isolation provides DOM samples that are intercomparable (Vetter et al. 2007; Koprivnjak et al. 2009) and the finding that DOC recoveries of replicate samples are generally consistent (see below).

## RESULTS

Initial seawater sample DOC concentrations were 39-88  $\mu\text{mol L}^{-1}$  and were concentrated by RO/ED to 1076-4298  $\mu\text{mol L}^{-1}$ . DOC recoveries for the RO/ED process (not including material recovered by rinsing the membranes with NaOH) ranged from 40-68% in the Atlantic Ocean samples (3 samples average = 51%) and 83-86% in the Pacific Ocean samples (2 samples average = 84%; Table 15). The low recovery (40%) observed in the North Atlantic 3000 m sample was likely due to the system not being adequately conditioned prior to use, but because its spectroscopic properties appeared consistent with the other samples, it was kept as part of this study. With the exception of this sample,

Table 15. Recovery of DOC by the RO/ED method. Only the "Initial" (seawater) and "Final" (concentrated and desalted) fractions were analyzed as part of this study, and only the "Final" fraction was amenable to solid-state NMR analysis.

Sample	Volume (l)			DOC ( $\mu\text{mol liter}^{-1}$ )			Yield (%)		
	Initial	Final	Rinse	Initial	Final	Rinse	Final	Rinse**	Total**
5m N. Atl. (upwelling)	473	6.6	4.3	88	4298	1104	68	11	79
5m N. Pac. (ALOHA)	142	6.1	4.4	69	1325	435	83	19	102
415m N. Atl. ( $\text{O}_2$ min.)	365	5.9	4.6	54	1523	421	46	10	56
3000m N. Atl. (ISOW)	355	5.4	4.5	41*	1076	323	40	10	50
3500m N. Pac. (ALOHA)	249	6.7	5.6	39*	1254	343	86	20	106

\*Yields were calculated using DOC values from previous studies (Hansell and Carlson 1998; Carlson et al.

2010). Measured DOC for deep ocean samples were higher,  $62 \mu\text{mol liter}^{-1}$  (ISOW) and  $52 \mu\text{mol liter}^{-1}$  (ALOHA), and were likely contaminated during sub-sampling for DOC.

\*\*Recent improvements in the RO/ED method have removed the need to collect separate final concentrates and NaOH rinses (N. Green, unpubl.).

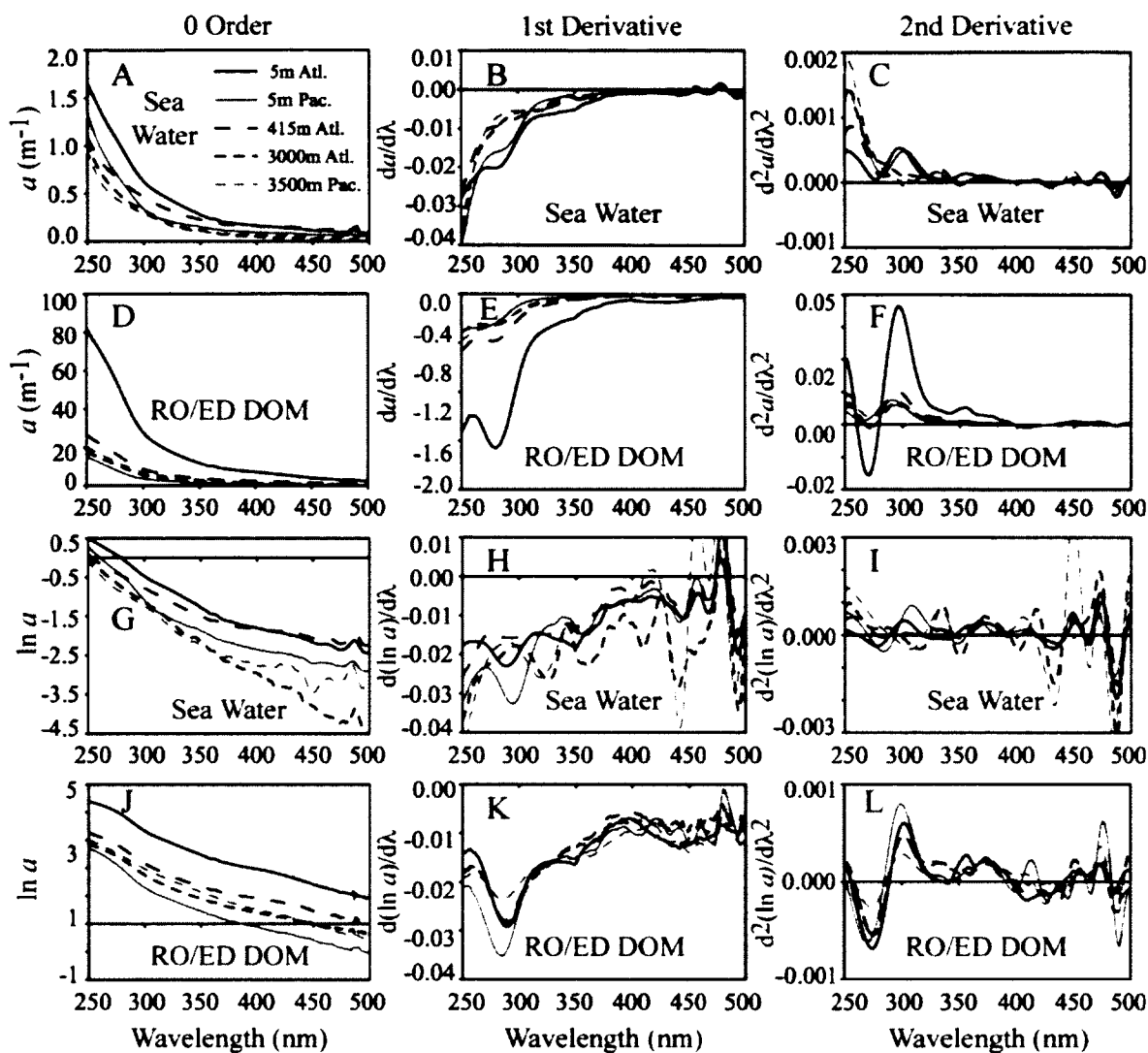


Fig. 33. UV-visible absorption spectra collected for (A) filtered seawater samples using 10 cm cuvette, (B) first-derivative, and (C) second-derivative. (D) Absorption spectra for RO/ED isolated samples using 1 cm cuvette, (E) first-derivative, and (F) second-derivative. (G) Natural log absorption spectra for filtered seawater samples, (H) first-derivative, and (I) second-derivative. (J) Natural log absorption spectra for RO/ED isolated samples, (K) first-derivative, and (L) second-derivative.

Table 16. Summary of optical properties measured for initial seawater samples and RO/ED isolates. Values in parentheses are the absorption coefficients predicted based on the measured seawater values, RO/ED concentration factors and DOC recoveries.

	Seawater samples				
	5m N. Atl. (Upwelling)	5m N. Pac. (ALOHA)	415m N. Atl. (O <sub>2</sub> min.)	3000m N. Atl. (ISOW)	3500m N. Pac. (ALOHA)
$a_{254}$ (m <sup>-1</sup> )	1.54	1.19	0.99	0.90	0.80
$a_{300}$ (m <sup>-1</sup> )	0.62	0.34	0.46	0.32	0.29
SUVA254	1.46	1.36	1.53	1.21	1.21
SUVA300	0.587	0.388	0.710	0.430	0.440
$S_{300-700}$ (nm <sup>-1</sup> )	0.0087	0.0084	0.0071	0.0090	0.0067
$S_{275-295}$ (nm <sup>-1</sup> )	0.0225	0.0289	0.0156	0.0203	0.0174
$S_{350-400}$ (nm <sup>-1</sup> )	0.0101	0.0092	0.0064	0.0166	0.0095
$S_R$	2.22	3.13	2.42	1.22	1.83
	RO/ED isolates				
	5m N. Atl.	5m N. Pac.	415m N. Atl.	3000m N. Atl.	3500m N. Pac.
$a_{254}$ (m <sup>-1</sup> )	77.8 (75.1)	14.1 (23.0)	24.9 (28.2)	16.7 (23.7)	19.1 (25.6)
$a_{300}$ (m <sup>-1</sup> )	28.0 (30.2)	3.6 (6.6)	8.7 (13.0)	5.8 (8.4)	7.2 (9.3)
SUVA254	1.55	0.866	1.42	1.49	1.22
SUVA300	0.558	0.224	0.497	0.514	0.462
$S_{300-700}$ (nm <sup>-1</sup> )	0.0097	0.0125	0.0086	0.0080	0.0123
$S_{275-295}$ (nm <sup>-1</sup> )	0.0284	0.0351	0.0275	0.0279	0.0235
$S_{350-400}$ (nm <sup>-1</sup> )	0.0100	0.0112	0.0083	0.0097	0.0127
$S_R$	2.85	3.15	3.33	2.87	1.85
	CDOM Recovery (%)				
	5m N. Atl.	5m N. Pac.	415m N. Atl.	3000m N. Atl.	3500m N. Pac.
$a_{254}$ (%)	70	51	42	28	64
$a_{300}$ (%)	63	46	32	27	67

recoveries are consistent with Koprivnjak et al. (2009). Using the same RO/ED system used in this study, repeated isolation of samples collected at the same depth at the Natural Energy Laboratory of Hawaii (NELHA) led to consistent recoveries (9 replicates; 67%  $\pm$ 4%; unpublished data).

CDOM was effectively concentrated along with the bulk DOM (Fig. 33; Table 16). Generally, the RO/ED isolates exhibited slightly higher  $S$ ,  $S_R$  and SUVA values than the initial seawater samples; however, the 415 m North Atlantic and 5 m North Pacific isolates had slightly lower SUVA values, and the 415 m and 3000m North Atlantic isolates had significantly higher  $S_{275-295}$  and  $S_R$  values. RO/ED isolates showed lower absorbance in the 190-230 nm region compared to the original samples (data not shown) due to the removal of dissolved nitrate, nitrite and bromide. Electrodialysis cannot remove uncharged inorganic salts, which co-concentrated along with the organic matter by reverse osmosis. The freeze-dried isolates from deep ocean samples contained less organic carbon as a fraction of total dissolved solids than the surface ocean samples. The 5 m North Atlantic and 5 m North Pacific freeze-dried powders contained 22.1% and 16.5% organic carbon respectively. The 415 m North Atlantic sample contained 15.3% organic carbon, while the 3000 m North Atlantic sample contained 8.0% organic carbon and the 3500 m North Pacific sample contained 6.9% organic carbon. The inorganic fraction of the freeze-dried powders contained primarily borates (~75-82%) and silicates (~0.3-17%), which increased with increasing depth (E. M. Perdue pers. comm.).

The solid-state CP/TOSS  $^{13}\text{C}$  NMR spectra for the RO/ED DOM isolates are shown in Fig. 34. It is noteworthy that, with the exception of the deep Pacific sample, the spectra are markedly similar. This similarity was also observed using high-resolution

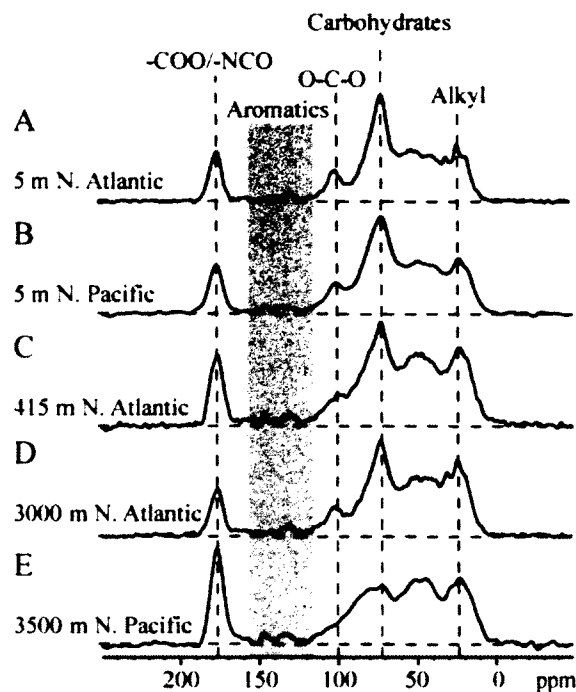


Fig. 34. Solid-state  $^{13}\text{C}$  NMR spectra measured by cross polarization with magic angle spinning and total suppression of sidebands (CP-TOSS). Samples collected at (A) a depth of 5 m from the Mauritanian upwelling zone in the N. Atlantic, (B) a depth of 5 m from station ALOHA in the N. Pacific, (C) a depth of 415 m in the eastern N. Atlantic, (D) a depth of 3000 m in the eastern N. Atlantic (Iceland Scotland Overflow Water), and (E) a depth of 3500 m from station ALOHA in the N. Pacific. Samples were isolated by RO/ED and freeze-dried.

Table 17. Integration ranges and normalized areas (total=100%) determined based on solid-state  $^{13}\text{C}$  CP/TOSS NMR spectra. Values are given as integrated signal (normalized to 100% total area). Uncertainty is reported as one standard deviation.

CP/TOSS Integrations	Functional Groups	5m N. Atl. (Upwelling)	5m N. Pac. (ALOHA)	415m N. Atl. (O <sub>2</sub> min.)	3000m N. Atl. (ISOW)	3500m N. Pac. (ALOHA)
0-25	CH <sub>3</sub> , CH <sub>2</sub>	12.4 ±0.1	11.3 ±0.2	13.8 ±0.3	13.3 ±0.2	12.5 ±0.2
25-35	CH <sub>2</sub> , CH	8.2 ±0.1	7.5 ±0.2	8.4 ±0.2	10.2 ±0.2	8.3 ±0.1
35-50	CH, CH <sub>2</sub> , Cq	13.1 ±0.1	12.9 ±0.4	14.3 ±0.3	14.5 ±0.4	13.8 ±0.3
50-60	Cq, OCH <sub>3</sub> , HC-NH	9.5 ±0.1	9.0 ±0.2	9.3 ±0.2	9.1 ±0.2	9.1 ±0.2
60-90	Carbohydrate-like	34.8 ±0.2	35.0 ±0.5	30.2 ±0.5	30.5 ±0.5	25.0 ±0.5
90-110	Anomeric O-C-O, Aromatic C	8.0 ±0.1	8.8 ±0.3	7.8 ±0.2	7.9 ±0.2	7.9 ±0.2
110-130	Aromatic C-H, Cq	1.9 ±0.1	2.8 ±0.1	2.2 ±0.1	2.3 ±0.1	2.4 ±0.1
130-150	Aromatic C-H, Cq	1.4 ±0.1	1.6 ±0.1	1.9 ±0.1	1.8 ±0.1	2.7 ±0.2
150-165	Aromatic C-O	0.8 ±0.1	0.8 ±0.1	1.2 ±0.1	1.3 ±0.1	1.3 ±0.1
165-190	COO-/COOH, ester, amide	9.6 ±0.1	9.9 ±0.3	10.8 ±0.3	8.6 ±0.3	16.3 ±0.2
190-220	Aldehyde, ketone, quinone	0.3 ±0.1	0.7 ±0.1	0.1 ±0.1	0.7 ±0.1	0.8 ±0.1

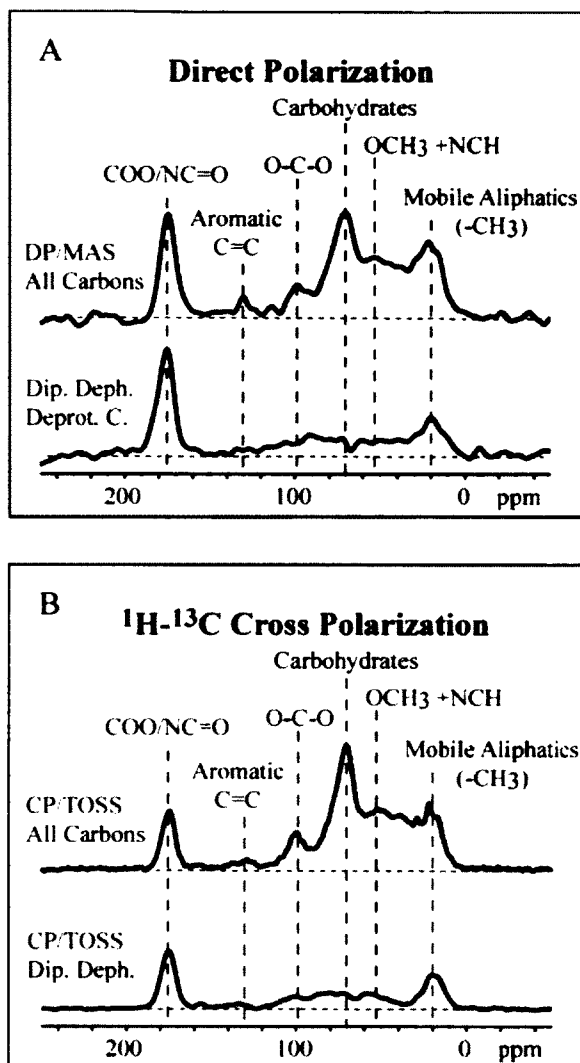


Fig. 35. A representative sample (5 m North Atlantic) was measured using both (A) direct polarization and (B) cross polarization  $^{13}\text{C}$  NMR.



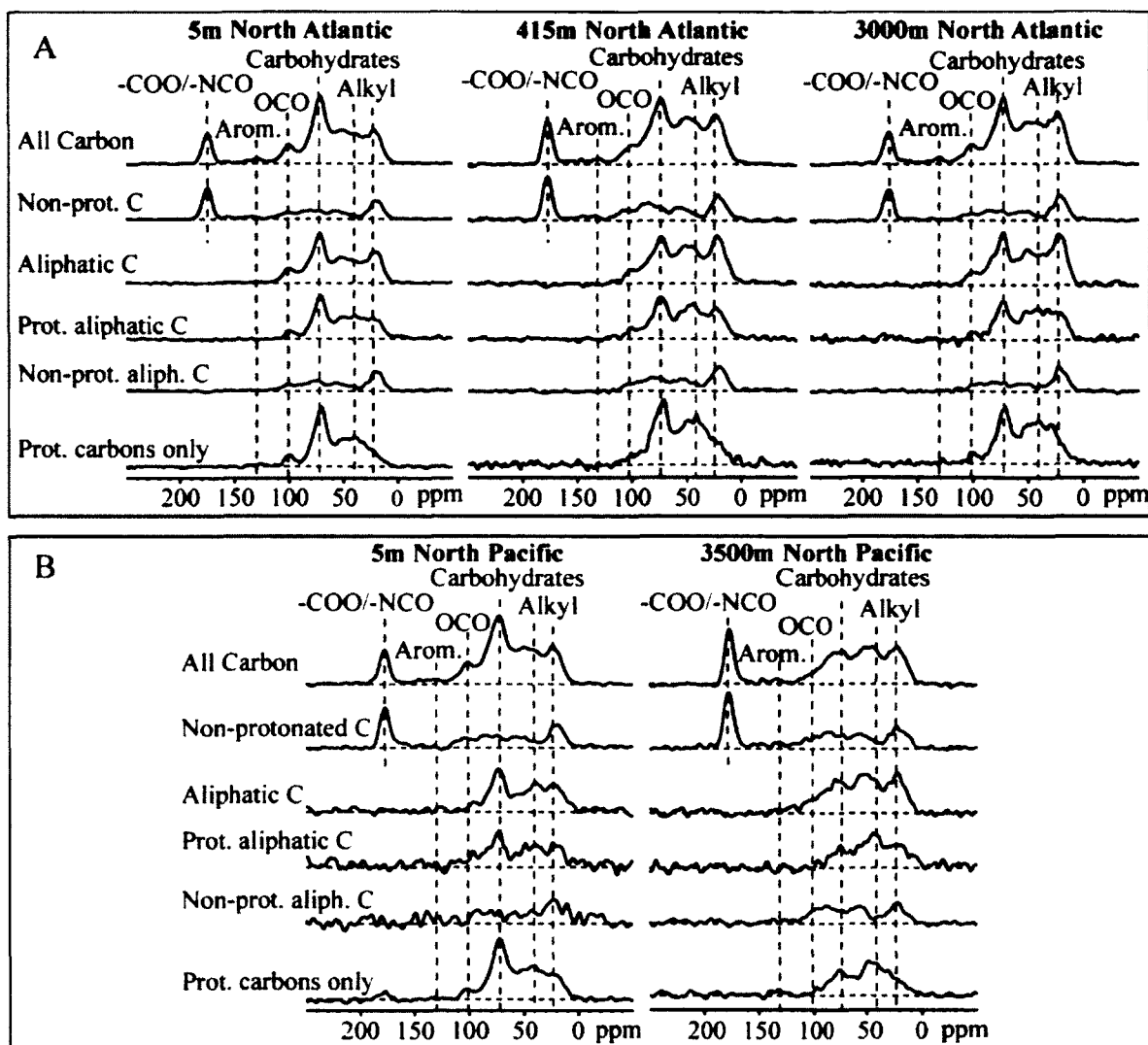


Fig. 36. Solid-state  $^{13}\text{C}$  CP/TOSS NMR spectra and CP/TOSS NMR spectra with spectral editing were collected for (A) RO/ED isolated DOM from the N. Atlantic and (B) RO/ED isolated DOM from the N. Pacific. CP/TOSS spectra, "All Carbon," are shown as reference spectra. CP/TOSS with dipolar dephasing: "Non-protonated C," CSA-filtered spectra: "Aliphatic C," short CP and CSA-filter: "Prot. aliphatic C," CSA-filter and dipolar dephasing: "Non-prot. Aliph. C." The spectra labeled "Protonated carbons only" show the difference between spectra collected using a short CP time and spectra combining the short CP time and dipolar dephasing.

mass spectrometry (H. Chen unpubl.). All five CP/TOSS spectra show that the isolated DOM contains very little aromatic material (90-160 ppm), but rather a mixture of substituted (50-120 ppm) and un-substituted (0-50 ppm) aliphatic carbons as well as a significant contribution from carboxylic carbons (acids, esters and amides; 160-190 ppm). All samples show strong indications of carbohydrate-like material (60-90 ppm C-O and 90- 120 ppm O-C-O) though the signals in those regions are weaker for the 3500 m North Pacific Ocean sample. The 3500 m North Pacific and 415 m North Atlantic samples have the strongest carboxyl signals. The functional groups assigned to each spectral region and the integrated signals from each CP/TOSS spectrum are listed in Table 17.

The DP/MAS  $^{13}\text{C}$  NMR and CP/TOSS NMR spectra obtained for the surface North Atlantic (Mauritanian upwelling zone) sample are compared in Fig. 35. Cross polarization NMR peak area integrations are semi-quantitative, having lower signal for aromatic carbons and carboxylic carbons than DP NMR spectra. However, despite this bias, Fig. 35 shows that routine semi-quantitative CP spectra are reasonably representative and therefore can be used to investigate compositional differences between samples.

The signal in the 90-115 ppm region of the CP/TOSS reference spectrum represents the combined contributions of anomeric carbons and some aromatic carbons, while the CSA-filtered spectra exclude the aromatic signals. Anomeric carbons clearly dominate this region of the spectra for the open ocean samples (Fig. 36 “Aliphatic C”). Comparing the CSA-filtered/dipolar-dephased spectrum and the CSA-filtered spectrum with short CP shows that the majority of these anomeric moieties are protonated (Fig.

Table 18. The relative abundances (%) of functional groups in RO/ED isolated DOC estimated based on NMR integration data (Table 17) and NMR spectral editing results (Fig. 36). Uncertainties are listed as one standard deviation and were calculated based on the signal to noise ratios determined for each integration region of the CP/TOSS, dipolar dephased, CSA-filtered, and/or combined dipolar dephased and CSA-filtered spectra.

Integrated Region	Functional Group Category	5m N. Atl. (Upwelling)	5m N. Pac. (ALOHA)	415m N. Atl. (O <sub>2</sub> min.)	3000m N. Atl. (ISOW)	3500m N. Pac. (ALOHA)
0-25	CH <sub>3</sub>	8.9 ±0.1	7.6 ±0.2	10.2 ±0.3	11.2 ±0.2	10.5 ±0.2
15-45	CH <sub>2</sub>	13.3 ±0.1	12.0 ±0.3	13.9 ±0.3	13.6 ±0.2	12.0 ±0.2
35-50	Aliphatic CH	8.7 ±0.1	11.6 ±0.3	9.1 ±0.2	11.9 ±0.3	8.5 ±0.2
35-60	Aliphatic Cq	4.1 ±0.7	4 ±2	5.1 ±0.5	5.1 ±0.6	6.6 ±1.0
50-60	Aliphatic C-OH and NCH	7.9 ±0.1	7.2 ±0.2	7.2 ±0.2	7.1 ±0.2	6.1 ±0.1
60-110	Carbohydrate-like C	38.1 ±0.3	34 ±2	31.8 ±0.8	31.1 ±0.6	25 ±1
90-110	O-Cq-O	2.6 ±0.1	1.8 ±0.4	4.4 ±0.2	2.3 ±0.1	5 ±0.6
100-165	Protonated aromatics	3.0 ±0.1	5.5 ±0.6	2.4 ±0.2	4.1 ±0.2	2 ±0.6
100-165	Non-protonated aromatics	2.6 ±0.1	4.5 ±0.6	3.4 ±0.4	4.0 ±0.2	5 ±0.6
165-190	COO-/COOH, ester, amide	10.3 ±0.1	10.3 ±0.3	11.7 ±0.3	9.1 ±0.3	17.7 ±0.2
190-220	Aldehyde, ketone, quinone	0.3 ±0.1	0.7 ±0.1	0.1 ±0.1	0.7 ±0.1	0.9 ±0.1

36). The signal from the 90-115 ppm region of the CSA-filtered/dipolar dephased spectrum, labeled in Table 18 as O-Cq-O (quaternary anomeric carbon; Fig. 37), was least abundant in the surface Pacific and most abundant in the deep Pacific sample. The integrated signal from the 90-165 ppm regions of the spectra labeled “Non-protonated C” and “Protonated carbons only” in Fig. 36, corrected for the contribution from anomeric carbons, was used to estimate the relative contribution from protonated and non-protonated aromatics (Table 18). Non-protonated aromatics include substituted ring carbons and olefinics as well as carbons in the interior of condensed aromatic structures, such as black carbon.

The surface sample collected in the Mauritanian upwelling zone shows the highest percentage of carbohydrate-like carbons (~75 ppm and ~100ppm) and the lowest percentage of non-protonated aromatic carbons (Tables 17 & 18). The surface sample from station ALOHA is similar to the Mauritanian upwelling zone sample, but with slightly lower carbohydrate-like carbon signals and slightly higher aromatic and/or olefinic carbon signals. The alkyl carbon signals of the two surface samples (0-50 ppm) are also similar (Tables 17 and 18). The ISOW (3000 m North Atlantic) DOM contains the lowest percentage of carboxylic carbon, while the 3500 m North Pacific DOM contains the lowest percentage of carbohydrate-like material (but highest percentage of quaternary anomeric carbons), lowest percentage of protonated aromatic carbon, highest percentage of non-protonated carbon, and largest percentage of carboxylic carbon (Table 18).

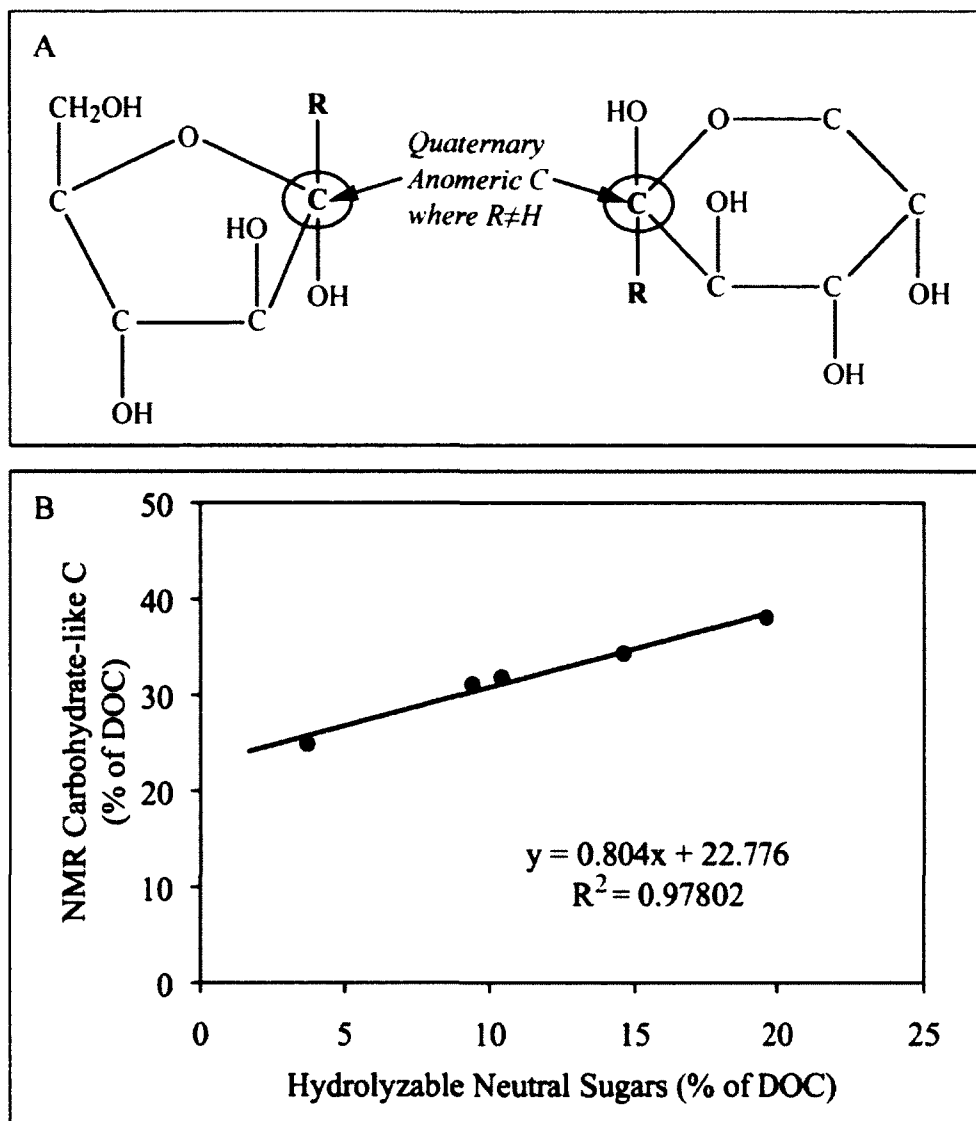


Fig. 37. (A) Quaternary anomeric carbons in furanose (left) and pyranose (right) sugars. (B) Hydrolyzable neutral sugars determined by the MBTH method versus carbohydrate-like C determined by CP/TOSS NMR and CP/TOSS with CSA-filter (includes O-CH-O, but excludes O-C<sub>q</sub>-O). MBTH data provided by H. Chen (unpubl.).

Comparing NMR quantification of carbohydrate-like DOC with the wet chemical determination of total hydrolysable neutral sugars (THNS), as measured for these samples by H. Chen (unpubl.), shows that while the two methods are strongly correlated ( $R^2 = 0.98$ ; Fig. 37B). However, the size of the NMR “carbohydrate-like” pool is approximately 23% larger (y-intercept = 22.8) and about 20% less dynamic (slope ~0.8) than the THNS pool.

## DISCUSSION

*Characterization of RO/ED isolated ocean DOM by solid-state  $^{13}\text{C}$  NMR* – In general, the recoveries were higher than those reported for other isolation techniques such as XAD or PPL SPE and ultrafiltration, which typically recover ~10-40% of oceanic DOC (Benner et al. 1992; Mopper et al. 2007; Dittmar et al. 2008; Koprivnjak et al. 2009). The most abundant inorganic materials in the isolates were silica and borate, which are not efficiently removed by RO/ED (E. M. Perdue pers. comm.). The large difference between residual inorganic solids in the deep and surface seawater samples was mainly due to silica, which has very low surface ocean concentrations (Chester 1990). Beyond their dilution of  $^1\text{H}$  and  $^{13}\text{C}$ , silica and borate are not expected to cause significant errors in the CP/TOSS NMR spectra.

DP/MAS  $^{13}\text{C}$  NMR (Fig. 35) provided spectra that were more quantitative than CP/TOSS with respect to proximity of  $^1\text{H}$  and  $^{13}\text{C}$  nuclei. However, time constraints meant that DP/MAS spectra could not be obtained for all of the samples. It is worth noting that CP/TOSS spectra were moderately biased against detection of carboxylic

Table 19. Comparison of CP/TOSS results for RO/ED isolates with CP/MAS

results from previous studies. Analytical uncertainties are reported as one standard deviation (for this study only).

Chemical Shift Range, ppm	0-60	60-110	110-160	160-190	190-220
Structural category	Alkyl	Alkoxy	Aromatic	Carboxyl	Carbonyl
<i>Open Ocean DOM Isolated by RO/ED</i>					
5m N. Atl. (upwelling)	42.8 $\pm$ 0.4	43.2 $\pm$ 0.2	3.8 $\pm$ 0.1	9.9 $\pm$ 0.1	0.3 $\pm$ 0.1
5m N. Pac. (ALOHA)	40.3 $\pm$ 0.9	44.0 $\pm$ 0.7	4.9 $\pm$ 0.2	10.1 $\pm$ 0.3	0.7 $\pm$ 0.1
415m N. Atl. (O <sub>2</sub> min.)	45.8 $\pm$ 0.8	37.8 $\pm$ 0.6	5.1 $\pm$ 0.2	11.1 $\pm$ 0.3	0.2 $\pm$ 0.1
3000m N. Atl. (ISOW)	47.0 $\pm$ 0.8	38.2 $\pm$ 0.6	4.9 $\pm$ 0.2	9.2 $\pm$ 0.3	0.7 $\pm$ 0.1
3500m N. Pac. (ALOHA)	45.3 $\pm$ 0.7	32.4 $\pm$ 0.7	5.2 $\pm$ 0.2	16.8 $\pm$ 0.2	0.3 $\pm$ 0.1
<i>Coastal Marine DOM isolated by RO/ED</i>					
Ogeechee R. 2m (Koprivnjak et al. 2009)	43	32	10	11	4
GA Bight 20m* (Koprivnjak et al. 2009)	37	37	11	12	3
GA Bight 84m (Koprivnjak et al. 2009)	44	36	7	11	2
<i>DOM isolated by UltraFiltration</i>					
10m N. Pac. (Benner et al. 1992)	25	53	7	12	3
20m N. Pac. (Sannigrahi et al. 2005)	26	66	0	8	
4000m N. Pac. (Benner et al. 1992)	30	28	21	16	5
4000m N. Pac. (Sannigrahi et al., 2005)	46	43	0	11	
<i>HA and FA isolated with XAD-2 resin</i>					
5m N. Pac. (Hedges et al. 1992)	45	18	18	15	4
4200m N. Pac. (Hedges et al. 1992)	46	17	19	15	3
<i>Freshwater NOM (RO isolated)</i>					
Suwannee R. (Perdue and Ritchie 2003)	27	24	25	19	5

\*Average of three samples.

moieties (165-190 ppm) and aromatics (100-165 ppm), which are thus underestimated by approximately 15% and 11% respectively in Tables 17 and 18.

Compared to surface samples, DOM isolated from the deep North Pacific and Atlantic oxygen minimum layer showed lower abundance of O-alkyl carbons (60-120 ppm) and higher abundance of carboxylic functionality (160-190 ppm; Fig. 36; Table 17). Dipolar dephased spectra (non-protonated C) show that these two samples exhibit the greatest contribution from quaternary alkyl carbons (50-100 ppm; Fig. 36). Similarly, CSA-filtered spectra indicated that these two samples had the weakest signal from anomeric carbons (90-115 ppm; Fig. 36). By contrast, the surface samples, which were expected to contain the largest fraction of freshly produced algal DOM, show the highest content of carbohydrate-like material, more protonated carbons, and a lower content of carboxyl carbons (Figs. 34 and 36; Tables 17 and 18).

*Comparison with previously published results* – Aromatic carbon (NMR-based) in surface waters vary from ~25% of organic carbon in DOM-rich freshwater (RO isolated Suwannee River NOM; (Perdue and Ritchie 2003) to 10% of organic carbon in coastal seawater (isolated by RO/ED; Koprivnjak et al. 2009) and 4-5% in open ocean surface water (Table 19). NMR data (Table 19) showed that deep Pacific UF isolated DOM (UDOM) is similar to the RO/ED isolated DOM (using the average of the two deep Pacific UDOM results), while surface Pacific UDOM is more enriched in O-alkyl groups and depleted in unsubstituted alkyl groups (Benner et al. 1992; Sannigrahi et al. 2005) compared to the RO/ED isolated DOM. Isolation of DOM from acidified seawater with XAD-2 resin (Hedges et al. 1992) recovers a fraction of marine DOM that is enriched in



alkyl, aromatic, and carboxyl carbons, and depleted in O-alkyl carbons relative to comparable RO/ED isolates (Table 19).

The discrepancy between the size of the two carbohydrate pools (spectrophotometric vs. NMR) shown in Fig. 37B may have arisen from sugar monomers that are degraded during hydrolysis and polysaccharides that are resistant to acid hydrolysis (Benner et al. 1992; Skoog and Benner 1997; Mao et al. 2010) or non-carbohydrate NMR signals that resonate in the 60-100 ppm range (McCarthy et al. 1996; Skoog and Benner 1997). However, the strong correlation ( $R^2 = 0.98$ ) indicates that the NMR signal in this spectral range mainly reflects carbohydrates and carbohydrate-like material.

Hertkorn et al. (2006) showed evidence of a refractory DOM component referred to as carboxyl-rich alicyclic molecules (CRAM) based on characterization of deep and surface ocean UDOM samples using two-dimensional NMR and ultra-high resolution mass spectrometry. While the one-dimensional NMR results presented here cannot confirm these specific DOM structures, the abundance of carboxylic functional groups as a fraction of DOC is highest in the deep Pacific sample, which supports the findings of Hertkorn et al (2006).

*Compositional and bulk structural changes to oceanic DOC* – The apparent  $^{14}\text{C}$  ages of the DOC and RO/ED isolated DOM from the water samples collected in this study have not been measured; however, based on values published for water samples from comparable depths and locations (Williams and Druffel 1987; Guo et al. 1996;

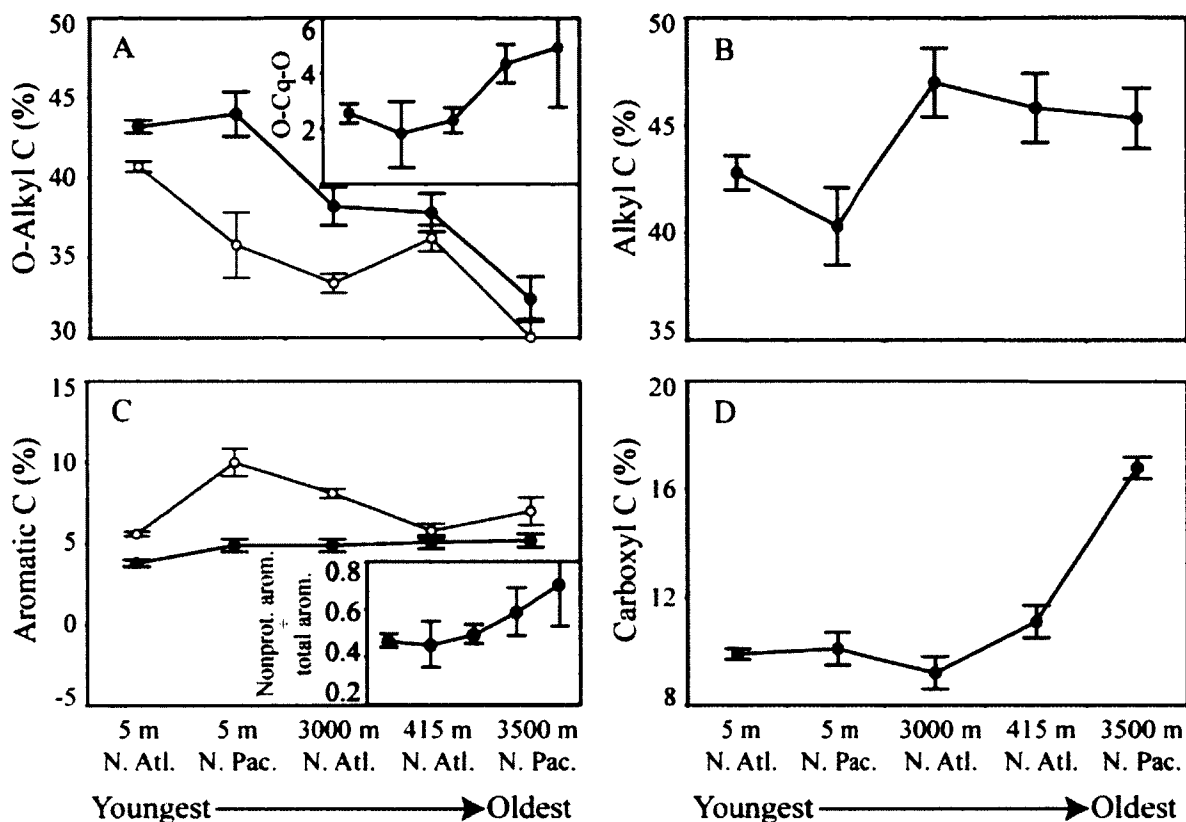


Fig. 38. Functional group relative abundance displayed on a carbon percentage

basis. (A) O-alkyl and quaternary anomeric carbons (inset), (B) alkyl carbons, (C) aromatic carbons and non-protonated aromatic C as a fraction of total aromatic C (inset), and (D) carboxyl carbons quantified in the RO/ED isolates by CP-TOSS  $^{13}\text{C}$  NMR. Error bars represent analytical uncertainty calculated based on the propagated standard deviations of from the CP/TOSS, CSA-filtered, dipolar dephased, and/or combined CSA-filtered/ dipolar-dephased spectra. Black symbols are based on CP/TOSS. Gray symbols and inset trends are based on spectral editing techniques. Error bars are shown as two standard deviations (95% confidence interval).

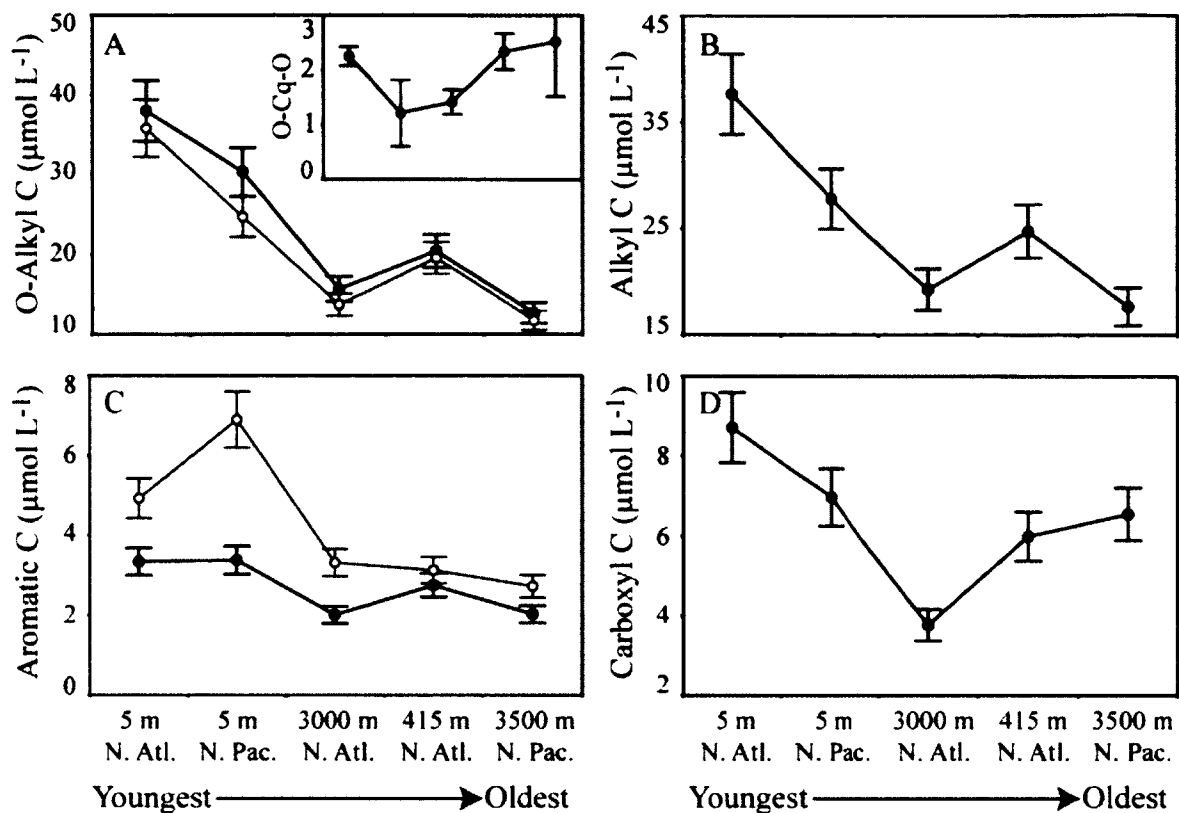


Fig. 39. Estimated in situ concentrations, assuming that RO/ED isolates are

reflective of total organic carbon pool irrespective of the recovery. (A) O-alkyl and quaternary anomeric carbons, (B) alkyl carbons, (C) aromatic carbons, and (D) carboxyl carbons extrapolated to their approximate in situ concentrations by normalizing to the original DOC concentrations. Black symbols are based on CP/TOSS. Gray symbols and inset are based on spectral editing techniques. Error bars represent the combined analytical error of the NMR spectra and the DOC measurements and are shown as two standard deviations (95% confidence interval).

Bauer and Druffel 1998; Bauer et al. 2002), the DOC in these samples have the following order of increasing apparent age: 5 m North Atlantic < 5 m North Pacific < 3000 m North Atlantic < 415 m North Atlantic < 3500 m North Pacific. In order to estimate the impact of age/degradation on the bulk structural characteristics and composition of DOM, several moieties quantified by solid-state  $^{13}\text{C}$  NMR are shown in order of their estimated apparent ages in Fig. 38. The NMR integration data were extrapolated to the approximate in situ concentration by normalizing to the seawater DOC concentration (Fig. 39). Figs. 38 & 39, together with the NMR spectra in Figs. 35 and 36, reveal several general trends that may reflect processes important to the cycling of DOM in the oceans. Carbohydrate-like compounds decrease both as a fraction of DOC and in concentration as DOM ages within the ocean (Figs. 38A and 39A). However, part of the carbohydrate pool, characterized by quaternary anomeric carbons is either refractory or produced during marine DOM aging (Figs. 38A inset and 39A inset). Alkyl carbons do not show a trend as a fraction of DOC (Fig. 38B), but appear to decrease in concentration (Fig. 39B) indicating that some alkyl carbons are part of the labile or semi-labile fraction of DOC.

Quaternary anomeric carbons (Table 18, Figs. 38 and 39A inset) appear to have a biogeochemical cycle that differs significantly from the overall carbohydrate-like pool (Table 18). Generally, samples expected to contain the freshest algae-derived DOM have the lowest O-Cq-O percentages, while the oldest, most-degraded DOM samples are the richest. Additionally, O-Cq-O carbons appear to be more abundant in the surface Atlantic Ocean than in the surface Pacific Ocean. Quaternary anomeric carbons are present in some furanose sugars (Poulin and Lowary 2010) and sugars that are functionalized at the anomeric carbon, e.g. keto-deoxyoctulosonate in bacterial lipopolysaccharides

(Herschberger and Binkley 1968; Strain and Armitage 1985). Furanose containing glycoconjugates are common constituents of bacterial cell walls, but furanose containing sugars (e.g. fructose, sucrose), oligosaccharides and polysaccharides are also produced by plants, fungi, and archaea (Poulin and Lowary 2010). Thus, the quaternary anomeric carbons observed in these samples may have been produced by bacteria or released during microbial degradation of organic matter (Ogawa et al. 2001), or released/preserved during bacterial mortality (Nagata and Kirchman 1999). Compounds containing O-Cq-O may be inherently resistant to microbial degradation or rapidly transported from surface waters to sediments and protected by strong adsorption or encapsulation (Hedges and Keil 1995; Henrichs 1995) and then released later to bottom waters by microbial processing at the sediment-water interface (Burdige 2002). Each of the above possibilities is consistent with the trend of their increasing abundance with apparent DOC age, however a predominantly bacterial source would explain the greater abundance of O-Cq-O in the North Atlantic surface (compared to the North Pacific surface) as this sample site exhibits the more active microbial food web and microbial-DOM loop. It should be noted that the difference between these two samples is based on the dual filtered (CSA and dipolar dephasing) spectra for which the 5 m Pacific sample has a low signal to noise ratio (see spectrum in Fig. 36 and error bars in Table 18 and Figs. 38 and 39). Further efforts to identify specific, naturally produced carbohydrates with these O-Cq-O structures, and investigations of their sources and cycling in the marine environment are clearly needed.

Aromatic carbons do not show an obvious trend with depth or age (Fig. 38C); however, non-protonated aromatic carbons, e.g., black carbon, (Fig. 38C inset) clearly

exhibit refractory behavior (Dittmar and Paeng 2009; Ziolkowski and Druffel 2010). However, when total aromatic and olefinic carbon concentrations are considered (Fig. 39C), a trend that is the opposite of that reported by Benner et al. (1992) and Hedges et al. (1992) was observed. Aromatic carbon represented a larger fraction of DOC and a higher concentration in surface waters than in deep waters (Figs. 38C and 39C). The non-protonated aromatic carbons (Table 18) likely include a significant amount of carbons from condensed aromatic structures (Masiello and Druffel 1998; Ziolkowski and Druffel 2010). Condensed aromatics typically have a pyrogenic source (e.g. fossil fuel and biomass burning) and reach the ocean via transport through soil pore waters and riverine export or via atmospheric deposition (Hockaday et al. 2006; Flores-Cervantes et al. 2009; Watanabe et al. 2010). Condensed aromatics are inherently resistant to microbial degradation due to the small amount of energy derived from their oxidation and the small number of species capable of utilizing aromatics as a source of carbon or energy (Rogoff and Wender 1962; Semple et al. 1999). Recent work has also suggested a possible hydrothermal source for condensed aromatics (Dittmar and Koch 2006). Radiocarbon ages for black carbon (Ziolkowski and Druffel 2010) indicate that it is probably the oldest and therefore most recalcitrant component of ocean DOM. The results show the largest percentage of non-protonated aromatic carbon in the deep North Pacific (Table 18) and that non-protonated aromatic carbon increases relative to protonated aromatic carbon during aging (Fig. 38C inset), which suggests aging within the ocean's interior plays some role in the distribution and cycling of condensed aromatics, possibly including selective preservation or hydrothermal processing of DOM.

Carboxylic groups make up a larger fraction of DOC in the 415 m Atlantic and 3500 m Pacific samples (Fig. 38D), which may reflect the formation of refractory carboxyl-rich structures, such as CRAM (Hertkorn et al. 2006), within the DOC pool or their preferential removal (or dilution) within the DOC pool at the surface. The minimum in the concentration of carboxyl carbons in the ISOW sample (Fig. 39D) is not understood, but may be related to the terrestrial DOM that is entrained during deep-water formation (Hernes and Benner 2006) or to the low isolation efficiency for this sample (Table 15). The processing of DOM has been described here as a function of DOC age, suggesting that the differences in carboxylic content are due to refractory carboxyl-rich compounds. The low abundance of carboxyl groups in surface water DOC, while probably due to dilution by fresh algal DOM, may also be due to photodegradation reactions. Thorn et al. (2010) have described rapid de-carboxylation of terrestrial DOM upon exposure to UV radiation, with the residual becoming more hydrophobic; an analogous process may be occurring in the euphotic zone and mixed layer of the oceans. Such a process might partly explain the lower relative abundance of carboxyl carbons (Fig. 38D) and higher concentration of alkyl-C (Fig. 39B) observed in both surface ocean RO/ED isolates.

*Cycling of semi-labile and refractory DOM in the ocean* – Oceanic DOM exhibits a continuum of biological lability, ranging from algal exudates which may be remineralized within minutes or days (Fuhrman and Ferguson 1986; Carlson and Ducklow 1996; Carlson et al. 1999) to refractory deep ocean DOM that recycles over thousands of years (Williams and Druffel 1987; Ziolkowski and Druffel 2010). Recent

attempts to conceptualize the production, processing, and preservation of DOM within the ocean have proposed a three-pool DOC model where DOC is classified according to time scales over which it is removed or preserved (Carlson 2002; Hansell et al. 2009). In this model, bio-labile carbon is released during photosynthesis, lysis, and grazing and is rapidly removed or recycled by heterotrophic activity (Carlson et al. 2002); semi-labile carbon is identified as DOM that resists rapid removal but cycles over months to years (Ogura 1972; Kirchman et al. 1993; Carlson and Ducklow 1995); and refractory carbon resists degradation, remaining in the ocean for centuries or millennia (Williams and Druffel 1987; Bauer et al. 1992).

The marked structural/compositional similarity of DOM isolated from different oceanic regimes suggests a significant fraction of all of the samples is comprised of a highly degraded, and amorphous “background” DOM. In our data set, this background DOM is best represented by the “old” deep North Pacific sample. Above this background, compositional differences between the samples are likely due to localized processes of production and removal (Figs. 34 and 36; Carlson 2002). Comparing DOC concentrations (Table 15) suggests that the Atlantic and Pacific surface samples and the North Atlantic 3000 m sample contain an excess of DOC that is probably semi-labile. Assuming that the N. Pacific sample is representative of the “background” DOM, subtracting its normalized NMR spectrum from those of the other samples yields compositional information about the semi-labile DOC pool (Tables 20 and 21). Negative values in Tables 20 and 21 reflect the substances that build up within the refractory pool in old, deep water masses, or may be preferentially removed from surface waters by photochemical degradation, particle adsorption or other processes. Since the biologically



Table 20. Semi-labile carbon characterization obtained by subtracting the refractory carbon signature of the deep N. Pacific sample from that of each sample (DOC normalized NMR integrations).

Functional groups		5m N. Atl. (Upwelling)	5m N. Pac. (ALOHA)	415m N. Atl. (O <sub>2</sub> min.)	3000m N. Atl. (ISOW)
		Sample conc. - 3500 N. Pac. Conc. ( $\mu\text{mol C L}^{-1}$ )			
0-25	CH <sub>3</sub> , CH <sub>2</sub>	6.0	2.9	2.6	0.6
25-35	CH <sub>2</sub> , CH	4.0	1.9	1.3	0.9
35-50	CH, CH <sub>2</sub> , Cq	6.1	3.5	2.3	0.6
50-60	Cq, OCH <sub>3</sub> , HC-NH	4.8	2.7	1.5	0.2
60-90	Carbohydrate-like C	20.9	14.4	6.6	2.8
90-110	Anomeric O-C-O, Aromatic C	4.0	3.0	1.1	0.2
110-130	Aromatic C-H, Cq	0.7	1.0	0.3	0.0
130-150	Aromatic C-H, Cq	0.2	0.1	0.0	-0.3
150-165	Aromatic C-O	0.2	0.0	0.1	0.0
165-190	COO-/COOH, ester, amide	2.1	0.5	-0.5	-2.8
190-220	Aldehyde, ketone, quinone	0.0	0.2	-0.3	0.0

Table 21. Semi-labile carbon characterization obtained by subtracting the refractory carbon signature of the deep N. Pacific sample from that of each sample (DOC normalized NMR integrals with spectral editing data).

	Functional Group Category	5m N. Atl. (Upwelling)	5m N. Pac. (ALOHA)	415m N. Atl. (O <sub>2</sub> min.)	3000m N. Atl. (ISOW)
Sample conc. - 3500 N. Pac. Conc. ( $\mu\text{mol C L}^{-1}$ )					
0-25	CH <sub>3</sub>	3.7	1.1	1.4	0.5
15-45	CH <sub>2</sub>	7.0	3.6	2.8	0.9
35-50	Aliphatic CH	4.3	4.7	1.6	1.6
35-60	Aliphatic Cq	1.0	0.2	0.2	-0.5
50-60	Aliphatic C-OH and NCH	4.6	2.6	1.5	0.5
60-110	Carbohydrate-like C	23.8	13.7	7.4	3.0
90-110	O-Cq-O	0.3	-0.7	0.4	-1.0
100-165	Protonated aromatics	1.9	3.0	0.5	0.9
100-165	Non-protonated aromatics	0.3	1.2	-0.1	-0.3
165-190	COO-/COOH, ester, amide	2.2	0.2	-0.6	-3.2
190-220	Aldehyde, ketone, quinone	-0.1	0.1	-0.3	-0.1

Table 22. Semi-labile carbon characterization obtained by subtracting the refractory carbon signature of the deep N. Pacific sample from that of each sample (NMR integrals with spectral editing data normalized to total area=100%).

	Functional Group Category	5m N. Atl. (Upwelling)	5m N. Pac. (ALOHA)	415m N. Atl. (O <sub>2</sub> min.)	3000m N. Atl. (ISOW)
Sample C % - 3500 N. Pac. C % (%)					
0-25	CH <sub>3</sub>	-1.71	-3	-0.38	0.62
15-45	CH <sub>2</sub>	1.26	0.02	1.84	1.58
35-50	Aliphatic CH	0.13	3.07	0.51	3.28
35-60	Aliphatic Cq	-2.43	-2.32	-1.48	-2.04
50-60	Aliphatic C-OH and NCH	1.72	1.05	1.07	0.99
60-110	Carbohydrate-like C	13.18	9.44	6.93	6.22
90-110	O-Cq-O	-2.39	-3.12	-0.59	-2.64
100-165	Protonated aromatics	0.95	3.47	0.38	2.13
100-165	Non-protonated aromatics	-2.21	-0.32	-1.39	-0.78
165-190	COO-/COOH, ester, amide	-7.42	-7.37	-6.01	-8.6
190-220	Aldehyde, ketone, quinone	-0.57	-0.19	-0.75	-0.14

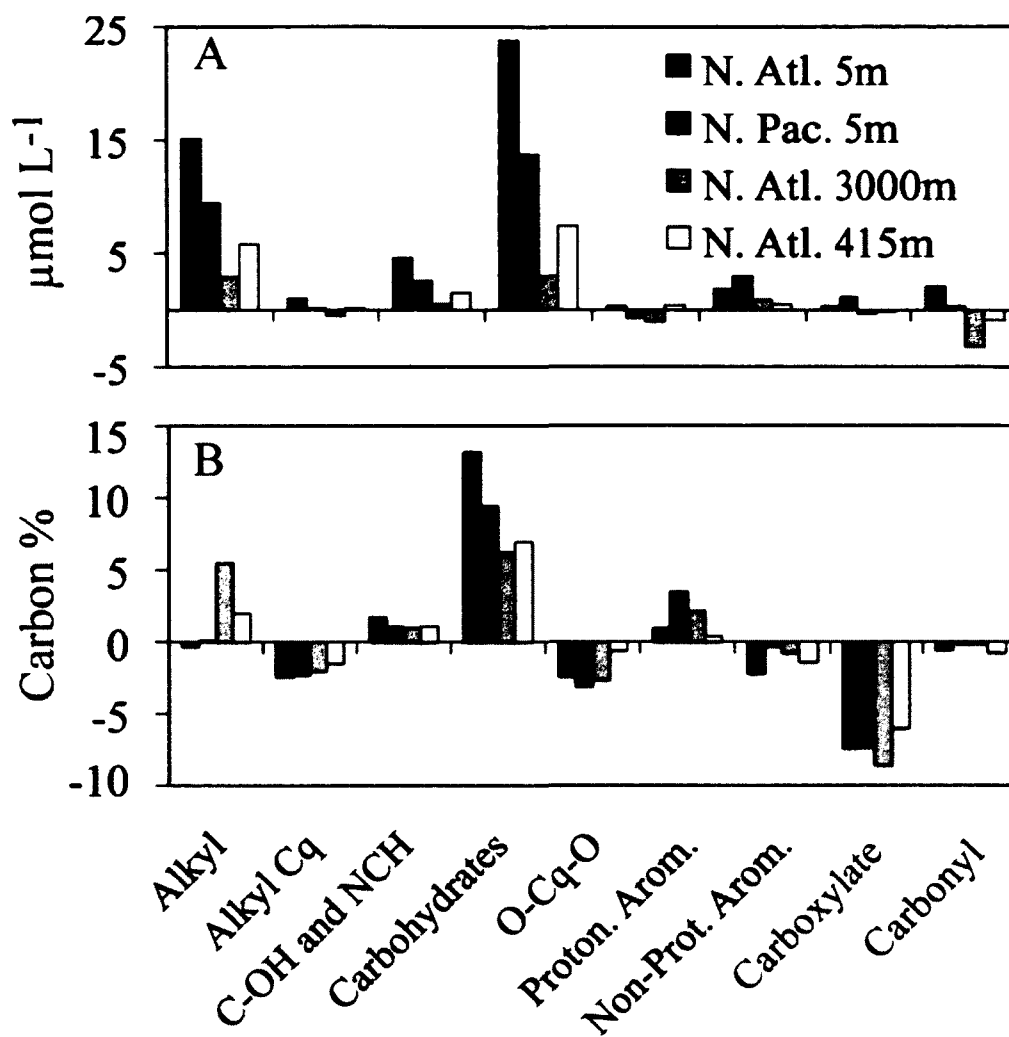


Fig. 40. Comparison of sample NMR signals after subtraction of the background refractory (N. Pacific 3500 m) DOM signal calculated using (A) DOC normalized and (B) total area=100% normalized data. Cq refers to quarternary carbons. O-Cq-O refers to quaternary anomeric carbons.

labile carbon pool has a residence time in the ocean that ranges from minutes to days, it may be largely absent from all of our samples.

There are two significant sources of uncertainty associated with this data treatment. The first is that the RO/ED system, while a significant improvement over earlier methods, still failed to recover at least 20% of the DOM; the second is that the definition of labile, semi-labile, and refractory in the context of three-pool DOC model is dominantly biological (e.g. largely ignores removal mechanisms such as adsorption, hydrothermal oxidation and photodegradation). It is therefore important to note that the 3000 m North Atlantic sample had lower than average DOC recovery (23%), and the surface samples likely reflect removal or transformation of photochemically-labile DOC (See Chapters III and IV).

Despite these caveats, several clear trends emerge (Fig. 40). The dominant constituents of semi-labile DOC are carbohydrate-like compounds followed by protonated alkyl groups and amide (NCH) groups, presumably from peptides (positive values in Tables 20, 21, and 22; Fig. 40). These components generally have substantial concentrations above the refractory background signal in the surface samples, but diminish with age/depth (Figs. 36, 38, and 39). Refractory DOC is enriched in quaternary aliphatic DOM (negative values in Table 21 and Fig. 40), which is not abundant in algal DOM (Mao et al. 2007a), but may arise from abiotic condensation or cross-linking reactions (Harvey et al. 1983; Kieber et al. 1989; Keil et al. 1994) or survive microbial degradation of macromolecular DOM (Amon and Benner 1996). Nonprotonated, i.e. condensed or substituted, aromatic rings typically have negative values in Tables 21 and 22 and Fig. 40, appear to increase as a fraction of total aromaticity with age (Fig. 38C

inset; Table 18), and are likely indicative of long-lived black carbon moieties (Ziolkowski and Druffel 2010).

DOM that survives in surface waters of the subtropical gyres can be expected to be photo-refractory due to the vertical stratification and long-term light exposure. Perhaps counter-intuitively, protonated aromatic and/or olefinic DOC (which resonate between 110-150 ppm, but is excluded from dipolar dephased NMR spectra; Fig. 36) appears to build up in the North Pacific gyre. Aromatic rich and heavily conjugated DOM is typically photo-labile (see Chapters II and III). This incongruence may be explained by a fraction of the photochemically altered aromatic (unsaturated) DOM having blue shifted absorption spectra (i.e. transparent to solar radiation; Helms et al. 2008; Chapter III). That is, the NMR signal in this spectral region could be due to compounds containing single rings (or rings connected by non-conjugated structures) that absorb at shorter wavelengths than condensed aromatics (Zhang et al. 2006), aromatics that are substituted with electron withdrawing groups (Stubbins et al. 2008), or olefinic or isoprenoid moieties, which contain some  $sp^2$  hybridized carbons, but absorb at wavelengths shorter than the solar irradiance cut-off ( $\sim 280$  nm) (Kirk 1994).

*Implications for the three-pool DOC model* – The decoupling of DOC and CDOM distributions observed in the upper oceans (Nelson et al. 2007; Swan et al. 2009) appears to be brought about, in part, by the two major removal processes: heterotrophic remineralization, which mainly affects DOC composition, and photobleaching (see Chapter II and Chapter III), which mainly affects CDOM. Thus, a comprehensive view of the oceanic carbon cycle does not fit neatly into either the biologically-controlled “three-

### Modified 3-pool DOM concept

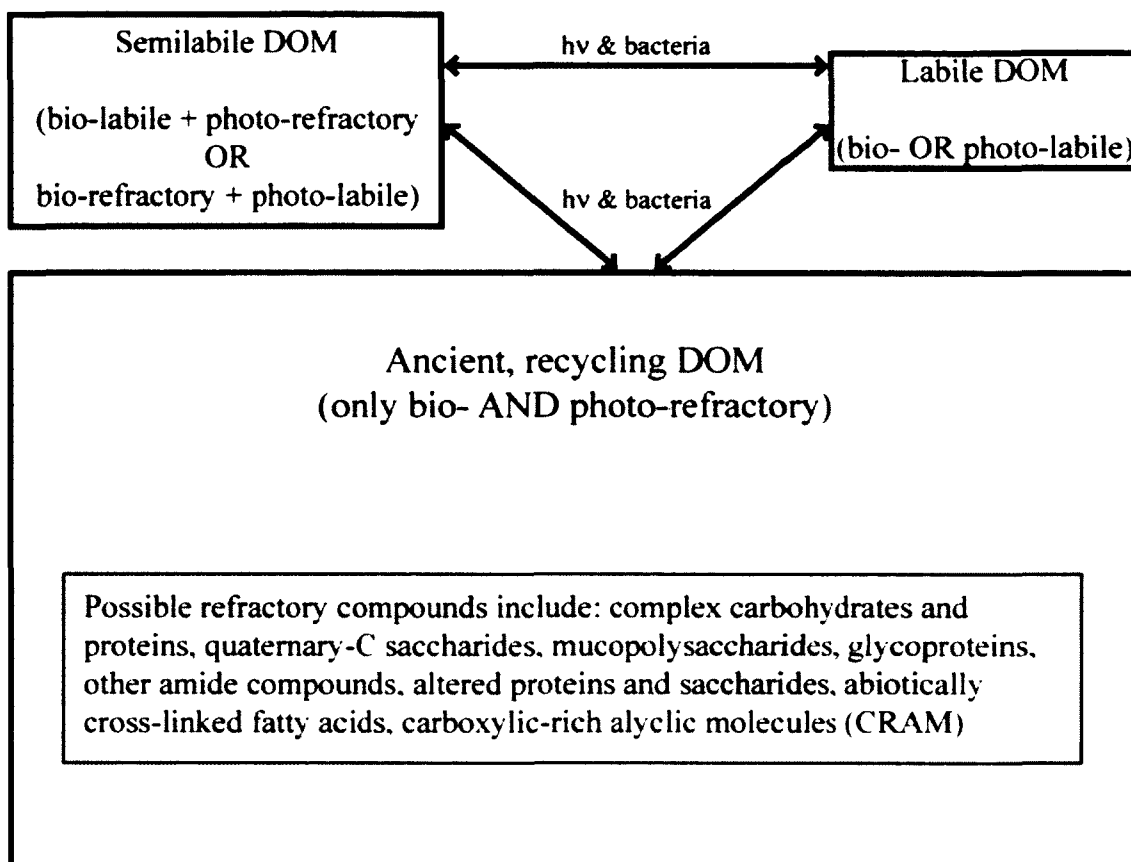


Fig. 41. Modifications expanding the applicability of the three-pool DOC model, proposed by Carlson (2002), to include photochemical reactivity of DOM, which can limit the ability of a given compound to cycle over time-scales longer than whole-ocean-overturn. The refractory category is narrowed to include only biologically and photochemically refractory compounds, while the labile category is expanded to include photo-labile compounds.

pool DOC model” proposed by Hansell and Carlson (2001), nor the “three-pool photochemical model” proposed by Stubbins et al. (2010). For example, the production of biologically labile carbon from DOM photolysis (Kieber et al. 1989; Miller et al. 2002), the microbial production of photo-labile CDOM (Rochelle- Newall and Fisher 2002a), the build up of photo-refractory DOM at the surface of the subtropical gyres (Hansell et al. 2009; Swan et al. 2009), and the build up of bio-refractory DOM in the deep ocean (Williams and Druffel 1987) reveal the lack of mutual exclusivity of the two conceptual models.

I propose an approach that incorporates aspects of both models by re-defining the three pools used by Hansell and Carlson (2001) and Carlson (2002). Refractory carbon remains a single pool, but consists of compounds that are both bio- and photo-refractory (Fig. 41). Possible examples of bio-/photo-refractory compounds are altered (and/or unaltered) complex carbohydrates and proteins (Repeta and Aluwihare 2006; Kaiser and Benner 2008), quaternary carbon containing saccharides, mucopolysaccharides (Alldredge et al. 1986), glycoproteins (Yamada and Tanoue 2003), other amide compounds (McCarthy et al. 1997, 1998; Aluwihare et al. 2002; Chapter II), abiotically cross-linked fatty acids (Kieber et al. 1997), and altered carboxylated aliphatic compounds (Hertkorn et al. 2006).

The semi-labile pool (Fig. 41) is re-defined as consisting of three groups of compounds including: 1) photo-refractory but semi-labile bio-compounds (e.g., unaltered to slightly altered peptides and oligosaccharides), 2) photo-labile and biologically semi-labile compounds (possibly produced by microbes below the photic zone; e.g., slightly altered pigments and other conjugated compounds, tryptophan -containing proteins and



peptides), and 3) photo-labile but biologically refractory compounds produced by microbes below the photic zone, slightly altered pigments and other conjugated compounds (Swan et al. 2009), and condensed aromatics (Dittmar 2008; Ziolkowski and Druffel 2010). Once the latter species (i.e., photolabile) are transported to the photic zone, photo-degradation will likely produce compounds that are biologically labile and compounds that are both biologically and photochemically refractory, thus partially shifting the resulting C to the refractory (background) and labile pools, respectively.

The “labile” carbon pool (Fig. 41) is broadened to incorporate two sub-pools including: 1) biologically labile molecules (e.g., simple biomolecules such as sugars, amino acids, LMW fatty acids and LMW carboxylic acids, and biologically labile photoproducts including LMW carbonyl compounds and LMW carboxylic acids); and 2) photochemically labile compounds (e.g., terrestrially derived lignin phenolics, brown algae derived phenolics, various pigments, fulvic substances and other LMW conjugated compounds).

*Conclusions and future directions* – The proposed revisions to the three-pool DOM concept suggest multiple lines of inquiry. Characterizing the molecular composition of microbially produced CDOM as well as understanding the molecular level and structural changes that occur during its photobleaching would provide important clues about the origin of biologically recalcitrant and photo-refractory DOM in the deep ocean. The identification of photo-labile and photo-refractory biomarkers within the pool of microbially produced and terrestrially derived CDOM would significantly help improve our understanding of the ocean carbon cycle. Enhanced compositional

characterization of irradiated and non-irradiated open ocean samples will also improve our understanding of the molecular level basis for observed optical properties and allow expanded use of optical properties as environmental tracers and possibly facilitate development of remote sensing technology.

The RO/ED isolated oceanic DOM analyzed in this study represents a larger and more representative fraction of open ocean DOC compared with UDOM and SPE isolates described previously. Advanced one-dimensional solid-state NMR revealed the presence and apparent preservation of quaternary anomeric carbons in biologically refractory carbohydrates. Future investigations of this class of marine DOM may eventually lead to the identification of the structures and sources of these compounds. The most abundant component of semi-labile DOM is carbohydrate-like material followed by aliphatics, both of which decrease with increasing apparent DOC age. The use of  $^{13}\text{C}$  NMR with dipolar dephasing facilitated the resolution of (photo-refractory) protonated, conjugated organics that accrue in subtropical gyre surface waters from non-protonated aromatics that preferentially accumulate in deep ocean waters. Bio-refractory DOM is enriched in carboxylate functionality, suggesting further investigation of CRAM structures remains a salient research objective. In fact, little is known about the sources of refractory oceanic DOM, which may consist of inherently resistant biomolecules or arise from biological, photochemical or thermal alteration of labile and semi-labile DOM. Understanding the biogeochemical processes affecting DOM and the compositional/structural features they impart to the refractory DOM pool are critical to our understanding of carbon sequestration and cycling in the ocean.

## CHAPTER VI

### SUMMARY AND CONCLUSIONS

#### SUMMARY OF MAJOR RESULTS

*Overview and summary* – The investigation of the largely ignored phenomenon of photochemical flocculation (Chapter II) and the long-term photochemical degradation of terrestrial DOM coupled with detailed analytical characterization (Chapter III) have increased our understanding of the fate and processing of terrestrial DOM in the oceans' margins. The nearly quantitative removal of terrestrial DOM tracers and previously ignored photo-flocculation phenomenon raise new questions regarding the removal of DOM from the water column and preservation of organic matter in coastal sediments.

The use of reverse osmosis coupled to electrodialysis (RO/ED) for the isolation of open ocean dissolved organic matter (DOM) represents a significant improvement in recovering a representative fraction of DOM, and the application of this technology has garnered considerable interest from the marine organic geochemistry community. The results presented in Chapter IV and Chapter V provide a basis for evaluating the potential of this new DOM isolation protocol, and set the stage for considerable advancement in the field of marine DOM characterization. The photochemical degradation of RO/ED-isolated DOM (Chapter IV) represents a totally new direction in the investigation of photodegradability of open ocean DOM, which has previously been hindered by the low concentrations of DOM found in situ and the chemical fractionation limitations of commonly used extraction techniques.

Photochemical degradation of terrestrial DOM led to extensive bleaching of absorbance and fluorescence, and the optical properties of the remaining material were

suggestive of marine derived DOM. The composition of extensively irradiated DOM, as revealed by  $^{13}\text{C}$  NMR, also more closely resembled marine DOM than the starting material. The emergence (or remainder) of dominant peaks at  $\sim 25$ ,  $\sim 75$ ,  $\sim 100$ , and  $\sim 175$  ppm in the  $^{13}\text{C}$  NMR spectra for irradiated tDOM (Chapter II and III) resembled marine and estuarine DOM  $^{13}\text{C}$  NMR spectra reported in a number of studies (Chapter II, Benner et al. 1992; Hedges et al. 1992; Abdulla et al. 2010). This similarity is most evident when considering the loss of signal from the aromatic region of the spectrum and the sharper and more intense peaks in the methyl (0-28 ppm), and O-alkyl/N-alkyl (50-115 ppm) regions of the NMR spectra. Photochemical degradation also removed some fraction of every major structural category except for amides. Carbohydrate-like and alkyl functional groups were relatively photo-resistant, while aromatic and carboxylic moieties (again with the exception of amides) were the most photo-labile. Dissolved lignin was almost completely removed during irradiation. Thus, the most commonly applied optical, structural, and molecular tracers of terrestrial DOM have now been proven susceptible to rapid photochemical removal. This result calls into question the current paradigm of the ocean DOM biogeochemical cycle, which presumes that terrestrial DOM does not contribute significantly to the ocean DOC inventory and that the dominant source of refractory DOC is in situ microbial (algal and bacterial).

In addition to photochemical removal of photo-labile DOM, removal of DOM by the relatively understudied process of photo-flocculation was investigated. Iron was found to resist flocculation initially, probably due to the abundance of iron-binding organic ligands. But, by the end of 30 d irradiation,  $\sim 86\%$  of the iron had flocculated. Initially, flocculated DOM was predominantly aliphatic, while DOM that flocculated

later showed greater structural diversity, suggesting multiple mechanisms are likely responsible for the phenomenon. The incorporation of a flocculation term in the oceanic carbon cycle significantly increases the potential for photochemical removal of terrestrial DOM from surface waters at the ocean margins (by as much as 13%).

DOM isolated by RO/ED from deep Pacific Ocean water (670 m) exhibited optical properties typical of deep ocean DOM. However, after extensive UV exposure DOC, absorbance and fluorescence all decreased leaving behind material with optical properties that were typical of surface ocean DOM. The absorbance of the dominant UV chromophore (~280 nm) shifted to shorter wavelengths upon irradiation, likely due to a reduction in conjugation and/or molecular size. Terrestrial humic-like fluorescence (EEMS Peak C) decreased more than the other major fluorescent DOM (FDOM) components, with the tyrosine-like fluorescence showing the smallest decrease. These results suggest that marine FDOM components that are similar to or derived from terrestrial FDOM is photo-labile, while protein-like FDOM components are relatively photo-refractory.

The solid-state  $^{13}\text{C}$  nuclear magnetic resonance (NMR) characterization of RO/ED isolated DOM reported in Chapter V revealed that open ocean DOM samples from widely varying locations and depths were very similar in composition and structure, suggestive of a significant background of recalcitrant DOM as put forth in the “three-pool” dissolved organic carbon (DOC) model of Carlson (2002). The three-pool model categorizes DOC according to its biological availability and the time scales over which it is recycled. “Refractory” DOC is recycled over century or millennia, semi-labile DOC is recycled over months to years, and labile DOC is recycled within minutes to days, after

release by primary producers. Advanced solid-state NMR also revealed two important aspects of the cycling of carbohydrates in the ocean: first that carbohydrates appear to dominate the semi-labile pool of carbon and second that a previously unknown and uncharacterized fraction of carbohydrates that contain quaternary anomeric carbons appear to resist biological degradation. Additionally, quaternary aliphatics and nonprotonated aromatics appear to be more biologically refractory than their protonated counterparts. Finally bio-refractory DOM appears to be enriched in carboxylic carbons, a result which supports the presence and refractory nature of carboxylic rich alicyclic molecules (CRAM) reported by Hertkorn et al. (2006).

*Common themes* – Photochemical de-carboxylation was observed in terrestrial DOM (Chapter II, Chapter III; Thorn et al. 2010), and RO/ED isolated DOM from surface waters generally contained less carboxylate than deep water (Chapter V). These results suggest that the carboxylate differential between deep and surface that is attributed to a build up of bio-refractory carboxyl rich compounds in deep water (Hertkorn et al. 2006), and is enhanced by the photochemical removal of carboxyl groups at the surface ocean.

Amide functional groups appear to be preserved (and possibly produced) during photochemical alteration of terrestrial DOM (Chapter II and Chapter III). Further, protein fluorescence is photochemically degraded slower than the other components of terrestrial FDOM (chapter III) open ocean FDOM (Chapter IV). The photo-refractory pool of DOM is therefore expected to include peptides and proteins. Additionally, abiotically produced amides (Chapter II; McKee and Hatcher 2010) may be constituents of both the bio-

refractory and photo-refractory DOM pools (terrestrial and marine).

Surface marine waters contain more carbohydrates than deep waters, but similar percentages of aliphatic material (Chapter V). When tDOM is photobleached, it becomes more aliphatic and contains more carbohydrates (Chapter III); however, flocculation may remove photochemically generated aliphatic material from the water column (Chapter II). Carbohydrates and predominantly aliphatic material do not exhibit UV-visible absorption (within the solar irradiance spectrum) and can therefore be classified as photo-resistant. The use of CSA-filter with CP/TOSS NMR facilitated the differentiation between pools of biologically semi-labile and bio-refractory carbohydrates. If it is assumed that, for each quaternary anomeric carbon, bio-refractory sugars contain at least four additional carbohydrate carbons, then this type of bio-refractory carbohydrate could account for  $\geq 79\%$  of the total carbohydrates in the deep North Pacific DOM sample (Chapter V).

Using routine CP/MAS or CP/TOSS and broad integration intervals to characterize open ocean DOM isolated by RO/ED suggest that all the marine DOM samples exhibited similar aromaticities. By using dipolar dephasing, however, it was shown that deprotonated aromatics are more bio-refractory and photo-labile, while the photo-refractory DOM pool appears to contain some protonated aromatics (Chapter V). The NMR results of Chapter III confirm that protonated aromatics are more photo-refractory than the non-protonated aromatics, while the optical spectroscopic results in Chapters III and IV suggest that the determining factor is simply the extent to which the UV absorption of the compounds overlap with the solar radiance spectrum (i.e. absorption spectra of protonated aromatic chromophores are probably more blue shifted and are therefore more likely to survive light exposure at the ocean's surface).

Several similarities between the photobleaching of open ocean DOM and terrestrial DOM were observed. Regardless of source, photobleaching led to increased UV spectral slopes and slope ratios. Fluorescence photobleaching led to reduced intensity across all wavelengths, though Peak M (marine derived humics) and Peak B (tyrosine-like fluorescence) became more prominent relative to Peak C (terrestrial humics) and Peak A (quinoid-like humics) in both terrestrially dominated and open ocean samples (Coble 1996). The presence and photo-lability of Peak C in the remote Pacific DOM supports the possibility that a significant fraction of nominally marine or microbial derived DOM may in fact represent heavily photobleached (and diluted) terrestrial DOM.

## MAJOR CONCLUSIONS AND FUTURE DIRECTIONS

*Conclusions* – Photochemically induced flocculation and enhancement of particle adsorption may represent significant sources of organic carbon, organic nitrogen, and iron to the sediments, and may contribute biologically refractory carbon and nitrogen to the sediments and deep ocean. Furthermore, photochemical flocculation may provide an important removal mechanism of terrestrial DOM from the water column.

It is widely thought that nearly all riverine DOM must be removed during transport from freshwaters to the open ocean within a few hundred to several hundred years (Kieber et al. 1990; Blough and Del Vecchio 2002; Nelson and Siegel 2002). However, the processes by which terrestrial DOM is removed are not well known and, based on the results of Chapters II, III and IV, a fraction of marine DOM may in fact be photobleached terrestrial DOM. The identification of terrestrially sourced bio-marker molecules that are resistant to both photochemical and microbial degradation would



greatly improve our ability to understand and quantify the oceanic carbon cycle (Spencer et al. 2009; Stubbins et al. 2010). Unfortunately, our present inability to optically, chemically, or isotopically (Spencer et al. 2009) differentiate the photo-resistant and photo-produced portions of terrigenous DOC (~5-25% of Dismal Swamp DOC; Chapter III) from in situ produced marine DOC continues to impede efforts to understand carbon cycling in the aquatic environment on global and oceanic scales.

The RO/ED isolated oceanic DOM analyzed in this study represents a larger and more representative fraction of open ocean DOC compared with ultrafiltration (UDOM) and solid phase extraction (SPE) isolates commonly used in previous studies.

Carbohydrate-like material is the most abundant component of semi-labile DOM, and also provides the most obvious trend with estimated DOC age (Figs. 38 and 39). Photo-refractory, conjugated organics that accrue in subtropical gyre surface waters are structurally distinct from aromatics that accumulate in deep ocean waters in that the former are more extensively protonated.

The decoupling of DOC and CDOM distributions observed in the oceans is brought about, in part, by the two dominant removal processes: heterotrophic remineralization in the case of DOC and photobleaching in the case of CDOM. Thus a comprehensive view of the oceanic carbon cycle requires an understanding of when the “three-pool DOC model” proposed by Hansell and Carlson (2001), or the “three-pool photochemical model” proposed by Stubbins et al. 2010 is the more appropriate. To address the limitations of these two models, a unifying approach is proposed in Chapter V that incorporates aspects of both models by re-defining the pools used by Hansell and Carlson (2001) and Carlson (2002). The “refractory” carbon pool is narrowed to include

only compounds that are both bio- and photo-refractory. The “semi-labile” pool is re-defined as consisting of three sub-pools including: photo-refractory but semi-labile bio-compounds, photo-labile but biologically refractory compounds, and photo-labile and biologically semi-labile compounds. Similarly, the “labile” C-pool, is redefined as consisting of two sub-pools including: biologically labile molecules and photochemically labile compounds.

By narrowing the definition of refractory DOC, a conceptual framework within which a significant fraction of DOC may survive multiple ocean overturn cycles is established, while expanding the definition of labile DOC to include photo-labile compounds reflects a significant removal mechanism that was ignored in the earlier model. As a significant fraction of terrestrial DOM is photo-labile and its organic photoproducts are bio-labile, the new model facilitates rectifying the perceived mismatch of the large autochthonous and allochthonous sources of DOM to the ocean and low oceanic DOC concentrations. The new model incorporates the relatively rapid remineralization of terrestrial DOM by a coupled photochemical-biological process at the ocean margins whereby only refractory (bio- AND photo-) and non-flocculating compounds are exported to the open ocean.

*Future directions* – The research described in this dissertation raises several new scientific questions. The processes controlling iron flocculation require further investigation; in particular, the extent to which photo-flocculation occurs in lower DOC waters is needed to gauge its potential global impact. Also, the extent to which photo-flocculation is offset by down-stream re-dissolution (e.g. Kieber et al. 2006) and under

what conditions the two processes compete with one another remains largely unknown. The physical properties (resistance to mechanical shear in turbulent environments, etc.) and physical dynamics (sinking velocities etc.) of photo-flocculated particles have yet to be investigated.

The loss of optical, structural, isotopic, and molecular indicators of terrestrial DOM source during photobleaching (Chapter II-IV) indicates that the identification of new photo-resistant biomarkers would significantly improve our ability to balance carbon budgets on ocean basin and global scales. The molecular level and bulk structural characterization of microbially produced ocean CDOM and the products of its photodegradation would significantly improve our understanding of the transformation and cycling of DOM in the ocean. The interfaces between abiotic and biological transformations of DOM, e.g., the bioavailability of hydrothermally and photochemically altered ocean DOM and the biological production of photolabile DOM, remain key areas of investigation.

The still-evolving technology of DOM isolation and de-salting remains a salient avenue of investigation. The demonstration that some biologically refractory carbohydrates contain quaternary anomeric carbons provides clues to their sources and the likely cause of their biological recalcitrance, and highlights the need for further investigation. Refractory DOM is enriched in carboxylate functionality, suggesting further investigation of CRAM structures remains a highly relevant research objective. Understanding the biogeochemical processes associated with DOM and the structural features they impart to the refractory DOM are important to our understanding of long-term carbon sequestration in the ocean.

## REFERENCES

- Abdulla, H. A. N., R. F. Dias, and E. C. Minor. 2009. Understanding the enhanced aqueous solubility of styrene by terrestrial dissolved organic matter using stable isotope mass balance and FTIR. *Org. Geochem.* **40**: 547-552, doi:10.1016/j.orggeochem.2009.02.011
- Abdulla, H. A. N., E. C. Minor, R. F. Dias, and P. G. Hatcher. 2010. Changes in the compound classes of dissolved organic matter along an estuarine transect: a study using FTIR and <sup>13</sup>C-NMR. *Geochim. Cosmochim. Acta* **74**: 3815-3838, doi:10.1016/j.gca.2010.04.006
- Aiken, G. R., and J. Leenheer. 1993. Isolation and Chemical Characterization of Dissolved and Colloidal Organic Matter. *J. Chem. Ecol.* **8**: 135-151, doi:10.1080/02757549308035305
- Aldredge, A. L., J. J. Cole, and D. A. Caron. 1986. Production of heterotrophic bacteria inhabiting macroscopic organic aggregates (marine snow) from surface waters. *Limnol. Oceanogr.* **31**: 68-78, doi:10.2307/2836640
- Aldredge, A. L., and M. W. Silver. 1988. Characteristics, dynamics and significance of marine snow. *Progr. Oceanogr.* **20**: 41-82, doi:10.2307/2836640
- Aluwihare, L. I., D. J. Repeta, S. Pantoja, and C. G. Johnson. 2005. Two chemically distinct pools of organic nitrogen accumulate in the ocean. *Science* **308**: 1007-1010, doi:10.1126/science.1108925
- Amon, R. M. W., and R. Benner. 1996. Bacterial utilization of different size classes of dissolved organic matter. *Limnol. Oceanogr.* **41**: 41-51, doi:10.4319/lo.1996.41.1.0041

- Barbeau, K. 2006. Photochemistry of organic iron(III) complexing ligands in oceanic systems. *Photochem. Photobiol.* **82**: 1505-1516, doi:10.1562/2006-06-16-IR-935
- Batoosingh, E., G. A. Riley, and B. Keshwar. 1969. An analysis of experimental methods for producing particulate organic matter in sea water by bubbling. *Deep-Sea Res.* **16**: 213-219.
- Bauer, J. E., P. M. Williams, and E. R. M. Druffel. 1992.  $^{14}\text{C}$  activity of dissolved organic carbon fractions in the north-central Pacific and Sargasso Sea. *Nature* **357**: 667-670, doi:10.1038/357667a0
- Bauer, J. E., and E. R. M. Druffel. 1998. Ocean margins as significant source of organic matter to the deep open ocean. *Nature* **392**: 482-485, doi:10.1038/33122
- Bauer, J. E., E. R. M. Druffel, D. M. Wolgast, and S. Griffin. 2002. Temporal and regional variability in sources and cycling of DOC and POC in the northwest Atlantic continental shelf and slope. *Deep-Sea Res. II* **49**: 4387-4419, doi:10.1016/S0967-0645(02)00123-6
- Baylor, E. R., and W. H. Sutcliffe. 1963. Dissolved organic matter in sea water as a source of particulate food. *Limnol. Oceanogr.* **8**: 369-371.
- Benner, R., J. D. Pakulski, M. McCarthy, J. I. Hedges, and P. G. Hatcher. 1992. Bulk chemical characterization of dissolved organic matter in the ocean. *Science* **255**: 1561-1564, doi:10.1126/science.255.5051.1561
- Benner, R., and B. Biddanda. 1998. Photochemical transformations of surface and deep marine dissolved organic matter: Effects on bacterial growth. *Limnol. Oceanogr.* **43**: 1373-1378, doi:10.4319/lo.1998.43.6.1373

- Benner, R., and S. Opsahl. 2001. Molecular indicators of the sources and transformations of dissolved organic matter in the Mississippi river plume. *Org. Geochem.* **32**: 597-611, doi:10.1016/S0146-6380(00)00197-2
- Benner, R. 2002. Chemical structure and reactivity, p. 59-151. *In* D. A. Hansell and C. A. Carlson [eds.], *Biogeochemistry of Marine Dissolved Organic Matter*. Academic Press. Amsterdam.
- Benner, R., and K. Kaiser. 2010. Biological and photochemical transformations of amino acids and lignin phenols in riverine dissolved organic matter. *Biogeochem.* **102**: 209-222, doi:10.1007/s10533-010-9435-4
- Bennet, A. E., C. M. Rienstra, M. Auger, K. V. Lakshmi, and R. G. Griffin. 1995. Heteronuclear decoupling in rotating solids. *J. Chem. Phys.* **103**: 6951-6958.
- Bertilsson, S., and L. J. Tranvik. 1998. Photochemically produced carboxylic acids as substrates for freshwater bacterioplankton. *Limnol. Oceanogr.* **43**: 885-895, doi:10.4319/lo.1998.43.5.0885
- Bertilsson, S., R. Stepanauskas, R. Cuadros-Hansson, W. Graneli, J. Wikner, and L. Tranvik. 1999. Photochemically induced changes in bioavailable carbon and nitrogen pools in boreal watersheds. *Aquat. Microb. Ecol.* **19**: 47-56, doi:10.3354/ame019047
- Bianchi, T. S., T. Filley, K. Dria, and P. G. Hatcher. 2004. Temporal variability in sources of dissolved organic carbon in the lower Mississippi River. *Geochim. Cosmochim. Acta* **68**: 959-967, doi:10.1016/j.gca.2003.07.011

- Birdwell, J. E., and A. S. Engel. 2010. Characterization of dissolved organic matter in cave and spring waters using UV-vis absorbance and fluorescence spectroscopy. *Org. Geochem.* **41**: 270-280, doi:10.1016/j.orggeochem.2009.11.002
- Birdwell, J. E., and K. T. Valsaraj. 2010. Characterization of dissolved organic matter in fogwater by excitation-emission matrix fluorescence spectroscopy. *Atmos. Environ.* **44**: 3246-3253, doi:10.1016/j.atmosenv.2010.05.055
- Black, A. P., F. B. Birkner, and J. J. Morgan. 1965. Destabilization of dilute clay suspensions with labeled polymers. *J. Am. Water Works Assoc.* **57**. 1547.
- Blough, N., O. Zafiriou, and J. Bonilla. 1993. Optical absorption spectra of waters from the Orinoco River outflow: Terrestrial input of colored organic matter to the Caribbean. *J. Geophys. Res.* **98**: 2271-2278, doi:10.1029/92JC02763
- Blough, N. V., and S. A. Green. 1995. Spectroscopic characterization and remote sensing of non-living organic matter, p. 23-45. *In* R. G. Zepp and C. Sontag [eds.], *The Role of Non-Living Organic Matter in the Earth's Carbon Cycle*. John Wiley and Sons. New York.
- Blough, N. V., and R. Del Vecchio. 2002. Chromophoric DOM in the coastal environment, p. 508-545. *In* D. A. Hansell and C. A. Carlson [eds.], *Biogeochemistry of Marine Dissolved Organic Matter*. Academic Press. San Diego, CA.
- Boehme, J., P. G. Coble, R. Conmy, and A. Stovall-Leonard. 2004. Examining CDOM fluorescence variability using principal component analysis: seasonal and regional modeling of three-dimensional fluorescence in the Gulf of Mexico. *Mar. Chem.* **89**: 3-14, doi:10.1016/j.marchem.2004.03.019

- Boyle, E. A., J. M. Edmond, and E. R. Sholkovitz. 1977. The mechanism of iron removal in estuaries. *Geochim. Cosmochim. Acta* **41**: 1313-1324.
- Brown, M. 1977. Transmission spectroscopy examinations of natural waters. *Estuar. Coast. Mar. Sci.* **5**: 309-317.
- Burdige, D. 2002. Sediment Pore Waters, p. 611-664. *In* D. A. Hansell and C. A. Carlson [eds.], *Biogeochemistry of Marine Dissolved Organic Matter*. Academic Press. Cambridge.
- Burdige, D. J., S. W. Kline, and W. Chen. 2004. Fluorescent dissolved organic matter in marine sediment pore waters. *Mar. Chem.* **89**: 289-311, doi:10.1016/j.marchem.2004.02.015
- Bushaw, K. L. and others 1996. Photochemical release of biologically available nitrogen from aquatic dissolved organic matter. *Nature* **381**: 404-407, doi:10.1038/381404a0
- Carder, K. L., R. G. Steward, G. R. Harvey, and P. B. Ortner. 1989. Marine humic and fulvic acids: Their effects on remote sensing of ocean chlorophyll. *Limnol. Oceanogr.* **34**: 68-81, doi:10.4319/lo.1989.34.1.0068
- Carlson, C. A., and H. W. Ducklow. 1995. Dissolved organic carbon in the upper ocean of the central Equatorial Pacific, 1992: Daily and fine-scale vertical variations. *Deep-Sea Res. II* **42**: 639-656, doi:10.1016/0967-0645(95)00023-J
- . 1996. Growth of bacterioplankton and consumption of dissolved organic carbon in the Sargasso Sea. *Aquat. Microb. Ecol.* **10**: 69-85, doi:10.3354/ame010069



- Carlson, C. A., N. R. Bates, H. W. Ducklow, and D. A. Hansell. 1999. Estimation of bacterial respiration and growth efficiency in the Ross Sea, Antarctica. *Aquat. Microb. Ecol.* **19**: 229-244, doi:10.3354/ame019229
- Carlson, C. A. 2002. Production and consumption processes, p. 91-151. *In* D. A. Hansell and C. A. Carlson [eds.], *Biogeochemistry of Dissolved Organic Matter in the Ocean*. Academic Press. San Diego.
- Carlson, C. A. and others 2002. Effect of nutrient amendments on bacterioplankton production, community structure, and DOC utilization in the northwestern Sargasso Sea. *Aquat. Microb. Ecol.* **30**: 19-36, doi:10.3354/ame030019
- . 2010. Dissolved organic export and subsequent remineralization in the mesopelagic and bathypelagic realms of the North Atlantic basin. *Deep-Sea Res. II* **57**: 1433-1445, doi:10.1016/j.dsr2.2010.02.013
- Chen, H. Unpubl. Molecular-level characterization of marine dissolved organic matter isolated by reverse osmosis and electrodialysis by Fourier transform ion cyclotron resonance mass spectrometry. Manuscript In Preparation
- Chester, R. 1990. *Marine Geochemistry*. Chapman and Hall. London.
- Chin, Y.-P., G. Aiken, and E. O. O'Loughlin. 1994. Molecular weight, polydispersity, and spectroscopic properties of aquatic humic substances. *Environ. Sci. Technol.* **28**: 1853-1858, doi:10.1021/es00060a015
- Chiou, C. T., R. L. Malcolm, T. I. Brinton, and D. E. Kile. 1986. Water solubility enhancement of some organic pollutants and pesticides by dissolved humic and fulvic acids. *Environ. Sci. Technol.* **20**: 502-508, doi:10.1021/es00147a010

- Christian, G. D., J. B. Callis, and E. R. Davidson. 1981. Array detectors and excitation-emission matrices in multicomponent analysis, p. 111-165. *In* E. L. Wehry [ed.], *Modern Fluorescence Spectroscopy*, 4. Plenum. New York, NY.
- Coble, P. G. 1996. Characterisation of marine and terrestrial DOM in seawater using excitation emission matrix spectroscopy. *Mar. Chem.* **51**: 325-346, doi:10.1016/0304-4203(95)00062-3
- Coble, P. G., C. E. Del Castillo, and B. Avril. 1998. Distribution and optical properties of CDOM in the Arabian Sea during the 1995 Southwest Monsoon. *Deep-Sea Res. II* **45**: 2195-2223, doi:10.1016/S0967-0645(98)00068-X
- Coble, P. G. 2007. *Marine Optical Biogeochemistry: The Chemistry of Ocean Color*. *Chem. Rev.* **107**: 402-419, doi:10.1021/cr050350+
- Compiano, A. M., J. C. Romano, F. Garabetian, P. Laborde, and I. de la Giraudiere. 1993. Monosaccharide composition of particulate hydrolysable sugar fraction in surface microlayers from brackish and marine waters. *Mar. Chem.* **42**: 237-251, doi:10.1016/0304-4203(93)90015-G
- Conrad, R., and W. Seiler. 1980. Photo-oxidative production and microbial consumption of carbon-monoxide in seawater. *FEMS Microbiol. Ecol.* **9**: 61-64, doi:10.1016/0378-1097(80)90113-5
- Conte, P., R. Spaccini, and A. Piccolo. 2004. State of the art of CP/MAS <sup>13</sup>C-NMR spectroscopy applied to natural organic matter. *Progr. Nucl. Magn. Res. Spectr.* **44**: 214-223, doi:10.1016/j.pnmrs.2004.02.002

- Cory, R. M., and D. M. McKnight. 2005. Fluorescence spectroscopy reveals ubiquitous presence of oxidized and reduced quinones in dissolved organic matter. *Environ. Sci. Technol.* **39**: 8142-8149, doi:10.1021/es0506962
- Cowie, G. L., and J. I. Hedges. 1992. The role of anoxia in organic-matter preservation in coastal sediments - relative stabilities of the major biochemicals under oxic and anoxic depositional conditions. *Org. Geochem.* **19** 229-234.
- Cutter, G. A., L. S. Cutter, and K. C. Filippino. 2004. Sources and cycling of carbonyl sulfide in the Sargasso Sea. *Limnol. Oceanogr.* **49**: 555–565, doi:10.4319/lo.2004.49.2.0555
- Dagg, M., R. Benner, S. Lohrenz, and D. Lawrence. 2004. Transformation of dissolved and particulate materials on continental shelves influenced by large rivers: plume processes. *Cont. Shelf Res.* **24**: 833-858, doi:10.1016/j.csr.2004.02.003
- Dalzell, B. J., E. C. Minor, and K. M. Mopper. 2009. Photodegradation of estuarine dissolved organic matter: a multi-method assessment of DOM transformation. *Org. Geochem.* **40**: 243-257, doi:10.1016/j.orggeochem.2008.10.003
- DeAzevedo, E. R., W.-G. Hu, T. J. Bonagamba, and K. Schmidt-Rohr. 2000. Principles of centerband-only detection of exchange in solid-state nuclear magnetic resonance, and extension to four-time centerband-only detection of exchange. *J. Chem. Phys.* **112**: 8988-9001, doi:10.1063/1.481511
- Del Castillo, C. E., P. G. Coble, J. M. Morrell, J. M. Lopez, and J. E. Corredor. 1999. Analysis of the optical properties of the Orinoco River plume by absorption and fluorescence spectroscopy. *Mar. Chem.* **66**: 35-51, doi:10.1016/S0304-4203(99)00023-7

- Del Castillo, C. E., F. Gilbes, P. G. Coble, and F. E. Muller-Karger. 2000. On the dispersal of riverine colored dissolved organic matter over the West Florida Shelf. *Limnol. Oceanogr.*: 1425-1432, doi:10.4319/lo.2000.45.6.1425
- Del Vecchio, R., and N. V. Blough. 2002. Photobleaching of chromophoric dissolved organic matter in natural waters: kinetics and modeling. *Mar. Chem.* **78**: 231-253, doi:10.1016/S0304-4203(02)00036-1
- . 2004a. On the origin of the optical properties of humic substances. *Environ. Sci. Technol.* **38**: 3885-3891, doi:10.1021/es049912h
- . 2004b. Spatial and seasonal distribution of chromophoric dissolved organic matter and dissolved organic carbon in the Middle Atlantic Bight. *Mar. Chem.* **89**: 169-187, doi:10.1016/j.marchem.2004.02.027
- Del Vecchio, R., and A. Subramaniam. 2004. Influence of the Amazon River on the surface optical properties of the western tropical North Atlantic Ocean. *J. Geophys. Res.* **109**: C11001, doi:10.1029/2004JC002503
- Deng, Y., and W. Stumm. 1994. Reactivity of aquatic iron(III) oxyhydroxides - implications for redox cycling of iron in natural waters. *Appl. Geochem.* **9**: 23-36.
- Deuser, W. 1988. Whither organic carbon? *Nature* **332**: 396-397, doi:10.1038/332396a0
- Dister, B., and O. C. Zafiriou. 1993. Photochemical free radical production rates in the eastern Caribbean. *J. Geophys. Res.* **98**: 2341-2352, doi:10.1029/92JC02765
- Dittmar, T., and B. P. Koch. 2006. Thermogenic organic matter in the abyssal ocean. *Mar. Chem.* **102**: 208-217, doi:10.1016/j.marchem.2006.04.003

- Dittmar, T. 2008. The molecular level determination of black carbon in marine dissolved organic matter. *Org. Geochem.* **39**: 396-407, doi:10.1016/j.orggeochem.2008.01.015
- Dittmar, T., B. Koch, N. Hertkorn, and G. Kattner. 2008. A simple and efficient method for the solid-phase extraction of dissolved organic matter (SPE-DOM) from seawater. *Limnol. Oceanogr.: Methods* **6**: 230-235, doi:10.4319/lom.2008.6.230
- Dittmar, T., and J. Paeng. 2009. A heat induced molecular signature in marine dissolved organic matter. *Nature Geosci.* **2**: 175-179, doi:10.1038/ngeo440
- Dixon, W. T. 1982. Spinning-sideband-free and spinning-sideband-only NMR spectra in spinning samples. *J. Chem. Phys.* **77**: 1800-1809, doi:10.1063/1.444076
- Druffel, E. R. M. and others 1989. Radiocarbon in dissolved organic and inorganic carbon from the central North Pacific. *Radiocarbon* **31**: 523-532.
- Eckert, J. M., and E. R. Sholkovitz. 1976. The flocculation of iron, aluminum and humates from river water by electrolytes. *Geochim. Cosmochim. Acta* **40**: 847-848, doi:10.1016/0016-7037(76)90036-3
- Eglinton, G., and R. J. Hamilton. 1963. The distribution of alkanes. *In* T. Swain [ed.], *Chemical plant taxonomy*. Academic Press.
- Esteves, V. I., M. Otero, and A. C. Duarte. 2009. Comparative characterization of humic substances from the open ocean estuarine water and fresh water. *Org. Geochem.* **40**: 942-950, doi:10.1016/j.orggeochem.2009.06.006
- Fasching, C. 2009. Impact on microbial degradation of dissolved organic carbon in streamwater and shallow groundwater. Masters. University of Vienna. Vienna.

- Faust, B. C., and R. G. Zepp. 1993. Photochemistry of aqueous iron (III)-polycarboxylate complexes: roles in the chemistry of atmospheric and surface waters. *Environ. Sci. Technol.* **27**: 2517-2522, doi:10.1021/es00048a032
- Fichot, C. G., and R. Benner. 2012. The spectral slope coefficient of chromophoric dissolved organic matter (S275-295) as a tracer of terrigenous dissolved organic carbon in river-influenced ocean margins. *Limnol. Oceanogr.* **57**: In Press.
- Fimmen, R. L., R. M. Cory, Y.-P. Chin, T. D. Trouts, and D. M. McKnight. 2007. Probing the oxidation-reduction properties of terrestrially and microbially derived dissolved organic matter. *Geochim. Cosmochim. Acta* **71**: 3003-3015, doi:10.1016/j.gca.2007.04.009
- Fitzwater, S. E., G. A. Knauer, and J. H. Martin. 1982. Metal contamination and its effect on primary production measurements. *Limnol. Oceanogr.* **27**: 544-551, doi:10.4319/lo.1982.27.3.0544
- Flores-Cervantes, D. X., D. I. Plata, J. K. MacFarlane, C. M. Reddy, and P. M. Gschwend. 2009. Black carbon in marine particulate organic carbon: Inputs and cycling of highly recalcitrant organic carbon in the Gulf of Maine. *Mar. Chem.* **113**: 172-181, doi:10.1016/j.marchem.2009.01.012
- Forsgren, G., M. Jansson, and P. Nilsson. 1996. Aggregation and sedimentation of Iron, Phosphorous and organic carbon in experimental mixtures of freshwater and estuarine water. *Estuar. Coast. Shelf Sci.* **43**: 259-268, doi:10.1006/ecss.1996.0068
- Forster, P. and others 2007. Changes in Atmospheric Constituents and in Radiative Forcing, p. 129-234. *In* S. Solomon et al. [eds.], *Climate Change 2007: The*

Physical Science Basis. Contribution of Working Group I to the Fourth Assessment Report of the Intergovernmental Panel on Climate. Cambridge University Press. New York.

- Fox, L. E. 1983. The removal of dissolved humic acid during estuarine mixing. *Estuar. Coast. Shelf Sci.* **16**: 431-440, doi:10.1016/0272-7714(83)90104-X
- Fuhrman, J. A., and F. Azam. 1982. Thymidine incorporation as a measure of heterotrophic bacterioplankton production in marine surface waters: evaluation and field results. *Mar. Biol.* **66**: 109-120, doi:10.1007/BF00397184
- Fuhrman, J. A., and R. L. Ferguson. 1986. Nanomolar concentrations and rapid turnover of dissolved free amino acids in seawater: Agreement between chemical and microbiological measurements. *Mar. Ecol. Prog. Ser.* **33**: 237-242, doi:10.3354/meps033237
- Gao, H. Z., and R. G. Zepp. 1998. Factors influencing photoreactions of dissolved organic matter in coastal river of the southern United States. *Environ. Sci. Technol.* **32**: 2940-2946, doi:10.1021/es9803660
- Goldstone, J. V., and B. M. Voelker. 2000. Chemistry of superoxide radical in seawater: CDOM associated sink of superoxide in coastal waters. *Environ. Sci. Technol.* **34**: 1043-1048, doi:10.1021/es9905445
- Goldstone, J. V., M. J. Pullin, S. Bertilsson, and B. M. Voelker. 2002. Reactions of hydroxyl radical with humic substances: Bleaching, mineralization, and production of bioavailable carbon substrates. *Environ. Sci. Technol.* **36**: 364-372, doi:10.1021/es0109646

- Gonsior, M., B. Peake, W. Cooper, D. Podgorski, J. D'Andrilli, and W. J. Cooper. 2009. Photochemically induced changes in dissolved organic matter identified by ultrahigh resolution Fourier transform ion cyclotron resonance mass spectrometry. *Environ. Sci. Technol.* **43**: 698-703, doi:10.1021/es8022804
- Green, F. I., and T. L. Highley. 1997. Mechanism of brown-rot decay: Paradigm or paradox. *Int. Biodeter. Biodegr.* **39**: 113-124.
- Green, N. W. and others unpubl. manuscript in preparation. An intercomparison of three methods of isolation of dissolved organic matter from deep and surface seawater.
- Green, S. A., and N. V. Blough. 1994. Optical absorption and fluorescence properties of chromophoric dissolved organic matter in natural waters. *Limnol. Oceanogr.* **39**: 1903-1916, doi:10.4319/lo.1994.39.8.1903
- Griffin, C. G., K. E. Frey, J. Rogan, and R. M. Holmes. 2011. Spatial and interannual variability of dissolved organic matter in the Kolyma River, East Siberia, observed using satellite imagery. *J. Geophys. Res.* **116**: G03018, doi:10.1029/2010JG001634
- Griffiths, P. R., and J. A. De Haseth. 2007. *Fourier Transform Infrared Spectroscopy*. Wiley Interscience. New Jersey.
- Guo, L., P. H. Santschi, and K. W. Warnken. 1995. Dynamics of dissolved organic carbon (DOC) in oceanic environments. *Limnol. Oceanogr.* **40**: 1392-1403, Doi:10.4319/lo.1995.40.8.1392
- Guo, L., P. H. Santschi, L. A. Cifuentes, S. E. Trumbore, and J. Southon. 1996. Cycling of high-molecular-weight dissolved organic matter in the Middle Atlantic Bight as



- revealed by carbon isotopic ( $^{13}\text{C}$  and  $^{14}\text{C}$ ) signatures. *Limnol. Oceanogr.* **41**: 1242-1252, doi:10.4319/lo.1996.41.6.1242
- Guo, W., C. Stedmon, Y. Han, F. Wu, X. Yu, and M. Hu. 2007. The conservative and non-conservative behavior of chromophoric dissolved organic matter in Chinese estuarine waters. *Mar. Chem.* **107**: 357-366, doi:10.1016/j.marchem.2007.03.006
- Gurtler, B. K., T. A. Vetter, E. M. Perdue, E. Ingall, J.-F. Koprivnjak, and P. H. Pfromm. 2008. Combining reverse osmosis and pulsed electrical current electrodialysis for improved recovery of dissolved organic matter from seawater. *J. Membr. Sci.* **323**: 328-336, doi:10.1016/j.memsci.2008.06.025
- Hansell, D. A., and C. A. Carlson. 1998. Deep-ocean gradients in the concentration of dissolved organic carbon. *Nature* **395**: 263-266, doi:10.1038/26200
- . 2001. Marine dissolved organic matter and the carbon cycle. *Oceanography* **14**: 41-49, doi:10.5670/oceanog.2001.05
- Hansell, D. A. 2002. DOC in the global ocean carbon cycle, p. 685-715. *In* D. A. Hansell and C. A. Carlson [eds.], *Biogeochemistry of Marine Dissolved Organic Matter*. Academic Press. San Diego.
- Hansell, D. A., C. A. Carlson, D. J. Repeta, and R. Schlitzer. 2009. Dissolved organic matter in the ocean: A controversy stimulates new insights. *Oceanography* **22**: 202-212, doi:10.5670/oceanog.2009.109
- Harvey, G. R., D. A. Boran, L. A. Chesal, and J. M. Tokar. 1983. The structure of marine fulvic and humic acids. *Mar. Chem.* **12**: 119-132, doi:10.1016/0304-4203(83)90075-0

- Hatcher, P. G. 1987. Chemical structural studies of natural lignin by dipolar dephasing solid-state  $^{13}\text{C}$  nuclear magnetic resonance. *Org. Geochem.* **11**: 31-39, doi:10.1016/0146-6380(87)90049-0
- Hedges, J. I., and J. R. Ertel. 1982. Characterization of lignin by gas capillary chromatography of cupric oxide oxidation products. *Anal. Chem.* **54**: 174-178, doi:10.1021/ac00239a007
- Hedges, J. I., P. G. Hatcher, J. R. Ertel, and K. J. Meyers-Schulte. 1992. A comparison of dissolved humic substances from seawater with Amazon River counterparts by  $^{13}\text{C}$ -NMR spectrometry. *Geochim. Cosmochim. Acta* **56**: 1753-1757, doi:10.1016/0016-7037(92)90241-A
- Hedges, J. I., and R. G. Keil. 1995. Sedimentary organic matter preservation: an assesment and speculative synthesis. *Mar. Chem.* **49**: 81-115, doi:10.1016/0304-4203(95)00008-F
- Hedges, J. I., R. G. Keil, and R. Benner. 1997. What happens to terrestrial organic matter in the ocean? *Org. Geochem.* **27**: 195-212, doi:10.1016/S0146-6380(97)00066-1
- Hedges, J. I. 2002. Why dissolved organics matter?, p. 1-33. *In* D. A. Hansell and C. A. Carlson [eds.], *Biogeochemistry of Marine Dissolved Organic Matter*. Academic Press. Amsterdam.
- Helms, J. R. 2006. Spectral shape as an indicator of molecular weight in chromophoric dissolved organic matter. Thesis. Old Dominion University, Norfolk, Virginia.
- Helms, J. R., A. Stubbins, J. Ritchie, E. C. Minor, D. J. Kieber, and K. Mopper. 2008. Absorption spectral slopes and slope ratios as indicators of molecular weight,

- source, and photobleaching of chromophoric dissolved organic matter. *Limnol. Oceanogr.* **53**: 955-969, doi:10.4319/lo.2008.53.3.0955
- Helms, J. R., X. Kong, E. Salmon, K. Schmidt-Rohr, P. G. Hatcher, and J.-D. Mao. 2012. Characterization of bitumen gilsonite using advanced solid-state NMR spectroscopy and FT-ICR-MS. *Org. Geochem.* **44**: 21-36, doi:10.1016/j.orggeochem.2011.12.001
- Henrichs, S. M., and P. T. Williams. 1985. Dissolved and particulate amino acids and carbohydrates in the surface microlayer. *Mar. Chem.* **17**: 141-163, doi:10.1016/0304-4203(85)90070-2
- Henrichs, S. M. 1995. Sedimentary organic matter preservation: an assessment and speculative synthesis - a comment. *Mar. Chem.* **49**: 127-136, doi:10.1016/0304-4203(95)00012-G
- Hernes, P. J., and J. I. Hedges. 1999. Geochemistry of tannin: Methods and applications. *In* G. G. Gross, R. Hemingway and T. Yoshida [eds.], *Plant Polyphenols 2: Chemistry, Biology, Pharmacology, Ecology*. Kluwer Academic / Plenum Publishers. New York.
- Hernes, P. J., and R. Benner. 2002. Transport and diagenesis of dissolved and particulate terrigenous organic matter in the North Pacific Ocean. *Deep-Sea Res. I* **49**: 2119-2132, doi:10.1016/S0967-0637(02)00128-0
- . 2006. Terrigenous organic matter sources and reactivity in the North Atlantic Ocean and a comparison to the Arctic and Pacific oceans. *Mar. Chem.* **100**: 66-79, doi:10.1016/j.marchem.2005.11.003

- Herschberger, C., and S. B. Binkley. 1968. Chemistry and metabolism of 3-deoxy-D-mannooctulosonic acid. *J. Biol. Chem.* **243**: 1578-1584.
- Hertkorn, N. and others 2006. Characterization of a major refractory component of marine dissolved organic matter. *Geochim. Cosmochim. Acta* **70**: 2990, doi:10.1016/j.gca.2006.03.021
- Hirschfeld, T. 1979. Diagnosis and correction of wedging errors in absorbance subtract Fourier transform infrared spectrometry. *Anal. Chem.* **51**: 495-499, doi:10.1021/ac50040a009
- Hockaday, W. C., A. M. Grannas, S. Kim, and P. G. Hatcher. 2006. Direct molecular evidence for the degradation and mobility of black carbon in soils from ultrahigh-resolution mass spectral analysis of dissolved organic matter from a fire-impacted forest soil. *Org. Geochem.* **37**: 501-510, doi:10.1016/j.orggeochem.2005.11.003
- Honghai, W., L. Yiyang, W. Jiayi, Z. Lixuan, Z. Dingcai, and D. Juan. 2008. Surface adsorption of iron oxide minerals for phenol and dissolved organic matter. *Earth Sci. Front.* **15**: 133-141.
- Hopmans, E. C., J. W. H. Weijers, E. Schefu, L. Herfort, J. S. Sinninghe Damste, and S. Schouten. 2004. A novel proxy for terrestrial organic matter in sediments based on branched and isoprenoid tetraether lipids. *Earth Planetary Sci. Let.* **224**: 107-116, doi:10.1016/j.epsl.2004.05.012
- Huguet, A., L. Vacher, S. Relexans, S. Saubusse, J. M. Froidefond, and E. Parlanti. 2009. Properties of fluorescent dissolved organic matter in the Gironde Estuary. *Org. Geochem.* **40**: 706-719, doi:10.1016/j.orggeochem.2009.03.002

- Jiao, N. and others 2010. Microbial production of recalcitrant dissolved organic matter: long-term carbon storage in the global ocean. *Nature Rev. Micro.* **8**: 593-599, doi:10.1038/nrmicro2386
- Johannessen, S. C., and W. L. Miller. 2001. Quantum yield for the photochemical production of dissolved inorganic carbon in seawater. *Mar. Chem.* **76**: 271–283, doi:10.1016/S0304-4203(01)00067-6
- Johnson, B. D. 1976. Nonliving Organic Particle Formation from Bubble Dissolution. *Limnol. Oceanogr.* **21**: 444-446, doi:10.4319/lo.1976.21.3.0444
- Johnson, B. D., and R. C. Cooke. 1980. Organic particle and aggregate formation resulting from the dissolution of bubbles in seawater. *Limnol. Oceanogr.* **25**: 653-661, doi:10.4319/lo.1980.25.4.0653
- Johnson, G. C., and J. M. Toole. 1993. Flow of deep and bottom waters in the Pacific at 10°N. *Deep-Sea Res. I* **40**: 371-394, doi:10.1016/0967-0637(93)90009-R
- Kaiser, K., and R. Benner. 2008. Major bacterial contribution to the ocean reservoir of detrital organic carbon and nitrogen. *Limnol. Oceanogr.* **53**: 99-112, doi:10.4319/lo.2008.53.1.0099
- Kalbitz, K., W. Geyer, and S. Geyer. 1999. Spectroscopic properties of dissolved humic substances: A reflection of land use history in a fen area. *Biogeochem.* **47**: 219-238, doi:10.1007/BF00994924
- Kalbitz, K. and others 2003. Changes in properties of soil-derived dissolved organic matter induced by biodegradation. *Soil Biol. Biochem.* **35**: 1129-1142, doi:10.1016/S0038-0717(03)00165-2

- Keeler, C., and G. E. Maciel. 2000.  $^{13}\text{C}$  NMR spectral editing of humic materials. *J. Molec. Struc.* **550-551**: 297-305, doi:10.1016/S0022-2860(00)00501-9
- Keil, R. G., D. B. Monthucon, F. G. Prahl, and J. Hedges. 1994. Sorptive preservation of labile organic matter in marine sediments. *Nature* **370**: 549-552, doi:10.1038/370549a0
- Kieber, D. J., and K. Mopper. 1987. Photochemical formation of glyoxylic and pyruvic acids in seawater. *Mar. Chem.* **21**: 135-149, doi:10.1016/0304-4203(87)90034-X
- Kieber, D. J., J. A. McDaniel, and K. Mopper. 1989. Photochemical source of biological substrates in seawater: Implications for carbon cycling. *Nature* **341**: 637-639, doi:10.1038/341637a0
- Kieber, R. J., X. Zhou, and K. Mopper. 1990. Formation of carbonyl compounds from UV-Induced photodegradation of humic substances in natural waters: Fate of riverine carbon in the sea. *Limnol. Oceanogr.* **35**: 1503-1515, doi:10.1021/es00080a003
- Kieber, R. J., J. D. Willey, R. F. Whitehead, and S. N. Reid. 2007. Photobleaching of chromophoric dissolved organic matter (CDOM) in rainwater. *J. Atmos. Chem.* **58**: 219-235, doi:10.1007/s10874-007-9089-3
- Kirchman, D. L., C. Lancelot, M. Fasham, L. Llegendre, G. Radach, and M. Scott. 1993. Dissolved organic matter in biogeochemical models of the ocean. *In* G. T. Evans and M. J. R. Fasham [eds.], *Towards a Model of Ocean Biogeochemical Processes*. Springer-Verlag. Berlin.
- Kirk, J. T. O. 1994. *Light and Photosynthesis in Aquatic Ecosystems*, Second ed. Cambridge University Press. Cambridge.

- Kitidis, V., A. P. Stubbins, G. Uher, R. C. U. Goddard, C. S. Law, and E. M. S. Woodward. 2006. Variability of chromophoric organic matter in surface waters of the Atlantic Ocean. *Deep-Sea Res. II* **53**: 1666-1684, doi:10.1016/j.dsr2.2006.05.009
- Kopáček, J., S. Klemntova, and S. Norton. 2005. Photochemical production of ionic and particulate aluminum and iron in lakes. *Environ. Sci. Technol.* **39**: 3656-3662, doi:10.1021/es048101a
- Kopáček, J., M. Maresova, S. Norton, P. Porcal, and J. Vesely. 2006. Photochemical source of metals for sediments. *Environ. Sci. Technol.* **40**: 4455-4459, doi:10.1021/es0600532
- Koprivnjak, J.-F., P. H. Pfromm, and E. M. Perdue. 2006. Coupling reverse osmosis with electrodialysis to isolate natural organic matter from fresh waters. *Wat. Res.* **40**: 3385-3392, doi:10.1016/j.watres.2006.07.019
- Koprivnjak, J.-F. and others 2009. Chemical and spectroscopic characterization of marine dissolved organic matter isolated using coupled reverse osmosis-electrodialysis. *Geochim. Cosmochim. Acta* **73**: 4215-4231, doi:10.1016/j.gca.2009.04.010
- Kowalczyk, P., W. J. Cooper, R. F. Whitehead, M. J. Durako, and W. Sheldon. 2003. Characterization of CDOM in an organic rich river and surrounding coastal ocean in the South Atlantic Bight. *Aquat. Sci.* **65**: 381-398, doi:10.1007/s00027-003-0078-1
- Kranck, K., and T. Milligan. 1980. Macroflocs: production of marine snow in the laboratory. *Mar. Ecol. Prog. Ser.* **3**: 19-24, doi:10.3354/meps003019

- Kujawinski, E. B., R. Del Vecchio, N. V. Blough, G. C. Klein, and A. G. Marshall. 2004. Probing molecular-level transformations of dissolved organic matter: insights on photochemical degradation and protozoan modification of DOM from electrospray ionization Fourier transform ion cyclotron resonance mass spectrometry. *Mar. Chem.* **92**: 23-37, doi:10.1016/j.marchem.2004.06.038
- Kulovaara, M., N. Corin, P. Backlund, and J. Tervo. 1996. Impact of UV254 radiation on aquatic humic substances. *Chemosphere* **33**: 783-790, doi:10.1016/0045-6535(96)00233-0
- Kuma, K., J. Nishioka, and K. Matsunaga. 1996. Controls on iron(III) hydroxide solubility in seawater: The influence of pH and natural organic chelators. *Limnol. Oceanogr.* **41**: 396-407, doi:10.4319/lo.1996.41.3.0396
- Kutser, T., D. C. Pierson, L. Tranvik, A. Reinart, S. Sobek, and K. Kallio. 2005. Using satellite remote sensing to estimate the colored dissolved organic matter absorption coefficient in lakes. *Ecosystems* **8**: 709-720, doi:10.1007/s10021-003-0148-6
- Laglara, L. M., and C. M. G. van den Berg. 2009. Evidence for geochemical control of iron by humic substances in seawater. *Limnol. Oceanogr.* **54**: 610-619, doi:10.4319/lo.2009.54.2.0610
- Lakowicz, J. R. 1999. *Principles of Fluorescence Spectroscopy*, 2nd ed. Kluwer Academic. New York.
- LeBel, D. A. and others 2008. The formation rate of North Atlantic Deep Water and Eighteen Degree Water calculated from CFC-11 inventories observed during WOCE. *Deep-Sea Res. I* **55**: 891-910, doi:10.1016/j.dsr.2008.03.009



- Leenheer, J. A. 1981. Comprehensive approach to preparative isolation and fractionation of dissolved organic carbon from natural waters and wastewaters. *Environ. Sci. Technol.* **15**, doi:10.1021/es00087a010
- . 2009. Systematic approaches to comprehensive analyses of natural organic matter. *Ann. Environ. Sci.* **3**: 1-130.
- Leifer, A. 1988. *The Kinetics of Environmental Aquatic Photochemistry: Theory and Practice*. American Chemical Society. Washington D.C.
- Liang, L., L. Luo, and S. Zhang. 2011. Adsorption and desorption of humic and fulvic acids on SiO<sub>2</sub> particles at nano- and micro-scales. *Colloids and Surfaces A: Physicochem. Eng. Aspects* **384**: 126-130, doi:10.1016/j.colsurfa.2011.03.045
- Louchouart, P., S. Opsahl, and R. Benner. 2000. Isolation and quantification of dissolved lignin from natural waters using solid-phase extraction and GC/MS. *Anal. Chem.* **72**: 2780-2787, doi:10.1021/ac9912552
- Mannino, A., and H. R. Harvey. 2000. Terrigenous dissolved organic matter along an estuarine gradient and its flux to the coastal ocean. *Org. Geochem.* **31**: 1611-1625, doi:10.1016/S0146-6380(00)00099-1
- Mantoura, R., and E. Woodward. 1983. Conservative behaviour of riverine dissolved organic carbon in the Severn Estuary: chemical and geochemical implications. *Geochim. Cosmochim. Acta* **47**: 1293-1309, doi:10.1016/0016-7037(83)90069-8
- Mao, J.-D., W.-G. Hu, K. Schmidt-Rohr, G. Davies, E. A. Ghabbour, and B. Xing. 2000. Quantitative characterization of humic substances by solid-state carbon-13 nuclear magnetic resonance. *Soil Sci. Soc. Am. J.* **64**: 873-884, doi:10.2136/sssaj2000.643873x

- Mao, J.-D., B. Xing, and K. Schmidt-Rohr. 2001. New structural information on a humic acid from two-dimensional  $^1\text{H}$ - $^{13}\text{C}$  correlation solid-state nuclear magnetic resonance. *Environ. Sci. Technol.* **35**: 1928-1934, doi:10.1021/es0014988
- Mao, J.-D., and K. Schmidt-Rohr. 2003. Recoupled long-range C-H dipolar dephasing in solid-state NMR, and its use for selection of fused aromatic rings. *J. Magn. Reson.* **162**: 217-227, doi:10.1016/S1090-7807(03)00012-0
- . 2004. Separation of aromatic-carbon  $^{13}\text{C}$  NMR signals from di-oxygen alkyl bands by a chemical-shift-anisotropy filter. *Solid State Nucl. Magn. Reson.* **26**: 36-45, doi:10.1016/j.ssnmr.2003.09.003
- Mao, J.-D., R. M. Cory, D. M. McKnight, and K. Schmidt-Rohr. 2007a. Characterization of a nitrogen-rich fulvic acid and its precursor algae from solid state NMR. *Org. Geochem.* **38**: 1277-1292, doi:10.1016/j.orggeochem.2007.04.005
- Mao, J.-D., L. Tremblay, J.-P. Gagne, S. Kohl, J. Rice, and K. Schmidt-Rohr. 2007b. Humic acids from particulate organic matter in the Saguenay Fjord and the St. Lawrence Estuary investigated by advanced solid-state NMR. *Geochim. Cosmochim. Acta* **71**: 5483-5499, doi:10.1016/j.gca.2007.09.022
- Mao, J.-D., K. M. Holtzman, and D. Franqui-Villanueva. 2010. Chemical structures of corn stover and its residue after dilute acid prehydrolysis and enzymatic hydrolysis: Insight into factors limiting enzymatic hydrolysis. *J. Agric. Food Chem.* **58**: 11680-11687, doi:10.1021/jf102514r
- Mao, J.-D., N. Chen, and X. Cao. 2011. Characterization of humic substances by advanced solid state NMR spectroscopy: Demonstration of a systematic approach. *Org. Geochem.* **42**: 891-902, doi:10.1016/j.orggeochem.2011.03.023

- Mao, J.-D., and Schmidt-Rohr, K. 2004. Separation of aromatic-carbon  $^{13}\text{C}$  NMR signals from di-oxygen alkyl bands by a chemical-shift-anisotropy filter. *Solid State Nucl. Magn. Reson.* **26**: 36-45.
- Masiello, C. A., and E. R. M. Druffel. 1998. Black carbon in deep-sea sediments. *Science* **280**: 1911-1913, doi:10.1126/science.280.5371.1911
- McCallister, S. L., J. E. Bauer, H. W. Ducklow, and E. A. Canuel. 2006. Sources of estuarine dissolved and particulate organic matter: A multi-tracer approach. *Org. Geochem.* **37**: 454-468, doi:10.1016/j.orggeochem.2005.12.005
- McCarthy, M., J. I. Hedges, and R. Benner. 1996. Major biochemical composition of dissolved high molecular weight organic matter in seawater. *Mar. Chem.* **55**: 281-298, doi:10.1016/S0304-4203(96)00041-2
- McCarthy, M., T. Pratum, J. Hedges, and R. Benner. 1997. Chemical composition of dissolved organic nitrogen in the ocean. *Nature* **390**: 150-154, doi:10.1038/36535
- McCarthy, M., J. Hedges, and R. Benner. 1998. Major bacterial contribution to marine dissolved organic nitrogen. *Science* **281**: 231-234, doi:10.1126/science.281.5374.231
- McKee, G. A., and P. G. Hatcher. 2010. Alkyl amides in two organic-rich anoxic sediments: A possible new abiotic route for N sequestration. *Geochim. Cosmochim. Acta* **74**: 6436-6450, doi:10.1016/j.gca.2010.08.004
- McKnight, D. M., E. W. Boyer, P. K. Westerhoff, P. T. Doran, T. Kulbe, and D. T. Andersen. 2001. Spectrofluorometric characterization of dissolved organic matter for indication of precursor organic material and aromaticity. *Limnol. Oceanogr.* **46**: 38-48, doi:10.4319/lo.2001.46.1.0038

- Mead, R. N., and M. A. Goni. 2008. Matrix protected organic matter in a river dominated margin: A possible mechanism to sequester terrestrial organic matter? *Geochim. Cosmochim. Acta* **72**: 2673-2686, doi:10.1016/j.gca.2008.03.007
- Menon, H. B., N. P. Sangekar, A. A. Lotliker, and P. Vetamony. 2011. Dynamics of chromophoric dissolved organic matter in Mandovi and Zuari estuaries - A study through in situ and satellite data. *ISPRS J. Photogramm.* **66**: 545-552, doi:10.1016/j.isprsjprs.2011.02.011
- Meyers-Schulte, K. J., and J. I. Hedges. 1986. Molecular evidence for a terrestrial component of organic matter dissolved in ocean water. *Nature* **321**: 61-64, doi:10.1038/321061a0
- Miller, W. L. 1994. Recent advances in the photochemistry of natural dissolved organic matter, p. 111 –128. *In* G. R. Helz, R. G. Zepp and D. G. Crosby [eds.], *Aquatic and Surface Photochemistry*. CRC Press. Danvers, MA.
- Miller, W. L., and R. G. Zepp. 1995. Photochemical production of dissolved inorganic carbon from terrestrial organic matter: significance to the oceanic organic carbon cycle. *Geophys. Res. Lett.* **22**: 417-420, doi:10.1029/94GL03344
- Miller, W. L., and M. A. Moran. 1997. Interaction of photochemical and microbial processes in the degradation of refractory dissolved organic matter from a coastal marine environment. *Limnol. Oceanogr.* **42**: 1317-1324, doi:10.4319/lo.1997.42.6.1317
- Miller, W. L., M. A. Moran, W. M. Sheldon, R. G. Zepp, and S. Opsahl. 2002. Determination of apparent quantum yield spectra for the formation of biologically

- labile photoproducts. *Limnol. Oceanogr.* **47**: 343-352,  
doi:10.4319/lo.2002.47.2.0343
- Minor, E. C., J. Pothén, B. J. Dalzell, H. Abdulla, and K. Mopper. 2006. Effects of salinity changes on the photodegradation and ultraviolet-visible absorbance of terrestrial dissolved organic matter. *Limnol. Oceanogr.* **51**: 2181-2186,  
doi:10.4319/lo.2006.51.5.2181
- Minor, E. C., B. J. Dalzell, A. Stubbins, and K. Mopper. 2007. Evaluating the photoalteration of estuarine dissolved organic matter using direct temperature-resolved mass spectrometry and UV-visible spectroscopy. *Aquat. Sci.* **69**: 440-455, doi:10.1007/s00027-007-0897-y
- Mitra, S., T. S. Bianchi, L. Guo, and P. H. Santschi. 2000. Terrestrially derived dissolved organic matter in the chesapeake bay and the middle atlantic bight. *Geochim. Cosmochim. Acta* **64**: 3547-3557, doi:10.1016/S0016-7037(00)00450-6
- Moore, W. S., J. L. Sarmiento, and R. M. Key. 1986. Tracing the amazon component of surface Atlantic water using  $^{228}\text{Ra}$ , salinity, and silica. *J. Geophys. Res.* **91**: 2574-2580, doi:10.1029/JC091iC02p02574
- Mopper, K., and E. T. Degens. 1979. Organic carbon in the ocean: Nature and cycling, p. 293-316. *In* B. Bolin, E. T. Degens, S. Kempe and P. Ketner [eds.], *The Global Carbon Cycle*. Wiley. New York.
- Mopper, K., and W. L. Stahovec. 1986. Sources and sinks of low molecular weight organic carbonyl compounds in seawater. *Mar. Chem.* **19**: 305-321,  
doi:10.1016/0304-4203(86)90052-6

- Mopper, K., J. Zhou, K. S. Ramana, U. Passow, H. G. Dam, and Drapeau. 1995. Role of surface active carbohydrates in the flocculation of a diatom bloom in a mesocosm. *Deep-Sea Res.* **42**: 47-73, doi:10.1021/cr050359b
- Mopper, K., and D. J. Kieber. 2002. Photochemistry and the cycling of carbon, sulfur, nitrogen and phosphorus, p. 455-507. *In* D. A. Hansell and C. A. Carlson [eds.], *Biogeochemistry of Marine Dissolved Organic Matter*. Academic Press. San Diego, CA.
- Mopper, K., A. Stubbins, J. D. Ritchie, H. M. Bialk, and P. G. Hatcher. 2007. Advanced instrumental approaches for characterization of marine dissolved organic matter: extraction techniques, mass spectrometry, and nuclear magnetic resonance spectroscopy. *Chem. Rev.* **107**: 419-442, doi:10.1021/cr050359b
- Moran, M. A., and R. G. Zepp. 1997. Role of photoreactions in the formation of biologically labile compounds from dissolved organic matter. *Limnol. Oceanogr.* **42**: 1307-1316, doi:10.4319/lo.1997.42.6.1307
- Moran, M. A., W. M. Sheldon, and R. G. Zepp. 2000. Carbon loss and optical property changes during long term photochemical and biological degradation of estuarine organic matter. *Limnol. Oceanogr.* **45**: 1254-1264, doi:10.4319/lo.2000.45.6.1254
- Nagata, T., and D. L. Kirchman. 1999. Bacterial mortality: a pathway for the formation of refractory DOM? *In* C. R. Bell, M. Brylinsky and P. Johnson-Green [eds.], *Mortality of Microbes in Aquatic Environments: New Frontiers*, Proc. of 8th Int. Symp. On Microbial Ecology. Atlantic Canada Soc. of Microbial Ecology.

- Nelson, N. B., and D. A. Siegel. 2002. Chromophoric DOM in the open ocean, p. 547-578. *In* D. A. Hansell and C. A. Carlson [eds.], *Biogeochemistry of Marine Dissolved Organic Matter*. Academic Press. San Diego, CA.
- Nelson, N. B., C. A. Carlson, and D. K. Steinberg. 2004. Production of chromophoric dissolved organic matter by Sargasso Sea microbes. *Mar. Chem.* **89**: 273–287, doi:10.1016/j.marchem.2004.02.017
- Nelson, N. B., D. A. Siegel, C. A. Carlson, C. Swan, W. M. Smethie Jr., and S. Khatiwala. 2007. Hydrography of chromophoric dissolved organic matter in the North Atlantic. *Deep-Sea Res. I* **54**: 710-731, doi:10.1016/j.dsr.2007.02.006
- Nierop, K. G., B. Jansen, and J. M. Verstraten. 2002. Dissolved organic matter, aluminum and iron interactions: precipitation induced by metal/carbon ratio, pH and competition. *Sci. Tot. Env.* **300**: 201-211, doi:10.1016/S0048-9697(02)00254-1
- O'Melia, C. R., and W. Stumm. 1967. Aggregation of Silica Despersions by Iron (III). *J. Colloid Interface Sci.* **23**: 437-447, doi:10.1016/0021-9797(67)90186-5
- Obernosterer, I., and R. Benner. 2004. Competition between biological and photochemical processes in the mineralization of dissolved organic carbon. *Limnol. Oceanogr.* **49**: 117-124, doi:10.4319/lo.2004.49.1.0117
- Ogawa, H., Y. Amagi, I. Koike, K. Kaiser, and R. Benner. 2001. Production of refractory dissolved organic matter by bacteria. *Science* **292**: 917-920, doi:10.1126/science.1057627
- Ogura, N. 1972. Rate and extent of decomposition of dissolved organic matter in the surface water. *Mar. Biol.* **13**: 89-93, doi:10.1007/BF00366559

- Opella, S. J., and M. H. Frey. 1979. Selection of nonprotonated carbon resonances in solid state nuclear magnetic resonance. *J. Am. Chem. Soc.* **101**: 5854-5856, doi:10.1021/ja00513a079
- Opsahl, S., and R. Benner. 1997. Distribution and cycling of terrigenous dissolved organic matter in the ocean. *Nature*. **386**: 480-482, doi:10.1038/386480a0
- . 1998. Photochemical reactivity of dissolved lignin in river and ocean waters. *Limnol. Oceanogr.* **43**: 1297-1304, doi:10.4319/lo.1998.43.6.1297
- Opsahl, S., R. Benner, and R. M. W. Amon. 1999. Major flux of terrigenous dissolved organic matter through the Arctic Ocean. *Limnol. Oceanogr.* **44**: 2017-2023, doi:10.4319/lo.1999.44.8.2017
- Orsetti, S., E. M. Andrade, and F. V. Molina. 2010. Modeling ion binding to humic substances: elastic polyelectrolyte network model. *Langmuir* **26**: 3134-3144, doi:10.1021/la903086s
- Ortega-Retuerta, E., I. Reche, E. Pulido-Villena, S. Austi, and C. Duarte. 2010. Distribution and photoreactivity of chromophoric dissolved organic matter in the Antarctic Peninsula (Southern Ocean). *Mar. Chem.* **118**: 129-139, doi:10.1016/j.marchem.2009.11.008
- Osburn, C. L., D. P. Morris, K. A. Thorn, and R. E. Moeller. 2001. Chemical and optical changes in freshwater dissolved organic matter exposed to solar radiation. *Biogeochem.* **54**: 251-278, doi:10.1023/A:1010657428418
- Osburn, C. L., C. R. Wigdahl, S. C. Fritz, and J. E. Saros. 2011. Dissolved organic matter composition and photoreactivity in prairie lakes of the U. S. Great Plains. *Limnol. Oceanogr.* **56**: 2371-2390, doi:10.4319/lo.2011.56.6.2371



Para, J., P. G. Coble, B. Charriere, M. Tedetti, C. Fontana, and R. Sempere. 2010.

Fluorescence and absorption properties of chromophoric dissolved organic matter CDOM in coastal surface waters of the northwestern Mediterranean Sea, influence of the Rhone River. *Biogeosciences* **7**: 4083-4103, doi:10.5194/bg-7-4083-2010

Pavia, D. L., G. M. Lampman, and G. S. Kriz. 1979. Introduction to spectroscopy: A guide for students of organic chemistry. Saunders. Philadelphia.

Perdue, E. M. pers. comm. April 22, 2011.

Perdue, E. M., and J. D. Ritchie. 2003. Dissolved organic matter in freshwaters, p. 273-318. *In* J. I. Drever [ed.], Surface and Ground Water, Weathering, Erosion and Soils. Elsevier-Pergamon. Oxford.

Pfeffer, P. E., W. V. Gerasimowicz, and E. G. Piotrowsik. 1984. Effect of paramagnetic Iron on quantitation in carbon-13 cross polarization magic angle spinning nuclear magnetic resonance spectroscopy of heterogeneous environmental matrices. *Anal. Chem.* **56**: 734-741, doi:10.1021/ac00268a032

Pisani, O., Y. Yamashita, and R. Jaffe'. 2011. Photo-dissolution of flocculent, detrital material in aquatic environments: contributions to the dissolved organic matter pool. *Water Res.* **45**: 3836-3844, doi:10.1016/j.watres.2011.04.035

Poulin, M. B., and T. L. Lowary. 2010. Methods to study the biosynthesis of bacterial furanosides, p. 611. *In* M. Fukuda [ed.], Glycomics. *Methods in Enzymology*. Academic Press.

- Powell, R., and A. Wilson-Finelli. 2003. Photochemical degradation of organic iron complexing ligands in seawater. *Aquat. Sci.* **65**: 367-374, doi:10.1007/s00027-003-0679-0
- Pullin, M. J., C. A. Progress, and P. A. Maurice. 2004. Effects of photoirradiation on the adsorption of dissolved organic matter on goethite. *Geochim. Cosmochim. Acta* **68**: 3643-3656, doi:10.1016/j.gca.2004.03.017
- Raymond, P. A., and J. E. Bauer. 2001. Use of  $^{14}\text{C}$  and  $^{13}\text{C}$  natural abundances for evaluating riverine, estuarine, and coastal DOC and POC sources and cycling: a review and synthesis. *Org. Geochem.* **32**: 469-485, doi:10.1016/S0146-6380(00)00190-X
- Reche, I., M. L. Pace, and J. J. Cole. 2000. Modeled effects of dissolved organic carbon and solar spectra on photobleaching in lake ecosystems. *Ecosystems* **3**: 419-432, doi:10.1007/s100210000038
- Repet, D. J., and L. I. Aluwihare. 2006. Radiocarbon analysis of neutral sugars in high-molecular-weight dissolved organic carbon: Implications for organic carbon cycling. *Limnol. Oceanogr.* **51**: 1045-1053, doi:10.4319/lo.2006.51.2.1045
- Riemer, D. D., P. J. Milne, R. G. Zika, and W. H. Post. 2000. Photoproduction of nonmethane hydrocarbons (NMHCs) in seawater. *Mar. Chem.* **71**: 177-198, doi:10.1016/S0304-4203(00)00048-7
- Rochelle-Newall, E. J., and T. R. Fisher. 2002a. Production of chromophoric dissolved organic matter fluorescence in marine and estuarine environments: an investigation into the role of phytoplankton. *Mar. Chem.* **77**: 7-21, doi:10.1016/S0304-4203(01)00072-X

- . 2002b. Chromophoric dissolved organic matter and dissolved organic carbon in Chesapeake Bay. *Mar. Chem.* **77**: 23-41, doi:10.1016/S0304-4203(01)00073-1
- Rogoff, M., and I. Wender. 1962. Oxidation of aromatic compounds by bacteria. *In* U. S. D. o. t. Interior [ed.]. Bureau of Mines. U.S. Government Printing Office.
- Romera-Castillo, C., H. Sarmiento, X. A. Alvarez-Salgado, J. M. Gasol, and C. Marrase. 2011. Net production and consumption of fluorescent colored dissolved organic matter by natural bacterial assemblages growing on marine phytoplankton exudates. *Appl. Environ. Microbiol.* **77**: 7490-7498, doi:10.1128/AEM.00200-11
- Sannigrahi, P., E. D. Ingall, and R. Benner. 2005. Cycling of dissolved and particulate organic matter at station ALOHA: Insights from <sup>13</sup>C NMR spectroscopy coupled with elemental, isotopic and molecular analyses. *Deep-Sea Res. I* **52**: 1429-1444, doi:10.1016/j.dsr.2005.04.001
- Sarpal, R. S., K. Mopper, and D. J. Kieber. 1995. Absorbance properties of dissolved organic matter in Antarctic sea water. *Antarct. J. Unit. States* **30**: 139-140.
- Schmitt-Kopplin, P., N. Hertkorn, H.-R. Schulten, and A. Kettrup. 1998. Structural changes in a dissolved soil humic acid during photochemical degradation processes under O<sub>2</sub> and N<sub>2</sub> atmosphere. *Environ. Sci. Technol.* **32**: 2531-2541, doi:10.1021/es970636z
- Semple, K. T., R. B. Cain, and S. Schmidt. 1999. Biodegradation of aromatic compounds by microalgae. *FEMS Microbiol. Ecol.* **170**: 291-300, doi:10.1111/j.1574-6968.1999.tb13386.x
- Sexton, P. F. and others 2011. Eocene global warming events driven by ventilation of oceanic dissolved organic carbon. *Nature* **471**: 349-352, doi:10.1038/nature09826

- Shank, G. C., R. F. Whitehead, M. L. Smith, S. A. Skrabal, and R. J. Kieber. 2006. Photodegradation of strong-copper complexing ligands in organic-rich estuarine waters. *Limnol. Oceanogr.* **51**: 884-892, doi:10.4319/lo.2006.51.2.0884
- Sharp, J. H. 2002. Analytical methods for total DOM pools, p. 35-58. *In* D. A. Hansell and C. A. Carlson [eds.], *Biogeochemistry of Marine Dissolved Organic Matter*. Academic Press. San Diego, CA.
- Sholkovitz, E. R. 1976. Flocculation of dissolved organic and inorganic matter during the mixing of river water and seawater. *Geochim. Cosmochim. Acta* **40**: 831-835, doi:10.1016/0016-7037(76)90035-1
- . 1978. The flocculation of dissolved Fe, Mn, Al, Cu, Ni, Co and Cd during estuarine mixing. *Earth Planet. Sci. Lett.* **41**: 77-86, doi:10.1016/0012-821X(78)90043-2
- Sholkovitz, E. R., E. A. Boyle, and N. B. Price. 1978. The removal of dissolved humic acids and iron during estuarine mixing. *Earth Planet. Sci. Lett.* **40**: 130-136, doi:10.1016/0012-821X(78)90082-1
- Skoog, A., M. Wedborg, and E. Fogelqvist. 1996. Photobleaching of fluorescence and the organic carbon concentration in a coastal environment. *Mar. Chem.* **55**: 333-345, doi:10.1016/S0304-4203(96)00044-8
- Skoog, A., and R. Benner. 1997. Aldoses in various size fractions of marine organic matter: Implications for carbon cycling. *Limnol. Oceanogr.* **42**: 1803-1813, doi:10.4319/lo.1997.42.8.1803
- Sleighter, R. L., and P. G. Hatcher. 2008. Molecular characterization of dissolved organic matter (DOM) along a river to ocean transect of the lower Chesapeake Bay by ultrahigh resolution electrospray ionization Fourier transform ion cyclotron

- resonance mass spectrometry. *Mar. Chem.* **110**: 140-152,  
doi:10.1016/j.marchem.2008.04.008
- Smith, D. C., and F. Azam. 1992. A simple economical method for measuring bacterial protein synthesis rates in sea water using <sup>3</sup>H-leucine. *Mar. Microb. Food Webs* **6**: 107-114.
- Sondergaard, M., C. A. Stedmon, and N. H. Borch. 2003. Fate of terrigenous dissolved organic matter (DOM) in estuaries: aggregation and bioavailability. *Ophelia* **57**: 161-176.
- Spencer, R. G. M., B. A. Pellerin, and B. A. Bergamaschi. 2007. Diurnal variability in riverine dissolved organic matter composition determined by in situ optical measurement in the San Joaquin River (California, USA). *Hydrol. Process.* **21**: 3181-3189, doi:10.1002/hyp.6887
- Spencer, R. G. M. and others 2009. Photochemical degradation of dissolved organic matter and dissolved lignin phenols from the Congo River. *J. Geophys. Res.* **114**: G03010, doi:10.1029/2009JG000968
- Spencer, R. G. M., G. R. Aiken, R. Y. Dyda, K. D. Butler, B. A. Bergamaschi, and P. J. Hernes. 2010. Comparison of XAD with other dissolved lignin isolation techniques and a compilation of analytical improvements for the analysis of lignin in aquatic settings. *Org. Geochem.* **41**: 445-453,  
doi:10.1016/j.orggeochem.2010.02.004
- Stedmon, C. A., S. Markager, and H. Kaas. 2000. Optical properties and signatures of chromophoric dissolved organic matter (CDOM) in Danish coastal waters. *Estuar. Coast. Shelf Sci.* **51**: 267-278, doi:10.1006/ecss.2000.0645

- Stedmon, C. A., and S. Markager. 2005. Resolving the variability in dissolved organic matter fluorescence in a temperate estuary and its catchment using PARAFAC analysis. *Limnol. Oceanogr.* **50**: 686-697, doi:10.4319/lo.2005.50.2.0686
- Stedmon, C. A., S. Markager, L. J. Tranvik, L. Kronberk, T. Slatis, and W. Martinsen. 2007. Photochemical production of ammonium and transformation of dissolved organic matter in the Baltic Sea. *Mar. Chem.* **104**: 227-204, doi:10.1016/j.marchem.2006.11.005
- Stedmon, C. A., C. L. Osburn, and T. Kragh. 2010. Tracing water mass mixing in the Baltic-North Sea transition zone using the optical properties of coloured dissolved organic matter. *Estuar. Coast. Shelf Sci.* **87**: 156-162, doi:10.1016/j.ecss.2009.12.022
- Stevenson, F. J. 1994. Humus chemistry: Genesis, composition, and reactions. John Wiley and Sons. New York.
- Strain, S. M., and I. M. Armitage. 1985. Selective detection of 3-deoxymannooctulosonic acid in intact lipopolysaccharides by spin-echo <sup>13</sup>C NMR. *J. Biol. Chem.* **260**: 12974-12977.
- Stubbins, A., G. Uher, C. S. Law, K. Mopper, C. Robinson, and R. C. Upstill-Goddard. 2006. Open-ocean carbon monoxide photoproduction. *Deep-Sea Res. II* **53**: 1695–1705, doi:10.1016/j.dsr2.2006.05.011
- Stubbins, A. and others 2008. Relating carbon monoxide photoproduction to dissolved organic matter functionality. *Environ. Sci. Technol.* **42**: 3271-3276, doi:10.1021/es703014q

- . 2010. Illuminated darkness: molecular signatures of Congo River dissolved organic matter and its photochemical alteration as revealed by ultrahigh precision mass spectrometry. *Limnol. Oceanogr.* **55**: 1467-1477, doi:10.4319/lo.2010.55.4.1467
- . 2012. Anthropogenic aerosols as a source of ancient dissolved organic matter in glaciers. *Nature Geosci.* **5**: 198-201, doi:10.1038/ngeo1403
- Stumm, W., and J. J. Morgan. 1981. *Aquatic Chemistry*, 2nd ed. Wiley-Interscience. New York.
- Sukenik, A., D. Bilanovic, and G. Shelef. 1988. Flocculation of microalgae in brackish and sea waters. *Biomass* **15**: 187-199, doi:10.1016/0144-4565(88)90084-4
- Sulzberger, B., and H. Laubscher. 1995. Reactivity of various types of iron(III) (hydr)oxides towards light-induced dissolution. *Mar. Chem.* **50**: 103-115, doi:10.1016/0304-4203(95)00030-U
- Sulzberger, B., and E. Durisch-Kaiser. 2009. Chemical characterization of dissolved organic matter (DOM): A prerequisite for understanding UV-induced changes of DOM absorption properties and bioavailability. *Aquat. Sci.* **71**: 104-126, doi:10.1007/s00027-008-8082-5
- Summers, R. S., P. K. Cornel, and P. V. Roberts. 1987. Molecular size distribution and spectroscopic characterization of humic substances. *Sci. Tot. Env.* **62**: 27-37, doi:10.1016/0048-9697(87)90478-5
- Sutcliffe, W. H., E. R. Baylor, and D. W. Menzel. 1963. Sea surface chemistry and Langmuir circulation. *Deep-Sea Res.* **10**: 233-243, doi:10.1016/0011-7471(63)90359-0

- Swan, C. M., D. A. Siegel, N. B. Nelson, C. A. Carlson, and E. Nasir. 2009. Biogeochemical and hydrographic controls on chromophoric dissolved organic matter distribution in the Pacific Ocean. *Deep-Sea Res. I* **56**: 2175-2192, doi:10.1016/j.dsr.2009.09.002
- Swift, R. S. 1985. Fractionation of soil humic substances, p. 387-407. *In* G. R. Aiken, D. M. McKnight, R. L. Wershaw and P. MacCarthy [eds.], *Humic Substances in Soil, Sediment, and Water*. John Wiley & Sons, Inc. New York.
- Tanoue, E., S. Nishiyama, M. Kamo, and A. Tsugita. 1995. Bacterial membranes: Possible source of a major dissolved protein in seawater. *Geochim. Cosmochim. Acta* **59**: 2643-2648, doi:10.1016/0016-7037(95)00134-4
- Tarr, M. A., W. Wang, T. S. Bianchi, and E. Englehaupt. 2001. Mechanisms of ammonia and amino acid photoproduction from aquatic humic and colloidal matter. *Wat. Res.* **35**: 3688-3696, doi:10.1016/S0043-1354(01)00101-4
- Thorn, K. A., S. J. Younger, and L. G. Cox. 2010. Order of Functionality Loss during Photodegradation of Aquatic Humic Substances. *J. Environ. Qual.* **39**: 1416-1428, doi:10.2134/jeq2009.0408
- Toole, D. A., D. Slezak, R. P. Kiene, D. J. Kieber, and D. A. Siegel. 2006. Effects of solar radiation on dimethylsulfide cycling in the western Atlantic Ocean. *Deep-Sea Res. I* **53**: 136–153, doi:10.1016/j.dsr.2005.09.003
- Turner, A., and M. C. Rawling. 2001. The influence of salting out on the sorption of neutral organic compounds in estuaries. *Wat. Res.* **35**: 4379-4389, doi:10.1016/S0043-1354(01)00163-4



- Turner, A. 2003. Salting out of chemicals in estuaries: implications for contaminant partitioning and modelling. *Sci. Tot. Env.* **314-316**: 599-612, doi:10.1016/S0048-9697(03)00076-7
- Twardowski, M. S., and P. L. Donaghay. 2002. Photobleaching of aquatic dissolved materials: absorption removal, spectral alteration and their interrelationship. *J. Geophys. Res.*, doi:10.1029/1999JC000281
- Twardowski, M. S., E. Boss, J. M. Sullivan, and P. L. Donaghay. 2004. Modeling the spectral shape of absorption by chromophoric dissolved organic matter. *Mar. Chem.* **89**: 69-88, doi:10.1016/j.marchem.2004.02.008
- Vähätalo, A. V., M. Salkinoja-Salonen, P. Taalas, and K. Salonen. 2000. Spectrum of the quantum yield for photochemical mineralization of dissolved organic carbon in a humic lake. *Limnol. Oceanogr.* **45**: 664-676, doi:10.4319/lo.2000.45.3.0664
- Vähätalo, A. V., and R. G. Wetzel. 2004. Photochemical and microbial decomposition of chromophoric dissolved organic matter during long (months-years) exposures. *Mar. Chem.* **89**: 313-326, doi:10.1016/j.marchem.2004.03.010
- VanLoon, G., and S. Duffy. 2010. *Organic Matter in Water. Environmental Chemistry: A Global Perspective.* Oxford University Press. New York.
- Verdugo, P., A. L. Alldredge, F. Azam, D. L. Kirchman, U. Passow, and P. H. Santschi. 2004. The oceanic gel phase: A bridge in the DOM-POM continuum. *Mar. Chem.* **92**: 67-85, doi:10.1016/j.marchem.2004.06.017
- Verney, R., R. Lafite, and J.-C. Brun-Cottan. 2009. Flocculation potential of estuarine particles: the importance of environmental factors and of the spatial and seasonal

- variability of suspended particulate matter. *Estuar. Coast.* **32**: 678-693,  
doi:10.1007/s12237-009-9160-1
- Vetter, T. A., E. M. Perdue, E. Ingall, J.-F. Koprivnjak, and P. H. Pfromm. 2007.  
Combining reverse osmosis and electrodialysis for more complete recovery of  
dissolved organic matter from seawater. *Sep. Purif. Technol.* **56**: 383-387,  
doi:10.1016/j.seppur.2007.04.012
- Vodacek, A., N. V. Blough, M. D. DeGrandpre, E. T. Peltzer, and R. K. Nelson. 1997.  
Seasonal variation of CDOM and DOC in the Middle Atlantic Bight: terrestrial  
inputs and photooxidation. *Limnol. Oceanogr.* **42**: 674-686,  
doi:10.4319/lo.1997.42.4.0674
- Wang, X., Y. Cai, and L. Guo. 2010. Preferential removal of dissolved carbohydrates  
during estuarine mixing in the Bay of Saint Louis in the northern gulf of Mexico.  
*Mar. Chem.* **119**: 130-138, doi:10.1016/j.marchem.2010.01.006
- Watanabe, A., S.-I. Ochi, C. Kato, K. Ikeya, and T. Nakamura. 2010. Relationship  
between  $^{14}\text{C}$  age and structural property of humic acids. 19th World Congress of  
Soil Science, Soil Solutions for a Changing World.
- Weishaar, J. L., G. R. Aiken, B. A. Bergamaschi, M. S. Fram, R. Fujii, and K. Mopper.  
2003. Evaluation of specific ultraviolet absorbance as an indicator of the chemical  
composition and reactivity of dissolved organic carbon. *Environ. Sci. Technol.*  
**37**: 4702-4708, doi:10.1021/es030360x
- Wetzel, R. G., P. G. Hatcher, and T. S. Bianchi. 1995. Natural photolysis by ultraviolet  
irradiance of recalcitrant dissolved organic matter to simple substrates for rapid

- bacterial metabolism. *Limnol. Oceanogr.* **40**: 1369-1380,  
doi:10.4319/lo.1995.40.8.1369
- White, E. M., D. J. Kieber, and K. Mopper. 2008. Determination of photochemically produced carbon dioxide in seawater. *Limnol. Oceanogr.: Methods* **6**: 441-453,  
doi:10.4319/lom.2008.6.441
- White, E. M., D. J. Kieber, J. Sherrard, W. L. Miller, and K. Mopper. 2010. Carbon dioxide and carbon monoxide photoproduction quantum yields in the Delaware Estuary. *Mar. Chem.* **118**: 11-21, doi:10.1016/j.marchem.2009.10.001
- Williams, P. M. 1971. The distribution and cycling of organic matter in the ocean, p. 145-163. *In* S. D. Faust and J. V. Hunter [eds.], *Organic Compounds in the Aquatic Environment*. Dekker. New York.
- Williams, P. M., and E. R. M. Druffel. 1987. Radiocarbon in dissolved organic matter in the central North Pacific Ocean. *Nature* **330**: 246-248, doi:10.1038/330246a0
- Williamson, C. E., P. J. Neale, G. Grad, H. T. De Lange, and B. R. Hargreaves. 2001. Beneficial and detrimental effects of UV on aquatic organisms: Implications of spectral variation. *Ecol. Appl.* **11**: 1843-1857, doi:10.1890/1051-0761(2001)011[1843:BADEOU]2.0.CO;2
- Wong, J. C. Y. 2009. Source tracing of dissolved organic matter (DOM) in watersheds using UV and fluorescence spectroscopy. Masters. University of Toronto. Toronto.
- Wu, X., and K. W. Zilm. 1993. Complete spectral editing in CPMAS NMR. *J. Magn. Reson. A* **102**: 205-213, doi:10.1006/jmra.1993.1092

- Wurl, O., L. Miller, R. Röttgers, and S. Vagle. 2009. The distribution of surface-active substances in the sea-surface microlayer and water column. *Mar. Chem.* **115**: 1-9, doi:10.1016/j.marchem.2009.04.007
- Yacobi, Y. Z., J. J. Alberts, M. Takacs, and M. McElvaine. 2003. Absorption spectroscopy of colored dissolved organic carbon in Georgia (USA) rivers: the impact of molecular size distribution. *J. Limnol.* **62**: 41-46, doi:10.4081/jlimnol.2003.41
- Yamada, N., and E. Tanoue. 2003. Detection and partial characterization of dissolved glycoproteins in oceanic waters. *Limnol. Oceanogr.* **48**: 1037-1048, doi:10.4319/lo.2003.48.3.1037
- Yamashita, Y., and E. Tanoue. 2003a. Distribution and alteration of amino acids in bulk DOM along a transect from bay to oceanic waters. *Mar. Chem.* **82**: 145-160, doi:10.1016/S0304-4203(03)00049-5
- . 2003b. Chemical characterization of protein-like fluorophores in DOM in relation to aromatic amino acids. *Mar. Chem.* **82**: 255-271, doi:10.1016/S0304-4203(03)00073-2
- . 2004. In situ production of chromophoric dissolved organic matter in coastal environments. *Geophys. Res. Lett.* **31**: L24302, doi:10.1029/2004GL019734
- Yamashita, Y., A. Tsukasaki, T. Nishida, and E. Tanoue. 2007. Vertical and horizontal distribution of fluorescent dissolved organic matter in the Southern Ocean. *Mar. Chem.* **106**: 498–509, doi:10.1016/j.marchem.2007.05.004

- Yamashita, Y., and E. Tanoue. 2008. Production of bio-refractory fluorescent dissolved organic matter in the ocean interior. *Nature Geosci.* **1**: 579–582, doi:10.1038/ngeo279
- . 2009. Basin scale distribution of chromophoric dissolved organic matter in the Pacific Ocean. *Limnol. Oceanogr.* **54**: 598–609, doi:10.4319/lo.2009.54.2.0598
- Zafiriou, O. C., J. Jousset-Dubien, R. G. Zepp, and R. G. Zika. 1984. Photochemistry of natural waters. *Environ. Sci. Technol.* **18**: 358A-371A, doi:10.1021/es00130a001
- Zafiriou, O. C., S. S. Andrews, and W. Wang. 2003. Concordant estimates of oceanic carbon monoxide source and sink processes in the pacific yield a balanced global "blue-water" CO budget. *Global Biogeochem. Cycles* **17**: 1015-1030, doi:10.1029/2001GB001638
- Zepp, R. G., and P. F. Schlotzhauer. 1981. Comparison of photochemical behavior of various humic substances in water: 3. Spectroscopic properties of humic substances. *Chemosphere* **10**: 479– 486, doi:10.1016/0045-6535(81)90148-X
- Zepp, R. G. 2002. Solar ultraviolet radiation and aquatic carbon, nitrogen, sulfur and metals cycles, p. 137–183. *In* E. W. Helbling and H. Zagarese [eds.], *UV Effects in Aquatic Organisms and Ecosystems*. Royal Society of Chemistry. Cambridge, UK.
- Zepp, R. G., W. M. Sheldon, and M. A. Moran. 2004. Dissolved organic fluorophores in southeastern US coastal waters: correction method for eliminating Rayleigh and Raman scattering peaks in excitation-emission matrices. *Mar. Chem.* **89**: 15-36, doi:10.1016/j.marchem.2004.02.006

- Zhang, L., G. H. Preslherbe, and H. M. Muchall. 2006. Ultraviolet absorption spectra of substituted phenols: A computational study. *Photochem. Photobiol.* **82**: 324-331, doi:10.1562/2005-07-08-RA-605
- Zhou, J., K. Mopper, and U. Passow. 1998. The role of surface-active carbohydrates in the formation of transparent exopolymer particles (TEP) by bubble adsorption. *Limnol. Oceanogr.* **43**: 1860-1871.
- Zika, R. G. 1980. The sunlight induced decay of seawater light absorbance and fluorescence. *EOS* **61**: 1010.
- Ziolkowski, L. A., and E. R. M. Druffel. 2010. Aged black carbon identified in marine dissolved organic carbon. *Geophys. Res. Lett.* **37**: L16601, doi:10.1029/2010GRL

## APPENDIX

### COPYRIGHT PERMISSIONS

#### ELSEVIER LICENSE TERMS AND CONDITIONS

Oct 24, 2011

This is a License Agreement between John R Helms ("You") and Elsevier ("Elsevier") provided by Copyright Clearance Center ("CCC"). The license consists of your order details, the terms and conditions provided by Elsevier, and the payment terms and conditions.

**All payments must be made in full to CCC. For payment instructions, please see information listed at the bottom of this form.**

Supplier	Elsevier Limited The Boulevard, Langford Lane Kidlington, Oxford, OX5 1GB, UK
Registered Company Number	1982084
Customer name	John R Helms
Customer address	509 Larchmont Dr. Wilmington, NC 28403
License number	2775521269464
License date	Oct 24, 2011
Licensed content publisher	Elsevier
Licensed content publication	Elsevier Books
Licensed content title	Biogeochemistry of Marine Dissolved Organic Matter
Licensed content author	Craig A. Carlson
Licensed content date	2002
Number of pages	61
Start Page	
End Page	
Type of Use	reuse in a thesis/dissertation
Portion	Figures/tables/illustrations
Number of Figures/tables/illustrations	1
Format	both print and electronic
Are you the author of this Elsevier chapter?	No
Will you be translating?	No
Order reference number	
Title of your thesis/dissertation	Nature and Photochemical Transformation of Terrestrial and Marine Dissolved Organic Matter

Expected completion date	Dec 2011
Estimated size (number of pages)	250
Elsevier VAT number	
Permissions price	0.00 USD
VAT/Local Sales Tax	
Total	0.00 USD

#### Terms and Conditions

### INTRODUCTION

1. The publisher for this copyrighted material is Elsevier. By clicking "accept" in connection with completing this licensing transaction, you agree that the following terms and conditions apply to this transaction (along with the Billing and Payment terms and conditions established by Copyright Clearance Center, Inc. ("CCC"), at the time that you opened your Rightslink account and that are available at any time at <http://myaccount.copyright.com>).

### GENERAL TERMS

2. Elsevier hereby grants you permission to reproduce the aforementioned material subject to the terms and conditions indicated.

3. Acknowledgement: If any part of the material to be used (for example, Figures) has appeared in our publication with credit or acknowledgement to another source, permission must also be sought from that source. If such permission is not obtained then that material may not be included in your publication/copies. Suitable acknowledgement to the source must be made, either as a footnote or in a reference list at the end of your publication, as follows:

"Reprinted from Publication title, Vol /edition number, Author(s), Title of article / title of chapter, Pages No., Copyright (Year), with permission from Elsevier [OR APPLICABLE SOCIETY COPYRIGHT OWNER]." Also Lancet special credit - "Reprinted from The Lancet, Vol. number, Author(s), Title of article, Pages No., Copyright (Year), with permission from Elsevier."

4. Reproduction of this material is confined to the purpose and/or media for which permission is hereby given.

5. Altering/Modifying Material: Not Permitted. However Figures and illustrations may be altered/adapted minimally to serve your work. Any other abbreviations, additions, deletions and/or any other alterations shall be made only with prior written authorization of Elsevier Ltd. (Please contact Elsevier at [permissions@elsevier.com](mailto:permissions@elsevier.com))

6. If the permission fee for the requested use of our material is waived in this instance, please be advised that your future requests for Elsevier materials may attract a fee.

7. Reservation of Rights: Publisher reserves all rights not specifically granted in the combination of (i) the license details provided by you and accepted in the course of this licensing transaction, (ii) these terms and conditions and (iii) CCC's Billing and Payment terms and conditions.

8. License Contingent Upon Payment: While you may exercise the rights licensed immediately upon issuance of the license at the end of the licensing process for the transaction, provided that you have disclosed complete and accurate details of your proposed use, no license is finally effective unless and until full payment is received from you (either by publisher or by CCC) as provided in CCC's Billing and Payment terms and conditions. If full payment is not received on a timely basis, then any license preliminarily granted shall be deemed automatically revoked and shall be void as if never granted. Further, in the event that you breach any of these terms and conditions or any of CCC's Billing and Payment terms and conditions, the license is automatically revoked and shall be void as if never granted. Use of materials as described in a revoked license, as well as any use of the materials beyond the scope of an unrevoked license, may constitute copyright infringement and publisher reserves the right to take any and all action to protect its copyright in the materials.

9. Warranties: Publisher makes no representations or warranties with respect to the licensed material.

10. Indemnity: You hereby indemnify and agree to hold harmless publisher and CCC, and their respective officers, directors, employees and agents, from and against any and all claims arising out of your use of the licensed material other than as specifically authorized pursuant to this license.

### INTRODUCTION

1. The publisher for this copyrighted material is Elsevier. By clicking "accept" in connection with completing this licensing transaction, you agree that the following terms and conditions apply to this transaction (along with the Billing and Payment terms and conditions established by Copyright



**If you would like to pay for this license now, please remit this license along with your payment made payable to "COPYRIGHT CLEARANCE CENTER" otherwise you will be invoiced within 48 hours of the license date. Payment should be in the form of a check or money order referencing your account number and this invoice number RLNK500651535.**

**Once you receive your invoice for this order, you may pay your invoice by credit card. Please follow instructions provided at that time.**

**Make Payment To:  
Copyright Clearance Center  
Dept 001  
P.O. Box 843006  
Boston, MA 02284-3006**

**For suggestions or comments regarding this order, contact RightsLink Customer Support: [customercare@copyright.com](mailto:customercare@copyright.com) or +1-877-622-5543 (toll free in the US) or +1-978-646-2777.**

**Gratis licenses (referencing \$0 in the Total field) are free. Please retain this printable license for your reference.**

NATURE PUBLISHING LICENSE  
TERMS AND CONDITIONS

Nov 09, 2011

This is a License Agreement between John R Helms ("You") and Elsevier ("Elsevier") provided by Copyright Clearance Center ("CCC"). The license consists of your order details, the terms and conditions provided by Elsevier, and the payment terms and conditions.

**All payments must be made in full to CCC. For payment instructions, please see information listed at the bottom of this form.**

Supplier	Nature Publishing Group
Registered Company Number	1982084
Customer name	John R Helms
Customer address	509 Larchmont Dr. Wilmington, NC 28403
License number	2785020798782
License date	Oct 24, 2011
Licensed content publisher	Nature Publishing Group
Licensed content publication	Journal of Investigative Dermatology
Licensed content title	Epidermal COX-2 Induction Following Ultraviolet Irradiation: Suggested Mechanism for the Role of COX-2 Inhibition in Photoprotection
Licensed content author	Catherine S Tripp, Eric A G Blomme, Kevin S Chinn, Medora M Hardy, Peter LaCelle, Alice P Pentland
Licensed content date	Sep 25, 2003
Fig.	Fig. 1. Emission spectrum of UVA 340 sunlamps compared to the solar spectrum
Type of Use	reuse in a thesis/dissertation
Portion	Figures/tables/illustrations
Number of Figures/tables/illustrations	1
Format	both print and electronic
Are you the author of this Elsevier chapter?	No
Will you be translating?	No
Order reference number	
Title of your	Nature and Photochemical Transformation of Terrestrial and Marine
Title of your thesis/dissertation	Nature and Photochemical Transformation of Terrestrial and Marine Dissolved Organic Matter

Expected completion date Dec 2011

Estimated size (number of pages) 250

Permissions price 0.00 USD

VAT/Local Sales Tax

Total 0.00 USD

Terms and Conditions

## INTRODUCTION

1. The publisher for this copyrighted material is Elsevier. By clicking "accept" in connection with completing this licensing transaction, you agree that the following terms and conditions apply to this transaction (along with the Billing and Payment terms and conditions established by Copyright Clearance Center, Inc. ("CCC"), at the time that you opened your Rightslink account and that are available at any time at <http://myaccount.copyright.com>).

## GENERAL TERMS

2. Elsevier hereby grants you permission to reproduce the aforementioned material subject to the terms and conditions indicated.

3. Acknowledgement: If any part of the material to be used (for example, Figures) has appeared in our publication with credit or acknowledgement to another source, permission must also be sought from that source. If such permission is not obtained then that material may not be included in your publication/copies. Suitable acknowledgement to the source must be made, either as a footnote or in a reference list at the end of your publication, as follows:

"Reprinted from Publication title, Vol /edition number, Author(s), Title of article / title of chapter, Pages No., Copyright (Year), with permission from Elsevier [OR APPLICABLE SOCIETY COPYRIGHT OWNER]." Also Lancet special credit - "Reprinted from The Lancet, Vol. number, Author(s), Title of article, Pages No., Copyright (Year), with permission from Elsevier."

4. Reproduction of this material is confined to the purpose and/or media for which permission is hereby given.

5. Altering/Modifying Material: Not Permitted. However Figures and illustrations may be altered/adapted minimally to serve your work. Any other abbreviations, additions, deletions and/or any other alterations shall be made only with prior written authorization of Elsevier Ltd. (Please contact Elsevier at [permissions@elsevier.com](mailto:permissions@elsevier.com))

6. If the permission fee for the requested use of our material is waived in this instance, please be advised that your future requests for Elsevier materials may attract a fee.

7. Reservation of Rights: Publisher reserves all rights not specifically granted in the combination of (i) the license details provided by you and accepted in the course of this licensing transaction, (ii) these terms and conditions and (iii) CCC's Billing and Payment terms and conditions.

8. License Contingent Upon Payment: While you may exercise the rights licensed immediately upon issuance of the license at the end of the licensing process for the transaction, provided that you have disclosed complete and accurate details of your proposed use, no license is finally effective unless and until full payment is received from you (either by publisher or by CCC) as provided in CCC's Billing and Payment terms and conditions. If full payment is not received on a timely basis, then any license preliminarily granted shall be deemed automatically revoked and shall be void as if never granted. Further, in the event that you breach any of these terms and conditions or any of CCC's Billing and Payment terms and conditions, the license is automatically revoked and shall be void as if never granted. Use of materials as described in a revoked license, as well as any use of the materials beyond the scope of an unrevoked license, may constitute copyright infringement and publisher reserves the right to take any and all action to protect its copyright in the materials.

9. Warranties: Publisher makes no representations or warranties with respect to the licensed material.

10. Indemnity: You hereby indemnify and agree to hold harmless publisher and CCC, and their respective officers, directors, employees and agents, from and against any and all claims arising out

## INTRODUCTION

1. The publisher for this copyrighted material is Elsevier. By clicking "accept" in connection with completing this licensing transaction, you agree that the following terms and conditions apply to this transaction (along with the Billing and Payment terms and conditions established by Copyright

**If you would like to pay for this license now, please remit this license along with your payment made payable to "COPYRIGHT CLEARANCE CENTER" otherwise you will be invoiced within 48 hours of the license date. Payment should be in the form of a check or money order referencing your account number and this invoice number RLNK500651535.**

**Once you receive your invoice for this order, you may pay your invoice by credit card. Please follow instructions provided at that time.**

**Make Payment To:  
Copyright Clearance Center  
Dept 001  
P.O. Box 843006  
Boston, MA 02284-3006**

**For suggestions or comments regarding this order, contact RightsLink Customer Support: [customercare@copyright.com](mailto:customercare@copyright.com) or +1-877-622-5543 (toll free in the US) or +1-978-646-2777.**

**Gratis licenses (referencing \$0 in the Total field) are free. Please retain this printable license for your reference.**

## VITA

John Robert Helms  
Department of Chemistry and Biochemistry  
Old Dominion University  
4541 Hampton Blvd.  
Norfolk, VA 23529

### *Education:*

B.A., Chemistry, Virginia Wesleyan College, Norfolk, VA, May 1998.  
M.S., Chemistry, Old Dominion University, Norfolk, VA, December 2006.  
PhD., Chemistry, Old Dominion University, Norfolk, VA, August 2012 (expected).

### *Professional:*

Chemist, K&M Environmental Inc. July 1998 - October 2001.  
Teaching Assistant, Old Dominion University. January 2002 – December 2007.  
Research Assistant, Old Dominion University. January 2003 – July 2011.  
Adjunct Assistant Professor, Tidewater Community College. January 2011 – May 2011.  
Postdoctoral Fellow, University of North Carolina, Wilmington. December 2011 –

### *Awards and affiliations:*

Virginia Wesleyan College Presidential Scholar (1994-1996)  
American Chemical Society (member since 1998)  
American Society of Limnology and Oceanography (member since 2005)  
Golden Key International Honour Society (inducted 2007)  
American Geophysical Union (member since 2008)

### *Selected Publications:*

- Helms, J.R., A. Stubbins, J. D. Ritchie, E.C. Minor, D. J. Kieber, and K. Mopper. 2008.  
Absorption spectral slopes and slope ratios as indicators of molecular weight and  
sources, and photobleaching of chromophoric dissolved organic matter.  
*Limnol. Oceanogr.* **53**: 955-969.
- Helms, J.R., K. Xueqian, E. Salmon, P.G. Hatcher, K. Schmidt-Rohr, and J.-D. Mao.  
2012. Structural characterization of gilsonite bitumen by advanced nuclear  
magnetic resonance spectroscopy and ultrahigh resolution mass spectrometry  
revealing pyrrolic and aromatic rings substituted with aliphatic chains. *Org.*  
*Geochem.* **44**: 21-36.